In The Name of God

University of Kashan
659

Climate System and Aeolian Erosion in Terrestrial Planets

Abolfazl Ranjbar

sokhanvaran pub.

سرشناسه	:	رنجبرفردوئی، ابوالفضل، ۱۳۳۹- AbolfazlRanjbar Fordoei ,
عنوان و نام پدیدآور	:	[Book]Climate system and aeolian erosion in terrestrial planets / Abolfazl Ranjbar.
مشخصات نشر	:	تهران : سخنوران، دانشگاه کاشان، ۱۳۹۹= ۲۰۲۰م.
مشخصات ظاهری	:	۳۰۶ص.
شابک	:	978-622-215814-9
وضعیت فهرست نویسی	:	فیپا
یادداشت	:	انگلیسی.
آوانویسی عنوان	:	کلایمیت...
موضوع	:	سیاره‌های درونی
موضوع	:	Inner planets
موضوع	:	سیاره‌ها -- زمین‌شناسی
موضوع	:	Planets -- Geology
موضوع	:	اقلیم‌شناسی
موضوع	:	Climatology
موضوع	:	خاک -- فرسایش
موضوع	:	Soil erosion
موضوع	:	فرسایش بادی
موضوع	:	Wind erosion
موضوع	:	تغییرات اقلیمی
موضوع	:	Climatic changes
شناسه افزوده	:	دانشگاه کاشان
رده بندی کنگره	:	۶۰۶QB
رده بندی دیویی	:	۴/۵۲۳
شماره کتابشناسی ملی	:	۷۳۰۰۶۶۳

۶۵۹

Climate System and Aeolian Erosion in Terrestrial Planets

مؤلف: ابوالفضل رنجبر فردوئی

ناشر: سخنوران - دانشگاه کاشان

طراح جلد: سخنوران

سال و نوبت چاپ: ۱۳۹۹ - اول

شمارگان: ۱۰۰۰ نسخه

شابک: ۹-۸۱۴-۲۱۵-۶۲۲-۹۸۷

قیمت: ۶۵۰۰۰ تومان

انتشارات دانشگاه کاشان - کیلومتر شش بلوار قطب راوندی - صندوق پستی: ۵۳۱۵۳-۸۷۳۱۷

انتشارات سخنوران: کارگر شمالی، بعد از ادوارد براون، شماره ۱۴۰۷، طبقه اول،

تلفن: ۶۶۴۷۶۳۰۶

*This book is dedicated to holy position of **Imam Ali** (peace be upon him) for inspiring human to learn.*

The space of any container becomes narrower due to its content, except for the container of knowledge, which it more expands with the study of science (Nāhjul-bālãgha).

Preface

At present eight plants orbiting sun. The inner, rocky planets are Mercury, Venus, Earth and Mars. Mercury is the smallest planet in our solar system and nearest to the Sun. Despite its proximity to the Sun, Mercury is not the hottest planet in our solar system.

Venus is a terrestrial plant and it is shrouded by an opaque layer of highly reflective clouds of sulfuric acid. Much of the Venus surface has been shaped by volcanic activity. About thousand impact craters on Venus are distributed. Venus has an extremely dense CO_2/N_2 atmosphere, and it is characterized as having an atmosphere 92 times more massive than that of the Earth. High winds circle the planet from east to west, at speeds 60 times faster than rotation of the solid planet. All winds on the planet are ultimately driven by convection. Venus's clouds as well as its CO_2 concentration further increase its opacity. The atmosphere is divided into a number of sections depending on altitude. The densest part of Venusian atmosphere is the troposphere. The troposphere contains 99% of the atmosphere's mass. Venus is Earth's twin in many ways, but without lack of liquid water.

In the absence of fluvial processes (or glacial abrasion, or freeze–thaw), it is hard to imagine how to make much sand. The observed aeolian features are dark mantles, wind streaks, yardangs and dunes. Dark mantles and wind streaks are rather common features on Venus, while yardangs and dunes large are observed in only a few localities. The prominent aeolian process on Venus is known as saltation in which grains hop along the surface in low angle trajectories. Formation of aeolian ripples is strongly influenced by size sorting of sand. Sand on Venus is scarce. It has attributed to the fact that erosion by water does not operate on Venus, and chemical weathering doesn't produce sand. Wind streaks are the most abundant aeolian features on Venus. A field of possible yardangs is observed in the vicinity of the crater Mead, the largest impact crater on the planet.

Earth "our home planet" is the third planet from the Sun, and the only place that is inhabited by living things. Earth is the only world in our solar system with liquid water on the surface. Some

geological evidence indicates that life may have arisen as early as 4.1 billion years ago. Of the Earth surface area, 70.8%, is below sea level and covered by ocean water. The remaining 29.2% has terrain that varies greatly from place to place and consists of mountains, deserts, plains, plateaus, and other landforms. The abundance of water on Earth's surface is a unique feature that distinguishes the "Blue Planet" from other planets in the Solar System.

Aeolian processes, involving erosion, transportation, and deposition of sediment by the wind, occur in a variety of environments, including the coastal zone, deserts, and agricultural fields. The landforms that result from aeolian erosion include ventifacts, ridge and swale systems, yardangs, desert depressions, and inverted relief. On Earth surface, three main factors influence the piling of sand into dunes with particular shapes: (1) wind magnitude (above the threshold velocity), direction, and frequency; (2) vegetation covers and (3) grain size.

Many attempts have been made to classify dunes based on a combination of shape, number and orientation relative to the prevailing wind and degree of form mobility. Based on these factors descriptive terms such as ‘longitudinal’ and ‘transverse’, have been used. For instance, the term the term longitudinal dune should be applied only where the orientation of the long axis of the dune deviates by less than 15° from the resultant sand transport direction, while a transverse dune should have long axes which are within 15° of being normal to the resultant sand transport direction. In another attempt Earth dunes were classified in self-accumulated dunes include barchans, transverse (barchanoid) ridges, unvegetated linear dunes (seif dunes), dome dunes, and star dunes, and dunes formed by the presence of vegetation include parabolic dunes, vegetated linear dunes, and coppice or hummock dunes.

Mars is a dusty, cold, desert world with a very thin atmosphere. The robotic explorers have found lots of evidence that Mars was much wetter and warmer, with a thicker atmosphere, billions of years ago. The days and seasons are likewise comparable to those of Earth. Liquid water cannot exist on the surface of Mars due to low atmospheric pressure. Data show Martian soil to be slightly

alkaline and containing elements such as magnesium, sodium, potassium and chlorine. These nutrients are found in soils on Earth, and they are necessary for growth of plants. Mars is scarred by a number of impact craters. The largest confirmed of these is the Hellass impact basin which is visible from Earth. Due to the smaller mass of Mars, the probability of an object colliding with the planet is about half that of Earth. Mars has two relatively small moons, Phobos and Deimos. Wind erosion and deposition are powerful agents of surface change on Mars. The topography on Mars shows a large scale asymmetry between the northern lowlands and the southern highlands. Mars exhibits many of the same dune forms as seen on the Earth, including barchan, transverse, yardangs, as well as star and climbing dunes. Many dunes are located in the floors of impact craters where sediment could accumulate. Mars is a very dusty planet. Dust storms on Mars are full of water. In 2018, the largest recorded dust storm circled the entire Martian globe, so thick that it hid the surface from the sun and killed the Opportunity rover. Most of the time the lofting and rearranging of dust is done by the dust devils that spin across the planetary surface. Dust on Mars is the most important driver of weather. The static electricity from rains rubbing against one another in these dry, sandy whirlwinds could be a problem. “It’s possible that all of the dust grains clattering together in these storms could produce a lot of electricity and disable electronics. The electric fields associated with dust devils on Mars are so much drier and dustier than in devils on Earth. Mechanical weathering is the primary mode for the generation of sand-sized particles on Mars, mainly because of the dearth of water under present Martian conditions. Impact craters also provide an intense but much localized means to break up near-surface rocks into smaller constituent pieces. The sand dunes are widespread around Mars, but not in a systematic manner.

A ring of sand called the North Polar Erg (NPE) surrounds the north polar cap on Mars. The dune field on the floor of Proctor crater was the first to be identified on Mars which covers an area approximately 2275 km^2 in area. A variety of dune types have been recognized on Mars over the years, including barchan, barchanoid ridge, transverse,

star, linear, dome, and complex dunes. Cater-related permanent wind streaks are observed around some craters on Mars.

Titan is the largest Saturn's moon. Titan is an icy world whose surface is completely obscured by a golden hazy atmosphere. The surface of Titan is one of the most Earthlike places in the solar system, albeit at vastly colder temperatures and with different chemistry. Here it is so cold (-179 degrees Celsius) that water ice plays the role of rock. Titan may have volcanic activity as well, but with liquid water "lava" instead of molten rock. At the surface of Titan, the atmospheric pressure is about 60 percent greater than on Earth—roughly the same pressure a person would feel swimming about 15 meters below the surface in the ocean on Earth. Titan's atmosphere is mostly nitrogen (about 95 percent) and methane (about 5 percent), with small amounts of other carbon-rich compounds. The low gravity and dense atmosphere on Titan make it a favorable environment for aeolian transportation of material in the sense that the wind speeds needed to saltate surface particles are rather low.

Our knowledge about erosional mechanisms on terrestrial planets is not even complete on Earth. We may gain further new insight in the future through space missions as well as by more observational, experimental and theoretical studies. However, in this book the reader finds base information as well as a discussion on what potential new results can tell us about the history of erosional mechanisms on sun terrestrial planets. I hope that this book can serve as guide for all those who are interested in aeolian processes on terrestrial planets with emphasize on Mercury, Venus, Earth, Mars and Earth's Moon. Because on these planets, the principal causes of erosion (e.g., running water, glacial abrasion and freeze thaw) are absent.

I would like to express my thanks to the authorities of University of Kashan.

University of Kashan, July 2020 **Abolfazl Ranjbar-Fordoei**

INDEX

Chapter 1
Our solar system

Introduction

Our galaxy has more planets than stars. Currently eight planets orbiting our star, the inner, rocky planets are Mercury, Venus, Earth and Mars. The outer planets are gas giants Jupiter and Saturn and ice giants Uranus and Neptune. Beyond Neptune, a newer class of smaller worlds called dwarf planets reign, including perennial favorite Pluto.

1.1. Mercury

The smallest planet in our solar system and nearest to the Sun, Mercury is only slightly larger than Earth's Moon. From the surface of Mercury, the Sun would appear more than three times as large as it does when viewed from Earth, and the sunlight would be as much as seven times brighter. Despite its proximity to the Sun, Mercury is not the hottest planet in our solar. It has no known satellites (moons).

Mercury's orbital velocity averages 47.6 km/s but varies from 56.6 km/s at perihelion to 38.7 km/s at aphelion. At perihelion the Sun's apparent diameter is over three times larger than its apparent diameter as seen from Earth.

Mercury's rotation period is 58.646 Earth days, and its orbital period is 87.969 Earth days. Therefore, it has a unique 3:2 resonance between its rotational and orbital periods: It makes exactly three rotations on its axis for every two orbits around the Sun. This resonance was apparently acquired over time as the natural consequence of the dissipative processes of tidal friction and the relative motion between a solid mantle and a liquid core. As a consequence of this resonance, a solar day (sunrise to sunrise) lasts

two Mercurian years or 176 Earth days. The obliquity of Mercury is close to 0◦; therefore, it does not experience seasons as do Earth and Mars. Consequently, the Polar Regions never receive the direct rays of sunlight and are always frigid compared to torrid sunlit equatorial regions.

Mercury has the most eccentric (0.205) and inclined (7°) orbit of any planet. However, over periods of a few million years, its eccentricity may vary from about 0.1 to 0.28 and its inclination from about 0° to 11°. Its average distance from the Sun is 0.3871 AU[1] (5.79 × 10^7 km). Because of its large eccentricity, however, the distance varies from 0.3075 AU (4.6 × 10^7 km) at perihelion to 0.4667 AU (6.98 × 10^7 km) at aphelion. As a consequence, Mercury's orbital velocity averages 47.6 km/s but varies from 56.6 km/s at perihelion to 38.7 km/s at aphelion. At perihelion the Sun's apparent diameter is over three times larger than its apparent diameter as seen from Earth (Munsell et al, 2009).

Mercury's rotation period is 58.646 Earth days, and its orbital period is 87.969 Earth days. Therefore, it has a unique 3:2 resonance between its rotational and orbital periods: It makes exactly three rotations on its axis for every two orbits around the Sun. This resonance was apparently acquired over time as the natural consequence of the dissipative processes of tidal friction and the relative motion between a solid mantle and a liquid core. As a consequence of this resonance, a solar day (sunrise to sunrise) lasts two Mercurian years or 176 Earth days. The obliquity of Mercury is close to 0◦; therefore, it does not experience seasons as do Earth and Mars. Consequently, the Polar Regions never receive the direct rays of sunlight and are always frigid compared to torrid sunlit equatorial regions.

Another effect of the 3:2 resonance between the rotational and orbital periods is that the same hemisphere always faces the Sun at alternate perihelion passages. This happens because the hemisphere

1 - Astronomical Unit (AU)

facing the Sun at one perihelion will rotate one and a half times by the next perihelion, so that it faces away from the Sun; after another orbit, it rotates another one-and-a half times so that it directly faces the Sun again. Because the sub-solar points of the 0◦ and 180◦ longitudes occur at perihelion they are called hot poles. The sub-solar points at the 90◦ and 270◦ longitudes are called warm poles because they occur at aphelion. Yet another consequence of the 3:2 resonances and the large eccentricity is that an observer on Mercury (depending on location) would witness a double sunrise, or a double sunset, or the Sun would backtrack in the sky at noon during perihelion passage. Near perihelion Mercury's orbital velocity is so great compared to its rotation rate that it overcomes the Sun's apparent motion in the sky as viewed from Mercury.

Mercury experiences the greatest range (day to night) in surface temperatures (650◦ C = 1170◦ F) of any planet or satellite in the solar system because of its close proximity to the Sun, its peculiar 3:2 spin orbit coupling, its long solar day, and its lack of an insulating atmosphere. Its maximum surface temperature is about 467◦ C (873◦ F) at perihelion on the equator; hot enough to melt zinc. At night just before dawn, the surface temperature plunges to about -183 ◦C (-297◦ F).

Radar images of Mercury obtained from both the Arecibo and the linked Goldstone—Very Large Array radar facilities discovered unusual features at Mercury's poles. The radar signals show very high reflectivities centered on the poles. The reflectivity and ratio values are similar to outer planet icy satellites and the residual polar water ice cap of Mars. Therefore, Mercury's polar radar features have been interpreted to be water ice. The radar characteristics are consistent with the ice being covered by a few centimeters of regolith. It has also been proposed that the radar characteristics are the result of volume scattering by inhomogeneities in elemental sulfur deposits. In this case, it is proposed that sulfur volatilized from sulfides in the regolith was cold-trapped at the poles.

Images taken by Mariner 10 from Mercury's Polar Regions show

cratered surfaces where ice or sulfur could be concentrated in permanently shadowed portions of the craters. Radar studies have shown that the anomalies are indeed concentrated in the permanently shadowed portions of these polar craters (Fig. 2). The south polar radar feature is centered at about 88◦ S and 150◦ Wand is largely confined within a crater (Chao Meng-Fu) 150 km in diameter, but a few smaller features occur outside this crater. In the North Polar Region, the deposits reside in about 25 craters down to latitude as low as 72° (Fig. 2). Because the obliquity of Mercury is near 0°, it does not experience seasons, and, therefore, temperatures in the polar regions should be <135 K. Water ice can be stable in the interiors of craters even down to 72° latitude if covered with only a few centimeters of regolith, or if it is relatively new. This means that water ice would still be present in its perpetually shadowed craters or even in illuminated craters at high latitude, if covered with a veneer of regolith (Mazarico et al., 2014).

1.2. Venus

Second planet from the Sun and our closest planetary neighbor, Venus is similar in structure and size to Earth, but it is now a very different world. Venus spins slowly in the opposite direction most planets do. Its thick atmosphere traps heat in a runaway greenhouse effect, making it the hottest planet in our solar system—with surface temperatures hot enough to melt lead. Glimpses below the clouds reveal volcanoes and deformed mountains.

Figure 1.1 Venus is a terrestrial planet and is sometimes called Earth's "sister planet" because of their similar size, mass, proximity to the Sun, and bulk composition (Hashimoto et al, 2008).

Venus is a terrestrial planet and is sometimes called Earth's "sister planet" because of their similar size, mass, proximity to the Sun, and bulk composition. It is radically different from Earth in other respects. It has the densest atmosphere of the four terrestrial planets, consisting of more than 96% carbon dioxide. The atmospheric pressure at the planet's surface is 92 times that of Earth, or roughly the pressure found 900 m (3,000 ft) underwater on Earth. Venus is by far the hottest planet in the Solar System, with a mean surface temperature of 735 °K (462 °C; 863 °F), even though Mercury is closer to the Sun. Venus is shrouded by an opaque layer of highly reflective clouds of sulfuric acid, preventing its surface from being seen from space in visible light. It may have had water oceans in the past (Hashimoto et al, 2008), but these would have vaporized as the temperature rose due to a runaway greenhouse effect. The water has probably photo-dissociated, and the free hydrogen has been swept into interplanetary space by the solar wind because of the lack of a planetary magnetic

field. Venus's surface is a dry desert scape interspersed with slab-like rocks and is periodically resurfaced by volcanism (Jakosky B.M., 1999).

1.2.1. Geography

About 80% of the Venusian surface is covered by smooth, volcanic plains, consisting of 70% plains with wrinkle ridges and 10% smooth or lobate plains. Two highland "continents" make up the rest of its surface area, one lying in the planet's northern hemisphere and the other just south of the equator. The northern continent is called Ishtar Terra after Ishtar, the Babylonian goddess of love, and is about the size of Australia. Maxwell Montes, the highest mountain on Venus, lies on Ishtar Terra. Its peak is 11 km (7 mi) above the Venusian average surface elevation. The southern continent is called Aphrodite Terra, after the Greek goddess of love, and is the larger of the two highland regions at roughly the size of South America. A network of fractures and faults covers much of this area (Kaufmann, 1994).

Most Venusian surface features are named after historical and mythological women. Exceptions are Maxwell Montes, named after James Clerk Maxwell, and highland regions Alpha Regio, Beta Regio, and Ovda Regio. The latter three features were named before the current system was adopted by the International Astronomical Union, the body which oversees planetary nomenclature (Carolynn, 1990).

The longitude of physical features on Venus is expressed relative to its prime meridian. The original prime meridian passed through the radar-bright spot at the centre of the oval feature Eve, located south of Alpha Regio. After the Venera missions were completed, the prime meridian was redefined to pass through the central peak in the crater Ariadne (Karttunen et al, 2007).

1.2.2. Surface Geology

Much of the Venusian surface appears to have been shaped by volcanic activity. Venus has several times as many volcanoes as Earth, and it has 167 large volcanoes that are over 100 km (62 mi) across. The only volcanic complex of this size on Earth is the Big Island of

Hawaii. This is not because Venus is more volcanically active than Earth, but because its crust is older. Earth's oceanic crust is continually recycled by subduction at the boundaries of tectonic plates, and has an average age of about 100 million years, whereas the Venusian surface is estimated to be 300–600 million years old Frankel, (Charles, 1996).

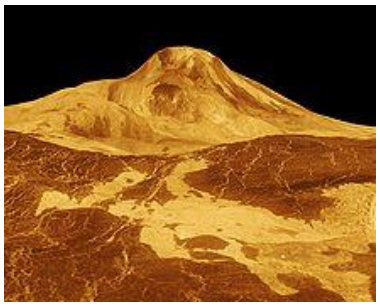

Figure 1.2 False-colour radar map of Maat Mons with a vertical exaggeration of 22.5 (NASA- Jet Propulsion Laboratory - photojournal.jpl.nasa.gov/catalog/pia00254).

Several lines of evidence point to ongoing volcanic activity on Venus. During the Soviet Venera program, the *Venera 9* orbiter obtained spectroscopic evidence of lightning on Venus, and the *Venera 12* descent probe obtained additional evidence of lightning and thunder. The European Space Agency's *Venus Express* in 2007 detected whistler waves further confirming the occurrence of lightning on Venus. One possibility is that ash from a volcanic eruption was generating the lightning. Another piece of evidence comes from measurements of sulfur dioxide concentrations in the atmosphere, which dropped by a factor of 10 between 1978 and 1986, jumped in 2006, and again declined 10-fold. This may mean that levels had been boosted several times by large volcanic eruptions (Glaze, 1999).

Almost a thousand impact craters on Venus are evenly distributed across its surface. On other cratered bodies, such as Earth and the Moon, craters show a range of states of degradation. On the Moon, degradation is caused by subsequent impacts, whereas on Earth it is

caused by wind and rain erosion. On Venus, about 85% of the craters are in pristine condition. The number of craters, together with their well-preserved condition, indicates the planet underwent a global resurfacing event about 300–600 million years ago (Nimmo and McKenzie, 1998), followed by a decay in volcanism (Romeo and Turcotte, 2009).

1.2.3. Internal Structure

Without seismic data or knowledge of its moment of inertia, little direct information is available about the internal structure and geochemistry of Venus (Goettel et al, 1981). The similarity in size and density between Venus and Earth suggests they share a similar internal structure: a core, mantle, and crust. Like that of Earth, the Venusian core is at least partially liquid because the two planets have been cooling at about the same rate. The slightly smaller size of Venus means pressures are 24% lower in its deep interior than Earth's. The principal difference between the two planets is the lack of evidence for plate tectonics on Venus, possibly because its crust is too strong to sub duct without water to make it less viscous. This results in reduced heat loss from the planet, preventing it from cooling and providing a likely explanation for its lack of an internally generated magnetic field. Instead, Venus may lose its internal heat in periodic major resurfacing events.

1.3. The Earth

Our home planet is the third planet from the Sun, and the only place we know of so far that’s inhabited by living things. While Earth is only the fifth largest planet in the solar system, it is the only world in our solar system with liquid water on the surface. Just slightly larger than nearby Venus, Earth is the biggest of the four planets closest to the Sun, all of which are made of rock and metal.

The name Earth is at least 1,000 years old. All of the planets, except for Earth, were named after Greek and Roman gods and goddesses. However, the name Earth is a Germanic word, which

simply means “the ground.”

Figure 1.3 The Blue Marble, the first full-view photograph of the planet, was taken by Apollo 17 astronauts en route to the Moon in 1972 (NASA Content Administrator, 2017).

Earth is the only astronomical object known to harbor life. According to radiometric dating and other sources of evidence, Earth formed over 4.5 billion years ago. Earth's gravity interacts with other objects in space, especially the Sun and the Moon, which is Earth's only natural satellite. Earth orbits around the Sun in 365.26 days, a period known as an Earth year. During this time, Earth rotates about its axis about 366.26 times (Manhesa et al, 1980). Earth's axis of rotation is tilted with respect to its orbital plane, producing seasons on Earth. The gravitational interaction between Earth and the Moon causes tides, stabilizes Earth's orientation on its axis, and gradually slows its rotation (Laskar et al, 2004). Earth is the densest planet in the Solar System and the largest and most massive of the four rocky planets.

Earth's lithosphere is divided into several rigid tectonic plates that

migrate across the surface over many millions of years. About 71% of Earth's surface is covered with water, mostly by oceans. The remaining 29% is land consisting of continents and islands that together contain many lakes, rivers and other sources of water that contribute to the hydrosphere. The majority of Earth's polar regions are covered in ice, including the Antarctic ice sheet and the sea ice of the Arctic ice pack. Earth's interior remains active with a solid iron inner core, a liquid outer core that generates the Earth's magnetic field and a convecting mantle that drives plate tectonics.

Within the first billion years of Earth's history, life appeared in the oceans and began to affect the Earth's atmosphere and surface, leading to the proliferation of anaerobic and, later, aerobic organisms. Some geological evidence indicates that life may have arisen as early as 4.1 billion years ago. Since then, the combination of Earth's distance from the Sun, physical properties and geological history have allowed life to evolve and thrive.

1.3.1. Geological History

Earth's atmosphere and oceans were formed by volcanic activity and outgassing. Water vapor from these sources condensed into the oceans, augmented by water and ice from asteroids, protoplanets, and comets. In this model, atmospheric "greenhouse gases" kept the oceans from freezing when the newly forming Sun had only 70% of its current luminosity. By 3.5 Bya, Earth's magnetic field was established, which helped prevent the atmosphere from being stripped away by the solar wind.

A crust formed when the molten outer layer of Earth cooled to form a solid. The two models (Rogers et al, 2004) that explain land mass propose either a steady growth to the present-day forms or, more likely, a rapid growth early in Earth history followed by a long-term steady continental area. Continents formed by plate tectonics, a process ultimately driven by the continuous loss of heat from Earth's interior. Over the period of hundreds of millions of years, the

supercontinents have assembled and broken apart. Roughly 750 Mya[1], one of the earliest known supercontinents, Rodinia, began to break apart. The continents later recombined to form Pannotia 600-540 Mya, then finally Pangaea, which also broke apart 180 Mya (Murphy and Nance, 1965).

The present pattern of ice ages began about 40 Mya, and then intensified during the Pleistocene about 3 Mya. High-latitude regions have since undergone repeated cycles of glaciation and thaw, repeating about every 40,000–100,000 years. The last continental glaciation ended 10,000 years ago (Staff, 2007).

1.3.2. Shape

The shape of Earth is nearly spherical. There is a small flattening at the poles and bulging around the equator due to Earth's rotation (Milbert and Smith, 2007). To second order, the Earth is approximately an oblate spheroid, whose equatorial diameter is 43 kilometres (27 mi) larger than the pole-to-pole diameter, although the variation is less than 1% of the average radius of the Earth.

The point on the surface farthest from Earth's center of mass is the summit of the equatorial Chimborazo volcano in Ecuador (6,384.4 km) (Senne, 2000). The average diameter of the reference spheroid is 12,742 kilometres (7,918 mi). Local topography deviates from this idealized spheroid, although on a global scale these deviations are small compared to Earth's radius: The maximum deviation of only 0.17% is at the Mariana Trench (10,911 metres) below local sea level), whereas Mount Everest (8,848 meters (29,029 ft) above local sea level) represents a deviation of 0.14%.

1.3.3. Surface

The total surface area of Earth is about 510 million km^2 (197 million sq mi). Of this, 70.8%, or 361.13 million km^2 (139.43 million sq mi), is below sea level and covered by ocean water. Below the ocean's surface are much of the continental shelf,

1 - million years ago (Mya)

mountains, volcanoes (Sandwell and Smith 2006), oceanic trenches, submarine canyons, oceanic plateaus, abyssal plains, and a globe-spanning mid-ocean ridge system. The remaining 29.2%, or 148.94 million km^2 (57.51 million sq mi), not covered by water has terrain that varies greatly from place to place and consists of mountains, deserts, plains, plateaus, and other landforms. Tectonics and erosion, volcanic eruptions, flooding, weathering, glaciation, the growth of coral reefs, and meteorite impacts are among the processes that constantly reshape the Earth's surface over geological time (Martin, 2011).

The continental crust consists of lower density material such as the igneous rocks granite and andesite. Less common is basalt, a denser volcanic rock that is the primary constituent of the ocean floors. Sedimentary rock is formed from the accumulation of sediment that becomes buried and compacted together. Nearly 75% of the continental surfaces are covered by sedimentary rocks, although they form about 5% of the crust (Jessey, 2007). The third form of rock material found on Earth is metamorphic rock, which is created from the transformation of pre-existing rock types through high pressures, high temperatures, or both. The most abundant silicate minerals on Earth's surface include quartz, feldspars, amphibole, mica, pyroxene and olivine. Common carbonate minerals include calcite (found in limestone) and dolomite (Wenk and Bulakh, 2004).

The elevation of the land surface varies from the low point of −418 m (−1,371 ft) at the Dead Sea, to a maximum altitude of 8,848 m (29,029 ft) at the top of Mount Everest. The mean height of land above sea level is about 797 m.

The pedosphere is the outermost layer of Earth's continental surface and is composed of soil and subject to soil formation processes. The total arable land is 10.9% of the land surface, with 1.3% being permanent cropland. Close to 40% of Earth's land surface is used for agriculture, or an estimated 16.7 million km^2 (6.4 million sq mi) of cropland and 33.5 million km^2 (12.9 million sq mi) of pastureland (Hooke et al, 2012).

1.3.4. Hydrosphere

The abundance of water on Earth's surface is a unique feature that distinguishes the "Blue Planet" from other planets in the Solar System. Earth's hydrosphere consists chiefly of the oceans, but technically includes all water surfaces in the world, including inland seas, lakes, rivers, and underground waters down to a depth of 2,000 m (6,600 ft). The deepest underwater location is Challenger Deep of the Mariana Trench in the Pacific Ocean with a depth of 10,911.4 m.

The mass of the oceans is approximately 1.35×10^{18} metric tons or about 1/4400 of Earth's total mass. The oceans cover an area of 361.8 million km^2 (139.7 million sq mi) with a mean depth of 3,682 m (12,080 ft), resulting in an estimated volume of 1.332 billion km^3 (320 million cu mi). If all of Earth's crustal surface were at the same elevation as a smooth sphere, the depth of the resulting world ocean would be 2.7 to 2.8 km (1.68 to 1.74 mi). About 97.5% of the water is saline; the remaining 2.5% is fresh water. Most fresh water, about 68.7%, is present as ice in ice caps and glaciers. The average salinity of Earth's oceans is about 35 grams of salt per kilogram of sea water (3.5% salt) (Kennish, 2001). Most of this salt was released from volcanic activity or extracted from cool igneous rocks. The oceans are also a reservoir of dissolved atmospheric gases, which are essential for the survival of many aquatic life forms. Sea water has an important influence on the world's climate, with the oceans acting as a large heat reservoir (Scott, 2006). Shifts in the oceanic temperature distribution can cause significant weather shifts, such as the El Niño–Southern Oscillation.

1.4. Mars

The fourth planet from the Sun, Mars is a dusty, cold, desert world with a very thin atmosphere. This dynamic planet has seasons, polar ice caps and weather and canyons and extinct volcanoes, evidence of an even more active past. Mars is one of the most explored bodies in our solar system, and it's the only planet where we've sent rovers to roam the alien landscape. NASA currently has three spacecraft in

orbit, one rover and one lander on the surface and another rover under construction here on Earth. India and ESA also have spacecraft in orbit above Mars. These robotic explorers have found lots of evidence that Mars was much wetter and warmer, with a thicker atmosphere, billions of years ago.

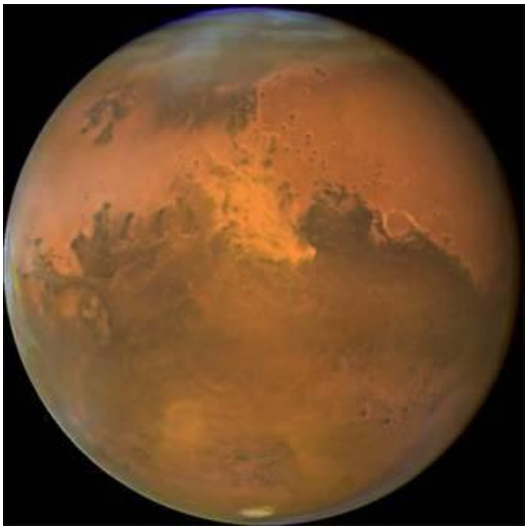

Figure 1.4 Mars is the fourth planet from the sun and the next planet beyond Earth.

The days and seasons are likewise comparable to those of Earth, because the rotational period as well as the tilt of the rotational axis relative to the ecliptic plane is very similar. Mars is the site of Olympus Mons, the largest volcano and highest known mountain in the Solar System, and of Valles Marineris, one of the largest canyons in the Solar System. The smooth Borealis basin in the northern hemisphere covers 40% of the planet and may be a giant impact feature (Yeager, A., 2008). Mars has two moons, Phobos and Deimos, which are small and irregularly shaped. These may be captured asteroids, similar to 5261 Eureka, a Mars trojan.

There are ongoing investigations assessing the past habitability potential of Mars, as well as the possibility of extant life. Future

astrobiology missions are planned, including the Mars 2020 and Rosalind Franklin rovers. Liquid water cannot exist on the surface of Mars due to low atmospheric pressure, which is less than 1% of the Earth's, except at the lowest elevations for short periods. The two polar ice caps appear to be made largely of water (Byrne and Ingersoll, 2003). The volume of water ice in the south polar ice cap, if melted, would be sufficient to cover the entire planetary surface to a depth of 11 meters (36 ft). In November 2016, NASA reported finding a large amount of underground ice in the Utopia Planitia region of Mars. The volume of water detected has been estimated to be equivalent to the volume of water in Lake Superior (NASA, 2016).

1.4.1. Physical Characteristics

Mars is approximately half the diameter of Earth, with a surface area only slightly less than the total area of Earth's dryland. Mars is less dense than Earth, having about 15% of Earth's volume and 11% of Earth's mass, resulting in about 38% of Earth's surface gravity. The red-orange appearance of the Martian surface is caused by iron (III) oxide, or rust. It can look like butterscotch; other common surface colors include golden, brown, tan, and greenish, depending on the minerals present (Peplow, 2004).

1.4.2. Surface Geology

Mars is a terrestrial planet that consists of minerals containing silicon and oxygen, metals, and other elements that typically make up rock. The surface of Mars is primarily composed of tholeiitic basalt, although parts are more silica-rich than typical basalt and may be similar to andesitic rocks on Earth or silica glass. Regions of low albedo suggest concentrations of plagioclase feldspar, with northern low albedo regions displaying higher than normal concentrations of sheet silicates and high-silicon glass. Parts of the southern highlands include detectable amounts of high-calcium pyroxenes. Localized concentrations of hematite and olivine have been found. Much of the surface is deeply covered by finely grained iron (III) oxide dust (Christensen et al, 2003).

Although Mars has no evidence of a structured global magnetic field, observations show that parts of the planet's crust have been magnetized, suggesting that alternating polarity reversals of its dipole field have occurred in the past. This paleomagnetism of magnetically susceptible minerals is similar to the alternating bands found on Earth's ocean floors. One theory, published in 1999 and re-examined in October 2005, is that these bands suggest plate tectonic activity on Mars four billion years ago, before the planetary dynamo ceased to function and the planet's magnetic field faded (Neal-Jones and O'Carroll, 2011).

It is thought that, during the Solar System's formation, Mars was created as the result of a stochastic process of run-away accretion of material from the protoplanetary disk that orbited the Sun. Mars has many distinctive chemical features caused by its position in the Solar System. Elements with comparatively low boiling points, such as chlorine, phosphorus, and Sulphur, are much more common on Mars than Earth; these elements were probably pushed outward by the young Sun's energetic solar wind (Halliday et al, 2001).

1.4.3. Soil

The Phoenix lander returned data showing Martian soil to be slightly alkaline and containing elements such as magnesium, sodium, potassium and chlorine. These nutrients are found in soils on Earth, and they are necessary for growth of planets. Experiments performed by the lander showed that the Martian soil has a basic pH of 7.7, and contains 0.6% of the salt perchlorate. This is a very high concentration and makes the Martian soil toxic (see also Martian soil toxicity) (Sample, 2017).

Streaks are common across Mars and new ones appear frequently on steep slopes of craters, troughs, and valleys. The streaks are dark at first and get lighter with age. The streaks can start in a tiny area, and then spread out for hundreds of meters. They have been seen to follow the edges of boulders and other obstacles in their path. The commonly accepted theories include that they are dark underlying layers of soil

revealed after avalanches of bright dust or dust devils. Several other explanations have been put forward, including those that involve water or even the growth of organisms (Gánti et al, 2003).

Figure 1.5 NASA's Mars Exploration Rover Spirit has found a patch of bright-toned soil so rich in silica that scientists propose water must have been involved in concentrating it (May 2007).

1.4.4. Mars Topography

The dichotomy of Martian topography is striking: northern plains flattened by lava flows contrast with the southern highlands, pitted and cratered by ancient impacts. Research in 2008 has presented evidence regarding a theory proposed in 1980 postulating that, four billion years ago, the northern hemisphere of Mars was struck by an object one-tenth to two-thirds the size of Earth's Moon. If validated, this would make the northern hemisphere of Mars the site of an impact crater 10,600 by 8,500 km (6,600 by 5,300 mi) in size, or roughly the area of Europe, Asia, and Australia combined, surpassing the South Pole–Aitken basin as the largest impact crater in the Solar System (Yeager, 2008).

Figure 1.6 Bonneville crater and Spirit rover's lander (NASA's Mars Exploration Rover Spirit drove off in 2004)

Mars is scarred by a number of impact craters: a total of 43,000 craters with a diameter of 5 km (3.1 mi) or greater have been found. The largest confirmed of these is the Hellas impact basin, a light albedo feature clearly visible from Earth. Due to the smaller mass of Mars, the probability of an object colliding with the planet is about half that of Earth.

1.4.5. Moons of Mars

Mars has two relatively small (compared to Earth's) natural moons, Phobos (about 22 km (14 mi) in diameter) and Deimos (about 12 km (7.5 mi) in diameter), which orbit close to the planet. Asteroid capture is a long-favored theory, but their origin remains uncertain. Both satellites were discovered in 1877 by Asaph Hall; they are named after the characters Phobos (panic/fear) and Deimos (terror/dread), who, in Greek mythology, accompanied their father Ares, god of war, into battle. Mars was the Roman counterpart of Ares (Hunt et al, 1978). In modern Greek, the planet retains its ancient name *Ares* (Aris: *Άρης*).

Figure 1.6 Image of Phobos (left side), showing a series of mostly parallel grooves and crater chains, with Stickney crater at right. Image of Deimos (right side), showing its smooth blanket of regolith (NASA's Mars Reconnaissance Orbiter).

Mars is located closer to the asteroid belt, so it has an increased chance of being struck by materials from that source. Mars is more likely to be struck by short-period comets, i.e., those that lie within the orbit of Jupiter (Wetherill, 1999). In spite of this, there are far fewer craters on Mars compared with the Moon, because the atmosphere of Mars provides protection against small meteors and surface modifying processes have erased some craters.

1.5. Jupiter, Our Solar System's Largest Planet

Jupiter has a long history surprising scientists—all the way back to 1610 when Galileo Galilei found the first moons beyond Earth. That discovery changed the way we see the universe. Fifth in line from the Sun, Jupiter is, by far, the largest planet in the solar system – more than twice as massive as all the other planets combined.

Jupiter's familiar stripes and swirls are actually cold, windy clouds of ammonia and water, floating in an atmosphere of hydrogen and helium. Jupiter’s iconic Great Red Spot is a giant storm bigger than Earth that has raged for hundreds of years.

Figure 1.7 This new Hubble Space Telescope view of Jupiter, taken on June 27, 2019, reveals the giant planet's trademark Great Red Spot, and a more intense color palette in the clouds swirling in Jupiter's turbulent atmosphere than seen in previous years. Hubble's Wide Field Camera 3 observed Jupiter when the planet was 400 million miles (640 million kilometers) from Earth, when Jupiter was near "opposition," or almost directly opposite the sun in the sky. (Image: NASA, ESA, A. Simon (Goddard Space Flight Center) and M.H. Wong (University of California, Berkeley).

The largest planet in the solar system, the gas giant Jupiter is approximately 318 times as massive as Earth. If the mass of all of the other planets in the solar system were combined into one "super planet," Jupiter would still be two and a half times as large.

Jupiter has a mean radius of 43,440.7 miles (69,911 kilometers), about a tenth that of the sun. However, its rapid rotation — it spins once every 9.8 hours — causes it to bulge at the equator, where the diameter is 88,846 miles (142,984 km). In contrast, the diameter at the poles is only 83,082 miles (133,708 km). This stretched shape is known as an oblate spheroid.

If you were to walk around the equator of Jupiter, you would travel 272,946 miles (439,264 km), over 10 times the distance around Earth's center line (Saumon and Guillot, 2004).

Because Jupiter is made of gas, mostly, its surface is considered uniform. As such, it lacks high and low points — mountains and valleys — such as those found on rocky terrestrial planets. These gases pile on top of one another, forming layers that extend downward. Because there is no solid ground, the surface of Jupiter is defined as the point where the atmospheric pressure is equal to that of Earth. At this point, the pull of gravity is almost two and a half times stronger than it is on our planet.

Trying to stand on that surface would be impossible, since it is simply another layer of gases. Spacecraft and astronauts would only sink into the mire. A probe or spacecraft traveling farther toward the center of the planet would continue to find only thick clouds until it reached the core.

1.5.1. Jupiter's Core

Details about Jupiter's core remain a challenge to find. Scientists think that the dense central core may be surrounded by a layer of metallic hydrogen, with another layer of molecular hydrogen on top. Scientists aren't certain of just how solid Jupiter's core might be. While some theorize that the core is a hot molten ball of liquid, other research indicates that it could be a solid rock 14 to 18 times the mass of the Earth. The temperature at the core is estimated to be about 35,000 degrees Celsius (63,000 degrees Fahrenheit).

Discussions about Jupiter's core didn't even begin until the late 1990s, when gravitational measurements revealed that the center of the gas giant was anywhere from 12 to 45 times the mass of Earth. And just because it had a core in the past doesn't mean that it still will today – new evidence suggests that the gas giant's core may be melting.

Jupiter is not quite a planet**.** Like the sun, Jupiter is composed predominantly of hydrogen and helium. But unlike the sun, it lacks the necessary amount to begin fusion, the process that fuels a star. Jupiter would need to be 75 to 80 times more massive than it is at present to be considered a star. If all of the planets in the solar system had

formed as part of the gas giant, it still would not have sufficient mass. Still, by itself, Jupiter is two and a half times larger than all of the other planets in the solar system combined.

1.5.2. Density, Mass and Volume

Known as a gas giant, Jupiter is composed primarily of hydrogen and helium. It weighs in at 1.9×10^{27} kilograms. Although it is significantly more massive than Earth, it is only a fifth as dense, at 1,326 kg/m^3, because it is made of gas rather than rock.

The volume of Jupiter is 1,431,281,810,739,360 cubic kilometers, 1,321 times that of Earth.

The surface area of this enormous planet is 23,713,907,537 square miles, or 6.1419×10^{10} square kilometers, 120 times that of our planet.

Jupiter's structure resembles that of the sun, but would need to be 75 times its present mass to undergo the fusion of hydrogen that fuels a star. The mass of the largest gas giant planets found outside of the solar system is often given in terms of the enormous planet.

1.5.3. Physical Characteristics

Jupiter is more than twice as massive as all the other planets combined. If the enormous planet was about 80 times more massive, it would have actually become a star instead of a planet. Jupiter's immense volume could hold more than 1,300 Earths. That means that if Jupiter were the size of a basketball, Earth would be the size of a grape. Jupiter has a dense core of uncertain composition, surrounded by a helium-rich layer of fluid metallic hydrogen that extends out to 80% to 90% of the diameter of the planet.

Jupiter's atmosphere resembles that of the sun, made up mostly of hydrogen and helium. The colorful light and dark bands that surround Jupiter are created by strong east-west winds in the planet's upper atmosphere traveling more than 335 mph (539 km/h). The white clouds in the light zones are made of crystals of frozen ammonia, while darker clouds made of other chemicals are found in the dark belts. At the deepest visible levels are blue clouds. Far from being static, the stripes of clouds change over time. Inside the atmosphere,

diamond rain may fill the skies.

The most extraordinary feature on Jupiter is the Great Red Spot, a giant hurricane-like storm that's lasted more than 300 years. At its widest, the Great Red Spot is about twice the size of Earth, and its edge spins counterclockwise around its center at speeds of about 270 to 425 mph (430 to 680 km/h). The color of the storm, which usually varies from brick red to slightly brown, may come from small amounts of sulfur and phosphorus in the ammonia crystals in Jupiter's clouds. The spot has been shrinking for quite some time, although the rate may be slowing in recent years.

Jupiter's gargantuan magnetic field is the strongest of all the planets in the solar system at nearly 20,000 times the strength of Earth's. It traps electrically charged particles in an intense belt of electrons and other electrically charged particles that regularly blasts the planet's moons and rings with radiation more than 1,000 times the lethal level for a human, enough to damage even heavily shielded spacecraft, such as NASA's Galileo probe. The magnetosphere of Jupiter swells out some 600,000 to 2 million miles (1 million to 3 million kilometers) toward the sun and tapers to a tail extending more than 600 million miles (1 billion km) behind the massive planet.

Jupiter also spins faster than any other planet, taking a little under 10 hours to complete a turn on its axis, compared with 24 hours for Earth. This rapid spin makes Jupiter bulge at the equator and flatten at the poles.

Jupiter broadcasts radio waves strong enough to detect on Earth. These come in two forms — strong bursts that occur when Io, the closest of Jupiter's large moons, passes through certain regions of Jupiter's magnetic field, and continuous radiation from Jupiter's surface and high-energy particles in its radiation belts.

1.5.4. Jupiter's Moons

With four large moons and many smaller moons in orbit around it, Jupiter by itself forms a kind of miniature solar system. Jupiter has 79 known moons, which are mostly named after the paramours of Roman

gods. The four largest moons of Jupiter, called Io, Europa, Ganymede and Callisto, were discovered by Galileo Galilei.

Ganymede is the largest moon in our solar system, and is larger than Mercury and Pluto. It is also the only moon known to have its own magnetic field. The moon has at least one ocean between layers of ice, although it may contain several layers of both ice and water, stacked on top of one another. Ganymede will be the main target of the European Jupiter Icy Moons Explorer (JUICE) spacecraft that's scheduled to launch in 2022 and arrive at Jupiter's system in 2030.

Io is the most volcanically active body in our solar system. The sulfur its volcanoes spew gives Io a blotted yellow-orange appearance that looks kind of like a pepperoni pizza. As Io orbits Jupiter, the planet's immense gravity causes "tides" in Io's solid surface that rise 300 feet (100 meters) high and generate enough heat for volcanic activity.

The frozen crust of Europa is made up mostly of water ice, and it may hide a liquid ocean that contains twice as much water as Earth does. Some of this liquid spouts from the surface in newly spotted sporadic plumes at Europa's southern pole. It would perform 40 to 45 flybys to examine the habitability of the moon. Callisto has the lowest reflectivity, or albedo, of the four Galilean moons. This suggests that its surface may be composed of dark, colorless rock.

1.6. Saturn

Saturn is the sixth planet from the Sun and the second largest planet in our solar system. Adorned with thousands of beautiful ringlets, Saturn is unique among the planets. It is not the only planet to have rings—made of chunks of ice and rock—but none are as spectacular or as complicated as Saturn's. Like fellow gas giant Jupiter, Saturn is a massive ball made mostly of hydrogen and helium.

This planet is surrounded by more than 60 known moons; Saturn is home to some of the most fascinating landscapes in our solar system. From the jets of water that spray from Enceladus to the methane lakes on smoggy Titan, the Saturn system is a rich source of scientific

discovery and still holds many mysteries.

The farthest planet from Earth discovered by the unaided human eye, Saturn has been known since ancient times. The planet is named for the Roman god of agriculture and wealth, who was also the father of Jupiter. With a radius of 36,183.7 miles (58,232 kilometers), Saturn is 9 times wider than Earth. If Earth were the size of a nickel, Saturn would be about as big as a volleyball ball.

From an average distance of 886 million miles (1.4 billion kilometers), Saturn is 9.5 astronomical units away from the Sun. One astronomical unit (abbreviated as AU), is the distance from the Sun to Earth. From this distance, it takes sunlight 80 minutes to travel from the Sun to Saturn.

1.6.1. Orbit and Rotation

Saturn has the second-shortest day in the solar system. One day on Saturn takes only 10.7 hours (the time it takes for Saturn to rotate or spin around once), and Saturn makes a complete orbit around the Sun (a year in Saturnian time) in about 29.4 Earth years (10,756 Earth days). Its axis is tilted by 26.73 degrees with respect to its orbit around the Sun, which is similar to Earth's 23.5^{o} tilt. This means that, like Earth, Saturn experiences seasons.

1.6.2. Formation

Saturn took shape when the rest of the solar system formed about 4.5 billion years ago, when gravity pulled swirling gas and dust in to become this gas giant. About 4 billion years ago, Saturn settled into its current position in the outer solar system, where it is the sixth planet from the Sun. Like Jupiter, Saturn is mostly made of hydrogen and helium, the same two main components that make up the Sun.

1.6.3. Structure

Like Jupiter, Saturn is made mostly of hydrogen and helium. At Saturn's center is a dense core of metals like iron and nickel surrounded by rocky material and other compounds solidified by the intense pressure and heat. It is enveloped by liquid metallic hydrogen

inside a layer of liquid hydrogen—similar to Jupiter's core but considerably smaller. It's hard to imagine, but Saturn is the only planet in our solar system whose average density is less than water. The giant gas planet could float in a bathtub if such a colossal thing existed.

1.6.4. Surface

As a gas giant, Saturn doesn't have a true surface. The planet is mostly swirling gases and liquids deeper down. While a spacecraft would have nowhere to land on Saturn, it wouldn't be able to fly through unscathed either. The extreme pressures and temperatures deep inside the planet crush melt and vaporize spacecraft trying to fly into the planet.

1.6.5. Atmosphere

Saturn is blanketed with clouds that appear as faint stripes, jet streams and storms. The planet is many different shades of yellow, brown and grey. Winds in the upper atmosphere reach 1,600 feet per second (500 meters per second) in the equatorial region. In contrast, the strongest hurricane-force winds on Earth top out at about 360 feet per second (110 meters per second). And the pressure—the same kind you feel when you dive deep underwater—is so powerful it squeezes gas into liquid.

Saturn's North Pole has an interesting atmospheric feature—a six-sided jet stream. This hexagon-shaped pattern was first noticed in images from the Voyager I spacecraft and has been more closely observed by the Cassini spacecraft since. Spanning about 20,000 miles (30,000 kilometers) across, the hexagon is a wavy jet stream of 200-mile-per-hour winds (about 322 kilometers per hour) with a massive, rotating storm at the center. There is no weather feature like it anywhere else in the solar system.

1.6.6. Potential for Life

Saturn's environment is not conducive to life as we know it. The temperatures, pressures and materials that characterize this planet are most likely too extreme and volatile for organisms to adapt to. While

planet Saturn is an unlikely place for living things to take hold, the same is not true of some of its many moons. Satellites like Enceladus and Titan, home to internal oceans, could possibly support life.

1.6.7. Saturn's Moons

Saturn is home to a vast array of intriguing and unique worlds. From the haze-shrouded surface of Titan to crater-riddled Phoebe, each of Saturn's moons tells another piece of the story surrounding the Saturn system. Currently Saturn has 53 confirmed moons with 29 additional provisional moons awaiting confirmation.

The moons of Saturn are numerous and diverse, ranging from tiny moonlets that are only tens of meters across to enormous Titan, which is larger than the planet Mercury. Saturn has 82 moons with confirmed orbits that are not embedded in its rings, 53 of which have names but only 13 of which have diameters larger than 50 kilometers, as well as dense rings which contain millions of embedded moonlets and innumerable smaller ring particles of their own. Seven Saturnian moons are large enough to be ellipsoidal in shape, yet only one or two of those, Titan and possibly Rhea, are currently in hydrostatic equilibrium. Particularly notable among Saturn's moons are Titan, the second-largest moon in the Solar System (after Jupiter's Ganymede), with a nitrogen-rich Earth-like atmosphere and a landscape featuring dry river networks and hydrocarbon lakes found nowhere else in the solar system, and Eneladus, due to its chemical composition being similar to that of comets. In particular, Enceladus emits jets of gas and dust, which could indicate the presence of liquid water under its south pole region, and may have a global ocean below its surface.

Twenty-four of Saturn's moons are *regular satellites*; they have prograde orbits not greatly inclined to Saturn's equatorial plane. They include the seven major satellites, four small moons that exist in a Trojan orbit with larger moons, two mutually co-orbital moons and two moons that act as shepherds of Saturn's F ring. Two other known regular satellites orbit within gaps in Saturn's rings. The relatively large Hyperion is locked in a resonance with Titan. The remaining

regular moons orbit near the outer edge of the A ring, within G ring and between the major moons Mimas and Enceladus. The regular satellites are traditionally named after Titans and Titanesses or other figures associated with the mythological Saturn.

The remaining 58, with mean diameters ranging from 4 to 213 km, are *irregular satellites*, whose orbits are much farther from Saturn, have high inclinations, and are mixed between prograde and retrograde. These moons are probably captured minor planets, or debris from the breakup of such bodies after they were captured, creating collisional families. The irregular satellites have been classified by their orbital characteristics into the Inuit, Norse, and Gallic groups, and their names are chosen from the corresponding mythologies. The largest of the irregular moons is Phoebe, the ninth moon of Saturn, discovered at the end of the 19th century.

The rings of Saturn are made up of objects ranging in size from microscopic to moonlets hundreds of meters across, each in its own orbit around Saturn. Thus a precise number of Saturnian moons cannot be given, because there is no objective boundary between the countless small anonymous objects that form Saturn's ring system and the larger objects that have been named as moons. Over 150 moonlets embedded in the rings have been detected by the disturbance they create in the surrounding ring material, though this is thought to be only a small sample of the total population of such objects (Tiscareno et al, 2008).

There are still 29 moons yet to be named (as of October 2019), using names from Gallic, Norse and Inuit mythology based on the orbital groups of the moons. Twenty of these moons are in line to receive permanent designations, with seventeen Norse, two Inuit, and one Gallic name expected.

Figure 1.8 Saturn, its rings and major icy moons (from Mimas to Rhea)

1.6.7.1. Rings

Saturn's rings are thought to be pieces of comets, asteroids or shattered moons that broke up before they reached the planet, torn apart by Saturn's powerful gravity. They are made of billions of small chunks of ice and rock coated with another material such as dust. The ring particles mostly range from tiny, dust-sized icy grains to chunks as big as a house. A few particles are as large as mountains. The rings would look mostly white if you looked at them from the cloud tops of Saturn, and interestingly, each ring orbits at a different speed around the planet.

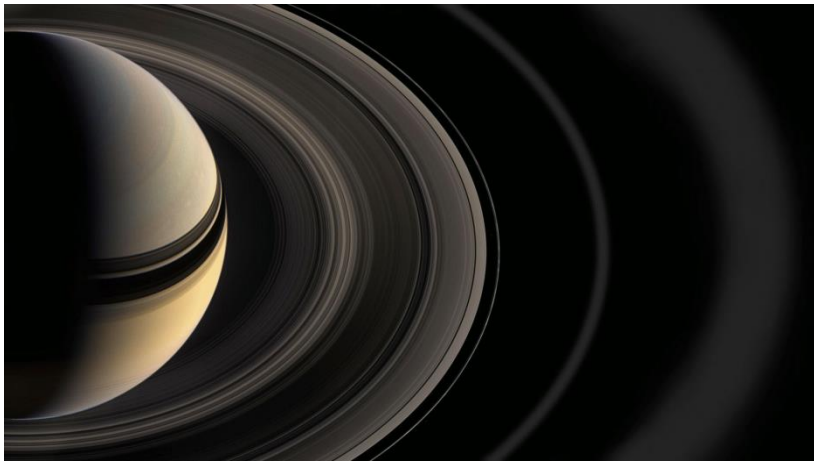

Figure 1.9 This Cassini image from 2012 shows Titan and its host planet Saturn. Image Credit: NASA/JPL-Caltech/SSI.

Saturn's ring system extends up to 175,000 miles (282,000 kilometers) from the planet, yet the vertical height is typically about 30 feet (10 meters) in the main rings. Named alphabetically in the order they were discovered, the rings are relatively close to each other, with the exception of a gap measuring 2,920 miles (4,700 kilometers) wide called the Cassini Division that separates Rings A and B. The main rings are A, B and C. Rings D, E, F and G are fainter and more recently discovered (Eposito, 2002).

Starting at Saturn and moving outward, there is the D ring, C ring, B ring, Cassini Division, A ring, F ring, G ring, and finally, the E ring. Much farther out, there is the very faint Phoebe ring in the orbit of Saturn's moon Phoebe.

1.6.7.2. Magnetosphere

Saturn's magnetic field is smaller than Jupiter's but still 578 times as powerful as Earth's. Saturn, the rings, and many of the satellites lie totally within Saturn's enormous magnetosphere, the region of space in which the behavior of electrically charged particles is influenced more by Saturn's magnetic field than by the solar wind.

Aurorae occur when charged particles spiral into a planet's atmosphere along magnetic field lines. On Earth, these charged particles come from the solar wind. Cassini showed that at least some of Saturn's aurorae are like Jupiter's and are largely unaffected by the solar wind. Instead, these aurorae are caused by a combination of particles ejected from Saturn's moons and Saturn's magnetic field's rapid rotation rate. But these "non-solar-originating" aurorae are not completely understood yet.

1.6.7.3. Titan

Titan is the largest Saturn's moon. Titan is an icy world whose surface is completely obscured by a golden hazy atmosphere. Titan is the second largest moon in our solar system. Only Jupiter's moon Ganymede is larger, by just 2 percent. Titan is bigger than Earth's moon, and larger than even the planet Mercury.

This mammoth moon is the only moon in the solar system with a

dense atmosphere, and it's the only world besides Earth that has standing bodies of liquid, including rivers, lakes and seas, on its surface. Like Earth, Titan's atmosphere is primarily nitrogen, plus a small amount of methane. It is the sole other place in the solar system known to have an earthlike cycle of liquids raining from clouds, flowing across its surface, filling lakes and seas, and evaporating back into the sky [akin to (similar) Earth's water cycle]. Titan is also thought to have a subsurface ocean of water.

Titan takes 15 days and 22 hours to complete a full orbit of Saturn. Titan is also tidally locked in synchronous rotation with Saturn, meaning that, like Earth's Moon, Titan always shows the same face to the planet as it orbits. Saturn takes about 29 Earth years to orbit the Sun (a Saturnian year), and Saturn's axis of rotation is tilted like Earth's, resulting in seasons. But Saturn's longer year produces seasons that each last more than seven Earth years. Since Titan orbits roughly along Saturn's equatorial plane, and Titan's tilt relative to the sun is about the same as Saturn's, Titan's seasons are on the same schedule as Saturn's—seasons that last more than seven Earth years, and a year that lasts 29 Earth years.

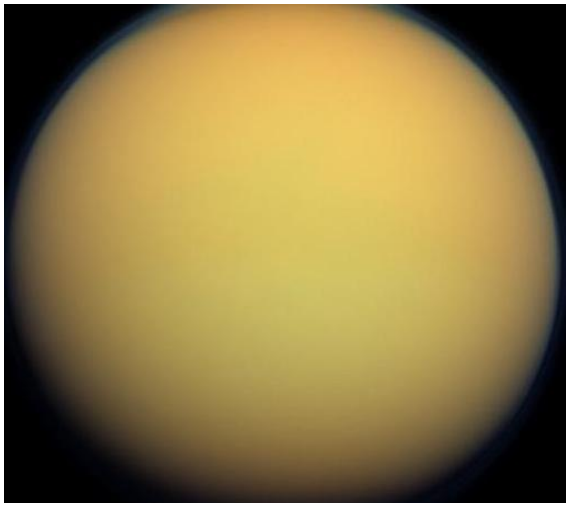

Figure 1.10 Titan in natural color, the thick atmosphere is orange due to a dense organo-nitrogen haze.

Scientists aren't certain about Titan's origin. However, its atmosphere provides a clue. Several instruments on the NASA and ESA Cassini-Huygens mission measured the isotopes nitrogen-14 and nitrogen-15 in Titan's atmosphere. The instruments found Titan's nitrogen isotope ratio most resembles that found in comets from the Oort Cloud—a sphere of hundreds of billions of icy bodies thought to orbit the Sun at a distance between 5,000 and 100,000 astronomical units from the Sun (Earth is about one astronomical unit from the Sun—roughly 93 million miles or 150 million kilometers). Titan's atmospheric nitrogen ratio suggests the moon's building blocks formed early in the solar system's history, in the same cold disk of gas and dust that formed the Sun (called the protosolar nebula), rather than forming in the warmer disk of material that Saturn later formed from (called the Saturn sub-nebula).

Titan's internal structure isn't entirely known, but one model based on data from the Cassini-Huygens mission suggests Titan has five primary layers. The innermost layer is a core of rock (specifically, water-bearing silicate rock) about 2,500 miles (4,000 kilometers) in diameter. Surrounding the core is a shell of water ice—a special type called ice-VI that is only found at extremely high-pressures. The high-pressure ice is surrounded by a layer of salty liquid water, on top of which sits an outer crust of water ice. This surface is coated with organic molecules that have rained or otherwise settled out of the atmosphere in the form of sands and liquids. The surface is hugged by a dense atmosphere.

The surface of Titan is one of the most Earthlike places in the solar system, albeit at vastly colder temperatures and with different chemistry. Here it is so cold (-290° F or -179° C) that water ice plays the role of rock. Titan may have volcanic activity as well, but with liquid water "lava" instead of molten rock. Titan's surface is sculpted by flowing methane and ethane, which carves river channels and fills great lakes with liquid natural gas. No other world in the solar system, aside from Earth, has that kind of liquid activity on its surface.

Vast regions of dark dunes stretch across Titan's landscape,

primarily around the equatorial regions. The "sand" in these dunes is composed of dark hydrocarbon grains thought to look something like coffee grounds. In appearance, the tall, linear dunes are not unlike those seen in the desert of Namibia in Africa. Titan has few visible impact craters, meaning its surface must be relatively young and some combination of processes erases evidence of impacts over time. Earth is similar in that respect as well; craters on our planet are erased by the relentless forces of flowing liquid (water, in Earth's case), wind, and the recycling of the crust via plate tectonics. These forces are present on Titan as well, in modified forms. In particular, tectonic forces—the movement of the ground due to pressures from beneath—appear to be at work on the icy moon, although scientists do not see evidence of plates like on Earth.

Our solar system is home to more than 150 moons, but Titan is unique in being the only moon with a thick atmosphere. At the surface of Titan, the atmospheric pressure is about 60 percent greater than on Earth—roughly the same pressure a person would feel swimming about 50 feet (15 meters) below the surface in the ocean on Earth. Because Titan is less massive than Earth, its gravity doesn't hold onto its gaseous envelope as tightly, so the atmosphere extends to an altitude 10 times higher than Earth's—nearly 370 miles (600 kilometers) into space.

Titan's atmosphere is mostly nitrogen (about 95 percent) and methane (about 5 percent), with small amounts of other carbon-rich compounds. High in Titan’s atmosphere, methane and nitrogen molecules are split apart by the Sun's ultraviolet light and by high-energy particles accelerated in Saturn's magnetic field. The pieces of these molecules recombine to form a variety of organic chemicals (substances that contain carbon and hydrogen), and often include nitrogen, oxygen and other elements important to life on Earth.

Some of the compounds produced by that splitting and recycling of methane and nitrogen create a kind of smog—a thick, orange-colored haze that makes the moon's surface difficult to view from space. (Spacecraft and telescopes can, however, see through the haze at

certain wavelengths of light outside of those visible to human eyes.) Some of the heavy, carbon-rich compounds settle to the moon's surface—these hydrocarbons play the role of "sand" in Titan's vast dune fields. And methane condenses into clouds that occasionally drench the surface in methane storms.

The methane in Titan's atmosphere is what makes its complex atmospheric chemistry possible, but where all that methane comes from is a mystery. Because sunlight continuously breaks down methane in Titan's atmosphere, some source must be replenishing it or it would be depleted over time. Researchers suspect methane could be belched into Titan's atmosphere by cryovolcanism—volcanoes releasing chilled water instead of molten rock lava—but they're not certain if this or some other process is responsible.

The Cassini spacecraft's numerous gravity measurements of Titan revealed that the moon is hiding an underground ocean of liquid water (likely mixed with salts and ammonia). The European Space Agency's Huygens probe also measured radio signals during its descent to the surface, in 2005, which strongly suggested the presence of an ocean 35 to 50 miles (55 to 80 kilometers) below the icy ground. The discovery of a global ocean of liquid water adds Titan to the handful of worlds in our solar system that could potentially contain habitable environments. Additionally, Titan's rivers, lakes and seas of liquid methane and ethane might serve as a habitable environment on the moon's surface, though any life there would likely be very different from Earth's life. Thus, Titan could potentially harbor environments with conditions suitable for life—meaning both lives as we know it (in the subsurface ocean) and life as we don't know it (in the hydrocarbon liquid on the surface). Although there is so far no evidence of life on Titan, its complex chemistry and unique environments are certain to make it a destination for continued exploration.

1.7. Uranus

The composition of Uranus' clouds had long been a mystery. In April 2017, a global research team found hydrogen sulfide, the odiferous

gas that most people avoid, in Uranus' cloud tops—a striking difference from the gas giant planets located closer to the Sun.

The first planet found with the aid of a telescope, Uranus was discovered in 1781 by astronomer William Herschel, although he originally thought it was either a comet or a star. It was two years later that the object was universally accepted as a new planet, in part because of observations by astronomer Johann Elert Bode. Herschel tried unsuccessfully to name his discovery Georgium Sidus after King George III. Instead the planet was named for Uranus, the Greek god of the sky, as suggested by Johann Bode.

Figure 1.11 This is an image of the planet Uranus taken by the spacecraft Voyager 2 in 1986. The Voyager project is managed for NASA by the Jet Propulsion Laboratory. Credit: NASA/JPL-Caltech

1.7.1. Orbit and Rotation

Uranus orbits the Sun once every 84 years, taking an average of seven years to pass through each constellation of the zodiac. In 2033, the planet will have made its third complete orbit around the Sun since

being discovered in 1781. The planet has returned to the point of its discovery northeast of Zeta Tauri twice since then, in 1862 and 1943, one day later each time as the procession of the equinoxes has shifted it 1° west every 72 years. Uranus will return to this location again in 2030-31. Its average distance from the Sun is roughly 20 AU (3 billion km; 2 billion miles). The difference between its minimum and maximum distance from the Sun is 1.8 AU, larger than that of any other planet, though not as large as that of dwarf planet Pluto (Richmond and Willmann-Bell, 1998). The intensity of sunlight varies inversely with the square of distance, and so on Uranus (at about 20 times the distance from the Sun compared to Earth) it is about 1/400 the intensity of light on Earth (Fred E., 1994). Its orbital elements were first calculated in 1783 by Pirre-Simon Lapace. With time, discrepancies began to appear between the predicted and observed orbits, and in 1841, John Couch Adams first proposed that the differences might be due to the gravitational tug of an unseen planet.

The rotational period of the interior of Uranus is 17 hours, 14 minutes. As on all the giant planets, its upper atmosphere experiences strong winds in the direction of rotation. At some latitudes, such as about 60 degrees south, visible features of the atmosphere move much faster, making a full rotation in as little as 14 hours (Gierasch, and Nicholson 2004).

1.7.2. Axial Tilt

The Uranian axis of rotation is approximately parallel with the plane of the Solar System, with an axial tilt of 97.77° (as defined by prograde rotation). This gives it seasonal changes completely unlike those of the other planets. Near the solstice, one pole faces the Sun continuously and the other faces away. Only a narrow strip around the equator experiences a rapid day–night cycle, but with the Sun low over the horizon. At the other side of Uranus' orbit the orientation of the poles towards the Sun is reversed. Each pole gets around 42 years of continuous sunlight, followed by 42 years of darkness (Sromovsky and Lawrence, 2006). Near the time of the equinoxes, the Sun faces

the equator of Uranus giving a period of day–night cycles similar to those seen on most of the other planets. Uranus reached its most recent equinox on 7 December 2007.

One result of this axis orientation is that, averaged over the Uranian year, the polar regions of Uranus receive a greater energy input from the Sun than its equatorial regions. Nevertheless, Uranus is hotter at its equator than at its poles. The underlying mechanism that causes this is unknown. The reason for Uranus' unusual axial tilt is also not known with certainty, but the usual speculation is that during the formation of the Solar System, an Earth-sized protoplanet collided with Uranus, causing the skewed orientation (Matthews, 1991). Research by Jacob Kegerreis of Durham University suggests that the tilt resulted from a rock larger than the Earth crashing into the planet 3 to 4 billion years ago. Uranus' south pole was pointed almost directly at the Sun at the time of Voyager 2's flyby in 1986. The labelling of this pole as "south" uses the definition currently endorsed by the International Astronomical Union, namely that the north pole of a planet or satellite is the pole that points above the invariable plane of the Solar System, regardless of the direction the planet is spinning (Seidelmann et al, 2000). A different convention is sometimes used, in which a body's north and south poles are defined according to the right-hand ruler in relation to the direction of rotation (NASA, 2004).

1.7.3. Visibility

The mean apparent magnitude of Uranus is 5.68 with a standard deviation of 0.17, while the extremes are 5.38 and +6.03. This range of brightness is near the limit of naked-aye visibility. Much of the variability is dependent upon the planetary latitudes being illuminated from the Sun and viewed from the Earth (Nowak, 2006). Its angular diameter is between 3.4 and 3.7 arcseconds, compared with 16 to 20 arcseconds for Saturn and 32 to 45 arcseconds for Jupiter. At opposition, Uranus is visible to the naked eye in dark skies, and becomes an easy target even in urban conditions with binoculars. In larger amateur telescopes with an objective diameter of between 15

and 23 cm, Uranus appears as a pale cyan disk with distinct limb darkening. With a large telescope of 25 cm or wider, cloud patterns, as well as some of the larger satellites, such as Taitania and Oberon, may be visible (Espenak, 2005).

1.7.4. Internal Structure

Uranus' mass is roughly 14.5 times that of Earth, making it the least massive of the giant planets. Its diameter is slightly larger than Neptune's at roughly four times that of Earth. A resulting density of 1.27 g/cm^3 makes Uranus the second least dense planet, after Saturn (Gunter and Teresa, 2007). This value indicates that it is made primarily of various ices, such as water, ammonia, and methane. The total mass of ice in Uranus' interior is not precisely known, because different figures emerge depending on the model chosen; it must be between 9.3 and 13.5 Earth masses. Hydrogen and helium constitute only a small part of the total, with between 0.5 and 1.5 Earth masses. The remainder of the non-ice mass (0.5 to 3.7 Earth masses) is accounted for by rocky material (Podolak et al, 1995).

The standard model of Uranus' structure is that it consists of three layers: a rocky core in the centre, an icy mantle in the middle and an outer gaseous hydrogen/helium envelope. The core is relatively small, with a mass of only 0.55 Earth masses and a radius less than 20% of Uranus'; the mantle comprises its bulk, with around 13.4 Earth masses, and the upper atmosphere is relatively insubstantial, weighing about 0.5 Earth masses and extending for the last 20% of Uranus' radius. Uranus' core density is around 9 g/cm^3, with a pressure in the centre of 8 million bars (800 GPa) and a temperature of about 5000 K (Sarah K., 2017). The ice mantle is not in fact composed of ice in the conventional sense, but of a hot and dense fluid consisting of water, ammonia and other volatiles. This fluid, which has a high electrical conductivity, is sometimes called a water–ammonia ocean.

The extreme pressure and temperature deep within Uranus may break up the methane molecules, with the carbon atoms condensing into crystals of diamond that rain down through the mantle like

hailstones. Very-high-pressure experiments at the Lawrence Livermore National Laboratory suggest that the base of the mantle may comprise an ocean of liquid diamond, with floating solid 'diamond-bergs'. Scientists also believe that rainfalls of solid diamonds occur on Uranus, as well as on Jupiter, Saturn, and Neptune (Sean K., 2016).

The bulk compositions of Uranus and Neptune are different from those of Jupiter and Saturn, with ice dominating over gases, hence justifying their separate classification as ice giants. There may be a layer of ionic water where the water molecules break down into a soup of hydrogen and oxygen ions, and deeper down superionic water in which the oxygen crystallises but the hydrogen ions move freely within the oxygen lattice (Bland, 2010).

Although the model considered above is reasonably standard, it is not unique; other models also satisfy observations. For instance, if substantial amounts of hydrogen and rocky material are mixed in the ice mantle, the total mass of ices in the interior will be lower, and, correspondingly, the total mass of rocks and hydrogen will be higher. Presently available data does not allow a scientific determination which model is correct. The fluid interior structure of Uranus means that it has no solid surface. The gaseous atmosphere gradually transitions into the internal liquid layers (Podolak et al, 1995). For the sake of convenience, a revolving oblate spheroid set at the point at which atmospheric pressure equals 1 bar (100 kPa[1]) is conditionally designated as a "surface". It has equatorial and polar radii of 25,559 ± 4 km (15,881.6 ± 2.5 mi) and 24,973 ± 20 km (15,518 ± 12 mi), respectively. This surface is used throughout this article as a zero point for altitudes.

1.7.5. Internal Heat

Uranus' internal heat appears markedly lower than that of the other giant planets; in astronomical terms, it has a low thermal flux (Pearl et

1 - kilo Pascal

al, 1990). Why Uranus' internal temperature is so low is still not understood. Neptune, which is Uranus' near twin in size and composition, radiates 2.61 times as much energy into space as it receives from the Sun (Sromovsky and Fry, 2005), but Uranus radiates hardly any excess heat at all. The total power radiated by Uranus in the far infrared (i.e. heat) part of the spectrum is 1.06±0.08 times the solar energy absorbed in its atmosphere. Uranus' heat flux is only 0.042±0.047 W/m^2, which is lower than the internal heat flux of Earth of about 0.075 W/m^2. The lowest temperature recorded in Uranus' tropopause is 49 K (−224.2 °C; −371.5 °F), making Uranus the coldest planet in the Solar System (Hanel et al, 1986).

One of the hypotheses for this discrepancy suggests that when Uranus was hit by a supermassive impactor, which caused it to expel most of its primordial heat, it was left with a depleted core temperature. This impact hypothesis is also used in some attempts to explain the planet's axial tilt. Another hypothesis is that some form of barrier exists in Uranus' upper layers that prevent the core's heat from reaching the surface. For example, convection may take place in a set of compositionally different layers, which may inhibit the upward heat transport; perhaps double diffusive convection is a limiting factor (Lunine, 1993).

1.7.6. Atmosphere of Uranus

Although there is no well-defined solid surface within Uranus' interior, the outermost part of Uranus' gaseous envelope that is accessible to remote sensing is called its atmosphere. Remote-sensing capability extends down to roughly 300 km below the 1 bar (100 kPa) level, with a corresponding pressure around 100 bar (10 MPa) and temperature of 320 K (47 °C; 116 °F). The tenuous thermosphere extends over two planetary radii from the nominal surface, which is defined to lie at a pressure of 1 bar (Herbert et al, 1987). The Uranian atmosphere can be divided into three layers: the troposphere, between altitudes of −300 and 50 km (−186 and 31 mi) and pressures from 100 to 0.1 bar (10 MPa to 10 kPa); the stratosphere, spanning altitudes

between 50 and 4,000 km (31 and 2,485 mi) and pressures of between 0.1 and 10^{-10} bar (10 kPa to 10 μPa); and the thermosphere extending from 4,000 km to as high as 50,000 km from the surface. There is no mesosphere.

1.8. Neptune

Dark, cold and whipped by supersonic winds, ice giant Neptune is the eighth and most distant planet in our solar system, more than 30 times as far from the Sun as Earth. Neptune is the only planet in our solar system not visible to the naked eye and the first predicted by mathematics before its discovery. In 2011 Neptune completed its first 165-year orbit since its discovery in 1846. NASA's Neptune Voyager 2 is the only spacecraft to have visited Neptune up close. It flew past in 1989 on its way out of the solar system.

Neptune is the eighth and farthest known planet from the Sun in the Solar System. In the Solar System, it is the fourth-largest planet by diameter, the third-most-massive planet, and the densest giant planet. Neptune is 17 times the mass of Earth, slightly more massive than its near-twin Uranus. Neptune is denser and physically smaller than Uranus because its greater mass causes more gravitational compression of its atmosphere. Neptune orbits the Sun once every 164.8 years at an average distance of 30.1 au (4.5 billion km; 2.8 billion mi). It is named after the Roman god of the sea and has the astronomical symbol ♆, a stylized version of the god Neptune's trident.

Neptune is not visible to the unaided eye and is the only planet in the Solar System found by mathematical prediction rather than by empirical observation. Unexpected changes in the orbit of Uranus led Alexis Bouvard to deduce that its orbit was subject to gravitational perturbation by an unknown planet. The position of Neptune was subsequently calculated from Bouvard's observations, independently, by John Couch Adams and Urbain Le Verrier after his death. Neptune was subsequently observed with a telescope on 23 September 1846 (Hamilton, 2001) by Johann Galle within a degree of the position

predicted by Le Verrier. Its largest moon, Triton, was discovered shortly thereafter, though none of the planet's remaining known 13 moons were located telescopically until the 20th century. The planet's distance from Earth gives it a very small apparent size, making it challenging to study with Earth-based telescopes.

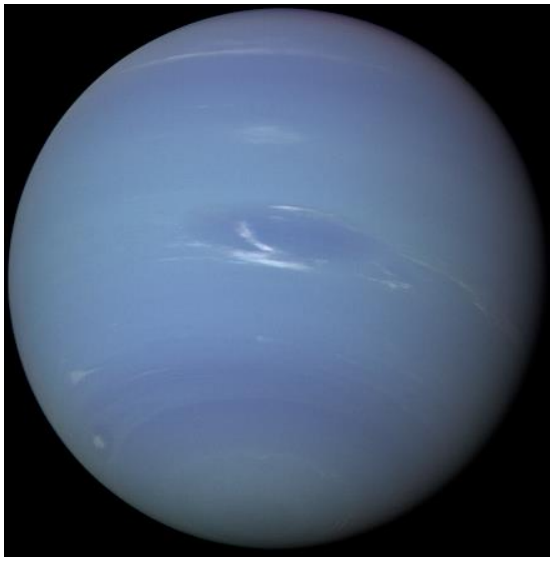

Figure 1.12 Image of Neptune taken by NASA's Voyager 2 in 1989.

Like Jupiter and Saturn, Neptune's atmosphere is composed primarily of hydrogen and helium, along with traces of hydrocarbons and possibly nitrogen, though it contains a higher proportion of "ices" such as water, ammonia and methane. However, similar to Uranus, its interior is primarily composed of ices and rock (Podolak et al, 1995); Uranus and Neptune are normally considered "ice giants" to emphasise this distinction (Lunine, 1993). Traces of methane in the outermost regions in part account for the planet's blue appearance. Neptune's atmosphere has active and visible weather patterns. For example, at the time of the *Voyager 2* flyby in 1989, the planet's southern hemisphere had a Great Dark Spot comparable to the Great Red Spot on Jupiter.

1.8.1. Physical Characteristics

Neptune's mass of 1.0243×10^{26} kg is intermediate between Earth and the larger gas giants: it is 17 times that of Earth but just 1/19th that of Jupiter. Its gravity at 1 bar is 11.15 m/s^2, 1.14 times the surface gravity of Earth, and surpassed only by Jupiter. Neptune's equatorial radius of 24,764 km is nearly four times that of Earth. Neptune, like Uranus, is an ice giant, a subclass of giant planet, because they are smaller and have higher concentrations of volatiles than Jupiter and Saturn. In the search for extrasolar planets, Neptune has been used as a metonym: discovered bodies of similar mass are often referred to as "Neptunes", just as scientists refer to various extrasolar bodies as "Jupiters". Internal structure Neptune's internal structure resembles that of Uranus. Its atmosphere forms about 5% to 10% of its mass and extends perhaps 10% to 20% of the way towards the core, where it reaches pressures of about 10 GPa[1], or about 100 times that of Earth's atmosphere. Increasing concentrations of methane, ammonia and water are found in the lower regions of the atmosphere.

The mantle is equivalent to 10 to 15 Earth masses and is rich in water, ammonia and methane. As is customary in planetary science, this mixture is referred to as icy even though it is a hot, dense fluid. This fluid, which has a high electrical conductivity, is sometimes called a water–ammonia ocean. The mantle may consist of a layer of ionic water in which the water molecules break down into a soup of hydrogen and oxygen ions, and deeper down supersonic water in which the oxygen crystallises but the hydrogen ions float around freely within the oxygen lattice. At a depth of 7,000 km, the conditions may be such that methane decomposes into diamond crystals that rain downwards like hailstones. Scientists also believe that this kind of diamond rain occurs on Jupiter, Saturn, and Uranus. Very-high-pressure experiments at the Lawrence Livermore National Laboratory suggest that the top of the mantle may be an ocean of liquid carbon with floating solid 'diamonds'.

---

1 - Giga Pascal

The core of Neptune is likely composed of iron, nickel and silicates, with an interior model giving a mass about 1.2 times that of Earth. The pressure at the centre is 7 Mbar (700 GPa), about twice as high as that at the centre of Earth, and the temperature may be 5,400 K.

1.8.2. Atmosphere

At high altitudes, Neptune's atmosphere is 80% at high altitudes; Neptune's atmosphere is 80% hydrogen and 19% helium. A trace amount of methane is also present. Prominent absorption bands of methane exist at wavelengths above 600 nm, in the red and infrared portion of the spectrum. As with Uranus, this absorption of red light by the atmospheric methane is part of what gives Neptune its blue hue, although Neptune's vivid azure differs from Uranus's milder cyan. Because Neptune's atmospheric methane content is similar to that of Uranus, some unknown atmospheric constituent is thought to contribute to Neptune's colour (Munsell et al., 2007).

Neptune's atmosphere is subdivided into two main regions: the lower troposphere, where temperature decreases with altitude, and the stratosphere, where temperature increases with altitude. The boundary between the two, the tropopause, lies at a pressure of 0.1 bars (10 kPa). The stratosphere then gives way to the thermosphere at a pressure lower than 10^{-5} to 10^{-4} bars (1 to 10 Pa). The thermosphere gradually transitions to the exosphere.

Models suggest that Neptune's troposphere is banded by clouds of varying compositions depending on altitude. The upper-level clouds lie at pressures below one bar, where the temperature is suitable for methane to condense. For pressures between one and five bars (100 and 500 kPa), clouds of ammonia and hydrogen sulfide are thought to form. Above a pressure of five bars, the clouds may consist of ammonia, ammonium sulfide, hydrogen sulfide and water. Deeper clouds of water ice should be found at pressures of about 50 bars (5.0 MPa), where the temperature reaches 273 K (0 °C). Underneath, clouds of ammonia and hydrogen sulfide may be found (Elkins and

Linda, 2006).

High-altitude clouds on Neptune have been observed casting shadows on the opaque cloud deck below. There are also high-altitude cloud bands that wrap around the planet at constant latitude. These circumferential bands have widths of 50–150 km and lie about 50–110 km above the cloud deck. These altitudes are in the layer where weather occurs, the troposphere. Weather does not occur in the higher stratosphere or thermosphere. Unlike Uranus, Neptune's composition has a higher volume of ocean, whereas Uranus has a smaller mantle.

Neptune's spectra suggest that its lower stratosphere is hazy due to condensation of products of ultraviolet photolysis of methane, such as ethane and ethylene (Hubbard, 1997). The stratosphere is also home to trace amounts of carbon monoxide and hydrogen cyanide. The stratosphere of Neptune is warmer than that of Uranus due to the elevated concentration of hydrocarbons.

For reasons that remain obscure, the planet's thermosphere is at an anomalously high temperature of about 750 K (Herbert and Bill, 1999**)**. The planet is too far from the Sun for this heat to be generated by ultraviolet radiation. One candidate for a heating mechanism is atmospheric interaction with ions in the planet's magnetic field. Other candidates are gravity waves from the interior that dissipate in the atmosphere. The thermosphere contains traces of carbon dioxide and water, which may have been deposited from external sources such as meteorites and dust (Encrenaz, 2003).

1.8.3. Magnetosphere

Neptune resembles Uranus in its magnetosphere, with a magnetic field strongly tilted relative to its rotational axis at 47° and offset at least 0.55 radii, or about 13,500 km from the planet's physical center. Before Voyager 2's arrival at Neptune, it was hypothesized that Uranus's tilted magnetosphere was the result of its sideways rotation. In comparing the magnetic fields of the two planets, scientists now think the extreme orientation may be characteristic of flows in the planets' interiors. This field may be generated by convective fluid

motions in a thin spherical shell of electrically conducting liquids (probably a combination of ammonia, methane and water) resulting in a dynamo action, (Stanley and Bloxham, 2004).

The dipole component of the magnetic field at the magnetic equator of Neptune is about 14 microteslas (μT) (0.14 G[1]). The dipole magnetic moment of Neptune is about 2.2×10^{17} Tm^3 ($14\ \mu T \cdot R_N^3$, where R_N is the radius of Neptune). Neptune's magnetic field has a complex geometry that includes relatively large contributions from non-dipolar components, including a strong quadrupole[2] moment that may exceed the dipole moment in strength. By contrast, Earth, Jupiter and Saturn have only relatively small quadrupole moments, and their fields are less tilted from the polar axis. The large quadrupole moment of Neptune may be the result of offset from the planet's center and geometrical constraints of the field's dynamo generator.

Neptune's bow shock, where the magnetosphere begins to slow the solar wind, occurs at a distance of 34.9 times the radius of the planet. The magnetopause, where the pressure of the magnetosphere counterbalances the solar wind, lies at a distance of 23–26.5 times the radius of Neptune. The tail of the magnetosphere extends out to at least 72 times the radius of Neptune, and likely much farther (Ness et al, 1989).

1.8.4. Climate

Neptune's weather is characterized by extremely dynamic storm systems, with winds reaching speeds of almost 600 m/s (2,200 km/h; 1,300 mph)—nearly reaching supersonic flow. More typically, by tracking the motion of persistent clouds, wind speeds have been shown to vary from 20 m/s in the easterly direction to 325 m/s westward (Hammel et al, 1989). At the cloud tops, the prevailing winds range in speed from 400 m/s along the equator to 250 m/s at the poles. Most of the winds on Neptune move in a direction opposite the

---

1 - Gauss

2- a distribution of electric charge or magnetization consisting of four equal monopoles, or two equal dipoles,

planet's rotation. The general pattern of winds showed *prograde rotation*[1] at high latitudes vs. retrograde rotation at lower latitudes. The difference in flow direction is thought to be a "skin effect" and not due to any deeper atmospheric processes. At 70° S latitude, a high-speed jet travels at a speed of 300 m/s.

Neptune differs from Uranus in its typical level of meteorological activity. Voyager 2 observed weather phenomena on Neptune during its 1989 flyby, but no comparable phenomena on Uranus during its 1986 fly-by.

The abundance of methane, ethane and acetylene at Neptune's equator is 10–100 times greater than at the poles. This is interpreted as evidence for upwelling at the equator and subsidence near the poles because photochemistry cannot account for the distribution without meridional circulation.

In 2007, it was discovered that the upper troposphere of Neptune's south pole was about 10 K warmer than the rest of its atmosphere, which averages approximately 73 K (−200 °C). The temperature differential is enough to let methane, which elsewhere is frozen in the troposphere, escape into the stratosphere near the pole. The relative "hot spot" is due to Neptune's axial tilt, which has exposed the south pole to the Sun for the last quarter of Neptune's year, or roughly 40 Earth years. As Neptune slowly moves towards the opposite side of the Sun, the South Pole will be darkened and the north pole illuminated, causing the methane release to shift to the north pole (Orton and Encrenaz, 2007).

Because of seasonal changes, the cloud bands in the southern hemisphere of Neptune have been observed to increase in size and albedo. This trend was first seen in 1980 and is expected to last until about 2020. The long orbital period of Neptune results in seasons lasting forty years.

---

1 - means the direction of rotation is same as that of the sun

1.8.5. Storms

In 1989, the Great Dark Spot, an anti-cyclonic storm system spanning 13,000 × 6,600 km, was discovered by NASA's Voyager 2 spacecraft. The storm resembled the Great Red Spot of Jupiter. Some five years later, on 2 November 1994, the Hubble Space Telescope did not see the Great Dark Spot on the planet. Instead, a new storm similar to the Great Dark Spot was found in Neptune's northern hemisphere (Hammel et al, 1995).

The Scooter is another storm, a white cloud group farther south than the Great Dark Spot. This nickname first arose during the months leading up to the Voyager 2 encounter in 1989, when they were observed moving at speeds faster than the Great Dark Spot (and images acquired later would subsequently reveal the presence of clouds moving even faster than those that had initially been detected by Voyager 2). The Small Dark Spot is a southern cyclonic storm, the second-most-intense storm observed during the 1989 encounter. It was initially completely dark, but as Voyager 2 approached the planet, a bright core developed and can be seen in most of the highest-resolution images, (Lavoie, 1996).

Neptune's dark spots are thought to occur in the troposphere at lower altitudes than the brighter cloud features, so they appear as holes in the upper cloud decks. As they are stable features that can persist for several months, they are thought to be vortex structures. Often associated with dark spots are brighter, persistent methane clouds that form around the tropopause layer. The persistence of companion clouds shows that some former dark spots may continue to exist as cyclones even though they are no longer visible as a dark feature. Dark spots may dissipate when they migrate too close to the equator or possibly through some other unknown mechanism (Gibbard et al, 2003).

1.8.6. Internal Heating

Neptune's more varied weather when compared to Uranus is due in part to its higher internal heating. Although Neptune lies over 50%

farther from the Sun than Uranus, and receives only 40% its amount of sunlight,[16] the two planets' surface temperatures are roughly equal. The upper regions of Neptune's troposphere reach a low temperature of 51.8 K (−221.3 °C). At a depth where the atmospheric pressure equals 1 bar (100 kPa), the temperature is 72.00 K (−201.15 °C). Deeper inside the layers of gas, the temperature rises steadily. As with Uranus, the source of this heating is unknown, but the discrepancy is larger: Uranus only radiates 1.1 times as much energy as it receives from the Sun; whereas Neptune radiates about 2.61 times as much energy as it receives from the Sun (Pearl, and Conrath, 1991). Neptune is the farthest planet from the Sun, yet its internal energy is sufficient to drive the fastest planetary winds seen in the Solar System. Depending on the thermal properties of its interior, the heat left over from Neptune's formation may be sufficient to explain its current heat flow, though it is more difficult to simultaneously explain Uranus's lack of internal heat while preserving the apparent similarity between the two planets (Imke and Jack, 2001).

1.8.7. Orbit and Rotation

The average distance between Neptune and the Sun is 4.5 billion km (about 30.1 AU[1]), and it completes an orbit on average every 164.79 years, subject to a variability of around ±0.1 years. The perihelion distance is 29.81 AU; the aphelion distance is 30.33 AU (Jean, 1998).

On 11 July 2011, Neptune completed its first full barycentric orbit since its discovery in 1846, although it did not appear at its exact discovery position in the sky, because Earth was in a different location in its 365.26-day orbit. Because of the motion of the Sun in relation to the barycenter of the Solar System, on 11 July Neptune was also not at its exact discovery position in relation to the Sun; if the more common heliocentric coordinate system is used, the discovery longitude was reached on 12 July 2011. The elliptical orbit of Neptune is inclined

1 - astronomical units (AU)

1.77° compared to that of Earth (Nancy, 2010; Williams, 2005).

The axial tilt of Neptune is 28.32°, which is similar to the tilts of Earth (23°) and Mars (25°). As a result, Neptune experiences similar seasonal changes to Earth. The long orbital period of Neptune means that the seasons last for forty Earth years (Villard and Devitt, 2003). Its sidereal rotation period (day) is roughly 16.11 hours. Because its axial tilt is comparable to Earth's, the variation in the length of its day over the course of its long year is not any more extreme.

Because Neptune is not a solid body, its atmosphere undergoes differential rotation. The wide equatorial zone rotates with a period of about 18 hours, which is slower than the 16.1-hour rotation of the planet's magnetic field. By contrast, the reverse is true for the Polar Regions where the rotation period is 12 hours. This differential rotation is the most pronounced of any planet in the Solar System, and it results in strong latitudinal wind shear (Max et al, 2003).

Neptune's orbit has a profound impact on the region directly beyond it, known as the Kuiper belt. The Kuiper belt is a ring of small icy worlds, similar to the asteroid belt but far larger, extending from Neptune's orbit at 30 AU out to about 55 AU from the Sun. Over the age of the Solar System, certain regions of the Kuiper belt became destabilized by Neptune's gravity, creating gaps in the Kuiper belt's structure. The region between 40 and 42 AU is an example (Petit et al., 1999).

There exist orbits within these empty regions where objects can survive for the age of the Solar System. These resonances occur when Neptune's orbital period is a precise fraction of that of the object, such as 1:2, or 3:4. If, say, an object orbits the Sun once for every two Neptune orbits, it will only complete half an orbit by the time Neptune returns to its original position. The most heavily populated resonance in the Kuiper belt, with over 200 known objects, is the 2:3 resonances. Objects in this resonance complete 2 orbits for every 3 of Neptune, and are known as plutinos because the largest of the known Kuiper belt objects, Pluto, is among them. Although Pluto crosses Neptune's orbit regularly, the 2:3 resonance ensures they can never collide. The

3:4, 3:5, 4:7 and 2:5 resonances are less populated (John, 2001).

Neptune has a number of known trojan objects occupying both the Sun–Neptune L_4 and L_5 Lagrangian points—gravitationally stable regions leading and trailing Neptune in its orbit, respectively. Neptune trojans can be viewed as being in a 1:1 resonance with Neptune. Some Neptune trojans are remarkably stable in their orbits, and are likely to have formed alongside Neptune rather than being captured. The first object identified as associated with Neptune's trailing Lagrangian point was 2008 LC. Neptune also has a temporary quasi-satellite. The object has been a quasi-satellite of Neptune for about 12,500 years and it will remain in that dynamical state for another 12,500 years (De La Fuente and De La Fuente, 2012).

1.8.8. Planetary Rings

Neptune has a planetary ring system, though one much less substantial than that of Saturn. The rings may consist of ice particles coated with silicates or carbon-based material, which most likely gives them a reddish hue. The three main rings are the narrow Adams Ring, 63,000 km from the centre of Neptune, the Le Verrier Ring, at 53,000 km, and the broader, fainter Galle Ring, at 42,000 km. A faint outward extension to the Le Verrier Ring has been named Lassell; it is bounded at its outer edge by the Arago Ring at 57,000 km (Blue, 2004).

The first of these planetary rings was detected in 1968 by a team led by Edward Guinan. In the early 1980s, analysis of this data along with newer observations led to the hypothesis that this ring might be incomplete. Evidence that the rings might have gaps first arose during a stellar occultation in 1984 when the rings obscured a star on immersion but not on emersion. Images from Voyager 2 in 1989 settled the issue by showing several faint rings (Nicholson et al, 1990).

The outermost ring, Adams, contains five prominent arcs now named *Courage, Liberté, Egalité 1, Egalité 2* and F*raternité* (Courage, Liberty, Equality and Fraternity). The existence of arcs was difficult to

explain because the laws of motion would predict that arcs would spread out into a uniform ring over short timescales. Astronomers now estimate that the arcs are corralled into their current form by the gravitational effects of Galatea, a moon just inward from the ring.

Earth-based observations announced in 2005 appeared to show that Neptune's rings are much more unstable than previously thought. Images taken from the W.M. Keck Observatory in 2002 and 2003 show considerable decay in the rings when compared to images by *Voyager 2*. In particular, it seems that the *Liberté* arc might disappear in as little as one century (Salo and Hänninen 1998).

1.8.9. Moons

Neptune has 14 known moons. Triton is the largest Neptunian moon, comprising more than 99.5% of the mass in orbit around Neptune, and it is the only one massive enough to be spheroidal. Triton was discovered by William Lassell just 17 days after the discovery of Neptune itself. Unlike all other large planetary moons in the Solar System, Triton has a retrograde orbit, indicating that it was captured rather than forming in place; it was probably once a dwarf planet in the Kuiper belt (Agnor and Hamilton, 2006). It is close enough to Neptune to be locked into a synchronous rotation, and it is slowly spiralling inward because of tidal acceleration. It will eventually be torn apart, in about 3.6 billion years, when it reaches the Roche limit. In 1989, Triton was the coldest object that had yet been measured in the Solar System, with estimated temperatures of 38 K (−235 °C) (Nelson et al, 1990).

Neptune's second known satellite (by order of discovery), the irregular moon Nereid, has one of the most eccentric orbits of any satellite in the Solar System. The eccentricity of 0.7512 gives it an apoapsis that is seven times its periapsis distance from Neptune.

From July to September 1989, Voyager 2 discovered six moons of Neptune. Of these, the irregularly shaped Proteus is notable for being as large as a body of its density can be without being pulled into a spherical shape by its own gravity. Although the second-most-massive

Neptunian moon, it is only 0.25% the mass of Triton. Neptune's innermost four moons—Naiad, Thalassa, Despina and Galatea—orbit close enough to be within Neptune's rings. The next-farthest out, Larissa, was originally discovered in 1981 when it had occulted a star. This occultation had been attributed to ring arcs, but when *Voyager 2* observed Neptune in 1989, Larissa was found to have caused it. Five new irregular moons discovered between 2002 and 2003 were announced in 2004. A new moon and the smallest yet, Hippocamp, was found in 2013 by combining multiple Hubble images. Because Neptune was the Roman god of the sea, Neptune's moons have been named after lesser sea gods (Grush, 2019).

References

Agnor C.B., Hamilton D.P. (2006) "Neptune's capture of its moon Triton in a binary–planet gravitational encounter". Nature. 441 (7090): 192–94.

Bauer M. (2012). "Have Venusian volcanoes been caught in the act?". European Space Agency. Archived from the original on 3 November 2013.

Bergstralh J.T., Miner E., Matthews M. (1991) Uranus, pp. 485–486. ISBN 978-0-8165-1208-9.

Bland E., (2010) "Outer planets may have oceans of diamond". ABC Science. Retrieved 9 October 2017.

Blue J. (2004) "Nomenclature Ring and Ring Gap Nomenclature". Gazetteer of Planetary Nomenclature. USGS. Archived from the original on 5 July 2010. Retrieved 28 February 2008.

Boss Alan P. (2002) "Formation of gas and ice giant planets". Earth and Planetary Science. Letter, 202 (3-4): 513–23.

Bradley D.K., Eggert, J.H.; Hicks, D.G.; Celliers, P.M. (30 July 2004). "Shock Compressing Diamond to a Conducting Fluid" (PDF). Physical Review Letters. 93 (19): 195506.

Byrne S., Ingersoll A.P. (2003). "A Sublimation Model for Martian South Polar Ice Features". Science, 299 (5609): 1051–1053. doi:10.1126/science.1080148.

Carolynn Y., ed. (1990) The Magellan Venus Explorer's Guide. California: Jet Propulsion Laboratory. p. 93. Retrieved 13 January 2016.

"Cartographic Standards" (PDF). NASA. Archived from the original on 7 April 2004. Retrieved 13 June 2007.

Christensen et al, (2003). "Morphology and Composition of the Surface of

Mars: Mars Odyssey THEMIS Results". Science, 300 (5628): 2056–2061. doi:10.1126/science.1080885.

De La Fuente M.C., De La Fuente M.R. (2012) "(309239) 2007 RW10: a large temporary quasi-satellite of Neptune". Astronomy and Astrophysics Letters. 545 (2012)

Eggert J.H., Hicks D.G., Celliers P.M., Bradley D.K., et al. (2009) "Melting temperature of diamond at ultrahigh pressure". Nature Physics. 6(40): 40–43.

Elkins-Tanton, Linda T. (2006) Uranus, Neptune, Pluto, and the Outer Solar System. New York: Chelsea House. pp. 79–83. ISBN 978-0-8160-5197-7.

Encrenaz T. (2003) "ISO observations of the giant planets and Titan: what have we learnt?" Planetary and Space Science. 51 (2): 89–103.

Eposito L.W. (2002) Planetary rings. Reports on progress in physics, 65 (12): 1741-1783. Bibcode: 2002RPPh…65.1741E

Espenak F. (2005) "Twelve Year Planetary Ephemeris: 1995–2006". NASA. Retrieved 14 June 2007.

Fred E., (1994) Twelve-Year Planetary Ephemeries: 1995-2006. NASA reference publication 1349. Retrieved 9 June 2007.

Frankel, Charles (1996) Volcanoes of the Solar System, Cambridge University Press. ISBN 978-0-521-47770-3.

Gánti T., et al. (2003) "Dark Dune Spots: Possible Biomarkers on Mars?". Origins of Life and Evolution of the Biosphere. 33 (4): 515–557. 10.1023/A:1025705828948.

Gibbard S.G., de Pater I., Roe H.G., Martin, S. et al. (2003) "The altitude of

Neptune cloud features from high-spatial-resolution near-infrared spectra" (PDF). Icarus, 166 (2): 359–74.

Gierasch Peter J., Nicholson Philip D. (2004) "Uranus". World Book. Retrieved 8 March 2015.

Glaze L.S., (1999)"Transport of SO2 by explosive volcanism on Venus". J. Geophysical. Res., 104 (E8): 18899–18906. doi:10.1029/1998JE000619.

Goettel K.A., Shields J.A., Decker D.A. (1981) "Density constraints on the composition of Venus". Proceedings of the Lunar and Planetary Science Conference. Houston, TX: Pergamon Press. pp. 1507–1516.

Grush L. (2019) "Neptune's newly discovered moon may be the survivor of an ancient collision

Gunter and Teresa, (2007) "Uranus: What Happened Here?". In Faure, Gunter; Mensing, Teresa M. (eds.). Introduction to Planetary Science. Introduction to Planetary Science. Springer Netherlands. pp. 369–384.

Halliday A.N., Wänke H., Birck J.L., Clayton, R.N. (2001) The Accretion, Composition and Early Differentiation of Mars.Space Science Reviews, 96 (1/4): 197–230. doi:10.1023/A:1011997206080.

Hamilton, C.J. (2001) Neptune, Views of the Solar System. Archived from the original, 2007.

Hammel H.B., Lockwood G.W., Mills J.R., Barnet C.D. (1995) "Hubble Space Telescope Imaging of Neptune's Cloud Structure in 1994". Science, 268 (5218): 1740–42.

Hammel H.B., Beebe R.F., De Jong E.M., Hansen C.J., et al. (1989) "Neptune's wind speeds obtained by tracking clouds in Voyager 2 images". Science, 24 (4924): 1367–69.

Hanel R., Conrath B., Flasar F.M., Kunde V., Maguire W., Pear J., Pirraglia J., Samuelson R., Cruikshank D. (4 July 1986). "Infrared Observations of the Uranian System". Science, 233 (4759): 70–74.

Hashimoto G.L., Roos-Serote M., Sugita S., Gilmore M.S., Kamp L.W., Carlson R.W., Baines K.H. (2008). "Felsic highland crust on Venus suggested by Galileo Near-Infrared Mapping Spectrometer data". J. Geophysical. Res. Planets: 113 (E9).

Hashimoto G.L., Roos-Serote M., Sugita S., Gilmore M.S., Kamp L.W., Carlson R.W., Baines K.H. (2008) "Felsic highland crust on Venus suggested by Galileo Near-Infrared Mapping Spectrometer data". J. Geophysical. Res. Planets: 113 (E9): E00B24. doi:10.1029/2008JE003134

Herbert F., Sandel B.R., Yelle R.V., Holberg J.B., Broadfoot A.L., Shemansky D.E., Atreya S. K., Romani P.N. (1987) “The upper atmosphere of Uranus: EUV Occulations observed by Voyager 2”. J. Geophysical. Res., 92 (A13): 15, 093–15,109.

Herbert F., Sandel B.R. (August–September 1999) "Ultraviolet observations of Uranus and Neptune". Planetary and Space Science, 47 (8–9): 119–139.

Hooke, R.L.B., Martín-Duque, J.F., Pedraza, J. (2012) "Land transformation by humans: A review". GSA Today. 22 (12): 4–10. doi:10.1130/GSAT151A.1

"Horizons Output for Neptune 2010–2011". Archived from the original on 2 May 2013. Retrieved 25 February 2008.—Numbers generated using the Solar System Dynamics Group, Horizons On-Line Ephemeris System.

Hubbard W.B. (1997) "Neptune's Deep Chemistry". Science. 275 (5304): 1279–80.

Hunt G.E., Michael W.H., Pascu D., Veverka J., Wilkins G.A., Woolfson

M., (1978) "The Martian satellites—100 years on". Quarterly Journal of the Royal Astronomical Society. 19: 90–109.

Imke de Pater, Jack J. Lissauer (2001) Planetary Sciences, 1st edition, p. 224.

Jakosky, Bruce M. (1999) "Atmospheres of the Terrestrial Planets". In Beatty, J. Kelly; Petersen, Carolyn Collins; Chaikin, Andrew (eds.). The New Solar System (4th ed.). Boston: Sky Publishing. pp. 175–200. ISBN 978-0-933346-86-4.

Jean M. (1998) Astronomical Algorithms (Richmond, VA: Willmann-Bell) 273. Supplemented by further use of VSOP87. The last three aphelia were 30.33 AU, the next is 30.34 AU. The perihelia are even more stable at 29.81 AU.

Jessey, David. "Weathering and Sedimentary Rocks". Cal Poly Pomona. Archived from the original on 3 July 2007.

John D., (2001) Beyond Pluto: Exploring the outer limits of the solar system. Cambridge University Press, p. 104.

Karttunen H., Kroger P., Oja H., Poutanen M., Donner K.J., (2007) Fundamental Astronomy. Springer. p. 162. ISBN 978-3-540-34143-7.

Kaufmann W. J. (1994) Universe, New York: W. H. Freeman. p. 204. ISBN 978-0-7167-2379-0.

Kennish M.J. (2001) Practical handbook of marine science. Marine science series (3rd ed.). CRC Press. p. 35. ISBN 978-0-8493-2391-1.

Kraus D., et al. (2017) Formation of diamonds in laser-compressed hydrocarbons at planetary interior conditions. Nature Astronomy. 1(9): 606–11. Bibcode: 2017NatAs1.606K. doi: 10.1038/s41550-017-0219-9.

Laskar J., et al. (2004) "A long-term numerical solution for the insolation quantities of the Earth". Astronomy and Astrophysics, 428(1): 261–85. doi: 10.1051/0004-6361:20041335.

Lavoie S. (1996) "PIA00064: Neptune's Dark Spot (D2) at High Resolution". NASA JPL. Archived from the original on 13 August 2013.

Lindal G.F. (1992) "The atmosphere of Neptune – an analysis of radio occultation data acquired with Voyager 2". Astronomical Journal. 103: 967–82.

Lovis C., Mayor M., Alibert Y., Benz W. (2006) "Trio of Neptunes and their Belt". ESO. Archived from the original on 13 January 2010.

Lunine J.I., (1993) "The Atmospheres of Uranus and Neptune". Annual Review of Astronomy and Astrophysics. 31: 217–63.

Lunine J.I. (1993) "The Atmospheres of Uranus and Neptune". Annual Review of Astronomy and Astrophysics. 31: 217–263.

Manhesa G., Allègre Claude, J., Dupréa B., Hamelin B. (1980) "Lead isotope study of basic-ultrabasic layered complexes: Speculations about the age of the earth and primitive mantle characteristics", Earth and Planetary Science Letters, 47 (3): 370–82.

Martin, R. (2011) Earth's Evolving Systems: The History of Planet Earth. Jones and Bartlett Learning, ISBN 978-0-7637-8001-2.

Max C.E., Macintosh B.A., Gibbard S.G., Gavel D.T., et al. (2003) "Cloud Structures on Neptune Observed with Keck Telescope Adaptive Optics". The Astronomical Journal, 125 (1): 364–75.

Mazarico E., Antonio G.S., Lemoine F.G., Neumann G.A., et al., (2014) The gravity field, orientation, and ephemeris of Mercury from MESSENGER observations after three years in orbit. Journal of Geophysical Research: Planets. 119 (12): 2417–2436.

Milbert D.G., Smith D.A. "Converting GPS Height into NAVD88 Elevation with the GEOID96 Geoid Height Model". National Geodetic Survey,

NOAA. Retrieved 7 March 2007.

Munsell K., Smith H., Harvey S. (2009) "Mercury: Facts & Figures". Solar System Exploration, NASA. Retrieved April, 2008.

Munsell K., Smith H., Harvey S. (2007) "Neptune overview". Solar System Exploration, NASA. Archived from the original on 3 March 2008.

Murphy J. B., Nance R.D. (1965) "How do supercontinents assemble?". American Scientist, 92 (4): 324–33. doi:10.1511/2004.4.324.

Nancy Atkinson (2010) "Clearing the Confusion on Neptune's Orbit". Universe Today, Archived from the original on 27 July 2011.

Nancy A. (2010) "Clearing the Confusion on Neptune's Orbit". Universe Today, Archived from the original on 27 July 2011. Retrieved 10 July 2011. (Bill Folkner at JPL)

NASA, (2010) "Neptune Fact Sheet". NASA. Archived from the original on 1 July 2010.

NASA, 92016) "Lake of frozen water the size of New Mexico found on Mars – NASA". The Register. November 22, 2016. Retrieved November, 23, 2016.

Neal-Jones N., O'Carroll, C., (2011) "New Map Provides More Evidence Mars Once Like Earth". NASA/Goddard Space Flight Center. Retrieved December 4, 2011.

Nelson R.M., Smythe W.D., Wallis B.D., Horn L.J., et al. (1990) "Temperature and Thermal Emissivity of the Surface of Neptune's Satellite Triton". Science, 250 (4979): 429–31.

Ness N.F., Acuña M.H., Burlaga L.F., Connerney J.E.P., Lepping R.P., Neubauer F.M. (1989) "Magnetic Fields at Neptune".

Science, 246 (4936): 1473–78.

Nicholson P.D., et al. (1990) "Five Stellar Occultations by Neptune: Further Observations of Ring Arcs". Icarus. 87 (1): 1–39.

Nimmo F., McKenzie D. (1998) "Volcanism and Tectonics on Venus". Annual Review of Earth and Planetary Sciences, 26 (1): 23–53.

Nowak G.T. (2006) "Uranus: the Threshold Planet of 2006". Retrieved 14 June 2007.

Orton G., Encrenaz T. (2007) "A Warm South Pole? Yes, On Neptune!". ESO.

Pearl J.C., Conrath B.J., Hanel R.A., Pirraglia J.A., Coustenis A. (1990). "The albedo, effective temperature, and energy balance of Uranus, as determined from Voyager IRIS data". Icarus. 84 (1): 12–28

Pearl J.C., Conrath B.J. (1991) "The albedo, effective temperature, and energy balance of Neptune, as determined from Voyager data". Journal of Geophysical Research: Space Physics. 96: 18, 921–30

Peplow M. (2004). "How Mars got its rust". Nature. Macmillan Publishers Ltd. Retrieved March 10, 2007.

Petit J., Morbidelli A., Valsecchi G.B. (1999) "Large Scattered Planetesimals and the Excitation of the Small Body Belts". Icarus, 141 (2): 367–87

Podolak M., Weizman A., Marley M. (1995). "Comparative models of Uranus and Neptune". Planetary and Space Science, 43 (12): 1517–22.

Podolak M., Weizman A., Marley M. (1995) "Comparative models of Uranus and Neptune". Planetary and Space Science, 43 (12): 1517–1522.

Podolak M., Weizman A., Marley M. (December 1995) "Comparative

models of Uranus and Neptune". Planetary and Space Science, 43 (12): 1517–1522.

Richmond V.A., Willmann-Bell (1998) Astronomical Algorithms, p 271. From the 1841 aphelion to the 2092 one, perihelia are always 18.28 and aphelia always 20.10 astronomical units.

Rogers J.W., Santosh M. (2004) Continents and Supercontinents. Oxford University Press US. p. 48. ISBN 978-0-19-516589-0.

Romeo I., Turcotte D.L. (2009) "The frequency-area distribution of volcanic units on Venus: Implications for planetary resurfacing". Icarus, 203 (1): 13–19.

Salo Heikki, Hänninen Jyrki (1998) "Neptune's Partial Rings: Action of Galatea on Self-Gravitating Arc Particles". Science, 282 (5391): 1102–04.

Sample I. (2017). "Mars covered in toxic chemicals that can wipe out living organisms, tests reveal". The Guardian, Retrieved November 26, 2018.

Sandwell, D.T., Smith, W.H.F. (2006) "Exploring the Ocean Basins with Satellite Altimeter Data". NOAA/NGDC. Retrieved April 2007

Sarah Kaplan (2017) "It rains solid diamonds on Uranus and Neptune". The Washington Post. Retrieved 22 May 2019.

Saumon D., Guillot T. (2004). "Shock Compression of Deuterium and the Interiors of Jupiter and Saturn". The Astrophysical Journal, 609 (2): 1170–1180.

Scott M. (2006) "Earth's Big heat Bucket". NASA Earth Observatory.

Sean Kane (2016) "Lightning storms make it rain diamonds on Saturn and Jupiter". Business Insider, Retrieved 22 May 2019.

Seidelmann P.K., Abalakin V.K., Bursa M., Davies M.E., De Bergh C., Lieske J.H., Oberst J., Simon J.L., Standish E.M., Stooke P., Thomas P.C. (2000) "Report of the IAU/IAG working group on cartographic coordinates and rotational elements of the planets and satellites: 2000".

Senne J.H. (2000) "Did Edmund Hillary Climb the Wrong Mountain". Professional Surveyor. 20 (5): 16–21.

Sromovsky L.A., Fry P.M. (2005) "Dynamics of cloud features on Uranus". Icarus, 179 (2): 459–484.

Sromovsky L. (2006) "Hubble captures rare, fleeting shadow on Uranus". University of Wisconsin Madison. Archived from the original on 20 July 2011. Retrieved 9 June 2007.

Staff. "Paleoclimatology – The Study of Ancient Climates". Page Paleontology Science Center, Archived from the original 2007.

Stanley S., Bloxham J. (2004). "Convective-region geometry as the cause of Uranus' and Neptune's unusual magnetic fields". Nature, 428 (6979): 151–53.

Tiscareno M.S., Burns J.A., Hedman, M.M., Porco C.C (2008) "The population of propellers in Saturn's A Ring". Astronomical Journal 135(3): 1083–1091.

Villard, Ray; Devitt, Terry (15 May 2003) "Brighter Neptune Suggests a Planetary Change of Seasons"

Wenk H.R., Bulakh A.G. (2004) Minerals: their constitution and origin. Cambridge University Press. p. 359. ISBN 978-0-521-52958-7.

Wetherill G.W. (1999). "Problems Associated with Estimating the Relative Impact Rates on Mars and the Moon". Earth, Moon, and Planets, 9 (1–2): 227–231.

Williams D.R. (2005) "Planetary Fact Sheets". NASA, Archived from the original on 25 September 2008.

Yeager A. (2008) "Impact May Have Transformed Mars". Science News.org.

Chapter 2
Venus Atmosphere: Structure, Composition and Climatic Events

Introduction

Second planet from the Sun and our closest planetary neighbor, Venus is similar in structure and size to Earth, but it is now a very different world. It receives about twice as much solar energy as Earth. However, the bright H_2SO_4 clouds make Venus' albedo more than twice Earth's. Consequently there is less solar forcing of Venus' climate than of Earth's in spite of its greater proximity to the Sun.

Venus has an extremely dense CO_2/N_2 atmosphere, with an average surface pressure of 92 bar (Avduevskii et al, 1976). The atmosphere is 96.5% CO2 and 3.5% N_2 by volume, which is the same as the molar ratio (Oyama et al, 1979, 1980). It has trace amounts of water vapor, sulfur gases, and halogens that play important roles in the formation of the global cloud layers and in the chemistry and energy balance of the atmosphere. The atmosphere has three main cloud layers from 48 to 68 km above the surface (366 K and 1.4 bar to 235 K and 50 mbar) consisting of liquid H_2SO_4/water aerosols (Esposito et al, 1983; Knollenberg and Hunten, 1980). There are variable hazes above and below the main cloud decks. Large spatial and temporal variabilities in the middle and lower clouds, including aerosol populations, are evident from Galileo's Near Infrared Mapping Spectrometer (NIMS) (Carlson et al, 1993; Grinspoon et al, 1993) and from observations by the European Space Agency's Venus Express (VEX) spacecraft (Barstow et al., 2012; Wilson et al., 2008). The atmosphere near the surface is about one-tenth as dense as water, and the CO_2 is

supercritical (Pcrit, Tcrit for CO_2 is 72.9 bar, 304.25 ^{o}K). So while Venus' atmosphere, like Earth's, is a fluid, it is neither a gas nor a liquid. As a mixture of gas and supercritical fluid, it has some properties of both. The fluid dynamics and heat transport operate in a medium with a density somewhere between water and air, without significant Coriolis forces. Relative to Earth and Mars, Venus rotates slowly. Strong zonal winds at the cloud tops are assumed to reflect cyclostrophic balance, in which the equator ward component of centrifugal force is balanced by meridional pressure gradient (Gierasch, 1975).

High winds circle the planet from east to west, at speeds 60 times faster than rotation of the solid planet (Schubert, 1983). Peaking at 120 m s^{-1} at the equatorial cloud tops, this super rotating zonal flow decreases almost linearly with depth down to the surface. With its speed and mass, the atmosphere has 0.1% of the angular momentum of the entire planet, peaking at 21 km above the surface. Large-scale cells that arise from equatorial heating of the clouds transport heat and momentum to high latitudes. A deeper return flow, perhaps in the form of eddies beneath the clouds, must exist but has never been observed (Gierasch et al, 1997).

Zonal winds decrease with increasing latitude until they transition to the giant polar vortices (Piccioni et al, 2007; Limaye et al, 2009; Luz et al, 2011) at about the same latitude as the descending branch of the hemispheric meridional circulation (Imamura and Hashimoto, 1998). The high mass of Venus's atmosphere makes it very opaque across all wavelengths, making it the primary reason for the planet's high surface temperature. In addition, Venus's clouds as well as its CO_2 concentration further increase its opacity, though the latter only con-tributes at specific infrared wavelengths.

2.1. Pressure-Temperature Profile

Venus is characterized as having an atmosphere 92 times more massive than that of the Earth. Consequently, the surface pressure reaches 92 bars, which is also larger than the Earth by that same

amount. Like the Earth, Venus exhibits a temperature inversion above the cloud layers. However, clouds on Venus (~50 km) are at a much higher altitude than those on Earth (~10 km). Solar heating is primarily responsible for the temperature increase above 100 km.

At the middle altitudes in the upper stratosphere where the temperature is already constant as a function of height, the temperature is also mostly constant throughout each day-night cycle, despite Venus's incredibly slow rotation period. For example, at 115 km, the temperature is fixed at 180 K to within 15 K. However in both the upper and lower atmosphere, there is a much more significant difference due to the length of Venus's day. For example, at 150 km, the temperature reaches 300 K during the day, but drops to below 150 K during the night.

Venus has very little temperature variation as a function of latitude. Despite its high temperatures, the poles are only 30 K colder than the equator). Venus has very little temperature variation as a function of latitude. Despite its high temperatures, the poles are only 30 K colder than the equator (Taylor, 2014).

2.2. The Atmosphere Profiles

The middle parts of these profiles (40 to 100 km (the stratosphere) was measured with the radio occultation experiment aboard the Pioneer Venus Orbiter (Kliore and Patel, 1980). In this method, the orbiter emits a radio signal from behind Venus and through its atmosphere. The signal is then detected based on the atmosphere's precise temperature and pressure at the tangent point. After exiting the atmosphere, the signal travels to either JPL Deep Space Network (DSS-14) or Tidbinbilla, Australia (DSS-43) depending on the time of day. The orbiter uses two different wavelengths: the X-band (3.5 cm) and the S-band (13 cm). It also maintains a local oscillator at each of these frequencies in order to measure the detection later. Even with this local reference signal, determining the detection is not straightforward due to the signal's high wavelength. As a result, the detection can only be measured in directly through the signal's

Doppler shift, which is then decomposed into an index of refraction mathematically using an Abel transform a "Fourier transform" for spherically symmetric functions. The temperature and pressure can then be extracted from the index of refraction. Radio occultations are preferred for measuring these profiles because they have the highest resolution of any method at better than 1 km (Lellouch et al, 1997).

At higher altitudes (> 100 km - the thermosphere) corresponding to lower pressures, the temperature profiles were measured with thermal sensors on descent probes from Pioneer and Venera 8-12. The density profiles, which are needed for determining the pressure, are measured with accelerometers also on board the descent probes (Lellouch et al, 1997).

The lowest altitudes (< 40 km - the troposphere) are probed using near-infrared sounding at 0.9 to 2.5 μm on the night-side of the planet. This emission can be measured from the ground in addition to from space.

At these wavelengths, very little of the emission is scattered due to the size and properties of the sulfuric acid cloud droplets that scatter light. Similarly, very little of the emission is absorbed since the relevant CO2 spectral lines are not as broad as expected. As a result, the atmosphere is very optically thin, making the light that escapes into space perfect for examining the lower atmosphere (Taylor et al, 1997).

The temperature profile can also be measured through spectroscopy using assorted molecular bands (e.g. CO_2 4.3 μm or 15 μm) or lines (e.g. CO J = 2 → 1). This method takes advantage of the fact that specific frequency intervals correspond to particular altitudes depending on the transmission from a given pressure level to space. Spectroscopic methods only have a resolution of 5 to 10 km (Lellouch et al, 1997).

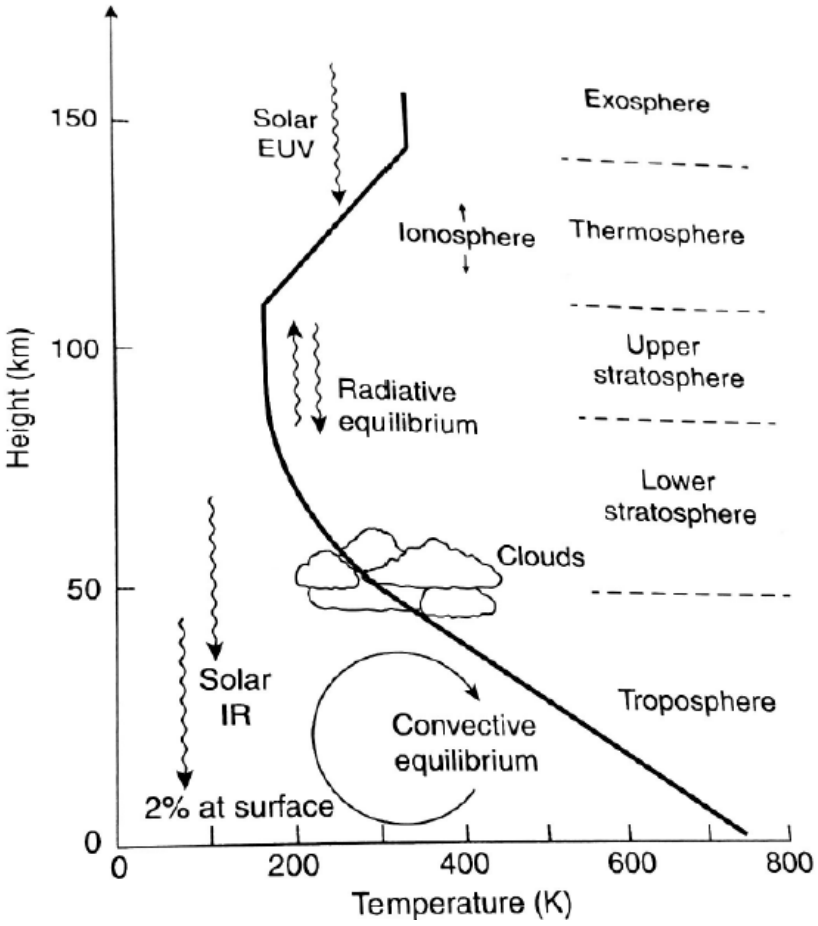

Figure 2.1 Altitude-temperature profile of Venus (Taylor 2014).

A second spectroscopic method involves extracting temperatures from relative strengths of spectral lines in nightglow emission. This emission can come from a variety of sources including cosmic ray luminescence, energy from chemical reactions, and atoms that were ionized during the day recombining.

2.3. Atmosphere Composition

The atmosphere of Venus is composed of 96.5% carbon dioxide, 3.5% nitrogen, and traces of other gases, most notably sulfur dioxide. The

amount of nitrogen in the atmosphere is relatively small compared to the amount of carbon dioxide, but because the atmosphere is so much thicker than that on Earth, its total nitrogen content is roughly four times higher than Earth's, even though on Earth nitrogen makes up about 78% of the atmosphere (Basilevsky and Head, 2003).

The atmosphere contains a range of compounds in small quantities, including some based on hydrogen, such as hydrogen chloride (HCl) and hydrogen fluoride (HF). There is carbon monoxide, water vapour and atomic oxygen as well. Hydrogen is in relatively short supply in the Venusian atmosphere. A large amount of the planet's hydrogen is theorized to have been lost to space, with the remainder being mostly bound up in sulfuric acid (H_2SO_4) and hydrogen sulfide (H_2S). The loss of significant amounts of hydrogen is proven by a very high D/H ratio measured in the Venusian atmosphere. The ratio is about 0.015–0.025, which is 100–150 times higher than the terrestrial value of 1.6×10^{-4} (Krasnopolsky et al, 2013). According to some measurements, in the upper atmosphere of Venus D/H ratio is 1.5 higher than in the bulk atmosphere.

2.3.1. Troposphere

The atmosphere is divided into a number of sections depending on altitude. The densest part of the atmosphere, the troposphere, begins at the surface and extends upwards to 65 km. At the furnace-like surface the winds are slow, but at the top of the troposphere the temperature and pressure reaches Earth-like levels and clouds pick up speed to 100 m/s (360 km/h) (Svedhem et al, 2007).

The atmospheric pressure at the surface of Venus is about 92 times that of the Earth, similar to the pressure found 900 m (3,000 ft) below the surface of the ocean. The atmosphere has a mass of 4.8×10^{20} kg, about 93 times the mass of the Earth's total atmosphere. The density of the air at the surface is 67 kg/m^3, which is 6.5% that of liquid water on Earth (Basilevsky and Head, 2003). The pressure found on Venus's surface is high enough that the carbon dioxide is technically no longer a gas, but a supercritical fluid. This supercritical carbon dioxide forms

a kind of sea that covers the entire surface of Venus. This sea of supercritical carbon dioxide transfers heat very efficiently, buffering the temperature changes between night and day (which last 56 terrestrial days) (Fegley et al, 1997).

The large amount of CO_2 in the atmosphere together with water vapour and sulfur dioxide create a strong greenhouse effect, trapping solar energy and raising the surface temperature to around 740 K (467 °C), hotter than any other planet in the Solar System, even that of Mercury despite being located farther out from the Sun and receiving only 25% of the solar energy (per unit area) Mercury does. The average temperature on the surface is above the melting points of lead (600 K, 327 °C), tin (505 K, 232 °C), and zinc (693 K, 420 °C). The thick troposphere also makes the difference in temperature between the day and night side small, even though the slow retrograde rotation of the planet causes a single solar day to last 116.5 Earth days. The surface of Venus spends 58.3 days in darkness before the sun rises again behind the clouds.

The troposphere on Venus contains 99% of the atmosphere by mass. Ninety percent of the atmosphere of Venus is within 28 km of the surface; by comparison, 90% of the atmosphere of Earth is within 10 km of the surface. At a height of 50 km the atmospheric pressure is approximately equal to that at the surface of Earth. On the night side of Venus clouds can still be found at 80 km above the surface (Nave, 2008).

The altitude of the troposphere most similar to Earth is near the tropopause—the boundary between troposphere and mesosphere. It is located slightly above 50 km. According to measurements by the *Magellan* and *Venus Express* probes, the altitude from 52.5 to 54 km has a temperature between 293 K (20 °C) and 310 K (37 °C), and the altitude at 49.5 km above the surface is where the pressure becomes the same as Earth at sea level. As manned ships sent to Venus would be able to compensate for differences in temperature to a certain extent, anywhere from about 50 to 54 km or so above the surface would be the easiest altitude in which to base an exploration or

colony, where the temperature would be in the crucial "liquid water" range of 273 K (0 °C) to 323 K (50 °C) and the air pressure the same as habitable regions of Earth (Landis et al., 2002). As CO_2 is heavier than air, the colony's air (nitrogen and oxygen) could keep the structure floating at that altitude like a dirigible.

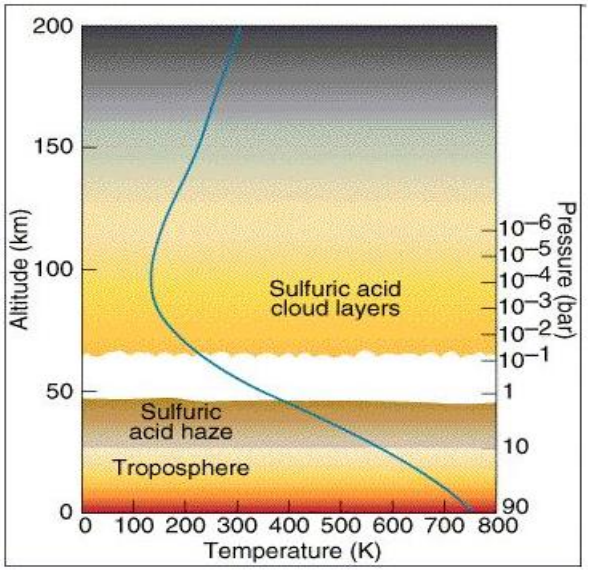

Figure 2.2 The structure of the atmosphere of Venus, as determined by U.S. probes.

2.3.2. Troposphere Circulation

The circulation in Venus's troposphere follows the so-called cyclostrophic flow. Its wind speeds are roughly determined by the balance of the pressure gradient and centrifugal forces in almost purely zonal flow. In contrast, the circulation in the Earth's atmosphere is governed by the geostrophic balance (Svedhem et al, 2007). Venus's windspeeds can be directly measured only in the upper troposphere (tropopause), between 60-70 km altitudes, which corresponds to the upper cloud deck. The cloud motion is usually observed in the ultraviolet part of the spectrum, where the contrast

between clouds is the highest. The linear wind speeds at this level are about 100 ± 10 m/s at lower than 50° latitude. They are retrograde in the sense that they blow in the direction of the retrograde rotation of the planet (Markiewicz et al, 2007).

The winds quickly decrease towards the higher latitudes, eventually reaching zero at the poles. Such strong cloud-top winds cause a phenomenon known as the super-rotation of the atmosphere (Svedhem et al., 2007). In other words, these high-speed winds circle the whole planet faster than the planet itself rotates. The super-rotation on Venus is differential, which means that the equatorial troposphere super-rotates more slowly than the troposphere at the mid-latitudes (Markiewicz et al, 2007). The winds also have a strong vertical gradient. They decline deep in the troposphere with the rate of 3 m/s per km (Svedhem et al, 2007). The winds near the surface of Venus are much slower than that on Earth. They actually move at only a few kilometers per hour (generally less than 2 m/s and with an average of 0.3 to 1.0 m/s), but due to the high density of the atmosphere at the surface, this is still enough to transport dust and small stones across the surface, much like a slow-moving current of water (Moshkin et al, 1979).

All winds on Venus are ultimately driven by convection. Hot air rises in the equatorial zone, where solar heating is concentrated, and flows to the poles. Such an almost-planetwide overturning of the troposphere is called Hadley circulation. However, the meridional air motions are much slower than zonal winds. The poleward limit of the planet wide Hadley cell on Venus is near ±60° latitudes (Svedhem et al, 2007). Here air starts to descend and returns to the equator below the clouds. This interpretation is supported by the distribution of the carbon monoxide, which is also concentrated in the vicinity of ±60° latitudes. Poleward of the Hadley cell a different pattern of circulation is observed. In the latitude range 60°–70° cold polar collars exist. They are characterised by temperatures about 30–40 K lower than in the upper troposphere at nearby latitudes (Piccioni et al, 2007).

The lower temperature is probably caused by the upwelling of the

air in them and by the resulting adiabatic cooling. Such an interpretation is supported by the denser and higher clouds in the collars. The clouds lie at 70–72 km altitude in the collars—about 5 km higher than at the poles and low latitudes (Svedhem et al, 2007). A connection may exist between the cold collars and high speed midlatitude jets in which winds blow as fast as 140 m/s. Such jets are a natural consequence of the Hadley–type circulation and should exist on Venus between 55–60° latitude (Markiewicz et al, 2007).

Odd structures known as polar vortices lie within the cold polar collars. They are giant hurricane-like storms four times larger than their terrestrial analogs. Each vortex has two "eyes"—the centres of rotation, which are connected by distinct S-shaped cloud structures. Such double eyed structures are also called polar dipoles. Vortices rotate with the period of about 3 days in the direction of general super-rotation of the atmosphere. The linear wind speeds are 35–50 m/s near their outer edges and zero at the poles (Piccioni et al, 2007). The temperature at the cloud-tops in the each polar vortex is much higher than in the nearby polar collars reaching 250 ^{o}K (−23 °C). The conventional interpretation of the polar vortices is that they are anticyclones with downwelling in the centre and upwelling in the cold polar collars. This type of circulation resembles a winter polar anticyclonic vortex on Earth, especially the one found over Antarctica. The observations in the various infrared atmospheric windows indicate that the anticyclonic circulation observed near the poles penetrates as deep as to 50 km altitude, i.e. to the base of the clouds (Piccioni et al, 2007). The polar upper troposphere and mesosphere are extremely dynamic; large bright clouds may appear and disappear over the space of a few hours. One such event was observed by Venus Express between 9 and 13 January 2007, when the South Polar Region became brighter by 30% (Markiewicz et al, 2007). This event was probably caused by an injection of sulfur dioxide into the mesosphere, which then condensed forming a bright haze (Markiewicz et al, 2007). The two eyes in the vortices have yet to be explained.

2.3.3. Upper Atmosphere and Ionosphere

The mesosphere of Venus extends from 65 km to 120 km in height, and the thermosphere begins at approximately 120 km, eventually reaching the upper limit of the atmosphere (exosphere) at about 220 to 350 km (Patzold et al, 2007). The exosphere is the altitude at which the atmosphere becomes collisionless.

The mesosphere of Venus can be divided into two layers: the lower one between 62–73 km and the upper one between 73-95 kms. In the first layer the temperature is nearly constant at 230 K (−43 °C). This layer coincides with the upper cloud deck. In the second layer temperature starts to decrease again reaching about 165 K (−108 °C) at the altitude of 95 km, where mesopause begins (Patzold, et al, 2007). It is the coldest part of the Venusian dayside atmosphere. In the dayside mesopause, which serves as a boundary between the mesophere and thermosphere and is located between 95–120 km, temperature increases to a constant "about 300–400 K (27–127 °C)"value prevalent in the thermosphere. In contrast, the nightside Venusian thermosphere is the coldest place on Venus with temperature as low as 100 K (−173 °C). It is even called a cryosphere (Bertaux et al, 2007).

The circulation patterns in the upper mesosphere and thermosphere of Venus are completely different from those in the lower atmosphere. At altitudes 90–150 km the Venusian air moves from the dayside to nightside of the planet, with upwelling over sunlit hemisphere and downwelling over dark hemisphere. The downwelling over the nightside causes adiabatic heating of the air, which forms a warm layer in the nightside mesosphere at the altitudes 90–120 km. The temperature of this layer—230 K (−43 °C) is far higher than the typical temperature found in the nightside thermosphere—100 °K (−173 °C) (Bertaux et al, 2007). The air circulated from the dayside also carries oxygen atoms, which after recombination form excited molecules of oxygen in the long-lived singlet state ($^1\Delta_g$), which then relax and emit infrared radiation at the wavelength 1.27 μm. This

radiation from the altitude range 90–100 km is often observed from the ground and spacecraft. The nightside upper mesosphere and thermosphere of Venus is also the source of non-local thermodynamic equilibrium emissions of CO_2 and nitric oxide molecules, which are responsible for the low temperature of the nightside thermosphere.

The Venus Express probe has shown through stellar occultation that the atmospheric haze extends much further up on the night side than the day side. On the day side the cloud deck has a thickness of 20 km and extends up to about 65 km, whereas on the night side the cloud deck in the form of a thick haze reaches up to 90 km in altitude—well into mesosphere, continuing even further to 105 km as a more transparent haze. In 2011, the spacecraft discovered that Venus has a thin ozone layer at an altitude of 100 km.

Venus has an extended ionosphere located at altitudes 120–300 km. The ionosphere almost coincides with the thermosphere. The high levels of the ionization are maintained only over the dayside of the planet. Over the nightside the concentration of the electrons is almost zero. The ionosphere of Venus consists of three layers: v1 between 120 and 130 km, v2 between 140 and 160 km and v3 between 200 and 250 km (Patzold, et al, 2007). There may be an additional layer near 180 km. The maximum electron volume density (number of electrons in a unit of volume) 3×10^{11} m^{-3} is reached in the v2 layer near the subsolar point. The upper boundary of the ionosphere—ionopause is located at altitudes 220–375 km and separates the plasma of the planetary origin from that of the induced magnetosphere (Russell, 1993). The main ionic species in the v1 and v2 layers is O_2^+ ion, whereas the v3 layer consists of O^+ ions (Patzold et al, 2007). The ionospheric plasma is observed to be in motion; solar photoionization on the dayside, and ion recombination on the nightside, are the processes mainly responsible for accelerating the plasma to the observed velocities. The plasma flow appears to be sufficient to maintain the nightside ionosphere at or near the observed median level of ion densities (Whitten et al, 1984).

2.4. Lapse Rates

A formal definition from the Glossary of Meteorology about lapse rate is:

The decrease of an atmospheric variable with height, the variable being temperature unless otherwise specified.

Typically, the lapse rate under consideration is the negative of the rate of temperature change with altitude change, thus

2.4.1. Dry Lapse Rate

$$\Gamma = -\frac{dT}{dz} \qquad (1)$$

Where Γ is the lapse rate given in units of temperature divided by units of altitude, T is temperature, and z is altitude.

The dry-lapse rate is given by

$$\Gamma_d = -\frac{dT}{dz} = \frac{g}{c_p}. \qquad (2)$$

With a mass of MV = 0:82 Mv = 4:87 ×10^{24} kg and a radius of RV = 0:95 Rv = 6:05 × 10^3 km, Venus has a surface gravity of gv= 8.87m.s^{-2}. The specific heat capacity at constant pressure, cp, can be determined easily by approximating the atmosphere which is 96:5% CO_2 as purely carbon dioxide. At the surface, Venus has an air pressure of 92 bars and a temperature of 740 K. Under these conditions, cp = 1.16 kJ.Kg^{-1}.K^{-1} for pure CO_2.

Just above the surface at 50 km, Venus has a pressure of 1.08 bars and a temperature of 350 ^oK, corresponding to cp = 0.90 kJ.Kg^{-1}.K^{-1}. Thus, at the surface, Venus has a dry lapse rate of Γd = 7.6 K.km^{-1}. At an altitude of 50 km, Γd = 9.9 K.km^{-1}, a sharp increase from the surface already.

2.4.2. Wet Lapse Rate

The wet lapse rate is given by

$$\Gamma_{\mathrm{w}} = g \frac{\left(1 + \frac{H_{\mathrm{v}}\, r}{R_{\mathrm{sd}}\, T}\right)}{\left(c_{\mathrm{pd}} + \frac{H_{\mathrm{v}}^2\, r}{R_{\mathrm{sw}}\, T^2}\right)} \qquad (3)$$

where g = 8.87 m / s^2 is Venus's surface gravity, H_v = 2.5 × 106 J.kg^{-1} is the latent heat of water, R_{sw} = 287.9 J.Kg^{-1}.K^{-1} is the specific gas constant of dry air, R_{sw} = 461.5 J.Kg^{-1}. K^{-1} is the specific gas constant of water vapor, cp = 1.16 kJ.Kg^{-1}.K^{-1} is the specific heat capacity, and r = (R*sd*=R*sw*) × pw=(p -pw) = 4×10^{-5} is the mixing ratio of water to air. Since the partial pressure of water pw/p = 10^{-4} ≪ 1, the difference between the dry lapse rate and the wet lapse rate is negligible. At the surface, Γw = 7.6 K.km^{-1}. At 50 km, = 9.8 K.km^{-1}. At 50 km, Γ_w = 9.8 K.km^{-1}.

2.4.3. Comparison

Below an altitude of 55 km (0.5 bars), the temperature gradient is in good agreement with the dry lapse rate. Figure 3 shows the atmosphere's static stability, the difference between the actual temperature gradient and the dry lapse rate (*d*T/*d*Z-Γ).

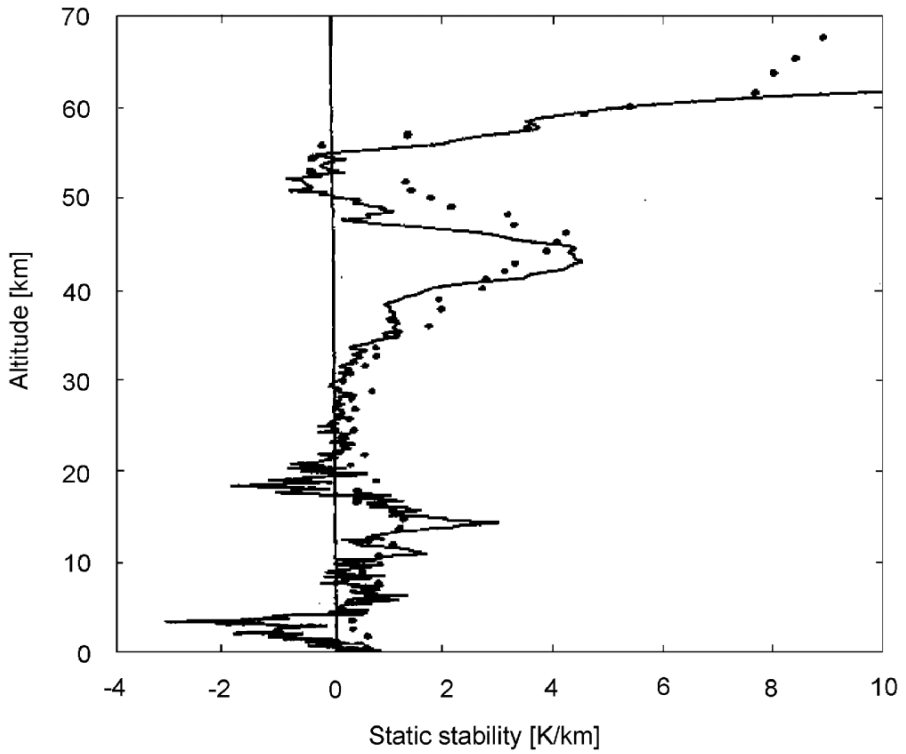

Figure 2.3 Static stability of atmosphere for VEGA 2 data (solid line) and the VIRA model (dots). The VEGA 2 data suggests the atmosphere is unstable at altitudes of 2-4 km, near 18 km, and at 49-55 km (Zasova et al. 2007).

At very close to the surface (2 to 4 km), in the middle of the troposphere (near 18 km), and near the top of the troposphere (49 to 55 km), the static stability is negative. This suggests the atmosphere is slightly unstable at these altitudes. The top region of instability may be due to the presence of clouds. Despite this agreement with the dry lapse rate, Venus is still much hotter than the blackbody temperature one would expect from just solar heating.

2.5. Greenhouse Effect

Like the Earth, Venus's actual surface temperature is much higher than the planet's effective temperature based on its albedo and its distance

from the Sun. Unlike the Earth, that difference is more than a factor of three, while on Earth it is only about 15%. This greenhouse effect results from the atmosphere's variation in opacity as a function

The origin of the greenhouse effect resides in the fact that planets do not emit light in the same wavelength range as the Sun. With the Sun's temperature of 5770 ^{o}K, it emits a Planck spectrum that peaks in the visible range. However, since Venus is much colder than the Sun, it emits a Planck spectrum that peaks in the infrared (μm) range that for the most part, does not overlap with the received light from the Sun. As a result, the light from the Sun may be able to pass through the atmosphere (in its wavelength range), but the energy re-emitted by the planet may not be able to escape the atmosphere into space (since it emits in a different wavelength range).

On Venus, only a very small fraction of sunlight reaches the planet, with 77% reflected and just 3% absorbed by the surface. Meanwhile, the remaining 20% is absorbed by the atmosphere, which then tries to reradiate it uniformly in all directions. However, the extremely high mass of the atmosphere makes it easy for the planet to trap any radiation that the atmosphere is re-emitting. The clouds further contribute to making the planet opaque to outgoing radiation. Yet even without these clouds, the planet's surface would still be extremely hot. Additionally, the atmosphere's high CO_2 concentration further increases the opacity, but only at the wavelengths where CO_2 absorbs. Since the planet needs to be opaque across the entire wavelength range where it is re-emitting light in order to have a strong greenhouse effect, CO_2 is not the primary driver of Venus's high surface temperature.

2.6. Atmosphere Circulation

The circulation in Venus's troposphere follows the so-called cyclostrophic flow. Its wind speeds are roughly determined by the balance of the pressure gradient and centrifugal forces in almost purely zonal flow. In contrast, the circulation in the Earth's atmosphere is governed by the geostrophic balance (Svedhem et al,

2007). Venus's wind speeds can be directly measured only in the upper troposphere (tropopause), between 60-70 km, altitude, which corresponds to the upper cloud deck. The cloud motion is usually observed in the ultraviolet part of the spectrum, where the contrast between clouds is the highest (Markiewicz et al, 2007). The linear wind speeds at this level are about 100 ± 10 m/s at lower than 50° latitude. They are retrograde in the sense that they blow in the direction of the retrograde rotation of the planet. The winds quickly decrease towards the higher latitudes, eventually reaching zero at the poles. Such strong cloud-top winds cause a phenomenon known as the super-rotation of the atmosphere. In other words, these high-speed winds circle the whole planet faster than the planet itself rotates. The super-rotation on Venus is differential, which means that the equatorial troposphere super-rotates more slowly than the troposphere at the midlatitudes (Markiewicz et al, 2007). The winds also have a strong vertical gradient. They decline deep in the troposphere with the rate of 3 m/s per km. The winds near the surface of Venus are much slower than that on Earth. They actually move at only a few kilometres per hour (generally less than 2 m/s and with an average of 0.3 to 1.0 m/s), but due to the high density of the atmosphere at the surface, this is still enough to transport dust and small stones across the surface, much like a slow-moving current of water (Moshkin et al, 1979).

All winds on Venus are ultimately driven by convection. Hot air rises in the equatorial zone, where solar heating is concentrated, and flows to the poles. Such an almost-planetwide overturning of the troposphere is called Hadley circulation. However, the meridional air motions are much slower than zonal winds. The poleward limit of the planet wide Hadley cell on Venus is near ±60° latitudes. Here air starts to descend and returns to the equator below the clouds. This interpretation is supported by the distribution of the carbon monoxide, which is also concentrated in the vicinity of ±60° latitudes. Poleward of the Hadley cell a different pattern of circulation is observed. In the latitude range 60°–70° cold polar collars exist (Piccioni et al, 2007).

They are characterized by temperatures about 30–40 °K lower than in the upper troposphere at nearby latitudes. The lower temperature is probably caused by the upwelling of the air in them and by the resulting adiabatic cooling. Such an interpretation is supported by the denser and higher clouds in the collars. The clouds lie at 70–72 km altitude in the collars- about 5 km higher than at the poles and low latitudes (Svedhem et al, 2007). A connection may exist between the cold collars and high speed midlatitude jets in which winds blow as fast as 140 m/s. Such jets are a natural consequence of the Hadley–type circulation and should exist on Venus between 55–60° latitude (Markiewicz et al, 2007).

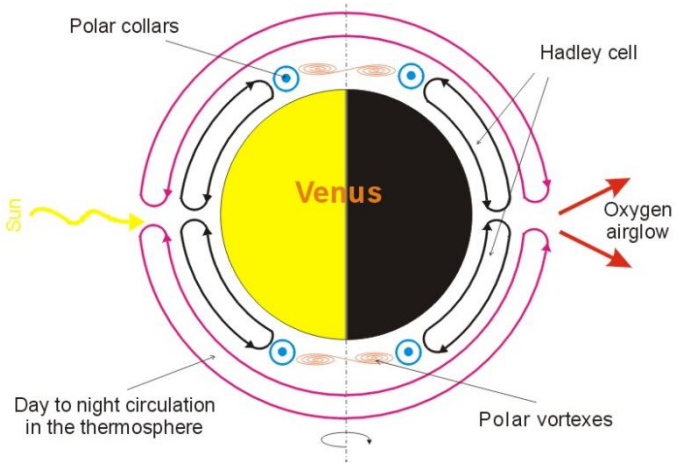

Figure 2.4 Meridional (north–south) component of the atmospheric circulation in the atmosphere of Venus.

Note that the meridional circulation is much lower than the zonal circulation, which transports heat between the day and night sides of the planet.

Odd structures known as polar vortices lie within the cold polar collars. They are giant hurricane-like storms four times larger than their terrestrial analogs. Each vortex has two "eyes"—the centres of rotation, which are connected by distinct S-shaped cloud structures. Such double eyed structures are also called polar dipoles (Piccioni et

al, 2007). Vortices rotate with the period of about 3 days in the direction of general super-rotation of the atmosphere. The linear wind speeds are 35–50 m/s near their outer edges and zero at the poles. The temperature at the cloud-tops in the each polar vortex is much higher than in the nearby polar collars reaching 250 K (−23 °C). The conventional interpretation of the polar vortices is that they are anticyclones with downwelling in the centre and upwelling in the cold polar collars (Piccioni et al, 2007). This type of circulation resembles a winter polar anticyclonic vortex on Earth, especially the one found over Antarctica. The observations in the various infrared atmospheric windows indicate that the anticyclonic circulation observed near the poles penetrates as deep as to 50 km altitude, i.e. to the base of the clouds. The polar upper troposphere and mesosphere are extremely dynamic; large bright clouds may appear and disappear over the space of a few hours. One such event was observed by Venus Express between 9 and 13 January 2007, when the South Polar Region became brighter by 30%. This event was probably caused by an injection of sulfur dioxide into the mesosphere, which then condensed forming a bright haze. The two eyes in the vortices have yet to be explained.

2.7. Atmosphere and Ionosphere

The mesosphere of Venus extends from 65 km to 120 km in height, and the thermosphere begins at approximately 120 km, eventually reaching the upper limit of the atmosphere (exosphere) at about 220 to 350 km. The exosphere is the altitude at which the atmosphere becomes collisionless.

The mesosphere of Venus can be divided into two layers: the lower one between 62–73 kmand the upper one between 73–95 km (Patzold et al, 2007). In the first layer the temperature is nearly constant at 230 K (−43 °C). This layer coincides with the upper cloud deck. In the second layer temperature starts to decrease again reaching about 165 K (−108 °C) at the altitude of 95 km, where mesopause begins. It is the coldest part of the Venusian dayside atmosphere. In the dayside mesopause, which serves as a boundary between the mesophere and

thermosphere and is located between 95–120 km, temperature increases to a constant—about 300–400 K (27–127 °C)—value prevalent in the thermosphere. In contrast, the nightside Venusian thermosphere is the coldest place on Venus with temperature as low as 100 K (−173 °C). It is even called a cryosphere.

The circulation patterns in the upper mesosphere and thermosphere of Venus are completely different from those in the lower atmosphere. At altitudes 90–150 km the Venusian air moves from the dayside to nightside of the planet, with upwelling over sunlit hemisphere and downwelling over dark hemisphere. The downwelling over the nightside causes adiabatic heating of the air, which forms a warm layer in the nightside mesosphere at the altitudes 90–120 km (Taylor and Witasse, 2007). The temperature of this layer—230 K (−43 °C) is far higher than the typical temperature found in the nightside thermosphere—100 K (−173 °C). The air circulated from the dayside also carries oxygen atoms, which after recombination form excited molecules of oxygen in the long-lived singlet state ($^1\Delta_g$), which then relax and emit infrared radiation at the wavelength 1.27 μm. This radiation from the altitude range 90–100 km is often observed from the ground and spacecraft. The nightside upper mesosphere and thermosphere of Venus is also the source of non-local thermodynamic equilibrium emissions of CO_2 and nitric oxide molecules, which are responsible for the low temperature of the nightside thermosphere.

The Venus Express probe has shown through stellar occultation that the atmospheric haze extends much further up on the night side than the day side. On the day side the cloud deck has a thickness of 20 km and extends up to about 65 km, whereas on the night side the cloud deck in the form of a thick haze reaches up to 90 km in altitude—well into mesosphere, continuing even further to 105 km as a more transparent haze. In 2011, the spacecraft discovered that Venus has a thin ozone layer at an altitude of 100 km.

Venus has an extended ionosphere located at altitudes 120–300 km (Patzold et al, 2007). The ionosphere almost coincides with the thermosphere. The high levels of the ionization are maintained only

over the dayside of the planet. Over the nightside the concentration of the electrons is almost zero. The ionosphere of Venus consists of three layers: v1 between 120 and 130 km, v2 between 140 and 160 km and v3 between 200 and 250 km. There may be an additional layer near 180 km. The maximum electron volume density (number of electrons in a unit of volume) 3×10^{11} m^{-3} is reached in the v2 layer near the subsolar point (Patzold, et al. 2007). The upper boundary of the ionosphere—ionopause is located at altitudes 220–375 km and separates the plasma of the planetary origin from that of the induced magnetosphere.[32][33] The main ionic species in the v1 and v2 layers is O_2^+ ion, whereas the v3 layer consists of O^+ ions (Patzold, et al, 2007). The ionospheric plasma is observed to be in motion; solar photoionization on the dayside, and ion recombination on the nightside, are the processes mainly responsible for accelerating the plasma to the observed velocities. The plasma flow appears to be sufficient to maintain the nightside ionosphere at or near the observed median level of ion densities.

2.8. Induced Magnetosphere

Venus is known not to have a magnetic field. The reason for its absence is not at all clear, but it may be related to a reduced intensity of convection in the Venusian mantle. Venus only has an induced magnetosphere formed by the Sun's magnetic field carried by the solar wind.[32] This process can be understood as the field lines wrapping around an obstacle—Venus in this case. The induced magnetosphere of Venus has a bow shock, magnetosheath, magnetopause and magnetotail with the current sheet (Zhang et al, 2007).

At the subsolar point the bow shock stands 1900 km (0.3 R_v, where R_v is the radius of Venus) above the surface of Venus. This distance was measured in 2007 near the solar activity minimum. Near the solar activity maximum it can be several times further from the planet. The magnetopause is located at the altitude of 300 km (Zhang et al, 2007). The upper boundary of the ionosphere (ionopause) is near 250 km. Between the magnetopause and ionopause there exists a magnetic

barrier—a local enhancement of the magnetic field, which prevents solar plasma from penetrating deeper into the Venusian atmosphere, at least near solar activity minimum. The magnetic field in the barrier reaches up to 40 nT (Zhang et al, 2007). The magnetotail continues up to ten radii from the planet. It is the most active part of the Venusian magnetosphere. There are reconnection events and particle acceleration in the tail. The energies of electrons and ions in the magnetotail are around 100 eV and 1000 eV respectively (Barabash et al, 2007).

Due to the lack of the intrinsic magnetic field on Venus, the solar wind penetrates relatively deep into the planetary exosphere and causes substantial atmosphere loss. The loss happens mainly via the magnetotail. Currently the main ion types being lost are O^+, H^+ and He^+. The ratio of hydrogen to oxygen losses is around 2 (i.e. almost stoichiometric) indicating the ongoing loss of water (Barabash et al, 2007).

2.9. Clouds

Venusian clouds are thick and are composed mainly (75-96%) of sulfuric acid droplets (Wilson, 2014). These clouds obscure the surface of Venus from optical imaging, and reflect about 75% of the sunlight that falls on them (Basilevsky and Head, 2003). The geometric albedo, a common measure of reflectivity, is the highest of any planet in the Solar System. This high reflectivity potentially enables any probe exploring the cloud tops sufficient solar energy such that solar cells can be fitted anywhere on the craft (Landis, 2001). The density of the clouds is highly variable with the densest layer at about 48.5 km, reaching 0.1 g/m^3 similar to the lower range of cumulonimbus storm clouds on Earth (Lee, 2012).

The cloud cover is such that typical surface light levels are similar to a partly cloudy day on Earth, around 5000–10000 lux. The equivalent visibility is about three kilometers, but this will likely vary with the wind conditions. Little to no solar energy could conceivably be collected by solar panels on a surface probe. In fact, due to the

thick, highly reflective cloud cover, the total solar energy received by the surface of the planet is less than that of the Earth.

Sulfuric acid is produced in the upper atmosphere by the Sun's photochemical action on carbon dioxide, sulfur dioxide, and water vapour. Ultraviolet photons of wavelengths less than 169 nm can photodissociate carbon dioxide into carbon monoxide and atomic oxygen. Atomic oxygen is highly reactive; when it reacts with sulfur dioxide, a trace component of the Venusian atmosphere, the result is sulfur trioxide, which can combine with water vapour, another trace component of Venus's atmosphere, to yield sulfuric acid (Krasnopolsky and Parshev, 1981).

$$CO_2 \rightarrow CO + O$$
$$SO_2 + O \rightarrow SO_3$$
$$2SO_3 + 4H_2O \rightarrow 2H_2SO_4 + H_2O$$

Surface level humidity is less than 0.1% Venus's sulfuric acid rain never reaches the ground, but is evaporated by the heat before reaching the surface in a phenomenon known as virga. It is theorized that early volcanic activity released sulfur into the atmosphere and the high temperatures prevented it from being trapped into solid compounds on the surface as it was on the Earth. In 2009 a prominent bright spot in the atmosphere was noted by an amateur astronomer and photographed by Venus Express. Its cause is currently unknown, with surface volcanism advanced as a possible explanation (Koehler, 1982).

2.10. Lightning

The clouds of Venus may be capable of producing lightning, but the debate is ongoing, with volcanic lightning and sprites also under discussion (Lorenz, 2018).

The Soviet Venera 9 and 10 orbiters obtained ambiguous optical and electromagnetic evidence of lightning (Russell and Phillips, 1990). The European Space Agency's Venus Express in 2007 detected whistler waves which could be attributed to lightning. Their

intermittent appearance indicates a pattern associated with weather activity. According to the whistler observations, the lightning rate is at least half of that on Earth, but this is incompatible with data from the JAXA Akatsuki spacecraft which indicate a very low flash rate (Lorenz et al, 2019).

The mechanism generating lightning on Venus, if present, remains unknown. Whilst the sulfuric acid cloud droplets can become charged, the atmosphere may be too electrically conductive for the charge to be sustained, preventing lightning (Michael et al, 2009).
Throughout the 1980s, it was thought that the cause of the night-side glow ("ashen glow") on Venus was lightning.

2.11. Absence of Water on Venus

Venus is Earth's twin in many ways, so its lack of liquid water oceans has perplexed scientists. A new study suggests that Venus might be about 7 million miles too close to the sun. Therein lies a steamy tale of early planetary evolution, one whose different endings were determined from the outset by location, rather than by processes that sent the two on divergent paths later in their histories, according to a new study.

If the analysis holds up to further scrutiny, it not only could help answer the Earth-Venus riddle. It also could help scientists studying extrasolar planets pin down more precisely a star's habitable zone, or help them identify rocky planets in habitable zones that are still working their way through their molten youth, some researchers say.

Figure 2.5 Of all the planetary-science questions we have, the question of why are the Earth and Venus different is the most gigantic and fundamental unanswered question we've got," says Lindy Elkins-Tanton, a researcher who studies planet evolution. If scientists want to say they know anything about what makes for a habitable planet, she says, "We'd better be able to answer that one.

Venus lost its water through a runaway greenhouse effect based on its closer proximity to the sun and the copious amounts of heat-trapping water vapor in its early atmosphere, reinforced by the lack of a carbon cycle, which partitions and recycles heat-trapping carbon dioxide (CO^2) among oceans, living things, and rocks. Earth retained its supply of water because it has these and other features. Each general explanation, however, presumes the planets had first cooled to host solid crusts.

The new work represents "the first model that suggests that the planets accreted with the same wet material, but Venus lost its water as it was solidifying, not afterwards," says Dr. Elkins-Tanton, who was not part of the research team.

The story, as set out by a trio of Japanese scientists led by the University of Tokyo's Keiko Hamano, begins with the generally

accepted picture of rocky planets building from primordial, rocky chunks that dominated the inner regions of the disk of dust and gas that surrounded the young sun some 4.6 billion years ago. Growth often was a violent process, aided by collisions with other massive objects trying to become planets. These collisions generated heat sufficient to periodically cover the planets with relatively deep oceans of magma. Meanwhile, water was ubiquitous in clouds of gas and dust that gave rise to stars and planets. The recurring collisions that kept the crust molten before Earth and Venus solidified released the water bound up in the once-solid minerals as steam.

How much water did that degassing deliver? In 1986, another team of planetary scientists in Japan calculated an amount comparable to the water contained in the modern world's oceans, lakes, ice, rivers, and in the atmosphere as water vapor. Since then, researchers have refined those estimates somewhat – and collisions with comets and asteroids have helped Earth maintain its inventory of water – but the findings essentially stand. In other words, a day at the beach means swimming in the distilled remains of Earth's early atmosphere.

The researchers then built a model of the processes that would affect an early Venus or Earth – such as the melting and cooling of a basaltic crust, the water content of the rock, the transport of heat from magma oceans to the greenhouse atmosphere, and the transfer of heat from the sun to a planet at Earth's and at Venus's distance. Even before the planets solidified, location made the big difference in this first-cut estimate. Earth's crust cooled substantially faster than did Venus's, according to the study. Despite the powerful greenhouse effect from all of the water vapor in the atmosphere, Earth shed more heat than it was receiving from the sun (which was some 20 to 30 percent fainter than it is today). As the planet cooled, so did the atmosphere. Water vapor condensed and formed oceans. The oceans formed faster than ultraviolet light from the sun could destroy the water molecules feeding the ocean.

Meanwhile, Venus's position closer to the sun meant its atmosphere was warmer, slowing the pace at which the molten surface cooled,

according to the model. This kept large quantities of water vapor in the atmosphere far longer than on Earth, exposing more of it to destruction from the sun's ultraviolet radiation. The radiation cut the bonds between the hydrogen and oxygen, leaving the lighter hydrogen atoms to be swept away by the solar wind.

Whereas Earth solidified in a few million years in this experiment, a similar planet at Venus's distance and with far more water than Earth's oceans contain would have cooled over perhaps 100 million years. The amount of water left would have been only about 10 percent of the Earth's oceans, mostly tied up in rocks in the planet's interior.

The team suggests that the break point between a Venus outcome and an Earth outcome sits at about 0.8 AU[1], or about 74.4 million miles from the sun. Venus orbits at about 0.70 AU.

"This is a first-order look at a really new idea," Elkins-Tanton says, and as such, it leaves additional factors to fresh iterations of the model. For instance, the model doesn't account for the effect of the sun's increasing intensity with time on the processes the model describes.

This has important implications for figuring out if a newly discovered extrasolar planet is habitable, adds Ralph Lorenz, a planetary scientist at the Johns Hopkins University's Applied Physics Laboratory in Laurel, Md. A star like the sun intensifies with time, shifting the location of the habitable zone outward. The carbon cycle, which makes Earth habitable, "relies on there being a lot of liquid water around. If you have a world that cooks out all of its water at the beginning, then even if its surface temperatures fall to nice levels later, it might not have enough water to have your warm little ponds" that serve as incubators for simple forms of life.

In summarize, since Venus is so similar to Earth in size and composition, one would expect a lot of water there, yet it is virtually absent. Because of the great similarities between the two planets, one would surmise that it must have had water in the past. Models for the

---

1- astronomical units (AU)

loss of the water involve the runaway greenhouse effect on Venus. Being closer to the Sun and having the carbon dioxide in the atmosphere, the atmosphere continued to heat, perhaps with enhanced trapping of heat due to water vapor. With sufficiently high temperatures, the water vapor could rise high enough in the atmosphere for the water molecules to be broken up by ultraviolet radiation from the Sun. The freed hydrogen could then escape from the atmosphere, leaving the oxygen only in the form of carbon and sulfur oxides.

The upper atmosphere of Venus is more heavily bombarded by the solar wind since it has no magnetic field to redirect some of the solar wind particles. This would hasten the breakup of the water molecules if the above model is correct.

References

Barabash S., Fedorov A., Sauvaud J.J., Lundin R., Russell C.T., Futaana Y., Zhang T.L., Andersson H., et al. (2007). "The loss of ions from Venus through the plasma wake". Nature, 450(7170): 650–653.

Basilevsky A.T., Head J.W. (2003) "The surface of Venus". Rep. Prog. Phys. 66 (10): 1699–1734.

Bertaux J., Vandaele A.C., Korablev O., Villard E., Fedorova A., Fussen D., Quémerais E., Belyaev D., et al. (2007) "A warm layer in Venus' cryosphere and high-altitude measurements of HF, HCl, H2O and HDO". Nature, 450(7170): 646–649. doi: 10.1038/nature05974. PMID 18046397

Fegley B., et al. (1997). Geochemistry of Surface-Atmosphere Interactions on Venus (Venus II: Geology, Geophysics, Atmosphere, and Solar Wind Environment). University of Arizona Press, ISBN 978-0-8165-1830-2.

Kliore A., Patel I. (1980) Vertical Structure of the atmosphere of Venus from Pioneer Venus Orbiter radio occultation studies, Journal of Geophysical Research, 85: 7957

Koehler H.W. (1982) "Results of the Venus sondes Venera 13 and 14". Sterne und Weltraum, 21: 282.

Krasnopolsky V.A., Belyaev D.A., Gordon I.E., Li G., Rothman L.S. (2013) "Observations of D/H ratios in H2O, HCl, and HF on Venus and new DCl and DF line strengths". Icarus, 224 (1): 57–65. doi:10.1016/j.icarus.2013.02.010

Krasnopolsky V.A., Parshev V.A. (1981) "Chemical composition of the atmosphere of Venus". Nature. 292 (5824): 610–613. doi:10.1038/292610a0.

Landis G.A. (2001) "Exploring Venus by Solar Airplane". AIP Conference Proceedings. American Institute of Physics. 522: 16–18.

doi:10.1063/1.1357898

Landis G.A., Colozza A., LaMarre C.M. (2002) "Atmospheric Flight on Venus". Proceedings, 40th Aerospace Sciences Meeting and Exhibit sponsored by the American Institute of Aeronautics and Astronautics. Reno, Nevada, January 14–17, 2002.

Lee Y.J. (2012) "Venus Cloud Structure and Radiative Energy Balance of the Mesosphere". p. 14.

Lellouch E., et al. (1997) Monitoring of Mesospheric Structure and Dynamics, in Bougher, S., Hunten, D., Phillips, R. Eds, Venus II. University of Arizona Press, Tucson.

Lorenz R.D., Imai M., Takahashi Y., Sato M., Yamazaki A., Sato T.M., Imamura T., Satoh T., Nakamura M. (2019) "Constraints on Venus Lightning From Akatsuki's First 3 Years in Orbit". Geophysical Research Letters. 46(14): 7955–7961. doi:10.1029/2019GL083311. ISSN 1944-8007

Lorenz Ralph D. (2018) "Lightning detection on Venus: a critical review". Progress in Earth and Planetary Science, 5(1): doi:10.1186/s40645-018-0181-x. ISSN 2197-4284.

Markiewicz W.J., Titov D.V., Limaye S.S., Keller H.U., Ignatiev N., Jaumann R., Thomas N., Michalik H., et al. (2007) "Morphology and dynamics of the upper cloud layer of Venus". Nature, 450 (7170): 633–636.

Michael M., Tripathi S.N., Borucki W.J., Whitten R.C., (2009) "Highly charged cloud particles in the atmosphere of Venus". J. Geophysical Res. 114 (E4). doi: 10.1029/2008je003258. ISSN 0148-0227

Moshkin B.E., Ekonomov A.P., Golovin I.M. (1979) "Dust on the surface of Venus". Kosmicheskie Issledovaniia (Cosmic Research). 17: 280–285. Bibcode: 1979KosIs.17. 280M

Nave C.R. (2008) "The Environment of Venus". Hyperphysics, Department of Physics and Astronomy, Georgia State University.

Patzold M., Hausler B., Bird M.K., Tellmann S., Mattei R., Asmar S.W., Dehant V., Eidel W., et al. (2007) "The structure of Venus' middle atmosphere and ionosphere". Nature, 450 (7170): 657–660.

Piccioni G., Drossart P., Sanchez-Lavega A., Hueso R., Taylor F.W., Wilson C.F., Grassi D., Zasova L., et al, (2007) "South-polar features on Venus similar to those near the North Pole". Nature, 450 (7170): 637–640.

Russell C.T. (1993) "Planetary Magnetospheres", Rep. Prog. Phys. 56(6): 687–732. doi: 10.1088/0034-4885/56/6/001

Russell C.T., Phillips J.L. (1990). "The Ashen Light". Advances in Space Research, 10(5): 137–141. doi:10.1016/0273-1177(90)90174-X

Russell C.T., Zhang T.L., Delva M., Magnes W., Strangeway R.J., Wei H.Y. (2007) "Lightning on Venus inferred from whistler-mode waves in the ionosphere". Nature, 450 (7170): 661–662. doi: 10.1038/nature0593

Svedhem Hakan, Titov D.V., Taylor Fredric V., Witasse O. (2007) "Venus as a more Earth-like planet". Nature, 450 (7170): 629–632. doi: 10.1038/nature06432

Taylor F. (2014) The Scientific Exploration of Venus, Cambridge University Press, New York.

Taylor F., et al, (1997) Near-infrared sounding of the lower atmosphere of Venus, in Bougher S., Hunten D., Phillips R. eds, Venus II. University of Arizona Press, Tucson.

Whitten R.C., McCormick P.T., Merritt D., Thompson K.W., Brynsvold R.R., Eich C.J., Knudsen W.C., Miller K.L., et al, (1984) "Dynamics of the Venus ionosphere: A two-dimensional model study". Icarus, 60(2):

317–326. doi:10.1016/0019-1035(84)90192-1

Wilson C.F. "Beyond sulphuric acid - what else is in the clouds of Venus?" Venus Exploration Targets Workshop (2014)

Zasova L., et al. (2007) Structure of the Venus atmosphere, Planetary and Space Science, 55, 1712

Zhang T.L., Delva M., Baumjohann W., Auster H.U., Carr C., Russell C.T., Barabash S., Balikhin M., et al. (2007) "Little or no solar wind enters Venus' atmosphere at solar minimum". Nature, 450(7170): 654–656. doi: 10.1038/nature06026

Chapter 3
Atmosphere system of the Earth

Introduction

The Earth's atmosphere is the gaseous coverage surrounding the planet. Like other planetary atmospheres, it figures centrally in transfers of energy between the sun, the Earth, and deep space. It also figures in transfers of energy from one region of the globe to another. By maintaining thermal equilibrium, such transfers determine the Earth's climate. However, among neighboring planets, the Earth's atmosphere is unique because it is related closely to ocean and surface processes that, together with the atmosphere, form the basis for life.

Because it is a fluid system, the atmosphere is capable of supporting a wide spectrum of motions. This range from turbulent eddies of a few meters to circulations with dimensions of the Earth itself. By rearranging mass, air motion influences other atmospheric components such as water vapor, ozone, and cloud, which figure prominently in radiative and chemical processes. Such influence makes the atmospheric circulation a key ingredient of the global energy budget.

3.1. Mechanisms Influencing Atmospheric Behavior

Of the factors influencing atmospheric behavior, gravity is the single most important.

Even though it has no upper boundary, the atmosphere is contained by the gravitational field of the Earth, which prevents atmospheric mass from escaping to space. Because it is such a strong body force, gravity determines many atmospheric properties. Most immediate is

the geometry of the atmosphere. Atmospheric mass is concentrated in the lowest 10 km – less than 1% of the Earth's radius. Gravitational attraction has compressed the atmosphere into a shallow layer above the Earth's surface in which mass and constituents are stratified vertically: They are layered.

Through stratification of mass, gravity imposes a strong kinematic constraint on atmospheric motion. Circulations with dimensions greater than a few tens of kilometers are quasi-horizontal. Vertical displacements of air are then much smaller than horizontal displacements. Under these circumstances, constituents such as water vapor and ozone fan out in layers or "strata." Vertical displacements are comparable to horizontal displacements only in small-scale circulations such as convective cells and fronts, which have horizontal dimensions comparable to the vertical scale of the mass distribution.

The compressibility of air complicates the description of atmospheric behavior by enabling the volume of a parcel to change as it experiences changes in surrounding pressure. Therefore, concentrations of mass and constituents for the parcel can change, even though the number of molecules remains fixed. The concentration of a chemical constituent can also change through internal transformations, which alter the number of a particular type of molecule. For example, condensation decreases the abundance of water vapor in an air parcel that passes through a cloud system.

Exchanges of energy with its environment and transformations between one form of energy and another likewise alter the properties of an air parcel. By expanding, an air parcel exchanges energy mechanically with its environment through work that it performs on the surroundings. Heat transfer, as occurs through absorption of radiant energy and conduction with the Earth's surface, represents a thermal exchange of energy with a parcel's environment. Absorption of water vapor by an air parcel (e.g., through contact with a warm ocean surface) has a similar effect. When the vapor condenses, latent heat of vaporization carried by the vapor is released to the surrounding molecules of dry air that comprise the parcel. If the condensed water

then precipitates back to the Earth's surface, this process leads to a net transfer of heat from the Earth's surface to the parcel.

The Earth's rotation, like gravity, exerts an important influence on atmospheric motion and, hence, on distributions of atmospheric properties. Because the Earth is a noninertial reference frame, the conventional laws of mechanics do not hold; they must be modified to account for its acceleration. Apparent forces introduced by the Earth's rotation are responsible for properties of the large-scale circulation, in particular, the flow of air around centers of low and high pressure. Those forces also inhibit meridional, e.g., NS (North-South) motion. Consequently, they inhibit transfers of heat and constituents between the equator and poles. For this reason, rotation tends to stratify properties meridionally, just as gravity tends to stratify them vertically.

The physical processes described in the preceding paragraphs do not operate independently. They are interwoven in a complex fabric of radiation, chemistry, and dynamics that govern the Earth-atmosphere system. Interactions among these can be just as important as the individual processes themselves. For instance, radiative transfer controls the thermal structure of the atmosphere, which determines the circulation. Transport by the circulation, in turn, influences the distributions of radiatively active components such as water vapor, ozone, and cloud. In view of their interdependence, understanding how one of these processes influences behavior requires an understanding of how that process interacts with others. This feature makes the study of the Earth-atmosphere system an eclectic one, involving the integration of many different physical principles (Murry, 2011).

3.2. Earth's Atmosphere and Its Composition

The Earth's atmosphere consists of a mixture of gases, mostly molecular nitrogen (78% by volume) and molecular oxygen (21% by volume); see Table 1.1. Water vapor, carbon dioxide, and ozone, along with other minor constituents, comprise the remaining 1% of the atmosphere. Although present in very small abundances, trace species

such as water vapor and ozone play a key role in the energy balance of the Earth through their involvement in radiative processes. Because they are created and destroyed in particular regions and are linked to the circulation through transport, these and other minor species are highly variable. For this reason, trace species are treated separately from the primary atmospheric constituents, which are referred to simply as "dry air."

3.2.1. Description of Air

The starting point for describing atmospheric behavior is the ideal gas law which constitutes the equation of state for a pure (single-component) gas.

Table 3.1 Atmospheric Composition, constituents are listed with volume mixing ratios representative of the Troposphere or Stratosphere, how the latter are distributed vertically, and controlling processes (Murry, 2011).

Constituent	Tropospheric Mixing Ratio	Vertical Distribution (Mixing Ratio)	Controlling Processes
N_2	.7808	Homogeneous	Vertical Mixing
O_2	.2095	Homogeneous	Vertical Mixing
$*H_2O$	≤0.030	Decreases sharply in Troposphere Increases in Stratosphere Highly Variable	Evaporation, Condensation, Transport Production by CH_4 Oxidation
Ar	.0093	Homogeneous	Vertical Mixing
$*CO_2$	380 ppmv	Homogeneous	Vertical Mixing Production by Surface and Anthropogenic Processes
$*O_3$	10 ppmv$	Increases sharply in Stratosphere Highly Variable	Photochemical Production in Stratosphere; secondarily through pollution in troposphere Destruction at Surface Transport
$*CH_4$	1.8 ppmv	Homogeneous in Troposphere Decreases in Middle Atmosphere	Production by Surface Processes Oxidation Produces H_2O
$*N_2O$	320 ppbv	Homogeneous in Troposphere Decreases in Middle Atmosphere	Production by Surface and Anthropogenic Processes Dissociation in Middle Atmosphere Produces NO Transport
$*CO$	70 ppbv	Decreases in Troposphere Increases in Stratosphere	Production Anthropogenically and by Oxidation of CH_4 Transport
NO	0.1 ppbv$	Increases Vertically	Production by Dissociation of N_2O Catalytic Destruction of O_3
$*CFC-11$	0.2 ppbv	Homogeneous in Troposphere	Industrial Production
$*CFC-12$	0.5 ppbv	Decreases in Stratosphere	Mixing in Troposphere
$*HFC-134A$	30 ppt		Photo-dissociation in Stratosphere

∗ Radiatively active; $ Stratospheric value

The *specific gas constant R* is related to the *universal gas constant* $R*$ through

$$\begin{aligned} pV &= nR^*T \\ &= \frac{m}{M}R^*T, \\ &= mRT \end{aligned} \qquad (1)$$

which constitutes the equation of state for a pure (single-component) gas. In (3.1), *p,T,* and *M* denote the pressure, temperature, and molar weight of the gas, and *V* , *m*, and $n = \frac{m}{M}$ refer to the volume, mass, and molar abundance of a fixed collection of matter (e.g., an air parcel).

The *specific gas constant R* is related to the *universal gas constant* R^* through

$$R = \frac{R*}{M} \qquad (2)$$

Equivalent forms of the ideal gas law that do not depend on the dimension of the system are

$$\begin{aligned} p &= \rho RT \\ pv &= RT, \end{aligned} \qquad (3)$$

where ρ and $v = \frac{1}{\rho}$ (also denoted α) are the density and specific volume of the gas.

Because it is a mixture of gases, air obeys similar relationships. So do its individual components. The *partial pressure pi* of the *i*th component is that pressure the ith component would exert in isolation at the same volume and temperature as the mixture.
It satisfies the equation of state

$$p_iV = m_iR_iT \qquad (4)$$

where *Ri* is the specific gas constant of the ith component. Similarly, the partial volume *Vi* is that volume the ith component

would occupy in isolation at the same pressure and temperature as the mixture. It satisfies the equation of state

$$pV_i = m_i R_i T \quad (5)$$

Dalton's law asserts that the pressure of a mixture of gases equals the sum of their partial pressures

$$P=\sum_i pi \quad (6)$$

Likewise, the volume of the mixture equals the sum of the partial volumes

$$V=\sum_i Vi \quad (7)$$

The equation of state for the mixture can be obtained by summing over all of the components

$$pV = T \sum_i miRi \quad (8)$$

yields the equation of state for the mixture $pV = m\bar{R}T$ (9)

Above 100 km, the mixing of air parcels is dominated by molecular diffusion. This part of the atmosphere is subjected to bombardment by radiation and high-energy particles from the Sun and outer space. This barrage has profound chemical effects on the composition of the atmosphere, especially the outer layers. In addition, gaseous molecules are influenced by gravity, leading to lighter molecules being found in the outer layers and heavier molecules closer to the Earth. Consequently, the composition of the atmosphere beyond the middle atmosphere is not uniform and is known as heterosphere. The upper boundary at which gases disperse into space lies at an altitude of approximately 1,000 km above sea level.

3.2.2. Homosphere and Heterosphere

Formation of the homosphere and heterosphere in the atmosphere can be explained as follows. Based on the concept of diffusion, the vertical molecular flux is given as

$$F = -D(\nabla N) \quad (10)$$

Where, D is the diffusion coefficient and N is the molecular number density. The negative sign indicates that the fluxes by diffusion are down-gradient.

The rate of change of N with respect to time is given by

$$\frac{\partial N}{\partial t} = -D(\nabla N) = D\nabla^2 N \qquad (11)$$

The vertical molecular flux in terms of the rate of change of N with height is

$$F = -D\frac{\partial N}{\partial z} \qquad (12)$$

The diffusion caused by eddies can be estimated by:

$$Feddy = -K_{eddy}\frac{\partial N}{\partial z} \qquad (3.13)$$

The solution to this diffusion equation for atmospheric conditions results in a time scale for diffusive travel, as time equals $< X^2 > /2D$.
Now, let us use kinetic theory to understand the molecular diffusion coefficient D.
The resulting expression for D is:

$$D = K_b \frac{(T)^{1.5}}{(p)(\frac{1}{m})^{0.5}} \qquad (3.14)$$

where K_b is the Boltzmann's constant ($1.38\times10^{-23} J.K^{-1}$), T is the temperature, p is the pressure, and m is the molecular mass. At the surface, D=2×105 $m^2.s^{-1}$. When $p = 5\times10^{-7}$ atm, T is constant, $D \sim 40$ $m^2.s^{-1}$.

When eddy diffusion dominates over molecular diffusion, the gases are well mixed and form the homosphere. When molecular diffusion dominates over eddy diffusion, the gases separate according to mass, as we see in the heterosphere.

3.2.3. Atmospheric Pressure

Atmospheric pressure is the pressure above any area of the Earth's atmosphere caused by the weight of the air. The air pressure varies spatially and temporally, because the amount and weight of air above the Earth vary with location and time.

Atmospheric pressure shows a semidiurnal variation caused by global atmospheric tides. The tidal effect is stronger in tropical zones and almost absent in Polar Regions. The average atmospheric pressure

at sea level is about 1,013.25 hectapascals (hPa).

3.2.4. Vertical Structure of Pressure and Density

Meteorological parameters, such as pressure and air density, vary dramatically with height in the atmosphere. The variation can be over many orders of magnitude and is very much larger than horizontal or temporal variations. It is therefore necessary to define a standard atmosphere in which geophysical quantities have been averaged horizontally and in time, and which vary as a function of height only. The quasiexponential height dependence of pressure and density can be inferred from the fact that the observed vertical profiles of pressure and density on the semilog plots closely resemble straight lines.

The standard atmospheric values specified by the International Civil Aviation Organisation (ICAO) are: (i) sea level pressure (p) is 1,013.25 hPa; (ii) sea level density (ρ) is 1.225 kg m^{-3}; (iii) sea level temperature (T) is 288.15n K; and fixed lapse rates for p and T.

The vertical variation of pressure (p) with height (z) may be derived as approximately (Wallace and Hobbs 2006) as:

$$p(z) = p(0)\exp\left(\frac{-z}{H}\right) \qquad (15)$$

where p(z) is the pressure at height z above sea level, p(0) is the sea level pressure, and H is a constant called the scale height of the atmosphere. Pressure decreases by a factor of e in passing upward through a layer of depth H. For the Earth's atmosphere, H is about 8.55 km. This equation is valid only for an isothermal atmosphere, in which the temperature remains constant with height.

A similar approximate expression may be derived for density ρ as follows:

$$\rho\,(z) = \rho\,(0)\exp\left(-\frac{z}{H}\right) \qquad (16)$$

Note that density also decreases rapidly with height. It can be shown that half of the mass of the Earth's atmosphere is below the 500 hPa level or an altitude of about 5.5 km. Figure 3.1 illustrates the vertical profiles of pressure in the troposphere and stratosphere. As

elevation increases, fewer air particles are above.

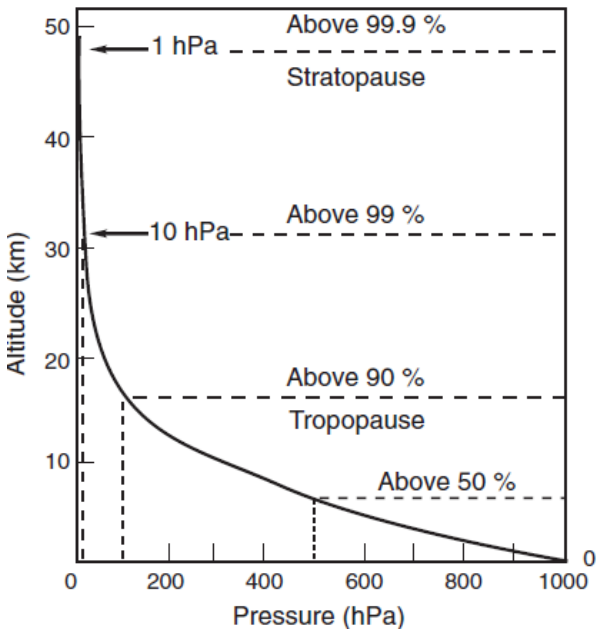

Figure 3.1 Vertical distribution of atmospheric pressure.

Therefore the atmospheric pressure decreases quasi-exponentially with increasing altitude. The atmospheric pressure drops by ~50% at a height of about 5 km above the Earth's surface (Fig. 3.1). At an altitude of 50 km the pressure (i.e., mass of particles above unit area at that level) is about 1 hPa so that only about 0.1% of the mass of the atmosphere lies above that level. Similarly, because the pressure at 90 km is about 0.001 hPa, only about one millionth of the mass of the atmosphere lies above that level.

3.2.5. Atmospheric Thermal Structure

The atmospheric layers of the Earth are characterized by variations in temperature produced by differences in the radiative and chemical composition of the atmosphere at different altitudes. With increasing distance from Earth's surface the chemical composition of air becomes progressively more dependent on altitude and the atmosphere

becomes enriched with lighter gases. Based on the temperature changes with height, the Earth's atmosphere is divided into mainly four concentric spherical strata by narrow transition zones. The four concentric layers of the atmosphere are termed as troposphere, stratosphere, mesosphere, and thermosphere. The vertical distribution of temperature in the Earth's atmosphere is shown in Fig. 3.2 (Brasseur and Solomon, 1984).

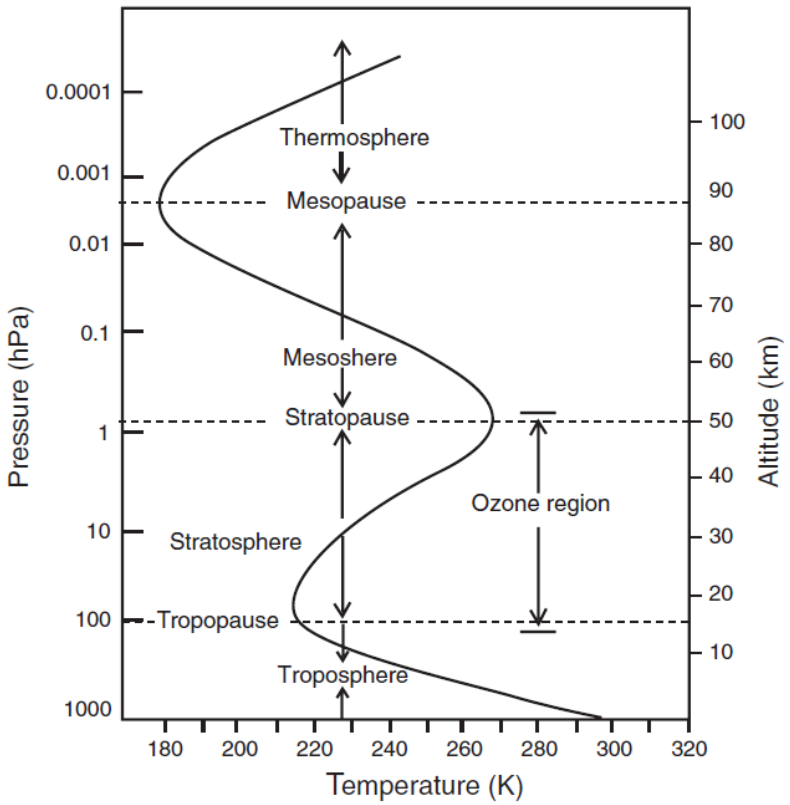

Figure 3.2 Vertical thermal structure of Earth's atmosphere up to 120 km (Brasseur and Solomon, 1984).

3.2.6. Troposphere

Troposphere is the lowest part of the atmosphere and is closer to the Earth, and extends about 8 km above the poles and 18 km over the equator. It is the densest part of the atmosphere which contains almost

all the water vapor, clouds, and precipitation.

Temperature generally decreases with height in the troposphere at about 6–7 ◦C km^{-1} in the lower half and 7–8 ◦C km^{-1} in the upper half. Because of the general decrease of temperature with height and the presence of weather systems, the troposphere is often characterized by fairly significant localized vertical motions, although these are generally much smaller than horizontal motions. Sometimes shallow layers may be present in the troposphere in which temperature increases with height. These *inversions* inhibit vertical motion. The presence of water vapor, clouds, storms, and weather, contributes to the significance of the troposphere.

Water vapor plays a major role in regulating air temperature because it absorbs solar energy and thermal radiation from the planet's surface. The troposphere contains 99% of the water vapor in the atmosphere. The water vapor content, however, decreases rapidly with altitude, thus reflecting the change in temperature. Water vapor concentrations also vary with latitudinal position, being greatest above the tropics and decreasing toward the Polar Regions. All weather phenomena occur within the troposphere, although turbulence may extend into the lower portion of the stratosphere. Troposphere means region of *turning* or *mixing*, and is so named because of vigorous convective air currents within the layer.

3.2.7. Stratosphere

The stratosphere is the second major stratum in the atmosphere. It resides above the tropopause up to 50 km as shown in Fig. 3.3. The air temperature in the stratosphere increases gradually to around 273 ^{o}K at the stratopause (∼50 km), which is marked by a reversal in the temperature trend. Because the air temperature in the stratosphere increases with altitude, it does not cause convection and has a stabilizing effect on atmospheric conditions in the region and confines turbulence to the troposphere.

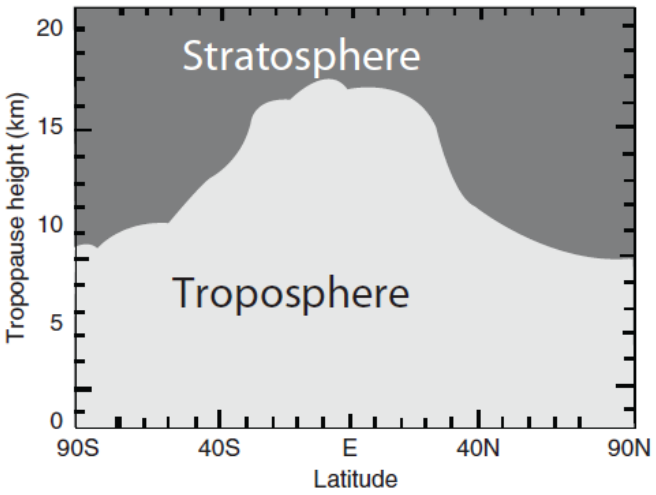

Figure 3.3 Latitudinal variation of the vertical extension of troposphere and lower stratosphere (Geerts and Linacre, 1997).

As water vapor content within the stratosphere is very low, ozone plays the major role in regulating the thermal regime of this layer. Temperature increases with ozone concentration. Solar energy is converted to kinetic energy when ozone molecules absorb ultraviolet radiation, resulting in heating of the stratosphere.

The stratosphere is a region of intense interactions among radiative, dynamical, and chemical processes, in which horizontal mixing of gaseous components proceeds much more rapidly than vertical mixing. The stratosphere is warmer than the upper troposphere, primarily because of a stratospheric ozone layer that absorbs solar ultraviolet radiation.

The stratosphere is relatively dry. However, it is rich in ozone as it is the main region of ozone production. Ozone absorbs ultraviolet radiation from the Sun and with the low densities present at stratospheric altitudes, this absorption is an efficient mechanism of transferring kinetic energy to a relatively small number of molecules due to which the air temperature becomes high. Ozone in the upper stratosphere therefore acts as a heat source.

3.2.8. Mesosphere

The mesosphere, a layer extending from 50 to 80 km, is characterized by decreasing temperatures with increasing altitude, reaching about 180 °K at 80 km. This characteristic is used to define its limits: it begins at the top of the stratosphere (sometimes called the stratopause), and ends at the mesopause, which is the coldest part of Earth's atmosphere with temperatures below −143 °C (−225 °F; 130 °K). Compared to lower regions, the concentrations of ozone and water vapor in the mesophere are negligible, hence the lower temperatures. Its chemical composition is fairly uniform. Pressures are very low. The *mesopause*, which separates the mesosphere from the next highest layer and like the other pauses, is a region where the temperature trend changes direction. Like the tropopause, however, the temperature of the mesopause can vary quite significantly, dropping as low as 150 K. In some instances *noctilucent clouds* can form here and affect global climate by absorbing and reflecting incoming solar radiation. The mesopause is the level at which the lowest atmospheric temperatures are usually found (Venkat et al, 2010).

3.2.9. Thermosphere

The thermosphere is a region of high temperatures above the mesosphere. It includes the ionosphere and extends out to several hundred kilometers. The temperatures in this region are of the order of 500–2,000 °K and the densities are very low. The thermosphere is that part of the heterosphere which does not have a constant chemical composition with increasing altitude. Rather, atoms tend to congregate in layers with the heavier species at lower altitudes.

The increase in temperature in the thermosphere is due to the absorption of intense solar radiation by the limited amount of molecular oxygen present. At an altitude of 100–200 km, the major atmospheric components are still nitrogen and oxygen, although at this high altitude gas molecules are widely separated. *Auroras* normally occur in this region between 80 and 160 km.

The *thermopause* is the level at which the temperature stops rising with height. Its height depends on the solar activity and is located between 250 and 500 km (Prölss and Bird, 2010).

3.2.10. Exosphere

The exosphere is the most distant atmospheric region from Earth's surface. The upper boundary of the layer extends to heights of perhaps 960–1,000 km.

The most common molecules within Earth's exosphere are those of the lightest atmospheric gases. Hydrogen is present throughout the exosphere, with some helium, carbon dioxide, and atomic oxygen near its base. The exosphere is a transitional zone between Earth's atmosphere and interplanetary space (Bauer and Lammer, 2004).

The upper atmosphere is divided into regions based on the behavior and number of free electrons and other charged particles. The importance of the upper atmosphere is that instead of absorbing or reflecting radiation it deflects ionized particles.

3.2.11. Ionosphere

The ionosphere is the region of the Earth's atmosphere in which the number of ions, or electrically charged particles, is large enough to affect the propagation of radio waves.

3.2.12. Plasmasphere

The plasmasphere is not really spherical but a doughnut-shaped region (a torus) with the hole aligned with Earth's magnetic axis. In this case the use of the suffix sphere is more in the figurative sense, like a *sphere of influence*. It is composed mostly of hydrogen ions (protons) and electrons, and is essentially an extension of the ionosphere.

3.2.13. Magnetosphere

The magnetic field of the Earth to a large extent shields it from the continual supersonic outflow of the Sun's ionized upper atmosphere, known as the solar wind.

Inside of the plasmapause, geomagnetic field lines rotate with the Earth. Outside the plasmapause, however, magnetic field lines are

unable to corotate because they are influenced strongly by electric fields produced by the solar wind (Blanc et al, 2005).

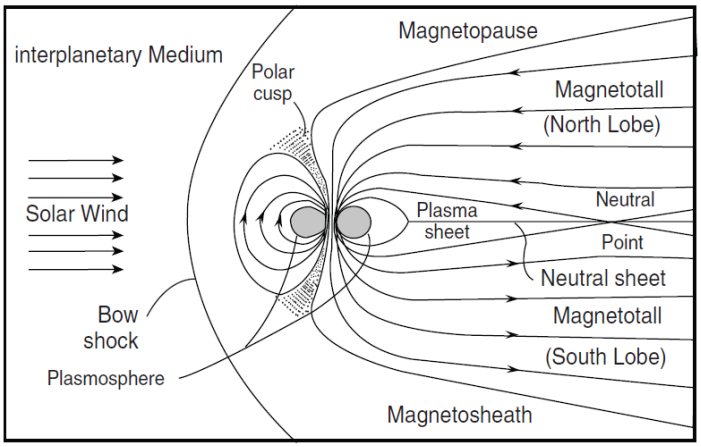

Figure 3.4 Earth's magnetosphere with principal particle regions (Russel, 1987).

3.3. The Tropopause

Tropopause separates the troposphere from the stratosphere, i.e., two volumes of air with significantly different properties. In this region the air ceases to cool, and the air becomes almost completely dry. Basically, it is the boundary between the upper troposphere and the lower stratosphere that varies in altitude between the poles and the equator.

Tropopause is the transition layer between the troposphere and the stratosphere, where an abrupt change in temperature lapse rate usually occurs. It is defined by the World Meteorological Organization (WMO) as the lowest level at which the lapse rate decreases to 2K km^{-1} or less, provided that the average lapse rate between this level and all higher levels within 2 km does not exceed 2K km^{-1}. Occasionally, a second tropopause may be found if the lapse rate above the first tropopause exceeds 3K km^{-1} fall below this value. This so-defined thermal tropopause can be obtained from single

temperature profiles and can be applied in both the tropics and the extratropics.

The highest tropopause is seen over south Asia during the summer monsoon season, where the tropopause occasionally peaks above 18 km. The oceanic warm pool of the western equatorial Pacific also exhibits higher tropopause height of 17.5 km. On the other hand, cold conditions lead to lower tropopause, evidently due to weak convection (Holton et al, 1995).

3.3.1 Dynamic Tropopause

Dynamic tropopause is used with potential vorticity instead of vertical temperature gradient as the defining variable. There is no universally used threshold, but the most common ones are that the tropopause lies at the 2 PVU (potential vorticity unit) or 1.5 PVU surface. This threshold will be taken as a positive or negative value (e.g., 2 and −2 PVU), giving surfaces located in the northern and southern hemisphere respectively.

To define a global tropopause in this way, the two surfaces arising from the positive and negative thresholds need to be joined near the equator using another type of surface such as a constant potential temperature surface as illustrated in Fig. 1.6.

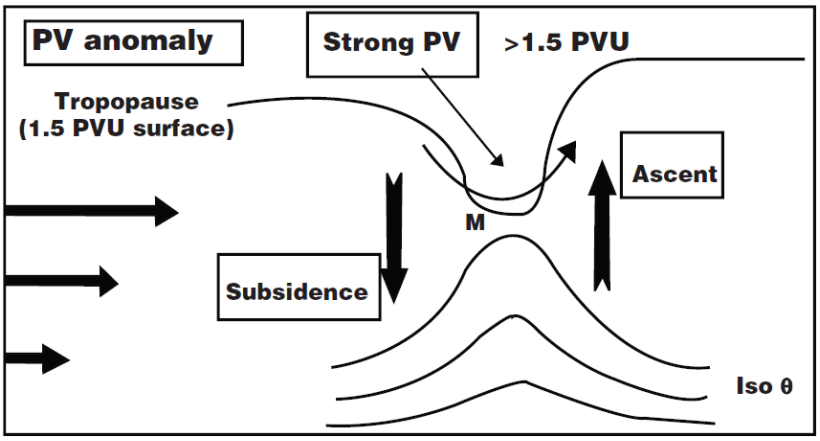

Figure 3.5 A typical dynamical tropopause (Wirth and Szabo, 2007).

3.3.2 Ozone Tropopause

Apart from *thermal* and *dynamical* tropopauses, there is another category for the definition of the tropopause based on the ozone content (Bethan et al, 1996) called *ozone tropopause*. In most seasons, ozone-mixing ratio similar to PV features a sharp positive vertical gradient at a particular altitude somewhere in the tropopause region. It can be used for defining an ozone tropopause from a single ozone sounding.

In addition, ozone-mixing ratio like PV is approximately materially conserved on synoptic timescales. Therefore one may expect that the ozone tropopause would behave like the dynamical tropopause (Reeves, et al., 2002).

3.3.3. Tropopause Folds

Tropopause fold is the extrusion of stratospheric air within an upper-tropospheric baroclinic zone which slopes downward from a normal tropopause level (~200–300 hPa) to the middle troposphere (~500–700 hPa). The tropopause fold is a mesoscale feature which forms in response to strong descent at the tropopause level. It constitutes an intense phase of upper tropospheric frontal development in which the tropopause undulation collapses.

The most vigorous tropopause folds occur during the winter and spring and are less frequent than cyclone development. They are usually observed downstream from a ridge, where there is large-scale descent in the entrance region of an upperlevel jet streak. Ozone-rich air originates in the lower stratosphere, west of the trough axis on the cyclonic side of the upper-level jet streak. This airstream then descends anticyclonically to the lower troposphere east of the surface high-pressure system or crosses the trough axis and ascends (Hartjenstein, 1999). Two major types of tropopause folds are noted. One is associated with the polar front jet (PFJ) and the other one is associated with the subtropical jet stream (STJ) and subtropical front, which is confined in the upper troposphere.

3.4. Climatology of the Lower and Middle Atmosphere

The vertical distribution of temperature and wind structure of the lower and middle atmosphere has been studied extensively for several decades using a variety of techniques. A large number of measurements have been made by using balloons, aircrafts, radiosonde, rocket and satellite observations, both spatially and temporally, on a global scale. Based on the global observations, and modeling information, Stratospheric Process and Its Influence on Climate (SPARC) have prepared reference climatology of the middle atmosphere (SPARC 2002). In this section, the temperature and wind climatology of the troposphere and stratosphere are mainly discussed.

3.4.1. Temperature

The temporal and latitudinal variability of mean temperature profile shows that there is considerable latitudinal and seasonal variability. Temperature decreases with latitude in the troposphere. The latitudinal gradient is about twice as steep in the winter hemisphere compared to that in the summer hemisphere. The tropopause is much higher and colder over the tropics than over the polar regions. The latitudinal distribution of temperature in the lower stratosphere is rather complicated.

The summer hemisphere has a cold equator and a warm pole. The winter hemisphere is cold at both equator and pole with a warmer region in middle latitudes. The cold pool of stratospheric air over the winter pole is highly variable. On occasions, it disappears for a period of a few weeks during midwinter. During these so-called *sudden stratospheric warmings*, the stratospheric temperatures over individual stations have been observed to rise by as much as 70 ◦C in 1 week (Labitzke and van Loon, 1999).

3.4.2. Wind

This is a latitude–height cross section of the zonal wind component, averaged with respect to longitude, during the month of January derived from METEO analyses (1,000–1.5 hPa), and a combination of

HALOE plus MLS data above 1.5 hPa, similar to that of temperature (Randel et al, 2004).

Prominent features are cores of strong westerly winds in middle latitudes at an altitude of 10 km. However, the strongest zonal winds occur in the mesosphere at an elevation of 60 km. Again there are two jet cores in middle latitudes, the stronger in the winter hemispheres westerly; the other in the summer hemisphere is easterly. During the equinoxes, these jets undergo dramatic reversals as the latitudinal temperature gradient reverses.

The sudden stratospheric warming phenomenon is accompanied by large changes in the longitudinally averaged zonal wind at high latitudes in the winter stratosphere. The midwinter warmings are accompanied by a pronounced weakening of the westerlies at stratospheric levels. Sometimes the westerlies disappear altogether. These changes in the stratosphere have little effect on the wind structure in the troposphere.

3.4.3. Zonal Mean Winds in the Equatorial and Mid-latitude Stratosphere

The direction and speed of the zonal mean winds in the tropics are dominated by the equatorial lower stratospheric phenomenon known as *Quasi Biennial Oscillation* (QBO). QBO in equatorial zonal winds alter from easterly to westerly at high altitudes above 30 km, with the easterly and westerly phases descending downward with height, so that the easterly winds will at one point be above the westerly winds and the westerly winds will at one point be above the easterly winds. The QBO extends to aproximately 10–15◦ latitudes on either side of the equator, although the effects of the QBO are felt in the subtropics to 30◦ latitude and even in high latitude regions (Matthew et al, 1997).

The zonal mean winds in the midlatitude winter hemisphere are westerly, with a maximum velocity of 80 ms^{-1} at 65 km altitude and 40◦ latitude. In summer hemisphere it becomes easterly, with a maximum velocity of about 50 ms^{-1} at 65 km altitude and 40◦ latitude. In the northern hemisphere, zonal mean winds change from westerly

to easterly in May, starting at the highest latitudes and altitudes and moving downward towards the tropics. Winds change from easterly to westerly in September, once again starting from high latitudes and altitudes.

As in the troposphere, the actual winds in the stratosphere have significant meridional components. Air parcels in midlatitudes typically traverse the globe in 1–2 weeks, depending on the location and the circumstances (Grotjahn, 2015).

3.4.4. Annual Oscillation

The *Annual Oscillation* (AO) is defined as the tendency of the lower stratospheric winds to become easterlies in the summer hemisphere and westerlies in the winter hemisphere. The AO is primarily an extratropical phenomenon and does not interact strongly with tropical circulation systems.

3.4.4.1. Semiannual Oscillation

One of the significant features of the low latitude upper stratosphere is the semiannual oscillation (SAO) of zonal winds. It is reported that the SAO is not generated by the solar declination changes in the low latitudes during the course of the year. It is however known that changes in the eddy momentum deposited to the zonal winds in the upper stratosphere and lower mesosphere is responsible for the equatorial westward current phase of the SAO which occurs shortly after the equinoxes.

Vertical variation of the amplitudes of QBO and SAO in temperature in the troposphere and stratosphere over the equatorial region derived from the ERA40 reanalysis data are shown in Fig. 3.6. In temperature, the QBO and SAO are generally weak in their amplitude but have the same phase in the troposphere. The semiannual oscillation is confined to tropics, with its phase decreasing with altitude in a manner similar to QBO. These features strongly suggest that the westerly phase of SAO should be due to the westerly momentum deposition at the relevant altitudes by Kelvin waves. The very rapid dissipation with heights of the long-period Kelvin waves

producing the westerly phase of the QBO implies that the longer-period Kelvin modes would not be available to transport energy and momentum to the mesospheric levels (Guharay et al, 2009).

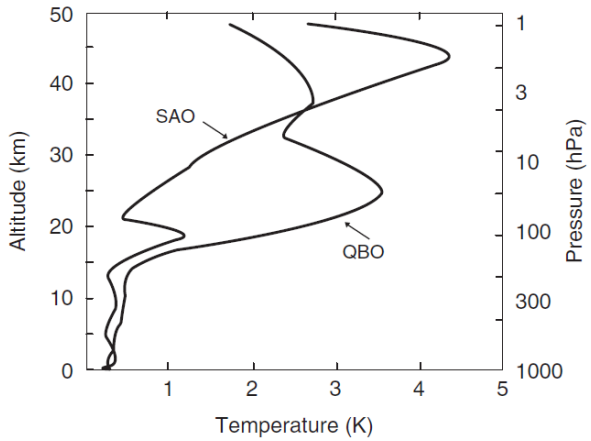

Figure 3.6 Vertical variations in the amplitudes of SAO and QBO in temperature (Courtesy: W.J.Randel).

3.4.4.2. Interannual and Intraseasonal Oscillations

Interannual variation is a year-to-year variation which is defined as a deviation from the climatological annual cycle of a meteorological quantity. It can be caused by a variation of an external forcing of the atmospheric circulation system, or can be generated internally within the system. On the other hand, *intraseasonal variation* is a low-frequency variation within a season, and it is considered to be the result of internal processes which may exist even under constant external conditions. Intraseasonal and interannual variations are defined as deviations from the periodic annual response. In general, intraseasonal variation means low-frequency variation with week-to-week or month-to-month timescales, while interannual variation means year-to-year variation. Some part of these variations is a response to the time variations of the external forcings or boundary conditions of the atmospheric circulation system, while the rest is generated internally within the system.

3.4.4.3. Jet Streams

Among the fascinating features of upper-air circulations are discontinuous bands of relatively strong winds of more than 30 ms−1, called jet streams. It is a narrow band of air that moves around the globe at relatively very high speed near the tropopause height. Strong vertical shear is experienced in the vicinity of the jet streams. As with other wind fields that increase with increasing height, jet streams can be explained as an application of the thermal wind equation. They are located above areas of particularly strong temperature gradients (e.g., frontal zones). In such areas, the pressure gradients and the resulting wind speeds increase with increasing height so long as the temperature gradients persist in the same direction. In general, this will extend to the tropopause, after which the temperature gradient reverses direction and the wind speeds diminish. Thus, jet streams are usually found in the upper troposphere (i.e., at levels of 9–18 km) (Fig. 3.7).

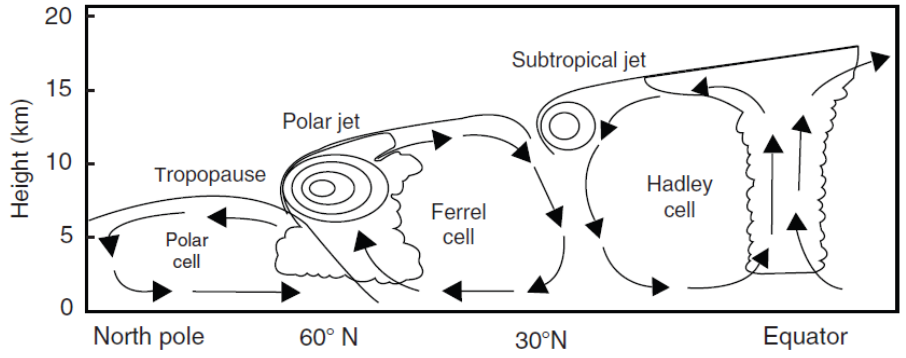

Figure 3.7 Positions of jet streams in the meridional circulation (adapted from National Weather Service, NOAA).

The polar front is the boundary between polar and midlatitude air. In winter this boundary may extend equatorward to 30◦, while in summer it retreats to 50–60◦.Winter fronts are also distinguished by stronger temperature contrasts than summer fronts. Thus, jet streams are located more equatorward in winter and are more intense during that time with jet core wind speed exceeding 75 $m.s^{-1}$.

A second jet stream is located at the poleward limit of the equatorial tropical air above the transition zone between tropical and midlatitude air. This *subtropical jet stream* (STJ) is usually found at latitudes of 30–40◦ in general westerly flow.

This jet may not be marked by pronounced surface temperature contrasts but rather by relatively strong temperature gradients in the mid-troposphere.Moreover, when the *polar-front jet* (PFJ) penetrates to subtropical latitudes; it may merge with the subtropical jet to form a single band. Also peculiar to the tropical latitudes of the northern hemisphere is a high-level jet called the *tropical easterly jet stream* (TEJ). Such jets are located about 15◦ N over continental regions due to the latitudinal heating contrasts over tropical landmasses that are not found over the tropical oceans.

3.4.4.4. Mean Meridional Winds

Schematic representation of meridional circulation is illustrated in Fig. 3.8. The arrows indicate the direction of air movement in the Hadley cell, Ferrel cell, and the polar cell in the meridional plane. The position and the direction of flow of the tropical easterly jet stream, subtropical jet stream, and the polar jet stream are also depicted.

The Hadley cell ends at about 30◦ north and south of the equator because it becomes dynamically unstable, creating eddies that are the reason for the weather disturbances of the midlatitude belts. These eddies force a downward motion just south of the jet axis and an upward motion between 40◦ and 60◦ north and south of the equator, forming the Ferrel cell. The eddies are also responsible for spreading the westerlies down to the surface.

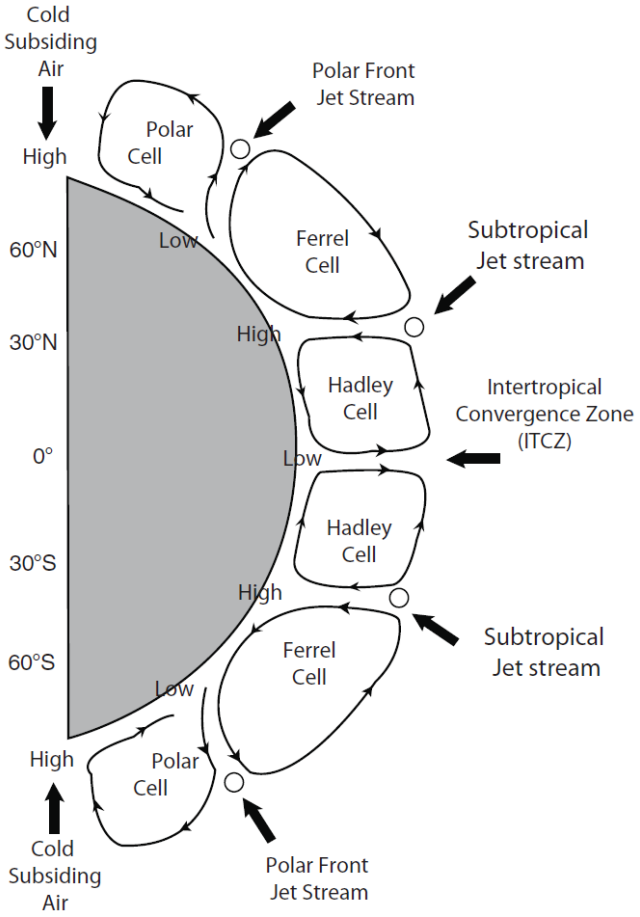

Figure 3.8 Mean meridional mass circulations in the atmosphere (Adapted from RMIT University).

3.4.4.5. The Polar Vortex

During the winter polar night, sunlight does not reach the South Pole. A strong circumpolar wind develops in the middle to lower stratosphere. These strong winds constitute the *polar vortex*.Wind speeds around the vortex may reach 100 ms^{-1}. The vortex establishes itself in the middle to lower stratosphere. It is important because it isolates the very cold air within it. In the absence of sunlight the air within the polar vortex becomes very cold. Special clouds can therefore form once the air temperature gets to below −80 ◦C.

Near the Arctic Circle the situation is considered to be less severe because its polar vortex is not as well defined as that of the Antarctic; thus, the Arctic stratosphere is warmer than its Antarctic counterpart (Mohanakumar, 2008).

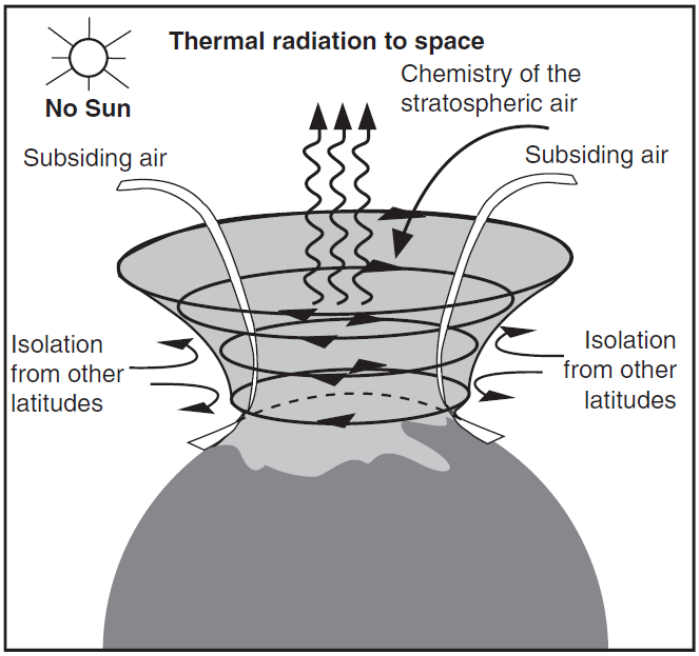

Figure 3.9 Schematic representation of Polar Vortex (Mohanakumar, 2008).

The stratosphere is cooled by the greenhouse gases. The extent of the cooling is more pronounced in the higher levels of the stratosphere. The differential cooling is suspected to have contributed to the tightening of the vortex. Contraction of the polar vortex will affect the weather changes throughout the northern hemisphere (Kodera and Kuroda 2000). Prior to 1970 the polar vortex was volatile in nature. Strengthening and weakening of the polar vortex occurred from week to week or month to month, especially during winter. After the 1970s, the vortex has shown a considerable preference toward strengthening.

The eastward circulation of the Antarctic polar vortex is strongest

in the upper stratosphere and strengthens over the course of the winter. The polar night jet is important because it blocks the transport between the southern polar region and the southern midlatitudes. It acts as a barrier and effectively blocks any mixing of air between inside and outside the vortex during the winter (Baldwin et al, 2003). Thus the ozone-rich air in the midlatitudes cannot be transported into the polar region.

Isolation of polar air allows the ozone loss processes to proceed without hindrance and replenishment by intrusions of ozone-rich air from midlatitudes. This isolation of the polar vortex is a key ingredient to polar ozone loss, since the vortex region can evolve without being disturbed by the more conventional chemistry of the midlatitudes. The polar night jet over the Arctic is not as effective in keeping out intrusions of warmer, ozone-rich midlatitude air. This is because there is more wave activity and hence more north–south mixing of air in the northern hemisphere than in the southern hemisphere.

3.4.4.6. Polar Stratospheric Clouds

Polar stratospheric clouds (PSCs) are important components of the ozone depletion process in the polar regions of the Antarctic and the Arctic. PSCs provide the surfaces upon which chemical reactions involved in ozone destruction take place. These reactions lead to the production of free chlorine and bromine, released from CFCs and other ozone-depleting chemicals (ODCs) which directly destroy ozone molecules.

Since the stratosphere is very dry, the clouds formed in this region entirely differ in character to those formed in the moist troposphere. In the extreme cold condition of the polar winter, two types of PSCs may form. Type I clouds, consisting of mainly nitric acid and sulphuric acid, are more frequent. Whereas, Type II clouds are rarer and contain water or ice which form only below −90 ◦C (Maturilli, 2007).

3.4.4.7. Sudden Stratospheric Warming

Sudden stratospheric warming (SSW) is an event where the polar

vortex of westerly winds in the northern winter hemisphere abruptly (i.e., in a few days' time) slows down or even reverses direction, accompanied by a rise of stratospheric temperature by several tens of degrees Celsius. During northern winter, occasionally the circulation becomes highly disturbed, accompanied by a marked amplification of planetary waves. The disturbed motion is characterized by marked deceleration of zonal mean westerlies or even a reversal into zonal mean easterlies. At the same time, temperature over the polar cap increases sharply by as much as 50 K, so the dark winter pole actually becomes warmer than the sunlit tropics. This dramatic sequence of events takes place in just a few days and is hence known as a sudden stratospheric warming. In northern hemisphere winter, a few of these so-called major SSWs take place along with several minor events. Major SSWs normally occur in the northern hemisphere because orography and land–sea temperature contrasts are responsible for the generation of long Rossby waves in the troposphere.

During major SSW, the north pole warms dramatically with reversal of meridional temperature gradient, and breakdown of polar vortex occurs. The polar vortex is replaced by blocking high over this region. The westerlies in the Arctic at 10 hPa are replaced by easterlies so that the center of the vortex moves south of 60–65◦N during the breakdown of polar vortex. The vortex is either displaced entirely or split into two.

There exists a link between sudden stratospheric warmings and the QBO (Labitzke and van Loon 1999). If the QBO is in its easterly phase, the atmospheric wave-guide is modified in such a way that upward-propagating Rossby waves are focused on the polar vortex, intensifying their interaction with the mean flow. The number of warming episodes is such that it agrees reasonably well with the number of QBO cycles in the equatorial lowermost stratosphere. A possible relationship with the equatorial QBO has been noted by several authors (Holton et al, 1995; Baldwin et al, 2001).

3.4.4.8. Arctic Oscillation

Arctic oscillation (AO) is an atmospheric circulation pattern in which the atmospheric pressure over the Polar Regions varies out of phase with that over middle latitudes (about 45◦N) on timescales ranging from weeks to decades. The oscillation extends through the entire depth of the troposphere. During late winter and early spring (January–March) it extends upward into the stratosphere where it modulates in the strength of the westerly vortex that encircles the Arctic polar cap region.

The Arctic oscillation exhibits a *negative phase* with relatively high pressure over the polar region and low pressure at midlatitudes, and a *positive phase* in which the pattern is reversed. In the positive phase, higher pressure at midlatitudes drives ocean storms farther north, and changes in the circulation pattern bring wetter weather to Alaska, Scotland, and Scandinavia, as well as drier conditions to the western United States and the Mediterranean. In the positive phase, frigid winter air does not extend as far into the middle of North America as it would during the negative phase of the oscillation. This keeps much of the United States east of the Rocky Mountains warmer than normal, but leaves Greenland and Newfoundland colder than usual. Weather patterns in the negative phase are in general opposite to those of the positive phase (Hansen, 2009).

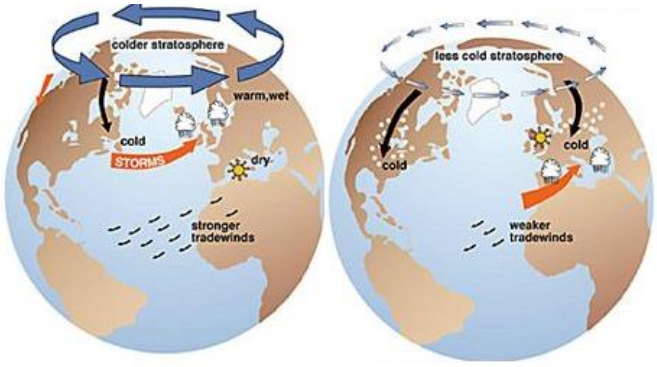

Figure 3.10 Effects of the positive and negative phases of the Arctic Oscillation (Stuwart 2005).

3.5. Atmospheric Tides

Atmospheric pressure, temperature, density, and winds are subject to variations with 24-hour (diurnal) and 12-hour (semidiurnal) periods. The minute but measurable variations of atmospheric parameters with lunar semidiurnal period are also caused by the gravitational attraction between the Moon and the Earth. But the variation of the atmospheric parameters with the solar diurnal and solar semidiurnal periods are caused predominantly by the heating of the atmosphere due to the absorption of solar radiation by water vapor in the troposphere and by ozone in the stratosphere and mesosphere. The heating generates pressure changes with peculiar patterns of variation with latitude, longitude, and altitude. In particular, the maximum heating rate and the associated pressure change at any given altitude travel with the subsolar point in the atmosphere, and for this reason the tides generated by solar heating are known as *migrating tides*.

Basically tides are generated by the daily variation of the atmospheric heating by solar radiation. The heating is generated by the absorption of solar UV radiation by ozone in the stratosphere and mesosphere, and the absorption of near-infrared bands by water vapor in the troposphere.

3.5.1. Greenhouse Gases in the Troposphere and Stratosphere

Atmospheric ozone, water vapor, and carbon dioxide are the major greenhouse gases which are abundant in the atmosphere and control the radiation balance of the Earth atmosphere system. These greenhouse gases are very good absorbers in the infrared part of the spectrum and regulate the temperature of the atmosphere. In this section the characteristics and distribution of these major greenhouse gases are discussed.

3.5.1.1. Stratospheric Ozone

Stratospheric ozone is the most important minor constituent present in the Earth's atmosphere. The more or less continuous increase in temperature with height in the stratosphere is mainly due to the

absorption of solar ultraviolet radiation by a layer of ozone molecules with peak abundance near 25 km. Although ozone is a minor constituent in the atmosphere, it absorbs ultraviolet radiation very effectively at wavelengths between 200 nm and 300 nm. This property of the ozone protects the life on Earth by preventing the harmful radiation reaching the Earth's surface. The word *ozone* is derived from the Greek word *ozein*, meaning to smell. Ozone has a pungent odour that allows ozone to be detected even in very low amounts. Ozone will rapidly react with many chemical compounds and is explosive in concentrated amounts.

More than 90% of ozone resides in the stratosphere in what is commonly known as the *ozone layer* or *ozonosphere*. The remaining ozone is found in the troposphere.

Ozone molecules have a relatively low abundance in the atmosphere. In the stratosphere near the peak of the ozone layer, there are up to 12,000 ozone molecules for every billion air molecules. Most air molecules are in the form of molecular oxygen (O_2) or molecular nitrogen (N_2). Near to the Earth's surface, ozone is even less abundant, with a typical range of 20–100 ozone molecules formed in each billion air molecules. The highest surface ozone values are due to the formation of ozone in polluted air by anthropogenic activities.

Stratospheric ozone is considered good for humans and other life forms because it absorbs UV*b* radiation from the Sun. Otherwise, UVb would reach Earth's surface in amounts that are harmful to a variety of life forms. In humans, as their exposure to UV*b* increases, so does their risk of skin cancer, cataracts, and a suppressed immune system. Excessive UV*b* exposure also can damage terrestrial plant life, single-cell organisms, and aquatic ecosystems. Other UV radiation, UV*a*, which is not absorbed significantly by ozone, causes premature aging of the skin (WMO, 2007).

Ozone is a natural component of the clean atmosphere. In the absence of human activities on Earth's surface, ozone would still be present near the surface and throughout the troposphere and stratosphere. Ozone's chemical role in the atmosphere includes

helping to remove other gases, both those occurring naturally and those emitted by human activities. If all the ozone were to be removed from the lower atmosphere, other gases such as methane, carbon monoxide, and nitrogen oxide would increase in abundance.

Ozone is constantly being produced and destroyed in a natural cycle. However, the overall amount of ozone is essentially stable. Large increases in stratospheric chlorine and bromine have upset that balance. Therefore, ozone levels are beginning to fall. The ozone depletion process begins when chloroflurocarbons (CFCs) and other ozone-depleting substances (ODS) leak or are released from equipment's.

Winds efficiently mix the troposphere and evenly distribute the gases. CFCs are extremely stable, and they do not dissolve in rain. After a period of a few years, ODS molecules reach the stratosphere. Strong UV light breaks apart the ODS molecule. CFCs release chlorine atoms and halons release bromine atoms. It is these atoms that actually destroy ozone, not the intact ODS molecule. It is estimated that one chlorine atom can destroy over 100,000 ozone molecules before finally being removed from the stratosphere.

3.5.1.2. Carbon Dioxide

The main sources of carbon dioxide are burning of fossil fuels, human and animal respiration, the oceans, and volcanic activity. The main sinks are photosynthesis and the production of carbonates (limestones) in the ocean/land system. The rate of removal of carbon dioxide is observed to be less than the generation (from fossil fuel burning) because the concentration of carbon dioxide in the atmosphere has been rising steadily during the 20th century. About 99% of the Earth's carbon dioxide is dissolved in the oceans. Because solubility is temperature-dependent the gas therefore enters or leaves the oceans. It is estimated that the annual amount of carbon dioxide entering or leaving the air by all mechanisms is about one tenth of the total carbon dioxide content of the atmosphere.

3.5.1.3. Water Vapor

Water vapor is unique among atmospheric trace constituents in that conditions for saturation are common in the atmosphere. This property is the most important factor governing the distribution of water vapor in the atmosphere, both in the troposphere, where it varies by asmuch as four orders of magnitude in a vertical profile, and in the stratosphere.

Water vapor is extremely important in radiative absorption and emission processes in the atmosphere. Its concentration is highly variable. Although always present, in some localities it is difficult to measure, but in the tropics its concentration can be as high as 3% or 4% by volume. Water vapor content of air is a strong function of air temperature. For example, air at 40◦ C can hold up to 49.8 g of water per kilogram of dry air, while at 5◦ C this reduces to 5.5 g per kilogram of dry air.

The major sources of water vapor are evaporation from water surfaces and transpiration from plant life. The main sink is condensation in clouds with resulting precipitation over oceans and land. On an average the concentration of atmospheric water vapor decreases with altitude, although this distribution may vary with space and time.

3.6. Atmospheric Aerosols

Atmospheric aerosols are small airborne particles of widely differing chemical composition.

They can either be of natural or of anthropogenic origin and it is estimated that anthropogenic aerosols constitute around 50% of the global mean aerosol optical thickness. The major sources of anthropogenic aerosols are from fossil fuel burning and biomass burning.

Atmospheric aerosols are important in many ways. Aerosol content affects the Earth’s albedo and plays a major role in the global radiation balance and climate.

Various aerosols act as cloud condensation nuclei and are

important in the formation of clouds and precipitation. In addition, the scattering property of the aerosols can be used by a number of next-generation active remote-sensing instruments in derivation of geophysical parameters. Most aerosol particles originate from blowing soil, smoke, volcanoes, and the oceans. Particles made of sodium chloride or magnesium chloride are hygroscopic and therefore act as good sites for the condensation of water to form cloud droplets.

The concentration of the aerosols varies considerably but is typically on the order of 103 cm^{-3} over oceans, 104 cm^{-3} over rural land, and 105 cm−3 over cities. The concentrations generally decrease with altitude.

The size of aerosol particles is usually given as the diameter of the particle assuming a spherical shape. The sizes of different aerosol particles in the atmosphere are illustrated in Fig. 1.29. Aerosols are usually assigned into three size categories:

(i) aitken particles, or *nucleation* mode (0.001–0.1 μm diameter); (ii) large particles, or *accumulation* mode (0.1–1 μm diameter); and (iii) giant particles, or *coarse particle* mode (>1 μm diameter).

The terms *nucleation* mode and *accumulation* mode refer to the mechanical and chemical processes by which aerosol particles in those size ranges are usually produced. The smallest aerosols, in the nucleation mode, are principally produced by gas-to-particle conversion, which occurs in the atmosphere.

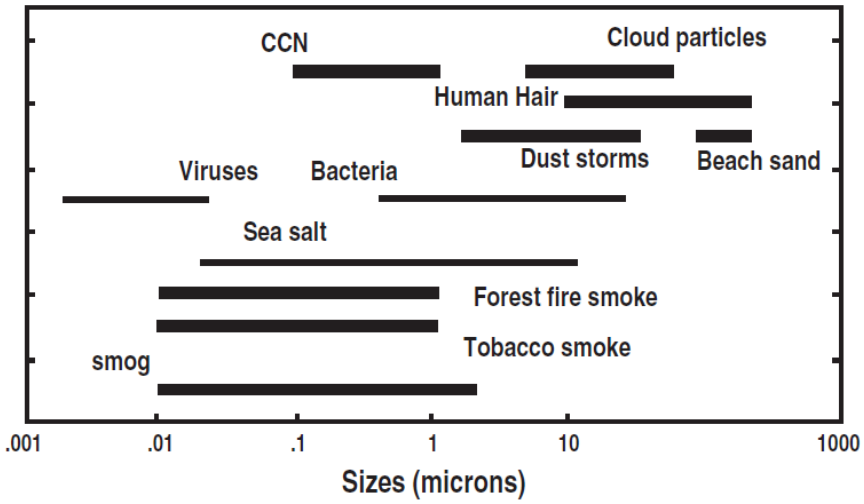

Figure 3.11 Size of different aerosols (Courtesy: Bruce Caron, New Media Studio).

Aerosols in the *accumulation* mode are generally produced by the *coagulation* of smaller particles and by the *heterogeneous* condensation of gas vapor onto existing aerosol particles.

3.6.1 Water-soluble Aerosols

Aerosols consist of water-soluble compounds, such as sulphate, nitrate, and sea salt, and are efficient cloud condensation nuclei (CCN). In unpolluted continental conditions, smaller particles are more likely to be water-soluble. Nearly 80% of the particles in the 0.1–0.3 μm size range are comprised of water-soluble particles. Over oceans, however, much of the coarse particle mode comprised of sea salt aerosols is water-soluble. Water-soluble aerosols are hygroscopic and they are capable of attracting water vapor from the air. The size of hygroscopic particles varies with relative humidity, leading to changes in optical properties as well. The presence of polar functional groups on organic aerosols, particularly carboxylic and dicarboxylic acids, makes many of the organic compounds in aerosols water-soluble and allows them to participate in cloud droplet nucleation. Aerosols, such as metal oxides, silicates, and clay minerals, originate from soil dust

or volcanoes and are insoluble.

3.6.2 Residence Time of Aerosols

The residence time of aerosols depends on their size, chemistry, and height in the atmosphere. Particle residence times range from minutes to hundreds of days.

Aerosols between 0.1 and 1.0 μm, known as the accumulation mode, remain in the atmosphere for a longer time. Smaller aerosols (the nucleation mode) are subject to Brownian motion. As a result, higher rates of particle collision and coagulation increase the size of individual particles and remove them from the nucleation mode. The coarser particles (>1 μm radius) have higher sedimentation rates and therefore the residence time is lower.

Aerosol lifetime is on the order of a few days or weeks, and aerosols are produced unevenly on the surface of the Earth. Variation between different parts of the globe in optical thickness and radiative forcing due to aerosols, can amount to tens of Wm^{-2}, which is a magnitude higher than the global means for these parameters.

3.6.3. Tropospheric Aerosols

Tropospheric aerosols are removed fairly rapidly by deposition or rainout and typically have residence times of about 1 week. Their spatial distribution is therefore very inhomogeneous and strongly correlated with the source regions. Routine satellite monitoring of tropospheric aerosols, when not obstructed by clouds, should provide insights into not only these aspects but also the way aerosols alter cloud optical properties.

3.6.4. Stratospheric Aerosols

Stratospheric aerosols have much longer residence times, on the order of about 1 year, and therefore have a more uniform distribution. As a result, volcanic explosions in which the debris reaches into the stratosphere can perturb global climate for several years. Satellite and sonde measurements indicate a steady increase in the background concentration of stratospheric sulphate of about 40–60% over the last

decade. It seems that this record is not affected by volcanic aerosols but could reflect an influx of increasing tropospheric aerosols. Emissions from subsonic aircraft flying in the stratosphere are also contributing aerosols in the stratosphere. Considering the expected growth in future air traffic, it is indeed necessary to regularly monitor the stratospheric aerosol trends on a global basis.

References

Baldwin M.P., Gray L.J., Dunkerton T.J., et al, (2001) The quasibiennial oscillation, Rev of Geophys, 39: 179–229.

Baldwin M.P., Stephenson D.B., Thompson D.W.J., et al, (2003) stratospheric memory and skill of extended range weather forecasts, Science, 301: 636–640.

Bauer S., Lammer H. Planetary Aeronomy: Atmosphere Environments in Planetary Systems, Springer Publishing, 2004.

Blanc M., Kallenbach R., Erkaev N.V. (2005) "Solar System Magnetospheres". Space Science Reviews, 116 (116): 227–298. doi: 10.1007/s11214-005-1958-y.

Brasseur G, Solomon S. (1984). Aeronomy of the Middle Atmosphere, D Riedel Publishing Company, Dordrecht.

Geerts B., Linacre E. (1997). The height of the tropopause, University of Wyoming (http://wwwdas/~geerts/cwx/notes/chap01/trop-height 01. gif).

Grotjahn R., Encyclopedia of Atmospheric Sciences, 2nd Edition, 2015.

Guharay A., Nath D., Pant P., Pande B., Russell J.M., Pandey K. (2009). Observation of semiannual and annual oscillation in equatorial middle atmospheric long term temperature pattern. Ann. Geophys., 27: 4273–4280.

Hansen J., Reto R., Makiko S., Ken L. (2009). "If It's That Warm, How Come It's So Damned Cold?".

Hartjenstein G. (1999) Tropopause folds and the related stratosphere

troposphere mass exchange, Project Report of University of Munich.(http://www.lrz-muenchen.de/projekte/hlr projects/1997-1999/cd/daten/pdf/uh22102. pdf).

Holton J.R., Haynes P.H., McIntyre M.E. et al, (1995) Stratosphere troposphere exchange, Rev. Geophys., 33: 403–440

Holton J.R., Haynes P.H., McIntyre M.E., Douglass A.R., Rood R.B., Pfister L., (1995) Stratosphere-troposphere exchange, Rev. Geophys, 33: 403–440.

Kodera K., Kuroda Y. (2000) Tropospheric and stratospheric aspects of the Artctic Oscillation, Geophys Res. Lett., 27: 3349–3352.

Labitzke K., van Loon H. (1999) The Stratosphere, Phenomena, History and Relevance, Springer, Berlin.

Labitzke K., van Loon H. (1999) The Stratosphere, Phenomena, History and Relevance, Springer, Berlin.

Matthew H.H., Erhan K., David C. F., Joleen M., Kugi et al, (1997). Mean winds in the tropical stratosphere and mesosphere during January 1993, March 1994 and August 1994. J. Geophysical Res., 102(22): 26033-26052.

Maturilli M. (2007). "Polar Stratospheric Clouds Above Spitsbergen". Alfred Wegener Institute for Polar and Marine Research.

Mohanakumar K. Stratosphere Troposphere Interactions: An Introduction. ISBN 978-1-4020-8216-0, 2008.

Murry L.S. (2011) Physics of the atmosphere and climate, 2nd ed., ISBN 978-0-521-76718-7 Hardback. USA.

Prölss G.W., Bird M.K., "Physics of the Earth's Space Environment",

Springer Verlag, Heidelberg, 2010.

Randel W.J., Udelhofen P., Fleming E., Geller M.A., Gelman M., et al., (2004) The SPARC Intercomparison of Middle Atmosphere Climatologies. J. Climate, 17: 986–1003.

Reeves C.E., Penkett S.A. et al, (2002) "Potential for photochemical ozone formation in the troposphere over the North Atlantic as derived from aircraft observations during ACSOE". J. Geophysical Res: Atmospheres. 107(D23): ACH 14–1–ACH 14–14. doi:10.1029/2002jd002415.

Russel C.T. (1987) The magnetosphere, in The Solar Wind and the Earth, edited by S.-I Akasofu and Y. Kamide, Terra Scientific Publishing Co., Tokyo.

Stuwart R.R. (2005) The oceanic influence on North American drought, in Oceanography in the 21st Century – An Online Textbook, Department of Oceanography, Texas A&M University.

Venkat R.M., Patra A.K., Krishna M.B. (2010) Tropical mesopause: Is it always close to 100 km? J. Geophysical Res., 115 (D6).

Wallace J.M., Hobbs P.V. (2006) Atmospheric Science – An Introductory Survey, Second edition, Elsevier, New York.

Wirth V., Szabo T. (2007) Sharpness of the extratropical tropopause in baroclinic life cycle experiments, J. Geophysical Res. Letts., 34: L02809, doi: 10.1029/2006GL028369.

Chapter 4
Climate of red planet (Mars)

Introduction

The particular importance of Mars among the other planets results primarily from the existence of its atmosphere. On the one hand, it endows Mars with a unique "Earth-like planet" status which motivates many studies aimed at testing the concepts, theories and tools developed for Earth climate sciences on a slightly different system. On the other hand, the atmosphere may have enabled the climatic conditions on Mars to have sometime been suitable for liquid water on its surface, and thus life. Mars present-day climate system is complex, highly variable and only partly understood. Mars, however, is cold and dry, and its atmosphere is so thin that the presence of liquid water, never detected, is unlikely on the surface. Nevertheless, the planet was probably different in the past. The surface of Mars is characterized by multiple geological evidences that suggest that liquid water existed at and near the Martian surface at various time in its history. Two concepts of past climate (or "paleoclimate") must be distinguished for Mars. On the one hand, it appears that the climate was sometime different from what it is today throughout most of its history and until quite recently on the geological timescale (a few millions ago, or even a few thousands of years ago) because of the oscillations of Mars orbit and rotation parameters. On the other hand, the observation of the geology and mineralogy f the oldest surface on Mars (dating back to more than 3 billion years ago) provide evidence that the Martian climate was then completely different then, with abundant liquid water on the surface, probably because of a thickest atmosphere or a higher

geothermal flux.

Mars is a small planet about half the diameter of the Earth and about one and a half time more distant from the sun. The atmospheric pressure at the surface range from 1mbar to 14mbardepending on location and season (compared to 1013mbar on average at sea level on Earth). The dominant gas is CO_2. In spite of these differences, the Martian climate system is similar to the Earth climate system in many aspects. The two planets rotate with almost the same rate and a similar obliquity. The length of day is thus almost the same (24h and 40 minutes on Mars) and the seasonal cycle is comparable. In such conditions, the general circulation is controlled by similar processes: On both planets, the Hadley circulation (the process that generates the trade winds) is important at low latitudes, whereas "baroclinic" planetary waves (a succession of low and high-pressure zones) dominate the weather system at mid-latitudes.

4.1. Weather

Mars' temperature and circulation vary every Martian year (as expected for any planet with an atmosphere and axial tilt). Mars lacks oceans, a source of much inter-annual variation on Earth. Mars Orbiter Camera data beginning in March 1999 and covering 2.5 Martian years show that Martian weather tends to be more repeatable and hence more predictable than that of Earth. If an event occurs at a particular time of year in one year, the available data (sparse as it is) indicate that it is fairly likely to repeat the next year at nearly the same location, give or take a week.

On September 29, 2008, the Phoenix lander detected snow falling from clouds 4.5 kilometres (2.8 mi) above its landing site near Heimdal Crater. The precipitation vaporized before reaching the ground, a phenomenon called virga.

4.2. Clouds

Martian dust storms can kick up fine particles in the atmosphere around which clouds can form. These clouds can form very high up,

up to 100 km (62 mi) above the planet (SPACE Staff, 2006). The first images of Mars sent by Mariner 4 showed visible clouds in Mars' upper atmosphere. The clouds are very faint and can only be seen reflecting sunlight against the darkness of the night sky.

Figure 4.1 Icy blue clouds swirl over the Martian mountain Syrtis Major (far right) in this Hubble telescope portrait of the Red Planet. According to a new study, the blue clouds of Mars may form as the result of tiny meteorite impacts in the planet's atmosphere (Brandon,. 2019).

Look up from the Red Planet on the right morning, and you might see a blue sky. All year round, wispy blue clouds of ice form in the Martian atmosphere, hovering between 18 and 37 miles (30 and 60 kilometers) above the planet's surface. There, they streak across the sky like the feathery cirrus clouds we see so often on Earth.

To form a cloud, airborne ice or water molecules need something solid to condense onto — a fleck of sea salt, maybe, or some stray dust tossed up on the wind. Scientists long assumed that bits of surface dust lofted into the Martian atmosphere might be the source of the planet's icy blue clouds. But a new study published today (June 17) in the journal Nature Geoscience argued that this might not be the

case.

4.3. Temperature

Measurements of Martian temperature predate the space age. However, early instrumentation and techniques of radio astronomy produced crude, differing results. Early flyby probes (Mariner 4) and later orbiters used radio occultation to perform aeronomy. With chemical composition already deduced from spectroscopy, temperature and pressure could then be derived. Nevertheless, flyby occultations can only measure properties along two transects, at their trajectories' entries and exits from Mars' disk as seen from Earth. This results in weather "snapshots" at a particular area, at a particular time. Orbiters then increase the number of radio transects. Later missions, starting with the dual Mariner 6 and 7 flybys, plus the Soviet Mars 2 and 3, carried infrared detectors to measure radiant energy. Mariner 9 was the first to place an infrared radiometer and spectrometer in Mars orbit in 1971, along with its other instruments and radio transmitter. Viking 1 and 2 followed, with not merely Infrared Thermal Mappers (IRTM). The missions could also corroborate these remote sensing datasets with not only their in situ lander metrology booms, but with higher-altitude temperature and pressure sensors for their descent (Pettit et al, 1924).

Differing *in situ* values have been reported for the average temperature on Mars (Eydelman, 2001), with a common value being −63 °C (210 °K; −81 °F). Surface temperatures may reach a high of about 20 °C (293 °K; 68 °F) at noon, at the equator, and a low of about −153 °C (120 °K; −243 °F) at the poles. Actual temperature measurements at the Viking landers' site range from −17.2 °C (256.0 °K; 1.0 °F) to −107 °C (166 °K; −161 °F). The warmest soil temperature estimated by the Viking Orbiter was 27 °C (300 K; 81 °F). The Spirit rover recorded a maximum daytime air temperature in the shade of 35 °C (308 K; 95 °F), and regularly recorded temperatures well above 0 °C (273 K; 32 °F), except in winter (Raly, 2007).

It has been reported that "On the basis of the nigh time air temperature data, every northern spring and early northern summer yet observed were identical to within the level of experimental error (to within ±1 °C)" but that the "daytime data, however, suggest a somewhat different story, with temperatures varying from year-to-year by up to 6 °C in this season This day-night discrepancy is unexpected and not understood". In southern spring and summer, variance is dominated by dust storms which increase the value of the night low temperature and decrease the daytime peak temperature. This results in a small (20 °C) decrease in average surface temperature, and a moderate (30 °C) increase in upper atmosphere temperature (Gurwell et al, 2005).

Before and after the Viking missions, newer, more advanced Martian temperatures were determined from Earth via microwave spectroscopy. As the microwave beam, of less than 1 arc minute, is larger than the disk of the planet, the results are global averages. Later, the Mars Global surveyor's Thermal Emission Spectrometer and to a lesser extent 2001 Mars Odyssey's THEMIS could not merely reproduce infrared measurements but intercompare lander, rover, and Earth microwave data. The Mars Reconnaissance's Mars Climate Sounder can similarly derive atmospheric profiles. The datasets "suggest generally colder atmospheric temperatures and lower dust loading in recent decades on Mars than during the Viking Mission (Bell et al, 2009), although Viking data had previously been revised downward. The TES[1] data indicates "Much colder (10–20 °K) global atmospheric temperatures were observed during the 1997 versus 1977 perihelion periods" and "that the global aphelion atmosphere of Mars is colder, less dusty, and cloudier than indicated by the established Viking climatology," again, taking into account the Wilson and Richardson revisions to Viking data (Clancy, 2000).

A later comparison, while admitting "it is the microwave record of air temperatures which is the most representative," attempted to merge

1 - Thermal Emission Spectrometer

the discontinuous spacecraft record. No measurable trend in global average temperature between Viking IRTM[1] and MGS[2] TES was visible. "Viking and MGS air temperatures are essentially indistinguishable for this period, suggesting that the Viking and MGS eras are characterized by essentially the same climatic state." It found "a strong dichotomy" between the northern and southern hemispheres, a "very asymmetric paradigm for the Martian annual cycle: a northern spring and summer which is relatively cool, not very dusty, and relatively rich in water vapor and ice clouds; and a southern summer rather similar to that observed by Viking with warmer air temperatures, less water vapor and water ice, and higher levels of atmospheric dust (Liu et al, 2003).

The Mars Reconnaissance Orbiter MCS[3] instrument was, upon arrival, able to operate jointly with MGS for a brief period; the less-capable Mars Odyssey THEMIS and Mars Express SPICAM datasets may also be used to span a single, well-calibrated record. While MCS and TES temperatures are generally consistent, investigators report possible cooling below the analytical precision. "After accounting for this modeled cooling, MCS MY 28 temperatures are an average of 0.9 (daytime) and 1.7 K (night-time) cooler than TES MY 24 measurements (Bandfield et al, 2013).

It has been suggested that Mars had a much thicker, warmer atmosphere early in its history. Much of this early atmosphere would have consisted of carbon dioxide. Such an atmosphere would have raised the temperature, at least in some places, to above the freezing point of water (Forget et al, 2013). With the higher temperature running water could have carved out the many channels and outflow valleys that are common on the planet. It also may have gathered together to form lakes and maybe an ocean. Some researchers have suggested that the atmosphere of Mars may have been many times as

---

1 - Mars infrared thermal mapper

2 - Mars Global Surveyor

3 - Mars Climate Sounder

thick as the Earth's; however research published in September 2015 advanced the idea that perhaps the early Martian atmosphere was not as thick as previously thought (Fassett, 2011).

4.4. Atmospheric pressure

The Martian atmosphere is composed mainly of CO_2 and has a mean surface pressure of about 600 Pascals (Pa), much lower than the Earth's 101,000 Pa. One effect of this is that Mars' atmosphere can react much more quickly to a given energy input than that of Earth's atmosphere (NASA, 2007). As a consequence, Mars is subject to strong thermal tides produced by solar heating rather than a gravitational influence. These tides can be significant, being up to 10% of the total atmospheric pressure (typically about 50 Pa). Earth's atmosphere experiences similar diurnal and semidiurnal tides but their effect is less noticeable because of Earth's much greater atmospheric mass.

Although the temperature on Mars can reach above freezing [0 °C (273 K; 32 °F)], liquid water is unstable over much of the planet, as the atmospheric pressure is below water's triple point and water ice sublimes into water vapor. Exceptions to this are the low-lying areas of the planet, most notably in the Hellas planitia impact basin, the largest such crater on Mars. It is so deep that the atmospheric pressure at the bottom reaches 1155 Pa, which is above the triple point, so if the temperature exceeded 0 °C liquid water could exist there.

4.5. Wind

The surface of Mars has a very low thermal inertia, which means it heats quickly when the sun shines on it. Typical daily temperature swings, away from the Polar Regions, are around 100 K. On Earth, winds often develop in areas where thermal inertia changes suddenly, such as from sea to land. There are no seas on Mars, but there are areas where the thermal inertia of the soil changes, leading to morning and evening winds akin to the sea breezes on Earth. The Antares

project "MSW[1]" has identified some minor weaknesses in current GCMs[2] due to the GCMs' more primitive soil modeling. "Heat admission to the ground and back is quite important in Mars, so soil schemes have to be quite accurate (NASA, 2007). Those weaknesses are being corrected and should lead to more accurate future assessments, but make continued reliance on older predictions of modeled Martian climate somewhat problematic.

At low latitudes the Hadley circulation dominates, and is essentially the same as the process which on Earth generates the trade winds. At higher latitudes a series of high and low pressure areas, called baroclinic pressure waves, dominate the weather. Mars is drier and colder than Earth, and in consequence dust raised by these winds tends to remain in the atmosphere longer than on Earth as there is no precipitation to wash it out (accepting CO_2 snowfall) (François, 2007). One such cyclonic storm was recently captured by the Hubble Space Telescope (pictured below).

One of the major differences between Mars' and Earth's Hadley circulations is their speed (NASA, 2007) which is measured on an overturning timescale. The overturning timescale on Mars is about 100 Martian days while on Earth, it is over a year.

4.6. Atmospheric Electricity

It is thought that Martian dust storms can lead to atmospheric electrical phenomena (Harrison et al, 2016). Dust grains are known to become electrically charged upon colliding with the ground or with other grains. Theoretical, computational and experimental analyses of lab-scale dusty flows and full-scale dust devils on Earth indicate that self-induced electricity, including lightning, is a common phenomenon in turbulent flows laden with dust (Renno et al, 2003). On Mars, this tendency would be compounded by the low pressure of the atmosphere, which would translate into much lower electric fields

1 - Mars small-scale weather

2 - Global climate models

required for breakdown. As a result, aerodynamic segregation of dust at both meso- and macro-scales could easily lead to a sufficiently large separation of charges to produce local electrical breakdown in dust clouds above the ground (Di and Urzay, 2018).

Nonetheless, in contrast to other planets in the Solar System, no in-situ measurements exist on the surface of Mars to prove these hypotheses (Aplin and Fischer, 2017). The first attempt to elucidate these unknowns was made by the Schiaparelli EDM lander of the ExoMars mission in 2016, which included relevant onboard hardware to measure dust electric charges and atmospheric electric fields on Mars. However, the lander failed during the automated landing on 19 October 2016 and crashed on the surface of Mars.

4.7. Methane

Methane (CH_4) is chemically unstable in the current oxidizing atmosphere of Mars. It would quickly break down due to ultraviolet radiation from the Sun and chemical reactions with other gases. The principal candidates for the origin of Mars' methane include non-biological processes such as water-rock reactions, radiolysis of water, and pyrite formation, all of which produce H_2 that could then generate methane and other hydrocarbons via Fischer–Tropsch synthesis with CO and CO_2 (Mumma et al, 2010). It has also been shown that methane could be produced by a process involving water, carbon dioxide, and the mineral olivine, which is known to be common on Mars.

Living microorganisms, such as methanogens, are another possible source, but no evidence for the presence of such organisms has been found on Mars (Krasnopolsky et al, 2004).

4.8. Mountains

Martian storms are significantly affected by Mars' large mountain ranges. Individual mountains like record holding Olympus Mons (26 km (85,000 ft)) can affect local weather but larger weather effects are due to the larger collection of volcanoes in the Tharsis region.

One unique repeated weather phenomenon involving mountains is a spiral dust cloud that forms over Arsia Mons. The spiral dust cloud over Arsia Mons can tower 15 to 30 km (49,000 to 98,000 ft) above the volcano. Clouds are present around Arsia Mons throughout the Martian year, peaking in late summer.

Clouds surrounding mountains display a seasonal variability. Clouds at Olympus Mons and Ascreaus Mons appear in northern hemisphere spring and summer, reaching a total maximum area of approximately 900,000 km^2 and 1,000,000 km^2 respectively in late spring. Clouds around Alba Patera and Pavonis Mons show an additional, smaller peak in late summer. Very few clouds were observed in winter. Predictions from the Mars General Circulation Model are consistent with these observations (Benson et al, 2006).

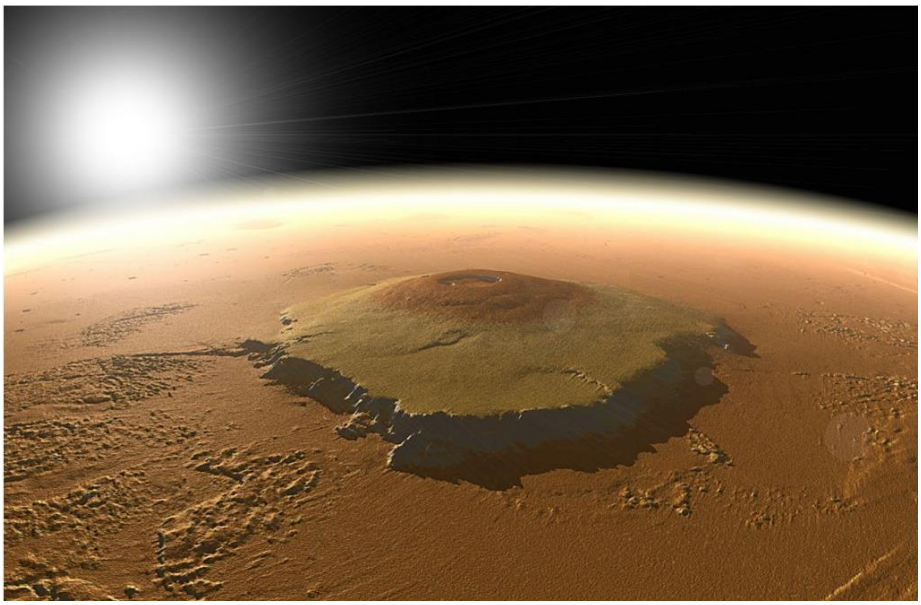

Figure 4.2 Olympus Mons is the largest volcano in the solar system. The massive Martian mountain towers high above the surrounding plains of the red planet, and may be biding its time until the next eruption (NASA/MOLA Science Team/ O. de Goursac, Adrian Lark, 2017).

4.8. Seasons

Mars has a Spring, Summer, Autumn, and Winter like Earth, but the Martian year is about 668.599 Martian sols long (687 Earth days), which means that all the seasons will be longer than on Earth. Mars' orbit is quite eccentric compared to that of Earth. Because of this, there are major differences in the orbital speed of Mars as it orbits the Sun. Mars is slowest when it is at aphelion (the farthest point from the Sun) and fastest at perihelion (the closest point to the Sun). Since the eccentricity of Mars' orbit exaggerates the *aphelion* and *perihelion* distances, Mars' seasons vary in duration more than those on Earth, which has a nearly circular orbit. The table below helps to illustrate these effects (Malin et al, 2010).

Table 4.1 Comparing of seasons length on Earth and Mars

Season (Northern Hemisphere)	Length of Season on Earth (Earth Days)	Length of Season on Mars (Martian Days
Spring	93	194
Summer	93	178
Autumn	90	142
Winter	89	154

Summer is the longest season on Earth because summer occurs when Earth is near aphelion. Similarly, most of spring and early summer occur near Mars' *aphelion*, resulting in a longer northern summer season than in the southern hemisphere. Although one would expect warmer summers in the northern hemisphere of Mars due to the extreme length of spring and summer, and the more direct radiation from the Sun reaching the surface, this is not the case. The eccentricity of Mars' orbit causes Mars to receive 44% more radiation from the Sun at perihelion (during southern summer) than at aphelion (is the point in the orbit of an object where it is farthest from the Sun). As a result, the southern hemisphere (the point in orbit where an

object is nearest to the sun is called the perihelion) summers are shorter, but hotter than northern hemisphere summers. This phenomenon is demonstrated by the fact that the southern polar ice cap frequently disappears entirely during summer, while the northern polar ice cap has never been known to do so. Southern summers can be as much as 30 degrees centigrade hotter than northern summers.

Table 4.2 The southern hemisphere also experiences longer, colder winters than the northern hemisphere since Mars is near aphelion during these seasons.

Season	Northern Hemisphere	Southern Hemisphere
Winter	Shorter and Warmer	Longer and Colder
Summer	Longer and Cooler	Shorter and Hotter

.

Since the inclination of Mars' axis (25^{o}) is quite close to that of Earth (23.5^{o}), the hours of daylight and darkness over the seasons vary nearly the same as on Earth. However, temperature variations on Mars follow the hours of sunlight more closely since the atmosphere is quite thin, and there are no bodies of water to retain heat after dark (Levy et al, 2008).

Seasonal variations may be more precisely specified by the parameter Ls, which is the areocentric longitude of the Sun. It is an angular measure of the position of a planet in its orbit. Ls = 0 corresponds to the first day of spring, or when the planet is on the Spring Equinox. Ls = 90 is the Summer Solstice, Ls = 180 is the Autumnal Equinox, and Ls = 270 is the Winter Solstice. So Ls provides a convenient way of measuring the changes in season. Incidentally, equinox is Latin for "equal night", and refers to the fact that on the day of the spring or Autumnal Equinox, there are equal hours (12) of day and night everywhere on the Earth. Also, solstice means "the Sun stands still", and refers to the observation that near the summer and Winter Solstice dates, the sunrise and sunset times do not vary appreciably (Carr, 1981).

4.8.1. Winter on Mars

Mars' polar caps essentially have two components: "Residual" and "seasonal" caps. The residual polar caps are the bulk of the polar cap that persists year after year. The residual northern polar cap remains pretty consistent over time, while the residual southern polar cap is changing quite a bit…but we'll save the complexities of the southern cap.

The residual northern polar cap is made up predominantly of water ice with some interspersed layers of dust and sand. In the central portion, it is about 2 kilometres thick—on par with the average thickness of the Antarctic ice sheet. The residual cap covers an area nearly twice the size of France, with a volume about half that of the Greenland ice sheet.

In winter however, the areal extent of the cap changes dramatically with the formation of the seasonal polar cap. The seasonal cap forms when carbon dioxide and water vapour in the atmosphere condense onto the Martian surface as frost. Depending on latitude, this frost layer can be up to a meter thick. The northern seasonal cap extends as far south as ~53°N latitude (Jakosky and Haberle, 1990).

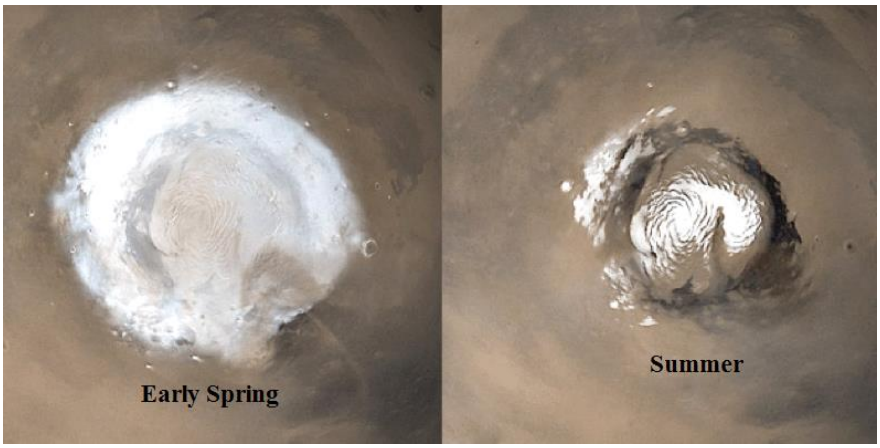

Figure 4.3 Mars' northern polar cap at near-maximum extent in early spring (left, showing the residual + seasonal cap) compared to mid-summer (right, showing the residual cap), imaged by the Mars Global Surveyor wide-angle Mars Orbiter Camera. Image credit: NASA/JPL-Caltech/MSSS.

For most of winter the cap is also shrouded in a thick veil of clouds known as the north polar hood. The "hood" forms from a series of storms like clockwork every year in late summer and persists through mid-winter. It is prominent enough to be seen from Earth. Once the cap peeks back over onto the day side of Mars in early spring, we're able to get a snapshot of the cap at its near-maximum extent from orbit.

Viking 2, at about 48°N latitude in *Utopia Planitia*, measured winter temperatures as low as 120°C (-184°F). For comparison, the lowest recorded temperature on Earth was nearly -90°C (-130°F) in Antarctica. Phoenix, way up at 68°N, (expectedly) didn't survive a Martian winter to make any temperature measurements due to the thickening clouds of the north polar hood blocking sunlight from reaching the solar panels. Even in summer however, it was cold enough at the Phoenix landing site for frost to form on the Martian surface on a nightly basis. The lowest temperature recorded by Phoenix was a frigid -98°C (-144°F)—not even in winter yet. Models and data from orbit suggest that the poles of Mars may get as cold as -130°C (-200°F) in wintertime (Madeleine, 2009).

The low water content of the Martian atmosphere means that the humidity is also extremely low, making winters there a dry cold. While we typically think of "deserts" as hot places like the Sahara, the term can refer to cold polar areas that receive little snow or rainfall as well, like the Antarctic Dry Valleys or Canada's Devon Island. Conditions on Mars fall into the category of a "cold polar desert."

Figure 4.5 Early summer morning water frost on the Martian surface imaged by the Phoenix lander on August 14, 2008. Image credit: NASA/JPL-Caltech/University of Arizona/Texas A&M University.

References

Aplin K.L., Fischer G. (2017) Lightning detection in planetary atmospheres. Weather, 72 (2): 46–50. doi: 10.1002/wea.2817

Bandfield J.L., et al. (2013) Radiometric Comparison of Mars Climate Sounder and Thermal Emission Spectrometer Measurements. Icarus, 225 (1): 28–39.

Bell J et al, (2009) "Mars Reconnaissance Orbiter Mars Color Imager (MARCI): Instrument Description, Calibration, and Performance". Journal of Geophysical Research, 114 (8): E08S92. doi:10.1029/2008je003315.

Benson et al, (2006) Interannual variability of water ice clouds over major Martian volcanoes observed by MOC. Icarus, 184 (2): 365–371. doi:10.1016/j.icarus.2006.03.014

Carr M.H. (1981) The Surface of Mars, Yale University

Clancy R. (2000) An inter-comparison of ground-based millimeter, MGS TES, and Viking atmospheric temperature measurements: Seasonal and inter-annual variability of temperatures and dust loading in the global Mars atmosphere". Journal of Geophysical Research, 105 (4): 9553–9571. doi:10.1029/1999JE001089

Di Renzo M., Urzay J. (2018) Aerodynamic generation of electric fields in turbulence laden with charged inertial particles. Nature Communications, 9 (1): 1676. doi:10.1038/s41467-018-03958-7.

Eydelman A. (2001) Temperature on the Surface of Mars, the Physics Fact book

Fassett C.J.H. (2011) Sequence and timing of conditions on early Mars. Icarus, 211 (2): 1204–1214. doi: 10.1016/j.icarus.2010.11.014

Forget F., et al. (2013) "3D modelling of the early Martian climate under a

denser CO_2 atmosphere: temperatures and CO_2 ice clouds. Icarus, 222 (1): 81–99. doi:10.1016/j.icarus.2012.10.019

François F. (2007) Alien Weather at the Poles of Mars, Science.

Gurwell M.A., Bergin E.A., Et al., (2005) "Mars surface and atmospheric temperature during the 2001 global dust storm". Icarus, 175 (1): 23–3. doi:10.1016/j.icarus.2004.10.009

Harrison R.G., Barth E., Esposito F. et al, (2016) Applications of electrified dust and dust devil electrodynamics to Martian atmospheric electricity. Space Sci. Rev. 203 (1–4): 299–345. doi: 10.1007/s11214-016-0241-8

Jakosky B.M., Haberle R.M. (1990) Year-to-year instability of the Mars Polar Cap. J. Geophysics. Res., 95: 1359–1365. doi:10.1029/JB095iB02p01359

Krasnopolsky V.A, Maillard J.P., Owen T.C. (2004) Detection of methane in the Martian atmosphere: evidence for life? Icarus, 172 (2): 537–547. doi: 10.1016/j.icarus.2004.07.004

Levy J., Head J., Marchant D., Kowalewski D. (2008) Identification of sublimation-type thermal contraction crack polygons at the proposed NASA Phoenix landing site: Implications for substrate properties and climate-driven morphological evolution. J. Geophysical Res. Lett., 35 (4): 555. doi:10.1029/2007GL032813.

Liu Junjun, Mark I.R., Wilson R.J. (2003) An assessment of the global, seasonal, and inter-annual spacecraft record of Martian climate in the thermal infrared. Journal of Geophysical Research, 108 (5089): 5089. doi: 10.1029/2002JE001921.

Madeleine J. et al. (2009) Amazonian northern mid-latitude glaciation on

Mars: A proposed climate scenario. Icarus, 203: 300–405.

Malin M. et al (2010) An overview of the 1985–2006 Mars Orbiter Camera science investigation, MARS INFORMATICS. http://marsjournal.org

Mumma M. et al, (2010) The Astrobiology of Mars: Methane and Other Candinate Biomarker Gases, and Related Interdisciplinary Studies on Earth and Mars. Astrobiology Science Conference 2010, Astrophysics Data System, Greenbelt, MD: Goddard Space Flight Center.

NASA (2007) Archived from the original, 2007 Mars General Circulation Modeling Group. Mars' low surface pressure.

(NASA 2007) Mars General Circulation Modeling Group. Mars' desert surface.

NASA (2008) NASA Mars Lander Sees Falling Snow, Soil Data Suggest Liquid Past.

Pettit et al, (1924) Radiation Measures on the Planet Mars, Publications of the Astronomical Society of the Pacific, 36 (9): 269–272. JSTOR 40693334

Raly A.J.S. (2007) Extreme Planet Takes, Toll Jet Propulsion Laboratory Featured Story

Renno N.O., Wang A.S., Atreya S.K., de Pater I., Roos-Serote M. (2003) Electrical discharges and broadband radio emission by Martian dust devils and dust storms. J. Geophysical 74 Res. Lett., 30 (22): 2140. doi:10.1029/2003GL017879.

SPACE Staff (2006) Mars clouds higher than any on Earth.

Chapter 5
Taitan's Climate

Introduction

Titan, the largest satellite of the planet Saturn, is unique among the icy satellites in its possession of a dense atmosphere. Like the Earth, the dominant atmospheric gas is nitrogen, but the interesting optical effects are controlled by the trace gases. After nitrogen, the most abundant gases are methane (4%) and hydrogen (~0.4%, Waite et al., 2005). Argon was thought to be present at a few percent levels, but recent measurements by the INMS measurement on the Cassini spacecraft indicate much smaller mixing ratios (~10−6). Solar UV penetrating into Titan's mesosphere breaks methane down into CH_3 radicals which combine at lower altitudes to form higher order hydro-carbons (such as C2H6 and C3H8). N2is also broken down (by cosmic rays and electrons from Saturn's magnetosphere) and combines with other molecules to form various nitriles. Titan's most visible feature is the optically thick haze layer enveloping the planet about 200 km above the surface. The ex-act composition of the haze particles is unknown, but spectra of laboratory produced compounds known as Titan tholin provide a good fit to the Voyager observations. These tholin are com-posed of carbon, nitrogen, and hydrogen molecules in various abundances but typical ratios are of order C/H≈1, C/N≈5 Titan's methane–ethane clouds231(McKay, 1996). Toon et al. (1992) and Barth and Toon (2003) have shown that these haze particles can be represented by a distribution of particles with radii ranging from 13 Å to 3.35 μm and peaking near 0.1 μm below 100 km. The largest of these particles take more than a (terrestrial) year to fall a scale height

of 30 km. However, the haze particles are the only known condensation nuclei on which clouds may form. Ground-based and HST observations show a change in the vertical haze profile in the lower stratosphere consistent with a gap in the haze.

Anderson et al. (2004) fit the gap between 25 and 75 km while Young et al. (2002) find the gap between the tropopause and 20 km. Rannou et al. (2003) characterized the haze vertical profile with a fractal model constrained by observations. They required a reduction in the haze extinction coefficient below 80 km for consistency with observations. Sagan and Thompson (1984) showed that Titan's various vapors will condense at a number of altitudes in the atmosphere, implying a layered structure to Titan's tropospheric clouds. Frere et al. (1990) produced the first Titan microphysics model to study the condensation of multiple organic and nitrile species (as detected by Voyager). They found that particles above 70 km are mainly composed of nitriles. Propane and C_2 hydrocarbons condense between 70 and 30 km. Below 30 km, methane dominates. Since many of the nucleation properties of these various nitriles and hydrocarbons have never been measured, it is impossible to simulate the full layering of Titan's cloud particles with sufficient accuracy. However, based on the lab measurements of Curtis et al. (2005) we can now study the effects of methane nucleation onto ethane coated tholin particles. Improvements in adaptive optics have allowed ground based observers to achieve much better resolution across Titan's disk. Recent observations by Brown et al. (2002) and Roe et al, (2002) have shown long lived south polar clouds. Roe et al. (2002) report three cloud features increasing in brightness and changing size within a period of 3 h. Brown et al, (2002) were able to locate the clouds at 16±5 km and determine a diameter of 200 km. Both papers found clouds to be about 0.3% brighter than Titan. Additional observations by Brown et al, (2002) found a larger cloud of 1400 km diameter and brightness of about 1% of Titan's total flux. All observations described above were made during southern hemisphere spring. Bouchez (2004) undertook an intensive imaging campaigning the fall

and winter of 2002–2003 to quantify properties of Titan's clouds such as location, duration, frequency, and size. They found transient clouds at southern latitudes of 70–80◦, consistent with a global coverage of 0.2–0.7%. The clouds traveled with an average speed of less than 3.5 m/s and rotated out of view without changing their size. Bouchez (2004) addition-ally located a bright scattering region seen near Titan's South Pole at an altitude of 35±10 km, above the region of the transient tropospheric clouds, citing possible cirrus-like, optically thin methane condensation clouds as a possible explanation. Additional cloud observations between 40 and 65 km are too high for methane condensation, but, as indicated by Sagan and Thompson (1984), Barth and Toon (2003) and this work, maybe a layer of ethane clouds.

Cassini and ongoing ground-based observations have both given us more information on the frequency and duration of these clouds and found evidence for clouds at mid-latitudes. Roe et al. (2005) reported the first evidence for mid-latitude clouds, located near 40◦S. Their altitudes are confined to the troposphere and spatial extents range from several hundred to several thousand kilometers. Porco et al. (2005) report on observations made by the Imaging Science Subsystem (ISS) onboard the Cassini orbiter. They imaged the south polar and mid-latitude clouds and describe a third class of clouds consisting of large-scale nearly zonal streaks (at latitudes of 36–39◦S and 67–72◦S).

Climatic conditions on Titan are a mixture of traits borrowed from Venus, Earth, and Mars. Titan has a N_2-based atmosphere with a surface pressure of 1.45 bars, similar to Earth and distinct from other satellites. The total column density of Titan's atmosphere exceeds Earth's and its surface temperature varies little with season and region. The difference between Titan's poles to equator surface temperature is more like that of Venus. Titan's atmosphere and seas is equivalent to a global precipitable methane layer of ~7 m. It is more similar to the water abundance on Mars, ~20 m, rather than the 2.7 km of water found on Earth. Yet unlike Mars and Earth, most of Titan's volatile inventory is found in the atmosphere rather than on the

surface. Surface features, while largely formed by erosion, appear more highly organized, as do the clouds. Unlike the current volatile inventory on any of the terrestrial planets, Titan's climate is not stable. Its methane abundance is continually dwindling and its climate evolving, unless a continual surface supply of CH_4 precisely matches the methane destruction rate by UV photolysis.

Starting with the basic observations that establish our level of understanding of Titan's atmosphere, one can ask whether it is possible to explain Titan's climate and weather as resulting from the different fundamental properties, such as Saturn's orbital eccentricity, Titan's smaller radius, longer spin period, larger distance from the Sun, higher atmospheric column abundance, effective temperature, and disparate chemistry. This chapter explores the processes by which these fundamental parameters establish the contrast between Titan's climate and those on other planetary bodies.

5.1. Composition of Taitan's Atmosphere

Most of the composition of Titan's atmosphere is established by photo-dissociation and ionization of the two main atmospheric components, N_2 and CH_4 (Yung et al, 1984). This chemistry produces mainly H_2, ethane (C_2H_6), acetylene (C_2H_2), hydrogen cyanide (HCN), propane (C_3H_8), and ethylene (C_2H_4) (Table 1). Notable exceptions are CO, CO_2, and H_2O, which require a source of oxygen, possibly due to ablation of micrometeorites and/or the deposition of energetic O^+ (Hörst et al, 2008).

As understood through UV to infrared (IR) spectroscopy of Titan's atmosphere, plasma measurements of the ionosphere, and in situ mass spectrometer measurements extending from the surface to the thermosphere, multiple energy sources contribute to this critical first step. Energetic photons and photoelectrons deposit their energy in the upper atmosphere (above 700 km) and are the dominant energy source in the daytime (Lavvas et al, 2011c).

Species	Abundance	Origin/Evolution
N_2	0.98	Interior/Stable
CH_4	0.014	Interior/Photodissociates
H_2	0.004	CH_4 photolysis/Escapes
C_2H_6	2×10^{-5}	CH_4 photolysis/Sediments
C_2H_2	3×10^{-6}	CH_4 photolysis/Sediments
HCN	7×10^{-7}	CH_4 photolysis/Sediments
C_3H_8	5×10^{-7}	CH_4 photolysis/Sediments
C_3H_4	1×10^{-8}	CH_4 photolysis/Sediments
C_2H_4	7×10^{-7}	CH_4 photolysis/Sediments
HC_3N	4×10^{-8}	CH_4 photolysis/Sediments
CO	4.7×10^{-5}	CH_4 photolysis/Meteorites
CO_2	1.5×10^{-8}	CO/Photodissociates
H_2O	8×10^{-9}	Meteorites/Photodissociates

Table 5.1 Average values for the lower stratosphere, (C_2H_6, C_2H_2, HCN, C_3H_8, C_3H_4, C_2H_4, C_2H_4, HC3N), (H_2O), and (CO) (Vinatier et al, 2010b).

Energetic particles and electrons from Saturn's magnetosphere supply a smaller and temporally variable energy source to the upper atmosphere (Galand et al, 2013). Galactic cosmic rays, which penetrate deeper in the atmosphere, close to 70 km, are the only source of N_2 dissociation in the stratosphere (Molina-Cuberos et al, 1999). Meteoroid ablation occurs between 500 and 800 km, depending on the properties of the incoming meteoroids, and mainly acts as a local source of ionization without impacting the background chemistry (Molina-Cuberos et al., 2001).

Among these contributions, it is the photons (with their corresponding photoelectrons) and the cosmic rays that primarily control the photochem among these contributions; it is the photons (with their corresponding photoelectrons) and the cosmic rays that primarily control the photochemistry and thus the production and loss of the main species affecting the atmospheric thermal balance. The photolysis of N_2 and CH_4 provides radicals and ions, which rapidly react to produce more complex hydrocarbons and nitrogen-containing molecules (Appendix A, Tables 3 and 4).

The mixing ratios of the photochemical species are largest in the upper atmosphere, where most of the solar energy that induces the chemical processes through the dissociation of N_2 and CH_4 is deposited. Diffusion and mixing transport these species to lower altitudes where their mixing ratios decrease away from the production region. Secondary production processes can affect the rate of decrease for each species, and for some cases the cosmic rays in the lower atmosphere can locally increase the mixing ratios. Eventually the cooler temperatures in the lower stratosphere and troposphere force most of the photochemical products to condense, thereby rapidly decreasing their mixing ratios to small values. Most of the byproducts end up on Titan's surface as liquid (e.g., ethane and propane) and solid sediments, e.g., C_2H_2, HCN, and the refractory haze (Lunine et al, 1983).

One important component of Titan's atmosphere is the vast photochemically produced haze. These complex organic molecules form an optically thick aerosol layer, which veils the planet at optical wavelengths and provides a strong radiative forcing of Titan's climate. The mass flux of aerosols implied by *in situ* Huygens Descent Imager-Spectral Radiometer (DISR) observations (3.0×10^{-14} g cm^{-2} s^{-1}), indicate that 29% of the photolyzed N_2 and CH_4 mass ends up as aerosols. *In situ* UV to IR observations (Koskinen et al, 2011) indicate that the aerosols are aggregates of ~3000 smaller quasi-spherical primary particles of 40 nm radius that can be traced back to the upper atmosphere as high up as the ionosphere. The mass flux of aerosols in the thermosphere at ~1000 km, 3.2×10^{-15} g cm^{-2} s^{-1} (Wahlund et al, 2009), is a significant fraction of that inferred for the main haze layer in the stratosphere at 200 km altitude (3.2×10^{-14} g cm^{-2} s^{-1}), which is comparable to that at 500 km (Caitlin et al, 2013).

The production of organic material through CH_4 photolysis and the continual depletion of CH_4 are possible only because CH_4 leaks into the stratosphere where UV photons break it apart. The culprit is the thermal profile (next section), which ironically is established by

methane through its radiative forcing and that of its photochemical byproducts.

In the lower atmosphere, both Earth's and Titan's temperatures reach minimum values at ~0.1 bar. Here, at the tropopause, the volume mixing ratio of each condensable is constrained to lie below its saturation value, which is ~3×10^{-6} for water on Earth and ~2×10^{-2} for methane on Titan. On Titan, significant methane reaches the upper stratosphere, where it is dissociated and constantly depleted. The atmospheric methane is probably related to a subsurface reservoir (Caitlin et al, 2013).

5.2. Temperature profile

Three different platforms have measured the temperature profiles of Titan's lower atmosphere. In 1980, Voyager 1 transmitted radio signals through Titan's atmosphere toward Earth, as the spacecraft passed behind Titan (egress) and reemerged (ingress). These occultations yielded the thermal structure of the atmosphere above 8.5°N latitude, 256°W longitude, and 6.2°N latitude, 77°W longitude, at dawn and dusk respectively, from the refraction of the radio signal by Titan's atmosphere (Lindal et al, 1983). Cassini similarly measured a dozen temperature profiles at latitudes extending from tropics to poles (Schinder et al, 2012).

The most notable characteristic of Titan's thermal profile is its lack of variability. Voyager egress and ingress measurements of the dawn and dust atmospheres indicate the same temperature pressure profiles within 0.7 K. Occultations by the ongoing Cassini mission, during 2004–2008, measured six profiles within ~35°N and S latitude circles; all these profiles match the Voyager profiles to within 1 K. The Huygens probe also measured the same profile, on January 14, 2005, during its descent. However, outward from the equator, temperatures decrease by ~ 1 K at 50° N and S latitudes and by 3–4 K pole ward of 70° latitude circles. A subtle ~1-K surface contrast exists between the summer and winter pole.

Titan's thermal structure resembles that of Earth: There is a well-

formed troposphere, stratosphere, and mesosphere (Griffith et al, 2005b). Within ~2.5 km of the surface, Titan's temperature profile follows a dry lapse rate, i.e., the change of temperature with pressure (or height) of adiabatically rising dry parcels (Schinder et al, 2011). This region defines the well-mixed "boundary layer," caused by the heating of the surface, which gives rise to dry convection. Titan's atmosphere is conditionally unstable; it is less steep than the dry lapse rate, but steeper than the moist lapse rate. Here parcels are unstable only if saturated, and therefore the stability of the atmosphere depends on the humidity profile.

Convective systems must originate below 15 km (Griffith et al., 2000). Cloud formation can initiate in the upper troposphere (15–45 km) as well, yet such strati form clouds, unlike convective systems, would exhibit little vertical evolution. Without tracking the vertical evolutions of clouds, it is difficult to distinguish strati form clouds from convective systems that form below 15 km and appear at higher altitudes because of convective upwelling (Schinder et al, 2012).

5.3. Methane profile

The methane profile of Titan's atmosphere has been measured by the Huygens probe during its descent to the surface at 10°S latitude and 192°W longitude. This profile is markedly simple. Cassini's Gas Chromatograph Mass Spectrometer (GCMS) determined a CH_4 mixing ratio of 0.057 (50% humidity) above a damp surface. The mixing ratio is essentially constant below ~7 km altitude, above which the atmosphere is cold enough to be saturated (Niemann et al, 2010). Between 9 km and 16 km altitude, the atmosphere is saturated with respect to the ambient condensate, a binary solution of liquid CH_4 and ~20% dissolved N_2. At 25–30 km altitude, it is saturated with respect to pure CH_4 ice, and an intermediate abundance exists between these two regions (Lavvas et al, 2011b).

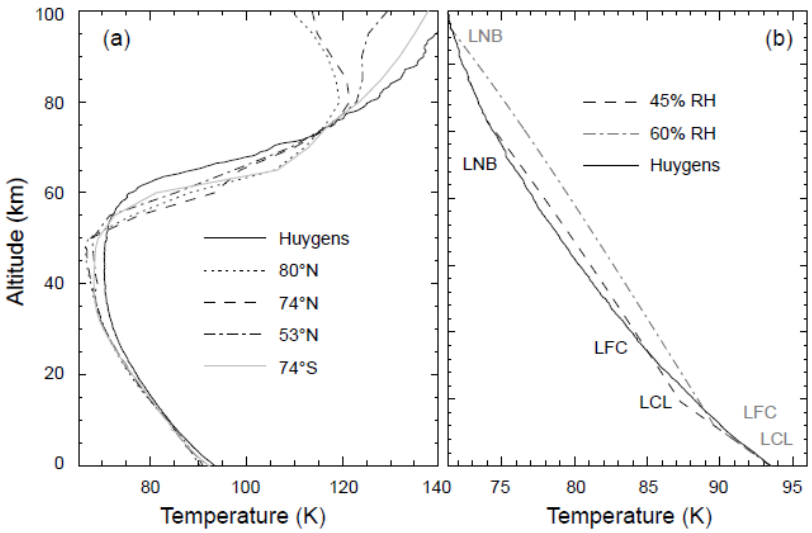

Figure 5.1 (a) Titan's temperature profile at several latitudes indicates a 3 K cooler surface temperature and a more stable atmosphere at the poles. (b) The path of convectively rising parcels at Titan's landing site, assuming surface relative humidity's of 45% and 60% are compared to the measured temperature profile (Schinder et al, 2012; Caitlin et al, 2013).

Such a profile clearly indicates that methane originates from the surface and mixes with the air up to 7 km, above which condensation of the ambient condensate controls its abundance.

The combined methane and temperature profiles measured at the landing site indicate the stability of the atmosphere with respect to convection.

Consider the path of surface parcels, which have the most amounts of methane and therefore latent heat to fuel convection. Assume that the parcel updrafts rapidly enough to be adiabatic. Then, since the atmosphere is under-saturated at the surface, the temperature of an up drafted parcel follows the dry lapse rate until it reaches the altitude, called the lifting condensation level, where the methane within the parcel condenses.

Above this point the parcel follows the wet adiabatic lapse rate and cools less quickly during its assent because of the release of latent

heat. This transition can be seen as a kink in the parcels paths in Fig. 4b. The parcel becomes buoyant when its temperature exceeds the atmospheric temperature and thus its density is smaller than the ambient values. Above this level, called the level of free convection, the parcel buoys upward until its temperature is smaller than ambient.

Research by Barth and Rafkin (2007, 2010), indicates that for a 60% humidity atmosphere, up to 1 m of precipitation may be produced in only a few hours. However, rainfall is a rare event; only two events have been witnessed during Cassini's now nine-year mission (Turtle et al, 2009, 2011a). For the conditions measured at the probe landing site, most raindrops evaporate before reaching the surface (Graves et al, 2008).

5.4. Atmospheric Energy Partitioning

Titan's main constituent, N_2, contributes to the moon's greenhouse effect and chemistry and provides a background gas that broadens the methane lines. Yet it is the second most abundant constituent, methane, and its photochemical byproducts that establish the atmosphere's structure and composition.

Titan's haze and methane heat its stratosphere and limit the radiation reaching the surface. These roles are witnessed from optical images of Titan, which reveal a hazy featureless moon and optical spectra that resemble a methane transmission spectrum.

Titan's haze is optically thick throughout optical wavelengths and optically thin in the infrared, precisely the opposite of a greenhouse gas (McKay et al, 1991). This anti-greenhouse component absorbs ~40% of the incident radiation, thereby cooling the surface by 9 K and heating the stratosphere ~9 K.

The resulting radiative forcing is complicated because the haze drifts from one hemisphere to the other with the seasonal winds, causing temporal changes in the haze density with altitude and latitude. This haze migration in turn affects the circulation (Rannou et al, 2012, 2012). Titan's atmosphere also experiences a greenhouse effect. Pressure-induced absorption of N2-N2, N2-CH_4, CH_4-CH_4, and

N_2-H_2 absorbs the 30–800 cm^{-1} radiation emitted by Titan, which warms the surface by 21 K on average (McKay et al, 1991), comparable to the 33 K greenhouse effect on Earth.

Titan's greenhouse effect is highly sensitive to the abundance of the minor constituent H2, which absorbs in the strong IR window at 400–600 cm–1. In Titan, CH_4 absorbs broadly in the IR and, as a condensable, its abundance is subject to climatic conditions. It is interesting to note that without methane, Titan's atmosphere would lack a stratosphere, strong greenhouse warming, and anti-greenhouse cooling.

Most radiative transfer derivations of the tropical temperature profile assume the global average incident solar radiation (3.7 Wm^{-2}) rather than the local insolation (McKay et al, 1991) and yield temperature profiles that match those measured in Titan's tropical latitudes.

The lack of radiative equilibrium in Titan's atmosphere on an average annual scale indicates that the circulation redistributes Titan's heat, which, as further discussed in section 7, gives rise to non-radiative surface fluxes particularly in the polar summers (Mitchell et al, 2012).

5.5. Methane Clouds

Titan's methane clouds are fastidiously organized by latitude and season. During Titan's southern summer (1999–2004), clouds appeared exclusively at latitudes pole ward of ~60°S (Bouchez and Brown, 2005). In 2004, bands of clouds emerged surrounding 40°S latitude (Roe et al, 2005). Roughly a year later the population of southern clouds diminished, and disappeared altogether in 2008 (Caitlin et al, 2013).

5.5.1. Cloud Evolution

Convection is also indicated by images of the cumuli structure and evolution of small polar cloud systems (Porco et al, 2005). Studies of small tropical clouds display a similar cumuli structure, but, in

contrast, appear lower in the atmosphere; none have been detected above 26 km altitude. These clouds are consistent with the Huygens temperature and methane profiles, for which convective clouds lie below ~26 km altitude (Griffith et al, 2009).

Usually less than 1% of Titan's disk is cloudy. This sparse coverage of clouds agrees with that expected, if one regards the atmosphere as a heat engine fueled by solar insolation that drives convective motion that is opposed by dissipation (Lorenz et al, 2005). The areal coverage of deep convection, which carries air aloft, is limited by the atmosphere's radiative cooling rate, which controls the downward flux of air, since on average the upward flux of air must equal the downward flux. Yet occasionally cloud systems emerge that are large enough to brighten Titan's disk by 9–66% (Turtle et al, 2011b).

5.5.2. Ethane Clouds

The cloud appears at latitudes where Titans general circulation concentrates and transports photochemical products, principally ethane, to lower altitudes, where they condense and may form clouds (Rannou et al, 2006). Methane (the second most abundant atmospheric constituent after nitrogen) is dissociated irreversibly by solar ultraviolet light, producing primarily ethane and, at one-sixth andone-10th of the ethane production rate, respectively, acetylene and haze, as well as other less abundant organic molecules (Coustenis and Be, 1995; Yung et al, 1984). These photochemical by-products precipitate to Titans surface. Titan's atmospheric composition and photochemical models indicate that ethane accumulates as a liquid (at the equatorial surface temperature of 93.5 K) at a rate of È300 m (if global) over Titans lifetime of 4.5 billion years, whereas solid sediments, including acetylene and haze particles, accumulate at roughly one-third of this rate (1995; Yung et al, 1984). Thus, unless methane is a recent addition to Titans atmosphere (Tobie et al., 2006) or ethane incorporates itself into surface solids (Osegovic and Max, 2005), it has been reasoned that a considerable fraction of the surface should be

covered with liquid ethane (Lunine et al, 1983). Titan's surface reveals dunes of solid sediments, probably including haze particles and acetylene ice (Lorenz et al, 2006). In addition, the surface is riddled with alluvial features (Porco, et al., 2005), suggesting the occurrence of methane rain in the past.

5.5.3. Methane Precipitation

If a situation could be reached where methane saturations could build up to a level high enough to allow a large number of these pure methane cloud particles to form (e.g., if there is a lack of suitable nuclei for some period of time or Sis suddenly ramped up by a change in temperature), they are able to grow to precipitation size and rain out in less than half a day. This time is several hours longer than indicated by the observations of Griffith and Hall (2000), but shorter than the lifetimes of the polar clouds observed by Brown et al. (2002). In our steady-state modeling, due to the slow resupply of methane vapor as the only mechanism for increasing the methane saturation, we do not see long lived optically thick clouds. However, we discuss a mechanism to form optically thick clouds with longer life-times in (Barth and Toon, 2004). Essentially relatively long-lived clouds can form due to dynamically driven temperature changes, but only over small fractions of the planet's surface. We do, however, see some precipitation, which is promising in light of the Huygens probe detection of methane in Titan's surface (Erika and Owen, 2006).

5.6. Titan's Seasons

Titan's orbital tilt with respect to the sun is very close to Saturn's axial tilt (about 27°), and its axial tilt with respect to its orbit is zero. This means that the direction of incoming sunlight is driven almost entirely by Titan's day-night cycle and Saturn's year cycle. The day cycle on Titan lasts 15.9 Earth days, which is how long it takes Titan to orbit Saturn. Titan is tidally locked, so the same part of Titan always faces Saturn, and there is no separate "month" cycle.

Seasonal change is driven by Saturn's year: it takes Saturn about

29.5 Earth years to orbit the sun, exposing different amounts of sunlight to Titan's northern and southern hemispheres during different parts of the Saturnian year. Seasonal weather changes include larger hydrocarbon lakes in the northern hemisphere during the winter, decreased haze around the equinoxes due to changing atmospheric circulation, and associated ice clouds in the South Polar regions (Flasar et al, 1981; Morrow, 2015). The last equinox occurred on August 11, 2009; this was the spring equinox for the northern hemisphere, meaning the southern hemisphere is getting less sunlight and moving into winter (Anderson and Samuelson, 2015).

Surface winds are normally low (<1 meter per second). Recent computer simulations indicate that the huge dunes of soot like material raining down from the atmosphere in the equatorial regions may instead be shaped by rare storm winds that happen only every fifteen years when Titan is in equinox (Piter, 2015). The storms produce strong downdrafts, flowing eastward at up to 10 meters per second when they reach the surface.

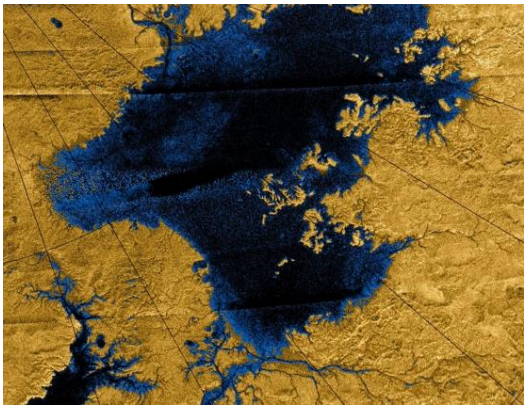

Figure 5.2 Images from the Cassini mission show river networks draining into lakes in Titan's North Polar Region. Image: NASA/JPL/USGS.

In late 2010, the equivalent of early spring in Titan's northern hemisphere, a series of methane storms, were observed in Titan's equatorial desert regions (Jia-Rui et al, 2011). Due to the eccentricity

of Saturn's orbit, Titan is about 12% closer to the sun during the southern hemisphere summer, making southern summers shorter but hotter than northern summers. This asymmetry may contribute to topological differences between the hemispheres - the northern hemisphere has many more hydrocarbon lakes (Stofan et al, 2007). Titan's lakes are largely placid, with few waves or ripples; however, *Cassini* has found evidence of increasing turbulence during the northern hemisphere summer, suggesting that surface winds may strengthen during certain times of the Titanian year. Waves and ripples have also been seen by Cassini (Hecht, 2011).

5.7. Carbon cycle in Titan

At present, Titan has an active methane cycle. It is characterized by the photochemical production of complex hydrocarbon species, cloud formation, rainfall, and the accumulation of hydrocarbon liquids in near-polar lakes and seas. However, it is still unclear if this cycle has existed during most of Titan's evolution or if it was triggered only relatively recently. Indeed, contrary to 15N/14N in nitrogen, the 13C/12C ratio measured in methane by the GCMS on Huygens (Niemann et al, 2010), and derived from the INMS and CIRS on Cassini (Nixon et al, 2012), is close to the ratio measured on Earth and several other solar system objects, indicating that the atmospheric methane inventory has not been affected by atmospheric escape (Nixon et al, 2012). This nearly unmodified ratio suggests that today's methane was injected in the atmosphere not more than 0.5^{-1} Gy[1] ago (Mandt et al, 2012) and that any methane released during the early stage of Titan's evolution should have been totally lost or rapidly re-trapped in the subsurface without being affected by atmospheric fractionation processes.

The building blocks that formed Titan probably contained a significant amount of methane, together with other carbon compounds, such as CO_2, CH_3OH, and more complex organic

1- Giga years

material (Tobie et al., 2012). The low abundance of CO in the present-day atmosphere suggests that the building blocks were depleted in CO (and N_2), which is consistent with the low $36Ar/N_2$ ratio, or that CO was efficiently converted during the accretion phase (Trigo-Rodriguez and Martin-Torres, 2012). The lack of extensive liquid reservoirs of ethane or methane at the surface suggests either that relatively little methane has been released from the interior through time, or that the ethane produced by methane-driven photochemistry, a liquid on Titan's surface, has been efficiently re-trapped in the crust as liquids and/or clathrates (Choukorun and Sotin, 2012).

References

Anderson C., Samuelson R. (2015) Monstrous Ice Cloud System in Titan's Present South Polar Stratosphere. NASA Science.

Anderson C.M., Chanover, N.J., McKay, C.P., Rannou, P., Glenar, D.A., 2004.Titan's haze structure in 1999 from spatially-resolved narrowband imaging surrounding the 0.94 μm methane window. J. Geophysical Res. Lett. 31, L17S06

Barth E.L., Rafkin S.C.R. (2010) Convective cloud heights as a diagnostic for methane environment on Titan. Icarus, 206, 467–484.

Barth E.L., Toon O.B. (2003) Microphysical modeling of ethane ice clouds in Titan's atmosphere. Icarus 162: 94–113.

Barth E.L., Toon O.B. (2004) Properties of methane clouds on Titan: Resultsfrom microphysical modeling. J. Geophys. Res. Lett. 31. L17S07.

Bouchez A.H., Brown M.E. (2005) Statistics of Titan's south polar tropospheric clouds. Astrophys. J. Lett., 618, L53–L56.

Bouchez A.H. (2004) Seasonal trend in Titan's atmosphere: Haze, wind, andclouds. Ph.D. thesis, CalTech, Pasadena, CA.

Brown M.E., Bouchez A.H., Griffith C.A. (2002) Direct detection of variable tropospheric clouds near Titan's south pole. Nature 240: 795–797.

Caitlin A.G., Jonathan L.M., Panayotis L., Gabriel T. Titan's Evolving Climate, in Comparative Climatology of Terrestrial Planets, Edited by Stephen J.M., Amy A.S-Miller, Jerald W.H. and Mark A.B. (2013).

The University of Arizona Press, ISBN 978-0-8165-3059-5.

Choukroun M., Sotin C. (2012) Is Titan's shape caused by its meteorology and carbon cycle? Geophys. Res. Lett., 39, 4201.

Coustenis A., Be´zard B. (1995) Titan's Atmosphere from Voyager Infrared Observations: IV. Latitudinal Variations in Temperature and Composition. Icarus,115: 126.

Curtis D.B., Glandorf D.L., Toon O.B., Tolbert M.A., McKay C.P., Khare B.N. (2005) Laboratory studies of butane nucleation on organic haze parti-cles: Application to Titan's clouds. J. Phys. Chem. A 109, 1382–1390

Erika L.B., Owen B.T. (2006) Methane, ethane, and mixed clouds in Titan's atmosphere: Properties derived from microphysical modeling. Icarus 182: 230–250

Flasar et al., (1981) Saturn's moon Titan shows surprising seasonal changes. Science Daily, 2012.

Frére C., Raulin F., Cabane M. (1990) Microphysical modeling of Titan's aerosols: Application to the in situ analysis. Adv. Space Res. 10:159–163.

Galand M., Coates A., Cravens T. et al, (2013) Titan's ionosphere. In Titan: Interior, Surface, Atmosphere, and Space Environment (I. Müller-Wodarg et al., eds.), in press. Cambridge Univ., New York.

Graves S.D.B., McKay C.P., Griffith C.A., et al, (2008) Rain and hail can reach the surface of Titan. Planet. Space Sci,. 56: 346–357.

Griffith C.A., Hall J.L., Geballe T.R., (2000) Detection of daily clouds on Titan. Science, 290: 509–513.

Griffith C.A., Penteado P., Greathouse T., et al, (2005b) Observations of Titan's mesosphere. Astrophysic J. Lett., 629, L57–L60.

Griffith C.A., Penteado P., Rodriguez S., et al, (2009) Characterization of clouds in Titan's tropical atmosphere. Astrophysic J. Lett., 702, L105–L109.

Hecht J. (2011) Ethane lakes in a red haze: Titan's uncanny moonscape. New Scientist, Retrieved 2011-07-25.

Hörst S.M., Vuitton V., Yelle R.V. (2008) Origin of oxygen species in Titan's atmosphere. J. Geophysic Res., 113(E10), E10006.

Jia-Rui C.C., Joe M., Michael B. (2011) Cassini Sees Seasonal Rains Transform Titan's Surface. NASA.

Koskinen T.T., Yelle R.V., Snowden D.S., et al. (2011) The mesosphere and lower thermosphere of Titan revealed by Cassini/ UVIS stellar occultations. Icarus, 216, 507–534.

Lavvas P., Sander M., Kraft M., et al (2011c) Surface chemistry and particle shape: Processes for the evolution of aerosols in Titan's atmosphere. Astrophysic J., 728-80.

Lindal G.F., Wood G.E., Hotz H.B., et al. (1983) The atmosphere of Titan — An analysis of the Voyager 1 radio occultation measurements. Icarus, 53, 348–363.

Lorenz R. et al., (2006). The sand seas of Titan: Cassini RADAR observations of longitudinal dunes. Science, 312: 724-727, doi:10.1126/science.1123257.

Lorenz R.D., Griffith C.A., Lunine J.I., et al, (2005) Convective plumes and the scarcity of Titan's clouds. J. Geophysical Res.

Lett., 32: 1201.

Lunine J.I., Stevenson D.J. (1987) Clathrate and ammonia hydrates at high pressure Application to the origin of methane on Titan. Icarus, 70, 61–77.

Lunine J.I., Stevenson D.J., Yung Y.L. (1983) Ethane Ocean on Titan. Science, 222: 1229.

Mandt K.E., Waite J.H., Teolis B., et al. (2012) The 12C/13C ratio on Titan from Cassini INMS measurements and implications for the evolution of methane. Astrophys J., 749: 160.

McKay C.P., Pollack J.B., Courtin R. (1991).The greenhouse and anti-greenhouse effects on Titan. Science, 253, 1118–1121.

McKay, C.P., (1996) Elemental composition, solubility, and optical properties of Titan's organic haze. Planet. Space Sci. 44: 741–747.

Mitchell J.L. (2012) Titan's transport-driven methane cycle. Astrophysic J. Lett., 756(2), L26.

Molina-Cuberos G.J., Lammer H., Stumptner W., et al. (2001) Ionospheric layer induced by meteoric ionization in Titan's atmosphere. Planet Space Sci., 49: 143–153.

Molina-Cuberos G.J., Löpez-Moreno J J., Rodrigo R., et al. (1999) Ionization by cosmic rays of the atmosphere of Titan. Planet. Space Sci., 47, 1347–1354.

Morrow A., (2015) "Monstrous Ice Cloud in Titan's South Polar Region". NASA. Retrieved January 30, 2019

Niemann H.B., Atreya S.K., Demick J.E., et al. (2010) Composition of

Titan's lower atmosphere and simple surface volatiles as measured by the Cassini-Huygens probe gas chromatograph mass spectrometer experiment. J. Geophys. Res. Planets, 115(E14), E12006.

Nixon C.A., Temelso B., Vinatier S., et al. (2012) Isotopic ratios in Titan's methane: Measurements and modeling. Astrophys. J., 749, 159–174.

Osegovice J.P., Max M.D. (2005) Compound clathrate hydrate on Titan's surface Journal of Geophysical Research, 110, Issue E8, CiteID E08004, doi: 10.1029/2005JE002435.

Piter K. (2015) Violent Methane Storms on Titan May Explain Dune Direction. Space Ref. April, 2015.

Porco C.C., et al., (2005) Imaging of Titan from the Cassini spacecraft. Nature, 434: 159-168, doi: 10.1038/nature03436.

Porco, C.C., and 35 colleagues, (2005) Imaging of Titan from the Cassini space craft. Nature 434: 159–168.

Rannou F.M., Hourdin F., Lebonnois S. (2006). The Latitudinal Distribution of Clouds on Titan

Rannou P., Le Mouélic S., Sotin C., et al. (2012) Cloud and haze in the winter polar region of Titan observed with visual and infrared mapping spectrometer on board Cassini. Astrophys. J., 748, 4

Rannou P., McKay, C.P., Lorenz, R.D., 2003. A model of Titan's haze of fractalaerosols constrained by multiple observations. Planet Space Sci. 51: 963–976.

Roe, H.G., Bouchez, A.H., Trujillo, C.A., Schaller, E.L., Brown,

M.E., (2005) Discovery of temperate latitude clouds on Titan. Astrophysic J. 618, L49–L52

Roe H.G., De Pater I., Macintosh B.A., McKay C.P., (2002) Titan's cloudsfrom Gemini and Keck adaptive optics imaging. Astrophys. J. 581, 1399–1406.

Sagan C., Thompson, W.R., (1984) Production and condensation of organic gases in the atmosphere of Titan. Icarus 59: 133–161.

Schinder P. J., Flasar F. M., Marouf E. A., et al. (2012) The structure of Titan's atmosphere from Cassini radio occultations: Occultations from the prime and equinox missions. Icarus, 221: 1020–1031.

Schinder P.J., Flasar F.M., Marouf E.A., et al. (2011) The structure of Titan's atmosphere from Cassini radio occultations. Icarus, 215: 460–474.

Stofan E.R., Elachi C., et al. (2007). The lakes of Titan. Nature, 445 (1): 61–64. doi:10.1038/nature05438.

Tobie G., Gautier D., Hersant F. (2012) Titan's bulk composition constrained by Cassini- Huygens: Implications for internal outgassing. Astrophys. J., 752, 125.

Tobie G., Lunine J.I., Sotin C. (2006) Episodic outgassing as the origin of atmospheric methane on Titan, Nature 440: 61.

Toon O.B., McKay C.P., Griffith C.A., Turco R.P., (1992) A physical model of Titan's aerosols. Icarus, 95: 24–53

Trigo-Rodriguez J.M., Martin-Torres J. (2012) Clues on the importance of comets in the origin and evolution of the

atmospheres of Titan and Earth. Planet Space Sci., 60, 3–9.

Turtle E.P., Del Genio A.D., Barbara J.M., et al. (2011b). Seasonal changes in Titan's meteorology. Geophys. Res. Lett., 38, 3203.

Vinatier S., Bézard B., Nixon C.N., et al. (2010b) Analysis of Cassini/CIRS limb spectra of Titan acquired during the nominal mission I: Hydrocarbons, nitriles, CO_2 vertical mixing ratio profiles. Icarus, 205: 559–570.

Wahlund J.E., Galand M., Müller-Wodarg I., et al. (2009) On the amount of heavy molecular ions in Titan's ionosphere. Planet Space Sci., 57(14–15): 1857–1865.

Waite J.H., Niemann H., et al., (2005) Ion neutral mass spectrometer results from the first flyby of Titan. Science 308: 982–986.

Young E.F., Rannou, P., McKay, C.P., Griffith, C.A., Noll, K., (2002) A three-dimensional map of Titan's tropospheric haze distribution based on HubbleSpace Telescope imaging. Astrophys. J. 123: 3473–3486.

Yung Y.L., Allen M., Pinto J.P., (1984) Photochemistry of the atmosphere of Titan: comparison between model and observations. Astrophys. J. Suppl. Ser.55: 465.

Chapter 6
Aeolian processes on Venus

Introduction

Venus is a planet that is similar to Earth in terms of some important planetary parameters (size, mass, position in the solar system, presence of atmosphere) and different in terms of other, equally important ones (absence of an intrinsic magnetic field, large atmospheric mass, carbon dioxide composition of the atmosphere, lack of water, very high surface pressure and temperature). The surface morphology of Venus is dominated by the signatures of basaltic volcanism and tectonic deformation. Other geological processes such as impact cratering, aeolian activity and gravity-driven down-slope mass movement, although active on the planet, are certainly of subordinate significance.

Venusian volcanism resulted in the formation of vast regional plains, occupying most of the planet's surface, and in the building of numerous volcanic edifices. Venusian tectonic deformation was both compressional and extensional. Scales and, periodically, rates of Venusian volcanism and tectonism were comparable to those on Earth. But Venus shows no evidence of the global plate-tectonic style so dominant in the geology of Earth. The morphological record seen in the Magellan radar images of Venus extends back into geological history not earlier than about 0.5–1 billion years. It is represented by a sequence of units from highly tectonized tessera and densely fractured plains, whose compositional nature is unclear, through moderately deformed basaltic lava plains, and then to only locally deformed basaltic plains and edifices. In the beginning of the time period during

which this sequence formed, the rates of volcanic and tectonic activity were significantly higher than in the subsequent time extending to the present. This change in volcanic and tectonic activity may correspond to a change in the convection style in the mantle of Venus.

6.1. Venus Atmosphere Dynamics

6.1.1. Lower Atmosphere

The lower atmosphere of Venus is observed to rotate in the same retrograde (westward) direction as the solid planet, to first approximation at constant angular velocity at any given altitude. The maximum superrotation rate, at cloudtop levels, is about once every 4 Earth-days, 60 times faster than that of Venus itself. This retrograde superrotating zonal (RSZ) flow has been known for over three decades, but at present there is still no adequate explanation. Not a single theoretical model using realistic formulations of the Venus atmosphere has been able to quantitatively reproduce this fundamental characteristic of the atmosphere of the nearest planet to Earth.

The large variability of the superrotating zonal winds between 90 and 110 km altitude may arise from gravity waves. Gravity waves are thus believed to play a major role in Venus upper atmosphere dynamics, in addition to their possible role (discussed above) in the lower atmosphere's RSZ flow. Wavelike density perturbations with horizontal scales of 100–600 km have been observed in the Venus thermosphere by the Pioneer Venus Orbiter Neutral Mass Spectrometer. These perturbations have been shown to be consistent with vertically propagating gravity waves from a source region at or below ~80 km altitude, well below thermospheric altitudes (Bougher et al, 1997).

6.1.2. Upper Atmosphere

The large-scale circulation of the upper atmosphere from ~90 to ~200 km altitude (upper mesosphere and thermosphere1) is a combination of two distinct flow patterns: (1) a relatively stable subsolar-to-antisolar (SS-AS) circulation cell driven by solar (EUV - UV) and IR

heating, and (2) a highly variable retrograde superrotating zonal (RSZ) flow, in part a continuation of the lower-atmosphere RSZ flow discussed above (Fig. 6.1). The effects of the superposition of these wind components in the Venus upper atmosphere are: (a) to shift the divergence of the flow from the subsolar point toward the evening terminator (ET), (b) to generate larger evening terminator winds than those along the morning terminator (MT), and (c) to shift the convergence of the flow away from midnight and toward the morning terminator. These components also vary as a function of altitude and reflect the changing importance of underlying drivers and their day-to-day and solar cycle variations (fig. 6. 1).

The sketch looks down on the north pole of the planet. The daylight hemisphere is light and the nightside hemisphere is dark. The overhead motion of the Sun is counterclockwise. SS-AS is the subsolar-antisolar circulation with upward motion and divergence under the Sun and sinking flow and convergence on the night side.

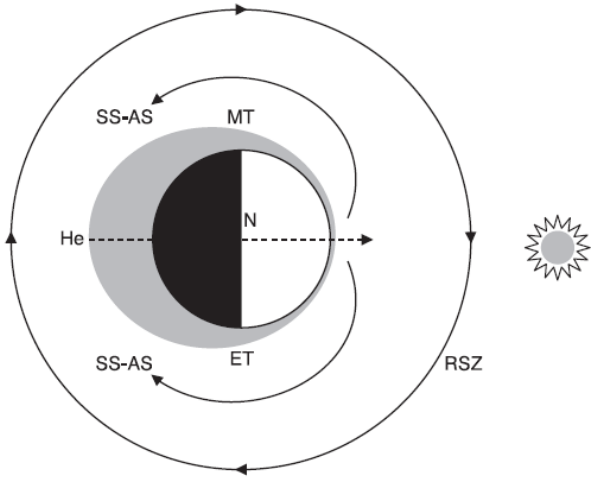

Figure 6.1 Sketch of the components that contribute to the upper atmospheric circulation on Venus (after Esposito et al, 2007).

RSZ is the retrograde superrotating zonal circulation which is clockwise, opposite to the overhead motion of the Sun. The lightly

shaded region represents the variation in the helium content of the upper atmosphere. The SS-AS flow transports helium from the day side to the night side resulting in a helium bulge on the night side. The RSZ and SS-AS winds are in the same direction at the evening terminator ET but in opposite directions at the morning terminator MT resulting in higher zonal wind velocities at the ET compared with the MT[1]. The effect of the superposition of the RSZ and SS-AS winds is to shift the center of dayside divergence toward the ET and shift the center of night side convergence and the center of the helium bulge toward the MT.

6.3. Venus Winds

Venus has a thick, torrid atmosphere. Although winds at altitude sweep the cloud tops rather swiftly in the sense of the planet's rotation, the near-surface winds are almost unknown except for a handful of radio tracking measurements of descent probes, some brief wind measurements on the surface, and indirect indication of winds such as the orientation of wind streaks.

Venus orbits the Sun in 224.7 terrestrial days, but because of the planet's slow retrograde rotation, a solar day (i.e., the time between successive solar noons, and thus the period with which atmospheric motions are forced) is 116.8 terrestrial days. The planet's orbital eccentricity is only 0.007, and the obliquity is 177.4_ (i.e., a tilt of 2.6_ with retrograde rotation), so seasons are effectively nonexistent. The cloud-tops can be tracked, especially at ultraviolet and infrared wavelengths, and the predominant motion is zonal, as noted above. The uneven deposition of sunlight drives a slow meridional (Hadley) circulation, and the angular momentum balance of this circulation is a key problem in Venus meteorology. Because the atmosphere is so massive, it has a large inertia or 'memory', which makes it rather challenging to simulate numerically.

Dobrovolskis (1993) suggests that slope winds on Venus may be

1 - morning terminator

significant, as on Mars, and that such winds may be strong enough to transport sand. This picture does seem to be borne out in part by the Magellan mapping of some 5700 wind streaks (Greeley et al. 1995) which show a preference in the downhill direction where slopes are observed (about 20 % of the total being biased downhill), even though the slopes themselves are typically only ~ 0.3°. They also argue that a Hadley-type flow may control many of the wind directions inferred from streaks, although their maps of streak orientation do not make this obvious. Most likely local terrain may modify directions substantially.

There are sadly very few surface wind speed measurements. The Venera 9 and 10 records have been characterized as having a means of 0.4 and 0.9 m/s respectively, with standard deviations of 0.1 and 0.15 m/s. Surface winds were also estimated from the intensity of sounds recorded by the Groza microphone on Venera 13 and 14 to be in a similar range (Ksanfomality et al. 1983). These data do seem to show winds within a factor of 2 or so of the saltation threshold, even for a small number of observations, so aeolian transport may be common. However, more data are sorely needed (Lorenz and Zimbelman, 2014).

In the absence of fluvial processes (or glacial abrasion, or freeze–thaw), it is hard to imagine how to make much sand. Similarly, the high atmospheric pressure on Venus prevents gas in magmas from expanding dramatically to produce Strombolian eruptions that erupt a lot of fine ash—most of the lava will have simply emerged from the ground and flowed. Some chemical weathering processes may produce some fines, and impact ejecta also produces fine particles (dark parabolic haloes around some impact craters may be radar-dark because they are made of smooth deposits of fine-grained material—these appear around the apparently youngest craters) (Lorenz and Zimbelman, 2014).

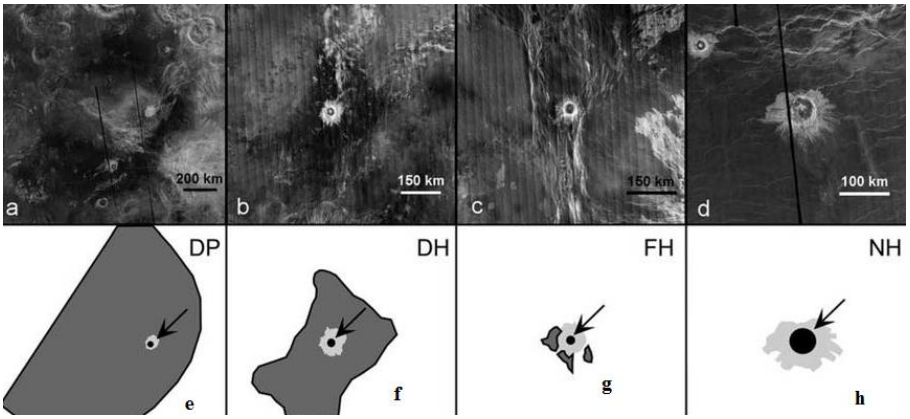

Figure 6.2 Craters with different types of associated radar-dark features arranged in order of increasing Age: (a) dark parabola (DP) crater Sabin; (b) clear dark halo (DH) crater Hwangcini; (c) faint dark halo (FH) crater Blackburne; (d) no halo (NH) crater Barto; (e) sketch of the dark deposits near the crater Sabin (Figure 2a); (f) sketch of the dark deposits near the crater Hwangcini (Figure 2b); (g) sketch of the dark deposits near the crater Blackburne (Figure 1c); (h) sketch of the crater Barto (Figure 2d). Legend: black circles are crater; light gray is continuous bright deposits; dark gray is radar-dark diffuse features (DDF); arrows show crater location; D is crater diameter (after Bondarenko and Head, 2009).

Marshall et al. (1991) studied the adhesion of basalt particles at a range of temperatures, noting that rocks may be appreciably softer at Venus surface temperatures. A small jet of air, pulsed by a valve at roughly once a second, was used to propel ~3 mm angular particles of rock at a polished target slab at known speeds inside a chamber.

They found that at temperatures below 440 K, abrasion occurred as expected. Results were highly variable between 440 and 570 K: above 570 K particles almost always accreted (i.e., welded themselves onto the target). This adhesion threshold of about 500 K is roughly 40 % of the melting temperature and is higher than temperatures even on Venus' highest coolest spot (Maxwell Montes, ~650 K) and so grain adhesion may well be an important aspect of aeolian processes on Venus.

6.4. Aeolian Features in Venus

In the absence of liquid water on Venus, exogenic resurfacing on this planet is essentially dominated by aeolian processes (Greeley et al, 1997). The observed aeolian features are represented by radar-dark mantles, wind streaks, yardangs and dunes. Dark mantles and wind streaks are rather common features on Venus, while yardangs and dunes large enough to be seen on the Magellan images are observed in only a few localities.

6.4.1. The Mechanism Responsible for the Formation of Aeolian Ripples

Wind driven ripples form the rearrangement of loosely packed sand grains on sand beds into ridge crest and troughs. The crests lie perpendicular to wind direction and with asymmetrical cross sections. The upwind slopes are much less steep than downwind slopes. These ripples are small, with a wave length of a few centimeters, and with heights roughly one-fifteenth or one-twentieth of their wavelength (fig. 6.3).

The mechanism responsible for the formation of aeolian ripples is thought to be the indirect action of wind on loose sand. When the wind strength is large enough, individual sand grains are lifted by the direct action of the shear stress exerted by the wind on the sand surface.

Figure 6.3 sand ripples atop a dune in the Maranjab desert (near Kashan) in Iran.

This process is known as saltation in which grains hop along the surface in low angle trajectories (fig. 6.4). During their flight; the grains reach a velocity that is approximately that of the wind and upon their impact with the surface, they impart their energy and momentum to the sand, ejecting other grains by a process known as reptation. These impacts further eject a number of grains on short, quasi-ballistic trajectories that are largely unaffected by wind. For sufficiently large wind velocities, the bombardment by sand grains accelerated by the wind generates a cascade process, and an entire population of saltating grains hopping on the sand surface emerges (Ungar and Haff, 1987). During strong winds, the layer of saltating grains can reach a thickness of more than 1 m.

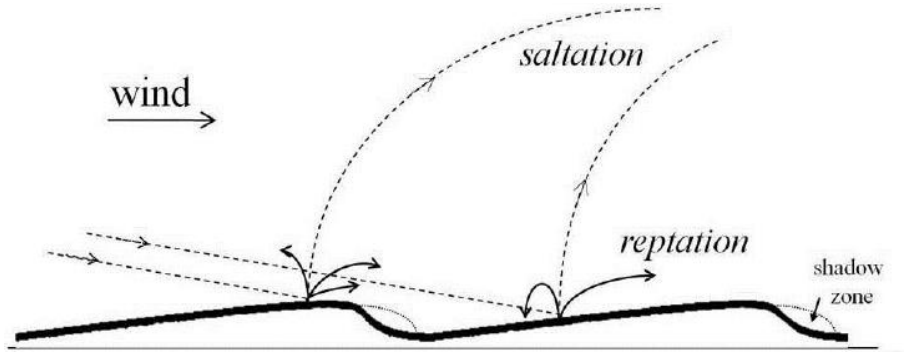

Figure 6.4 Interaction of saltating, reptating, and rolling sand grains in the model. Saltating particles follow by long trajectories (dashed lines), strike the sand bed. The impacts cause ejection of reptating grains from the bed surface.

These grains trajectories (solid lines with arrows) are short. The landing reptating grains may roll for some distance upon the bed surface (small circles) before they stop (Massoud, 2010). Saltating grains (dashed lines) impacting onto the sand bed ejects several particles which enter reptation (solid lines) (Prigozhin, 1999).

The ripple wavelength is not constant but grows with time; and the essential physics lies in the variation of reptation flux. The saltating grains gain their momentum from the wind, supply the energy

necessary for reptation, and decelerate the wind near the bed surface. As the dynamic equilibrium between the amount of saltating particles and wind shear stress establishes, the probability of direct entrainment of the bed particles into motion by wind becomes small.

Formation of aeolian ripples is strongly influenced by size sorting of sand. Ripples composed of homogeneous sand are small and flat because the surface grains are destabilized by saltation impacts and carried away by the wind, stronger on the ripple crests; these grains may be deposited in troughs. The final wavelength of such ripples, measured after a long period of a unidirectional wind, was correlated with the grain size. Ripples made of inhomogeneous sand become much bigger because coarser grains form an armoring layer on the ripple crests and stoss slopes; significantly less crude particles are found in the troughs. The armoring layer may be very thin, almost a monolayer, see (Tsoar 1990), or becomes thick near the ripple crest.

Probably, the inhomogeneous sand ripples continue growing till the wind starts to carry away also coarse grains from their crests. Contrary to ordinary ripples, no significant correlation between the wavelength and the mean grain size has been observed for megaripples (Tsoar 1990). Aeolian ripples larger than those commonly found in fine sands were variously termed ridges, granule ripples, megaripples or gravel ripples; such ripples were studied at various locations on Earth and, recently, also on Mars (Jerolmack et al, 2006).

Bagnold has postulated the following conditions necessary for megaripple growth: (i) availability of coarse grains with diameters 3-7 times larger than the mean diameter of grains in saltation; (ii) a constant supply of fine sand in saltation to sustain forward motion of coarse grains by creep; and (iii) wind velocity below the saltation threshold of the coarse grains. Formation and stabilization of ripples is observed on a time scale of minutes and hours, respectively, but, according to Bagnold, it takes decades or centuries to form huge megaripples.

Figure 6.5: The largest megaripples on Earth discovered On Argentina's Puna plateau, blistering winds have formed the largest known ripples on the planet (Juan Pablo Milana, 2009).

Sharp (1963), however, noted that, provided a suitable supply of coarse grains is available, it might take only weeks of sufficiently strong wind to form good granule ripples. Wind tunnel experiments, performed with sand collected from granule ripples, showed that, starting with a flat bed, usual ripples form, coarsen and gradually turn into megaripples. They may look like low dunes, but the cresting ridges pictured above is the world's largest "megaripples", a phenomenon that had been thought impossible on our planet.

6.5. Sands

Scarcity of sand on Venus has been considered as explanation for the scarcity of observed aeolian bedforms. It has attributed (Weitz et al, 1994) to the fact that erosion by water, the main source of sand-size particles on the Earth, does not operate on Venus, and chemical weathering is not likely to produce sand (Basilevsky et al, 2004). On Mars, sand is abundant, because the main terrestrial sink of sand, sedimentation at the sea floor, does not operate on Mars. Unlike Mars, Venus has an efficient sink of sand, lithification of beds accelerated by high surface temperatures. Some "stickiness" of particles at high temperatures has been predicted from the first principles (Starukhina, 2000) and observed in the wind tunnel experiments under Venus conditions (Marshall et al, 1991). "Stickiness" and quick-lithification

of sands can explain lack of saltation of Venus, even if the sand-size particles are abundant.

Impacts have been considered as the main source of sand on Venus; estimates (Garvin, 1990) give ~ 1 mm equivalent global layer (EGL), while from considerations in (Basilevsky et al, 2004) we got two orders of magnitude more optimistic value (~ 1 dm EGL). Material ejected by young large craters forms extended radar-dark diffuse features (DDFs) of parabolic plan form, dm to meters thick. According to (Basilevsky et al, 2004) they may contain a significant proportion of sand particles, but their surface usually remains flat for tens Ma (Kreslavsky and Bondarenko, 2012). Microdunes (Weitz et al, 1994), however, are formed on DDFs, and possibly, from their material. As noted in (Ivanov et al, 1992), impacts cause a wave of strong compression of the air followed by rarefaction, which can disintegrate slightly lithified deposits, extract sand from topographic traps, etc. This gives another explanation for concentration of wind streaks around impacts.

In addition to impacts, tectonics and associated mass wasting can disintegrate rocks to produce sand-size particles. No association of wind streaks with the youngest tectonic fractures has been noted. Pyroclastics is obvious and probably rich source of sand size material; however, there is no unambiguous association of wind streaks with young volcanoes (Kreslavsky and Bondarenko, 2012).

6.6. Dunes

Owing to the large atmospheric density of Venus, a minimal dune size of the order of 20cm is predicted from the scaling with ℓ_{drag} (Claudin and Andreotti, 2006). Indeed, wind tunnel experiments under constant wind and atmospheric pressure condition of Venus produced small transverse bedforms, named microdunes, with wavelengths within the range 10-30 cm. These *microdunes* displayed several features reminiscent of Earth aeolian dunes, such as a slip face and a separation bubble. Tests using mixed sand sizes did not lead to crest-coarsened bedforms as expected in the case of granule ripples, thus corroborating the conclusion that the microdunes were indeed small-

scale prototypes of terrestrial "full-scale transverse dunes" (Marshall and Greeley 1992).

Dune fields identified in images of the Venus orbiter Magellan contain long-crested dunes much larger than the microdunes of the wind tunnel (Weitz et al, 1994).

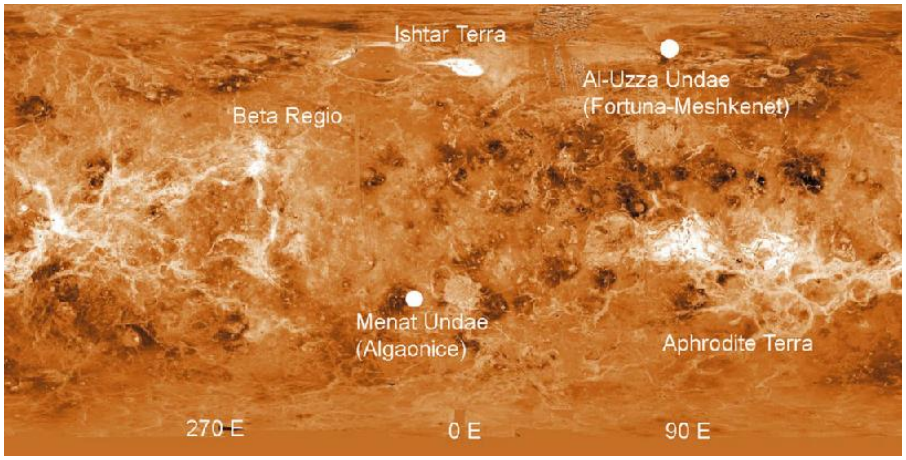

Figure 6.6 A global mosaic of radar reflectivity measured by the Magellan spacecraft (cylindrical projection). The two major dune fields are marked with circles (after Lorenz and Zimbelman, 2014).

The dunes have length ranging from 500 m to 10 km, width of about 200 m, and values of interdune spacing of the order of 500 m (Greeley et al, 1992b) these are dimensions akin to those of terrestrial dunes (Lancaster, 1995). The orientation of nearby surficial features indicates transverse dune alignment to the prevailing wind direction. Although microdunes are not visible as surface features in the Magellan images, their occasional occurrence has been indicated by Magellan's radar data. Because radar detection of the microdunes required their slip face be nearly perpendicular to the radar illumination, there might be many more (small) dunes on Venus not detected by Magellan due to inadequate angle of the radar beam (Greeley et al, 1995). Alternatively, the relative scarceness of dunes or microdunes on Venus might be a consequence of insufficient wind speeds, meager sand cover or a scarcity of sand-size particles on Venus, where the effect of weathering caused by water is negligible

compared to Mars or Earth (Weitz et al, 1994). The two prominent dune fields identified on Venus are Algaonice and Fortuna-Meshkenet (Greeley et al, 1992) (Fig. 6.7).

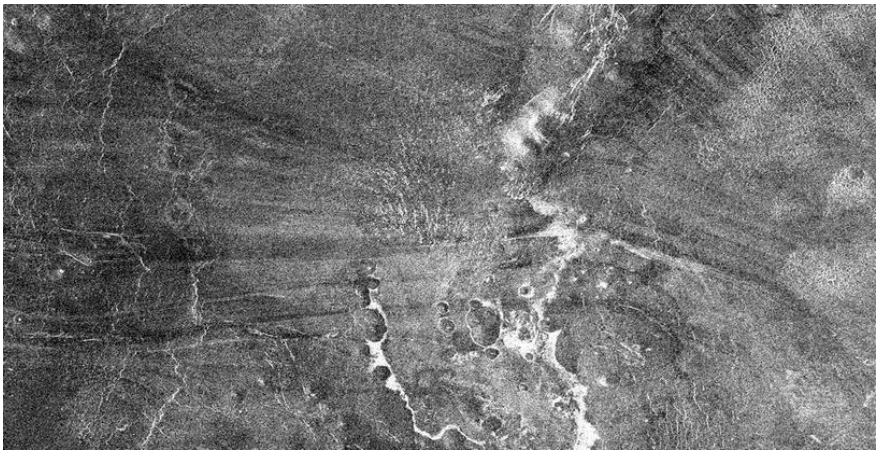

Figure 6.7 Magellan radar mosaic of the Algaonice dune field. The dunes form a roughly V-arrangement in the center of the image, just above the circular pts. More obvious than the small, bright dunes themselves are some background volcanic features and wind streaks that permeate the region (after Lorenz and Zimbelman, 2014).

Figure 6.8 Magellan radar mosaic of the Fortuna-Mesknet dune field. These appear rather more extensive than the Algaonice dunes. Similar to those, the dunes appear to be transverse, orthogonal to the prominent windstreaks (after Lorenz and Zimbelman, 2014).

The Algaonice dunes at 25_S, 340_E cover some 1300 km^2 (about the same size as the Lencois Maranhenses dunefield in Brazil) at the end of the ejecta outflow channel from the impact crater of that name (the dunes themselves were subsequently formally named Menat Undae, although the Algaonice name seems to have been more widely used). The dunes are 0.5–5 km in length and are quite bright, likely because there are slip faces oriented towards the radar illumination, which was at an incidence of 35°.

The more northern dune field, Fortuna-Meshkenet lies at 67_N, 91_E in a valley between Ishtar Terra and Meshkenet Tessera (the dunes are formally named Al-Uzza Undae). The dunes are 0.5–10 km long, 0.2–0.5 km wide and spaced by an average of 0.5 km. They appear to be transverse dunes, in that there are several bright wind streaks visible in the region, which seem generally orthogonal to the dunes. Glints are not observed strongly on these dunes, although here the incidence angle of the radar observation was 22–25°.

A significant reason for the lack of observed dunes may be a planet wide paucity of sediment. The Venusian surface may have been completely resurfaced by lava flows about 500 Myr ago and the kinetics of breakdown of basalt by the Venusian atmosphere is uncertain (and of course, other and-generating processes such as freeze–thaw, glacial action or fluvial erosion do not occur on present-day Venus). Indeed, the dominant source of sand-sized sediment may be the ejecta from impact craters. Garvin (1990) calculated that impacts could produce enough fine-grained materials (<1 mm) to form at most a globally-averaged layer 1 m thick. Note that the Fortuna and Algaonice dune fields likely account for only about 1000 km^3 of sediment in total.

Dark mantles are typically seen in association with impact craters forming halos of different sizes and forms. The source of the dark-mantle material is fine debris formed by crater-forming impacts, so one can consider it as a facies of an impact crater ejecta deposit. But this material did settle down through the atmosphere and even in its freshest state (crater-associated radar-dark parabolae) its deposition

was strongly controlled by wind, so it should also be considered aeolian. In many cases, the dark mantles have already lost direct contact with impact craters and occupy wind-shadow localities in local topographic lows and behind or against positive topographic features.

Wind streaks are the most abundant aeolian features on Venus. They are elongated features varying significantly in shape (linear, fan-like, wispy), size (from a few to tens of kilometres) and radar brightness (bright, dark, mixed). Wind streaks typically originate from topographic features that are obviously the accumulational and/or erosional products of behind-the-feature wind turbulence. It is quite typical that lateral boundaries of wind streaks are diffuse.

Wind streaks can result from either enhanced deposition or enhanced erosion, depending on the size of the particles involved in the creation of the brightness contrast that distinguishes the wind streak from its surroundings. A few wind streaks have been observed in radar images of the Venus surface which are indicative of near-surface winds (the more obvious parabolic ejecta features (Fig. 6.9) seen around some recent craters are formed by upper atmospheric winds and are not of particular interest in this book except perhaps as a source of sand).

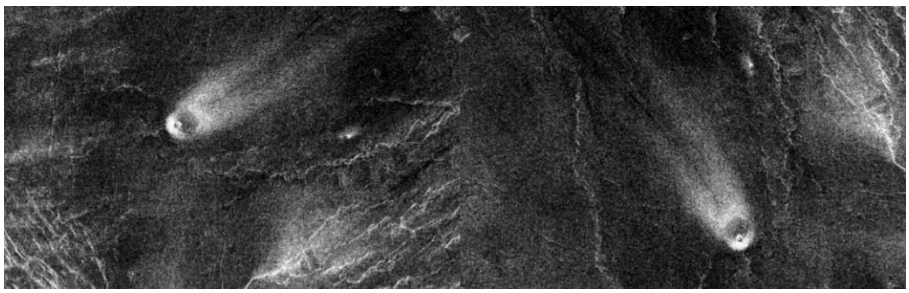

Figure 6.9 Magellan radar image shows bright wind streaks associated with small volcanoes located at 9.4S, 247.5E at the western end of Parga Chasma.

A field of possible yardangs, which are wind-erosional grooves, is observed in the vicinity of the crater Mead, the largest impact crater on Venus. The features described as yardangs are represented by sets

of parallel, linear, slightly sinuous grooves and ridges separating them. These features are a few tens of kilometers long and about 0.5 km wide, forming clusters with 0.5–2 km spacing. They differ from wind streaks in that they have well-defined boundaries and do not originate from topographic features, such as hills.

6.7. Dark mantles

Dark mantles commonly are seen in association with impact craters, forming halos of different sizes and forms. The source of the dark-mantle material is fine debris formed by crater-forming impacts. In many cases the dark mantles have lost direct contact with impact craters and occupy wind-shadow localities in local topographic lows and behind, or against, positive topographic features, becoming a variety of smooth plains (Sposito et al, 2007).

6.8. Rift Zones

The spatial distribution of rift zones of Venus, their topographic configuration, morphometric parameters, and the type of volcanism associating with rifts were analyzed. This allowed the main characteristic features of rifts to be revealed and two different types of rift-forming structures, serving for classification of rift zones as *rift valleys* and *graben belts*, to be isolated. These structural types (facies) of rift zones are differently expressed in the relief: rift valleys are individual deep (several kilometers) W-shaped canyons, while graben belts are clusters of multiple V-shaped and rather shallow (hundreds of meters) depressions. Graben belts are longer and wider, as compared to rift valleys. Rift valleys are spatially associated with dome_shaped volcanic rises and large volcanos (concentrated volcanic sources), while graben belts do not exhibit such associations. Volcanic activity in the graben belts are presented by spacious lava fields with no apparent sources of volcanism. Graben belts and rift valleys were formed during the Atlian Period of geologic history of Venus, and they characterized the tectonic style of the planet at the late stages of its geologic evolution. Formation of this or that structural facies of the

rift zones of Venus were probably governed by the thickness of the lithosphere, its rheological properties, and the development degree of the mantle diapirs associating with rift zones (Guseva, 2016).

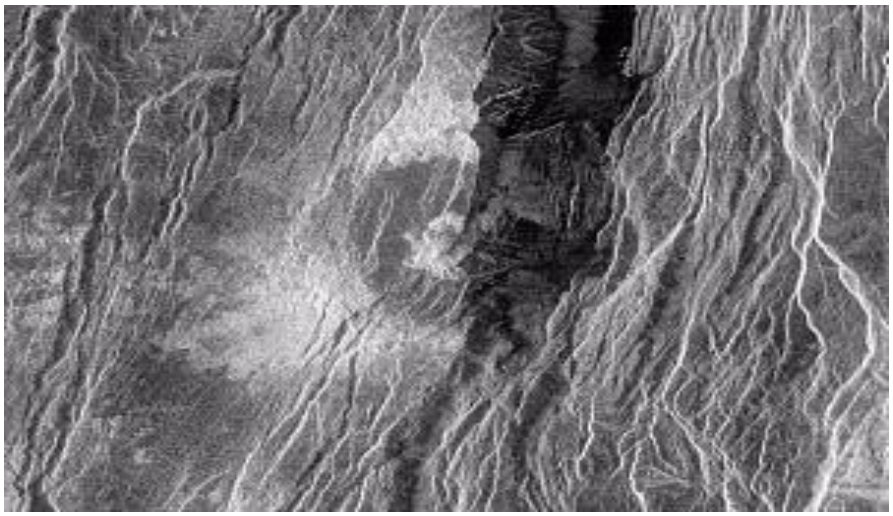

Figure 6.10: Rift zones as rift valleys and graben belts

Rift zones of Venus were for the first time distinguished from the radar data of the Pioneer Venus spacecraft. Later, a wider occurrence of rift zones on the surface of the planet was ascertained from the ground based radar survey and the data of the Venera-15, -16, and Magellan missions (Crumpler et al, 1993).

The photogeologic analysis of the images obtained in the course of the Venera-15, and -16 missions yielded the first description of rift zones. From the results of the Magellan expedition, the structures of rift valleys and fracture belts were classified as relatively young and relatively old, respectively (Basilevsky and Head, 2000a).

The considered unit of rift zones (Rz) occupies approximately 22.6 × 106 km^2 that amounts to around 5% of the surface of Venus. Rift zones are widespread predominately in the equatorial region of the planet (Ivanov and Head, 2011). They form a global rift system of Venus extending to approximately 40000–55000 km. The rift zones are associated with vast lava plains (Guseva, 2010) and large volcanos exceeding 100 km in diameter. These volcanos are mostly in the

regions of a triple junction of rift zones (Senske, 1990). The highest concentration of volcanic edifices is observed within the BAT (Beta–Atla–Themis) region, where they associate with positive gravitational anomalies. On Venus, volcanism is predominantly basaltic, close to alkaline and tholeiitic basalts of the Earth (Smrekar and Phillips, 1991).

6.9. Yardangs

Yardangs are elongated hills sculpted by the wind. They resemble inverted boat hulls and can be tens of meters high and many kilometers long. Although most yardangs develop in easily eroded material, such as volcanic ash, they have also been reported in crystalline rocks.

A field of possible yardangs, which are wind-erosional ridges, is observed in the vicinity of the crater Mead, the largest impact crater on Venus. They are represented by sets of parallel, linear, slightly sinuous grooves and ridges separating them (Figure 14D). Yardangs differ from wind streaks in that they have well-defined boundaries and lack a distinctive relation to topographic features, such as hills (Esposito et al, 2007).

Figure 6.11 A field of possible yardangs on Venus.

References

Basilevsky A.T., Head J.W. (2000a) Rifts and large volcanoes on Venus: global assessment of their age relations with regional plains, J. Geophys. Res, 105: 24583–24611.

Basilevsky et al. (2004) JGR, 109, E12003.

Bondarenko N.V., Head J.W. (2009) Crater-associated dark diffuse features on Venus: Properties of surficial deposits and their evolution.

Bougher S.W., Alexander M.J., Mayr H.G. (1997) Upper atmosphere dynamics: Global circulation and gravity waves, in Venus II: Geology, Geophysics, Atmosphere, and Solar Wind Environment, edited by Bougher S.W., Hunten D.M., and Phillips R.J., pp. 259–291, The University of Arizona Press, Tucson.

Claudin P., Andreotti B. (2006) A scaling law for aeolian dunes on Mars, Venus, Earth, and for subaqueous ripples Earth Planet. Sci. Lett., 252: 30-44.

Crumpler L.S., Head J.W., Aubele J.C. (1993) Relation of major volcanic center concentration on Venus to global tectonic patterns. Science, 261: 591–595.

Dobrovolskis A.R. (1993) Atmospheric tides on Venus IV. Topographic winds and sediment transport. Icarus 103: 276-289.

Esposito Larry W., Stofan Ellen R., Cravens Thomas E. (2007) Exploring Venus as a terrestrial planet. (Geophysical monograph; 176), ISBN 978-0-87590-441-2, p 225

Garvin J.B. (1990) EMP, 50/51, 175 – 190.

Greeley R., Arvidson R. E., Elachi C., et al, (1992b) Aeolian features on Venus: preliminary Magellan results J. Geophys. Res. 97: 13319-45

Greeley R., Bender K., Thomas P.E., Schubert G., Limonadi D., Weitz C. M. (1995) Wind-related features and processes on Venus — Summary of Magellan results. Icarus, 115, 399–420.

Greeley R., Bender K.C., Saunders R.C., Schubert G., Weitz C.M. (1997) Venus II ed S. Bougher et al (Tucson: University of Arizona Press) p 547.

Guseva E.N. (2011) Comparison of the volume of rift-related volcanic rocks on Venus and Earth, Proc. 41st Lunar and Planeary Dci Conf., Housto.

Guseva E.N. (2016) Classification of the Rift Zones of Venus: Rift Valleys and Graben Belts. Solar System Research, 50(3):184-196.

Ivanov B.A. et al. (1992) JGR, 97, 16167 – 16181

Ivanov M.A., Head J.W. (2011) Global geological map of Venus, Planet. Space Sci., 59:1559-1600.

Jerolmack D.J., Mohrig D., Grotzinger J.P., Fike D.A., Watters W.A. (2006) Spatial grain size sorting in aeolian ripples and estimation of wind conditions on planetary surfaces: Application to Meridiani Planum, Mars. Journal of Geophysical Research E, 111.

Juan P.M. (2009) Largest mega-ripples on Earth, possibly solar system, discovered. New scientist, 202(2730): page 13. doi: 10.1016/s0262-4079(09)60973-8.

Kreslavsky M.A., Bondarenko N.V. Third International Planetary Dunes Workshop (2012), Aeolian transport and aeolian depoists on venus: an overview of remote sensing observations. Earth and Planetary Sciences, University of California - Santa Cruz, CA, USA,

Lancaster N. (1995) Geomorphology of desert dunes (London: Routledge).

Marshall J. R. et al. (1991), JGR, 96: 1931–1947.

Marshall J.R., Greeley R. (1992) An experimental study of aeolian structures on Venus J. Geophys. Res., 97 E1 1007-16.

Massoud Ayah T. (2010) Dynamics and Self organization in Aeolian Ripples, department of physics, University of Illinois, Urbana-Champaign

Prigozhin L. (1999) Nonlinear dynamics of Aeolian sand ripples. Phys. Rev. E., 60: 729-33

Lorenz R.D., Zimbelman J.R. (2014) How Windblown Sand Shapes Planetary Dune Worlds Landscapes. ISBN 978-3-540-89724-8, doi:10.1007/978-3-540-89725-5. Springer Heidelberg, New York Dordrecht London

Senske D.A., (1990) Geology of the Venus equatorial region from Pioneer Venus radar imaging, Earth, Moon, Planets, 50/51: 305–327.

Schaller C.J., Melosh H.J. (1998) Venusian Ejecta Parabolas: Comparing Theory with Observations. Icarus, 123-137. Doi: 10.1006/icar.1997.5855.

Sharp R.P. (1963) wind ripples. J. Geol. 71: 617-633.

Smrekar S.E., Phillips R.J. (1991) Venusian highlands: geoid to topography ratios and their implications, Earth Planet. Sci. Lett., 107: 582–597.

Starukhina L. (2000) Solar System Res., 34: 295.

Tsoar H. (1990) Grain-size characteristics of wind ripples on a desert seif dune. Geography Research Forum 10: 37–50.

Ungar J., Haff P.K. (1987) Steady state saltation in air. Sedimentology, 34: 289-299.

Weitz C.M., Plaut J.J., Greeley R., Saunders R.S. (1994) Dunes and microdunes on Venus: why were so few found in the Magellan data? Icarus 112: 282-95.

Chapter 7
Aeolian processes on Earth

Introduction

Aeolian processes, involving erosion, transportation, and deposition of sediment by the wind, occur in a variety of environments, including the coastal zone, cold and hot deserts, and agricultural fields. Common features of these environments are a sparse or nonexistent vegetation cover, a supply of fine sediment (clay, silt, and sand), and strong winds. Aeolian processes are responsible for the emission and/or mobilization of dust and the formation of areas of sand dunes. They largely depend on other geologic agents, such as rivers and waves, to supply sediment for transport.

Aeolian erosion develops through two principal processes: deflation (removal of loosened material and its transport as fine grains in atmospheric suspension) and abrasion (mechanical wear of coherent material). The relative significance of each of these processes appears to be a function of the properties of surface materials and the availability of abrasive particles. The landforms that result from aeolian erosion include ventifacts, ridge and swale systems, yardangs, desert depressions, and inverted relief.

Areas of sand dunes occur in inland and coastal settings, where they often provide a distinctive environment that provides habitats for endemic and rare or threatened species. In both coastal and inland settings, dune migration and sand encroachment may impact neighboring ecosystems and resources, as well as infrastructure. Transport of fine sediment by wind may cause dust storms, events in

which visibility is reduced to less than 1 km by blowing dust. Dust storms impact air quality in their immediate vicinity as well as in areas downwind. Deposition of dust may have a significant effect on the composition and nature of soils in arid regions and beyond. Far-traveled dust from distant sources may have a significant effect on soil chemistry and nutrient status (Lancaster, 2005).

7.1. Aeolian Processes, Deposits, Landforms and Features

Wind erodes the Earth's surface by deflation (the removal of loose, fine-grained particles by the turbulent action of the wind) and by abrasion (the wearing down of surfaces by the grinding action and sandblasting by windborne particles).

Regions which experience intense and sustained erosion are called deflation zones. Most aeolian deflation zones are composed of desert pavement, a sheet-like surface of rock fragments that remains after wind and water have removed the fine particles. Almost half of Earth's desert surfaces are stony deflation zones.

Figure 7.1 Desert varnish (after Krinsley et al, 1995).

The rock mantle[1], a number of astroids, and some planetary moons have mantles) in desert pavements protects the underlying material from deflation.

---

1 - A mantle is a layer inside a planetary body bounded below by a core and above by a crust. Mantles are made of rock, and are generally the largest and most massive layer of the planetary body. Mantles are characteristic of planetary bodies that have undergone differentiation by density. All terrestrials (including Earth)

A dark, shiny stain, called desert varnish or rock varnish, is often found on the surfaces of some desert rocks that have been exposed at the surface for a long period of time.
Manganese, Iron oxides, hydroxides, and clay minerals form most varnishes and provide the shine.

Deflation[1] basins, called blowouts, are hollows formed by the removal of particles by wind. Blowouts are generally small, but may be up to several kilometers in diameter. Wind-driven grains abrade landforms[2]. Landforms are categorized by characteristic physical attributes such as elevation, slope, orientation, stratification, rock exposure, and soil type. Landforms do not include man-made features, such as canals, ports and many harbors; and geographic features, such as deserts.

Figure 7.2 Landform a feature of the desert's surface (Lut desert, Iran).

Grinding by particles carried in the wind creates grooves or small depressions. Ventifacts are rocks which have been cut, and sometimes polished, by the abrasive action of wind.

1 - Blowouts or deflations are sandy depressions in a sand dune ecosystem caused by the removal of sediments by wind

2 - A landform is a natural or artificial feature of the solid surface of the Earth or other planetary body

Figure 7.3 a ventifact (after Bourke and Viles, 2007).

Sculpted landforms, called yardangs, are up to tens of meters high and kilometers long and are forms that have been streamlined by desert winds. The famous Great Sphinx of Giza in Egypt may be a modified yardang.

7.2. Basic Aspects of Wind Erosion

7.2.1 Soil-Particle Characteristics

The processes of particle entrainment[1], transport and deposition involve a set of particle-to-flow, particle-to-surface and particle-to-particle interactions. The physical properties of individual particles, such as shape, size and density, play an important role in these interactions. These properties vary greatly and are difficult to measure precisely in practice, but they must be adequately (much) described in wind-erosion models. The shape of a grain includes all aspects of its external morphology, such as its general form (sphericity), its roundness (sharpness of edges and corners) and its surface roughness.

Observations show that the shape of soil particles is highly irregular (Pye, 1994), ranging from spheres to plates in their gross form, from very-angular to well-rounded in their roundness and from rough to smooth in their surface texture. In practice, the size of a

1 - When a fluid picks up and drags another fluid or a solid

particle can be determined by directly measuring its external caliper dimensions.

Several techniques are proposed to measure external caliper dimensions, among which sieving is the most-widely used direct-measuring method. A series of progressively finer square-mesh sieves is used to separate particles, principally on the basis of their intermediate axial diameters (Kennedy et al. 1985).

To overcome the difficulties in precisely measuring particle shape and size, we introduce the concept of *equivalent spherical diameter* (ESD)[1]. The aerodynamic behavior of particles is well-understood only for spherical particles.

Nearly all theoretical models for particle entrainment and motion are based on the assumption that the particles are spheres. The equivalent particle size is measured by the diameter of a sphere of which certain aerodynamic or optical properties are identical to those of the particle under consideration.

Table 7.1: Various equivalent particle sizes for particle P, defined by comparing a property with that of a sphere S (After Allen, 1981)

Symbol	Name	Definition	Formula
d_m	mass d	d of S, same density & mass as P	$m = \rho_p \frac{\pi d_m^3}{6}$
d_v	volume d	d of S, same volume as P	$V = \frac{\pi d_v^3}{6}$
d_s	surface d	d of S, same surface as P	$s = \pi d_s^2$
d_{sv}	surface-volume d	d of S, same external surface to volume ratio as P	$d_{sv} = d_v^3/d_s^2$
d_d	drag d	d of S, same resistance to motion as P in a fluid with same viscosity & velocity	$F_D = \frac{C_D \pi d_d^2 \rho v^2}{8}$
d_f	terminal-velocity d	d of S, same density & terminal velocity as P in a fluid of same density & viscosity	

d_m= mass diameter → d of S = sphere diameter; P = particle

d_v = volume diameter

d_s = surface diameter

1 - Scientifically, the equivalent spherical diameter (ESD) of an irregularly shaped object is the diameter of a sphere of equivalent volume.

d_{sv} = surface /volume diameter
d_d = drag diameter
d_f = terminal velocity diameter

For example, for a given particle mass, m, the particle mass equivalent diameter, dm, is calculated through:

$$d_m = \left(\frac{6m}{\pi \rho_p}\right)^{1/3} \quad (1)$$

where ρ_p is the particle density. There are many other definitions for equivalent particle size. Methods commonly used in sedimentology for measuring equivalent particle size include electro-optical and settling-velocity methods. For example, in the laser-diffraction method, the volume equivalent diameter is estimated on the basis of the optical properties, while in the settling-tube method (Malcolm and Raupach, 1991), the terminal-velocity equivalent diameter is estimated.

The definitions for equivalent particle diameter, as listed in Table 1, are adequate depends on the problems being studied. The usefulness of every definition may be limited to types of problems. For example, the *terminal velocity*[1] equivalent diameter is advantageous if we are interested in the *transport* and *deposition* of particles in the atmosphere, as the particle terminal velocity is the key aerodynamic property involved in these processes. But this definition of particle diameter may not be suitable, if our main concern is how dust particles suspended in air might influence the *radiation balance* of the atmosphere.

As far as wind-erosion modeling is concerned, the most useful

1 - Terminal velocity is the maximum velocity attainable by an object as it falls through a fluid (air). It occurs when the sum of the drag force (F_d) and the buoyancy is equal to the downward force of gravity (F_G) acting on the object. Since the net force on the object is zero, the object has zero acceleration.

equivalent particle diameters are mass equivalent diameter, drag equivalent diameter, terminal-velocity equivalent diameter, projected-area equivalent diameter, and sieve diameter.

From the view point of the dynamic processes involved in wind erosion, sieve diameter is not the best representation of particle size, but it is widely used because it is relatively easy to measure.

7.2.2 Forces on an Airborne Particle

The motion of an airborne particle is influenced by several forces, including the gravity force (F_g), aerodynamic drag (F_d), aerodynamic lift (F_l), the Magnus force due to particle rotation, (F_m), and the electric force (F_e).

The particle-to air density ratio is defined to be $\sigma p = \rho p/\rho a$, where the particle density (ρp), is around 2,600 kg m^{-3} while the air density (ρ), is approximately 1.2 kg m^{-3}.

Since σp is of order 103, the action of buoyancy upon an airborne soil particle is negligible and hence, Fg is simply the particle weight. The vertical only component of F_g is −mg with g being the acceleration of gravity.

The physical mechanism which leads to aerodynamic drag (F_d) is as illustrated in Figure 7.4a. If the particle moves relative to the surrounding fluid, a force in the opposite direction of that relative velocity is exerted by the fluid on the particle. This force is known as the drag (F_d) that arises from the pressure differences between the frontal region and the wake region of the particle and from *the viscous effect* (the transfer of momentum from the fluid to the particle through molecular motion).

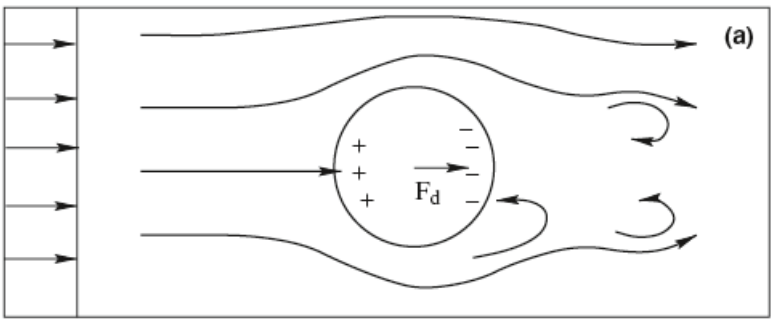

Figure 7.4a Aerodynamic drag due to the viscous effect, flow separation and turbulence in the *wake region* of the particle.

There is an equal and opposite force exerted by the particle on the fluid. The force exerted by the flow on the particle is equal to the integral of total stress (or momentum flux) over the surface of the particle. Higher fluid pressure on the sphere is indicated positive and lower pressure negative.

Aerodynamic lift (F_l) due to the *Bernoulli Effect* on a spherical particle in a shear flow (Fig.7.4b). The pressure is higher on the lower side of the particle where the fluid velocity is smaller, while the pressure is lower on the upper side, where the fluid velocity is higher.

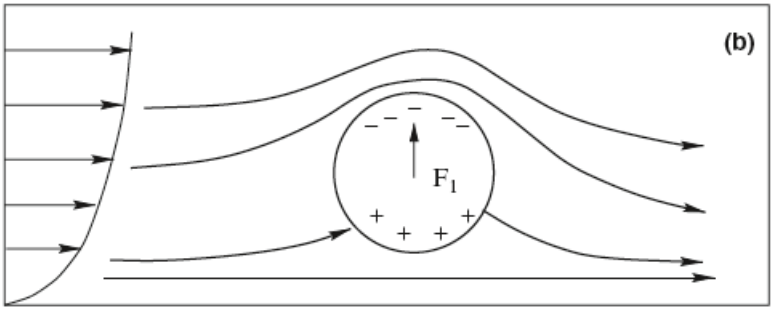

Figure 7.4b Aerodynamic lift due to the Bernoulli Effect on a spherical particle in a shear flow

Magnus force **(**F_m**)** due to a combination of the Bernoulli Effect and the viscous effect on a spinning particle.

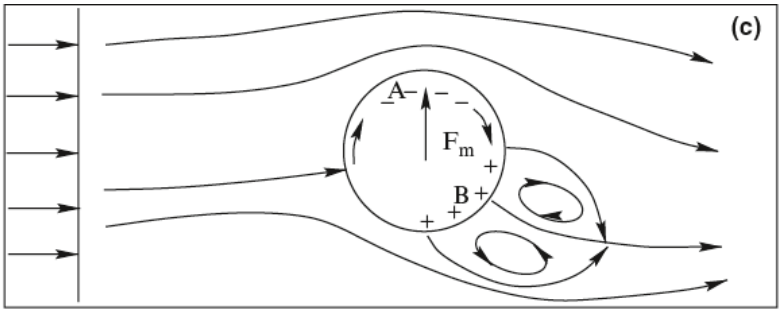

Figure 7.4c Magnus force due to a combination of the Bernoulli Effect and the viscous effect (after Allen, 1994)

On the upper side of the particle, where the particle spins in the same direction as the fluid motion, the fluid velocity is relatively higher and the pressure is relatively lower than on the lower side of the particle, where the particle spins in the opposite direction to the fluid.

The aerodynamic drag force (F_d) is often expressed in terms of particle-to-fluid relative velocity (**ur**), by

$$\mathbf{F_d} = -\frac{1}{2} C_d \rho A \mathbf{u_r} U_r \qquad (2)$$

Where:

Cd is the aerodynamic drag coefficient,

A is the particle cross-section in the ur direction (equal to $\pi d^2/4$ for spherical particles) and

Ur is the magnitude of ur.

ur = particle relative velocity / fluid relative velocity

If upi is ith component of the particle velocity and ui is the ith component of velocity of the fluid surrounding that particle respectively, then is the ith component of **ur**, and Ur is given by

$$U_r = (u_{r1}^2 + u_{r2}^2 + u_{r3}^2)^{1/2} \qquad (3)$$

The magnitude of the aerodynamic drag depends critically on the flow pattern around the particle. It means that Cd is a function of the particle Reynolds number (*Rep*),

Rep = *Udr*/*V*. → *Udr* is roughness-element size and v is particle

velocity.

For different regimes of *Rep*; *Cd* can be interpreted as:

•*For Rep*≪ 1, "called the Stokes region" the fluid motion in the vicinity of the particle is just influenced by viscous forces and fluid inertia[1] is negligible.

In this situation, *Cd* is inversely proportional to Rep. for this regime, the Stokes law *Cd* = 24/*Rep* applies. The Stokes law begins to fail at about Rep = 10.

$$F_d = 6\pi \mu R V \qquad (4)$$

where:

F_d is the frictional force – known as *Stokes' drag* – acting on the interface between the fluid and the particle

- μ is the viscosity (some authors use the symbol η)
- R is the radius of the spherical object
- V is the fluid velocity relative to the object.

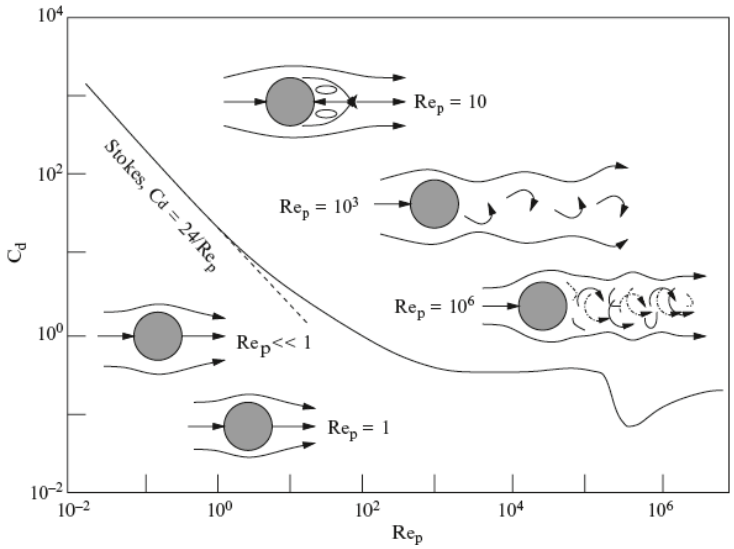

Figure 7.8 Aerodynamic drag coefficient, Cd, for a smooth spherical particle as a function of particle. Reynolds number, Re_p. Apart from the Stokes region, the relationship is based on experimental results (Allen, 1994)

1 - Inertia is the resistance of any physical object to any change in its velocity. This includes changes to the object's speed, or direction of motion.

•For the regime $10^3 < Re_p < 3\times10^5$, pressure-induced drag dominates over viscous drag, C_d is approximately 0.5 and nearly independent of Re_p.

•As $Re_p > 3\times10^5$, the boundary layer over the sphere undergoes a transition from laminar to turbulent and the pressure distribution around the particle is significantly altered, resulting in a large decrease in C_d from about 0.5 to about 0.1.

There are other simpler expressions. For example,

$$C_d = \frac{24}{Re_p}[1 + 0.15Re_p^{0.687}] \tag{5}$$

is fairly widely used.

An aerodynamic lift force (F_l) arises from a *shear flow*, which results in a pressure gradient to the shear in the direction of decreasing velocity. The aerodynamic lift can be approximately given by

$$\mathbf{F}_l = \frac{1}{2}C_l\rho A(\nabla U^2)d \tag{6}$$

Where; ∇U^2 is the gradient of $U \equiv |u|^2$; C_l is the aerodynamic lift coefficient, usually $C_l = 0.85C_d$. For spherical particles, F_l is generally important only if the particles are placed in a flow of strong shear.

For a non-spherical particle, F_l can be significant even in uniform flows, as the shape of the particle may lead to differing velocities, and hence pressure distributions over its surface.

The mechanism which results in the Magnus force (F_m) is illustrated in figure 5c.

A rotating particle experiences a force perpendicular to both the direction of rotation and the direction of motion.

The Magnus force can be partially explained using the Bernoulli equation, but it is necessary to take into consideration the viscous effect in relation to particle rotation. On side A of a top-spin particle the particle moves in the same direction as the fluid, the fluid velocity is increased due to the viscous effect and the pressure is reduced. The

opposite occurs on side B of the particle.

The magnitude of the Magnus force is dependent on Rep and the ratio vs/Ur, where vs is the circumferential speed of the particle (Ω_p). In studying the motion of sand grains in the atmosphere, Anderson and Hallet (1986) used the expression

$$\mathbf{F_m} = \pi\rho\frac{d^3}{8}(\mathbf{\Omega_p} \times \mathbf{u_r}) \tag{7}$$

if the particle Reynolds number is small, where Ω_p is the angular velocity of the particle.

For large particle Reynolds numbers, it is plausible (true) to assume that

$$\mathbf{F_m} = C_m\pi\rho\frac{d^3}{8}(\mathbf{\Omega_p} \times \mathbf{u_r}) \tag{8}$$

where C_m is a coefficient of the Magnus force which depends on Re_p and *vs/Ur*.

vs is the circumferential speed of the particle (Ω_p)

7.2.3 Electric force (F_e)

Zheng et al (2004) have reported that soil particles may be charged and an electric field (*E*) is generated near the surface due to the motion of windblown (bâd zā-dəh) particles, and the electric force (F_e) exerted by E on the windblown particles may be as large as the gravity force (F_g).

The electric force on a particle of mass m is

$$\mathbf{F_e} = mC_e\mathbf{E} \tag{9}$$

E has been found to vary from case to case, and the existing measurements of E range between some negative value and 166 kV m^{-1}. E appears to decrease rapidly with height *z* (Fig. 5.6).

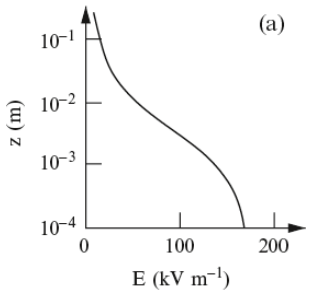

Figure 7.9 A profile of near-surface electric field E(z).

Also the charge of windblown sand particles can be either positive or negative, but it is generally considered to be negative and the magnitude of C_e (electric coefficient) is around $-60\mu C\ kg^{-1}$ (μC is micro Coulomb).

A negatively charged particle in the electric field would experience a F_e pointing to the ground surface. We can compare the magnitude of Fe with that of Fg. Assuming E = 100 kV m^{-1} and $C_e = -60\ \mu C\ kg^{-1}$, it is found that $F_e/F_g \approx 3/5$. Therefore, F_e appears to be quite significant and should be carefully considered in studying the motion of windblown particles.

7.2.4. Terminal Velocity

The terminal velocity of a particle is that velocity resulting from the gravity and drag forces. Commonly it is the freefalling speed of a particle in still (undisturbed; calm) air under the action of gravity. The relationship between the terminal velocity of a particle and its diameter depends on whether the flow local to the particle is laminar or turbulent. In laminar flow, the particle falls more quickly than in turbulent flow, where particles tend to align themselves for maximum drag and the drag is increased by eddies in the wake of the particles.
The general equation for the drag force F_d on a particle is:

$$\mathbf{F_d} = -\frac{1}{2} C_d \rho A \mathbf{u_r} U_r \qquad (10)$$

$$F_d = C_d^{\,n} V^n \mu^{2-n} \rho_0^{\,n-1} \qquad (11)$$

where C_d is the drag coefficient, depending on shape, surface, and so on;
V is relative velocity;
μ is fluid viscosity;
ρ_0 is fluid density; and
n varies from 1 for laminar flow to 2 for turbulent flow.
For example, for a sphere in laminar flow, $C_d = 3\pi$.
Hence for laminar flow spheres,

$$Fd = 3\pi d\, V\mu \qquad (12)$$

which is known as Stokes's law.

$$V_t = \sqrt{\frac{2mg}{\rho A C d}} \qquad (13)$$

Where;
V_t represents terminal velocity,
m is the mass of the falling object,
g is the gravity,
C_d is the drag coefficient,
ρ is the density of the fluid through which the object is falling, and
A is the particle cross-section (Projected area).
Projected area is two dimensional area measurement of a three-dimensional object by projecting its shape on to an arbitrary plane. This is often used in wind pressures, and terminal velocity.

For rectangular shape → area = L×W	projected area = L×W cosβ
For spherical shape → area = $4\pi r^2$	projected area = πr^2
For circular shape → area = πr^2	projected area = πr^2 cosβ

A = original area
β = the angle between the normal to the local plane and the line of sight to the surface

7.3. **Modes of Particle Motion**

Particles of different sizes adopt different modes of motion during a wind erosion event. Based on field and wind-tunnel observations, Bagnold classified particle motion into three categories; namely, *suspension*, *saltation* and *creep*. Figure 8 gives a schematic illustration of this classification.

7.3.1. Suspension

Once dust particles are entrained into the atmosphere, they often become suspended in air because of their small terminal velocities. They can be relatively easily dispersed away from the surface by turbulence in the atmospheric boundary layer and then carried by the atmospheric circulation over large distances, up to thousands of kilometers.

As the typical residence time of a dust particle in the atmosphere depends on its terminal velocity, suspension can be further divided into long- and short-term suspension. The suspension of particles smaller than 20 μm is referred to as *long-term suspension*. Particles with a diameter between 20 and 70 μm remain suspended only for a short period of time, typically several hours, and can hardly be transported more than several hundreds of kilometers, unless the weather situation is extremely favourable. The suspension of particles between 20 and 70 μm is therefore referred to as short-term suspension.

7.3.2. Saltation

Saltation is the bouncing motion of sand particles across the surface during an erosion event. It is the principal mechanism for the transport of large quantities of soil ad sand particles in the direction of the wind, resulting in the formation and evolution of sand seas, dunes, ripples and fence-line drifts.

Typical saltation trajectories are as illustrated in Fig. 7.10: i.e., sand particles are entrained into the atmospheric surface layer with an initial steep vertical ascent followed by a more horizontal movement

and eventual return to the surface with a small impact angle.

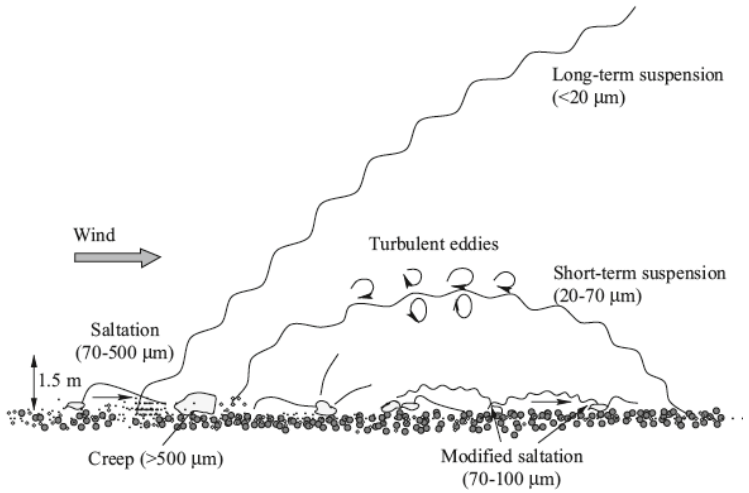

Figure 7.10 An illustration of creep, saltation and suspension of soil particles during an erosion event. Saltation is further classified into *pure* and *modified saltation* and suspension is further divided into short-term and long-term suspension (after Pyle, 1987).

7.3.3. Creep

Under normal atmospheric conditions, particles larger than 1,000 μm are too heavy to be lifted from the surface by wind. However, they can be pushed along the surface by wind or by the impact of saltating particles and this is known as *creep*.

The classification of particle motion described above is conceptually important, but does not explicitly account for the effect of flow conditions on particle motion. For wind-erosion modeling purposes, more objective definitions of suspension and saltation are required. A necessary condition for an airborne particle to remain suspended is that its terminal velocity is smaller than the mean vertical Lagrangian velocity for the air parcel in which the particle is contained.

The Lagrangian velocity is the velocity at which air parcels are dispersed upward by turbulence. In neutral atmospheric surface layers, the typical Lagrangian vertical velocity is approximately κu_*.

Therefore, for particles with $wt/\kappa u* \ll 1$, upward turbulent dispersion dominates over gravitational settling, so long-term suspension is a good approximation for these particles. For particles with $wt/\kappa u* \gg 1$, gravitational settling dominates over turbulent dispersion, so suspension is virtually not possible for these particles.

7.4. Threshold Friction Velocity for Sand Particles

Soil particles resting on the surface under the influence of an air stream experience several forces, including the aerodynamic drag, F_d, the aerodynamic lift, F_L, the gravity force, F_g, and the inter-particle cohesive force, F_i (Fig. 7.11). Driving forces for the lift off of sand-sized particles are F_d and F_l, which are related to the wind shear near the surface and hence are functions of the friction velocity ($u*$). The threshold friction velocity, $u*t$, is the minimum friction velocity required for the aerodynamic forces to overcome the retarding forces, namely F_g and F_i, and to initialize the movement of soil particles.

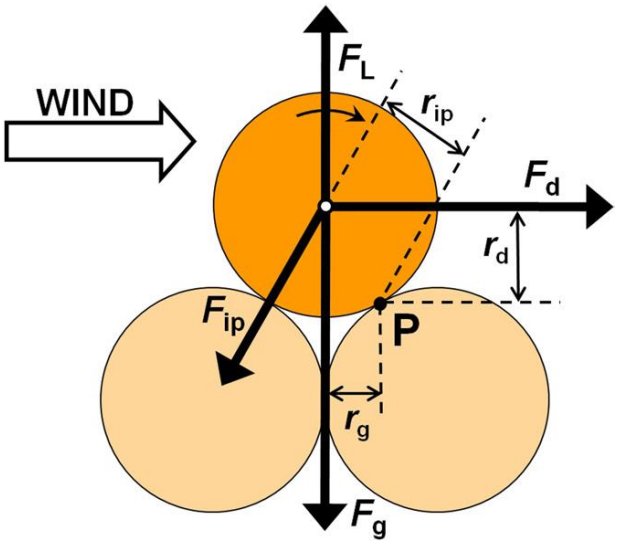

Figure 7.11 Schematic of the forces acting on a stationary sand particle resting on a bed of other particles (after Shao and Lu, 2000). Forces are denoted by thick arrows, and their moment arms relative to the pivoting point P are indicated by thin arrows. When the moment of the aerodynamic lift and drag forces exceeds that of the gravitational and antiparticle forces,

the particle will be entrained into the flow by pivoting around P in the indicated direction.

In wind-tunnel and field studies, u∗t is commonly set (regulated) to the value of u∗ at which a small percentage of soil particles start to move. Threshold friction velocity (u∗t) is essentially a property of the soil surface, rather than that of a soil particle. It describes the capacity of the surface to resist wind erosion and is affected by a range of factors. However, under ideal conditions, u∗t can be expressed as a function of only particle size.

7.5. Aeolian dune shapes

Three main factors (two climatic and one sedimentary) influence the piling of sand into dunes with particular shapes:

1. Wind magnitude (above the threshold velocity), direction, and frequency.
2. Vegetation covers.
3. Grain size.

In addition, other factors obstructions to wind flow, climatic changes manifested by dramatic change in wind direction, velocity and frequency of storms, sand availability, thickness of sand cover, and sudden removal of vegetation cover can affect dune morphology. Because dunes are bed-forms in which a great deal of energy has been invested, daily or seasonal changes in wind direction do not easily reshape them. Therefore dune shape is the manifestation of a long-term average of wind conditions.

Distinction of sand dunes into simple (basic), compound and complex forms was suggested by McKee (White and Tsoar, 1998). Simple dunes consist of individual dune forms which are spatially separate from nearby dunes. Compound dunes consist of two or more dunes of the same type which have coalesced or are superimposed.

Complex dunes consist of two or more different types of simple dunes which have coalesced or are superimposed. Complex and compound are in most cases megadunes and abound in most of the world's great sand seas. Simple sand dunes are small in most cases,

with wavelengths (shortest distance from one dune crest to the other) of 10 to 500 m.

Three general types of active sand dunes are classified by movement:

1. *Migrating* dunes: the whole dune body advances with little or no change in shape and dimension. Transverse and barchan dunes are the most representative specimens.

2. *Elongating* dunes: the dunes elongate and become extended in length with time. Linear dunes are the most representative specimens.

3. *Accumulating* dunes: the dunes have little or no net advance or elongation.

Star dunes best represent this type.

Dunes are segregated into three different categories of sand accumulation:

1. Accumulation as a consequence of topographic barriers (mostly cliffs) interfering with airflow. These dunes are not vegetated.

2. Accumulation of sand in areas of open terrain due to changes of bed roughness or aerodynamic fluctuations. These dunes are not vegetated.

3. Accumulation due to vegetation that determines dune formation and shape.

All dunes in this category are vegetated. If vegetation is destroyed by human impact the reaction is either transformation to a category 2 dune types, or the formation of superimposed dunelets on top of the main dune.

The second category, unvegetated dunes that are self-accumulated, is widespread mostly in arid lands. This category is subdivided according to the grain size into sand dunes with bimodal and unimodal sand-grains. The fine sand mode of the bimodal sand dunes is within the range of the mean size of unimodal desert dune sand (0.125–0.250 mm). All dunes composed of bimodal coarse sand have a moderate aspect ratio of $h/L < 0.3$ (where h is the hill height and L is the horizontal distance from the hilltop to the point where the elevation is half its maximum). Dunes composed of unimodal, well-sorted fine sand display slip-faces, pronounced crests and a much higher aspect

ratio ($1.3 > h/L > 0.3$).

Despite the upslope increase in wind shear stress, the effect of gravity (mg sin θ) on grains, which is dependent upon the weight of the grain (mg) and the slope angle (θ), is stronger. Bimodal sand with one coarse mode can only form sand-sheets and sand-strips. Coarse sand-sheets (also known as zebras) are the most common types of aeolian depositional surfaces in deserts, covering an area of 1,520,000 km^2 (White and Tsoar, 1998).

Many attempts have been made to classify dunes based on a combination of shape, number and orientation of slip-faces relative to the prevailing wind or resultant sand drift direction, and degree of form mobility (e.g. Wasson and Hyde 1983a, El-Baz 1986, Thomas 1989b). The relationship between wind regime, slip face orientation, and direction of dune movement (or extension) is complex, and descriptive terms such as 'longitudinal' and 'transverse', which carry genetic implications, are frequently used inappropriately. Hunter et al, (1985) suggested that the term longitudinal dune should be applied only where the orientation of the long axis of the dune deviates by less than 15° from the resultant sand transport direction, while a transverse dune should have long axes which are within 15° of being normal to the resultant sand transport direction. Dunes whose long axes show a larger deviation from the resultant sand transport direction are referred to as oblique dunes (Fig. 7.12). In practice, it is often difficult to classify dunes accurately in this way because long-term wind data are commonly not available from the dune areas, and local sand transport directions may deviate significantly from those predicted using data from the nearest weather station owing to the effects of topography and secondary circulations in the atmosphere. Many dune ridges show dynamic behavior typical of both transverse and longitudinal dunes, and Carson and MacLean (1985a, 1985b, 1986) suggested the term 'hybrid' to describe such dunes.

This term has not, however, been widely accepted and is considered inappropriate by some authors (Hunter et al, 1985).

Self-accumulated simple dunes include barchans, transverse (barchanoid) ridges, unvegetated linear dunes (seif dunes), dome

dunes, and star dunes. Dunes formed by accumulation of sand related to the presence of vegetation include parabolic dunes, vegetated linear dunes, and coppice or hummock dunes.

Linear dunes (vegetated and unvegetated) are by far the most common dune type found in deserts, followed by transverse dunes. However, there is considerable variation between different regions. In humid region coastal dune fields hummock dunes and parabolic dunes are the most common types, whereas in arid and semi-arid region coastal dune fields barchans and transverse barchanoid ridges are dominant (Illenberger, 1988).

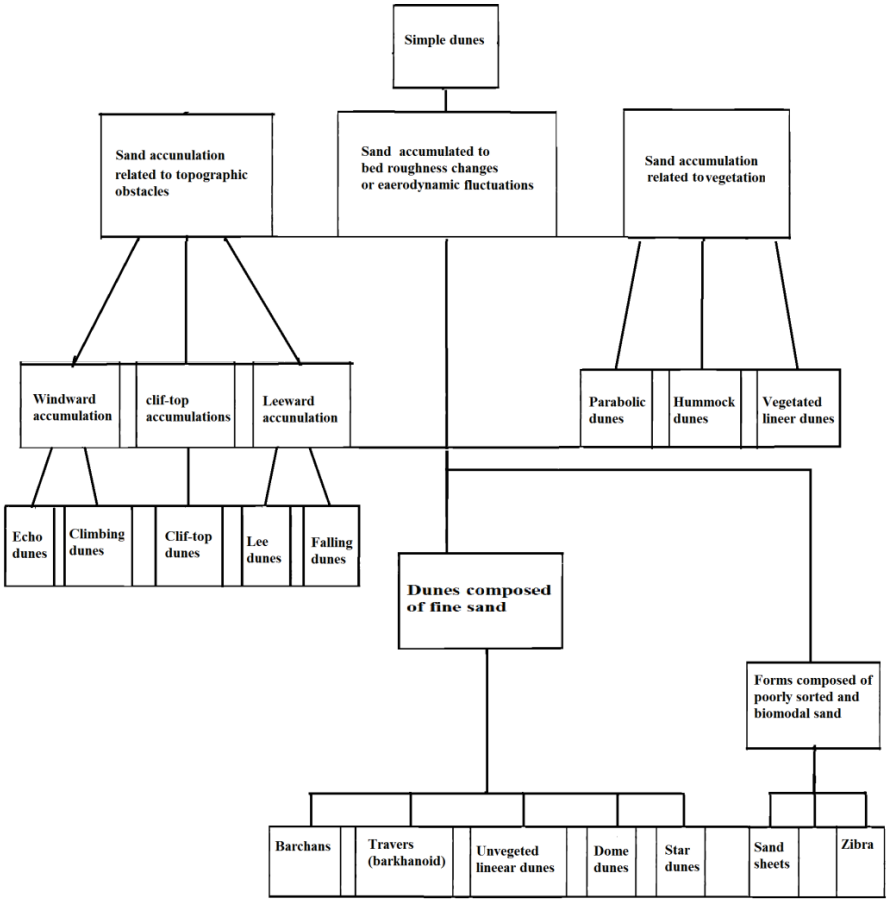

Figure 7.12 Classification of major dune types (after White and Tsoar, 1998)

7.6. Dune Accumulation Influenced by Topographic Obstacles

7.6.1. Lee Dunes

Topographic obstacles such as boulders, escarpments, and hills induce zones of airflow acceleration, deceleration, and enhanced turbulence. Consequently, there will be either erosion or accumulation of sand, or both simultaneously in different places. The resulting dunes are static, i.e. they do not advance or elongate once they have attained a steady state. Allen (1982) used the less specific term *current shadow* for such features in both aeolian and aqueous environments. However, the terms *lee dune* or shadow dune are more widely used in the aeolian literature.

As the airflow is deflected around and over the obstacle, a horseshoe vortex is created (Fig. 7.13), and sand is initially deposited both in front of the obstacle and on either side as two tapering wings (7.14).

The two wings eventually coalesce as the arms of the horseshoe vortex gradually transfer sand towards the centerline of the obstacle, and over time the shadow dune becomes higher, longer, and narrower.

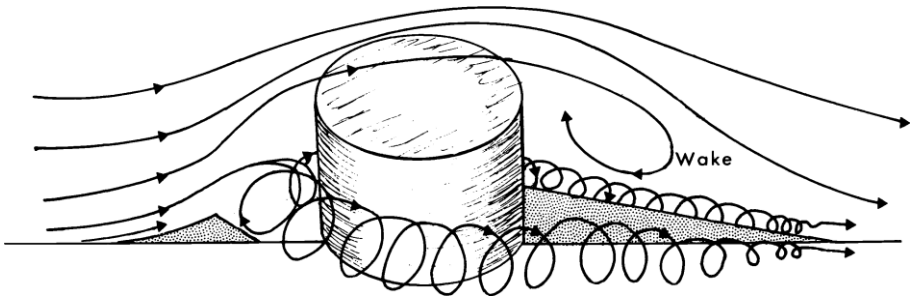

Figure 7.13 Schematic diagram shows the development of a horseshoe vortex around an obstacle. Sand accumulations are stippled (Greeley 1986).

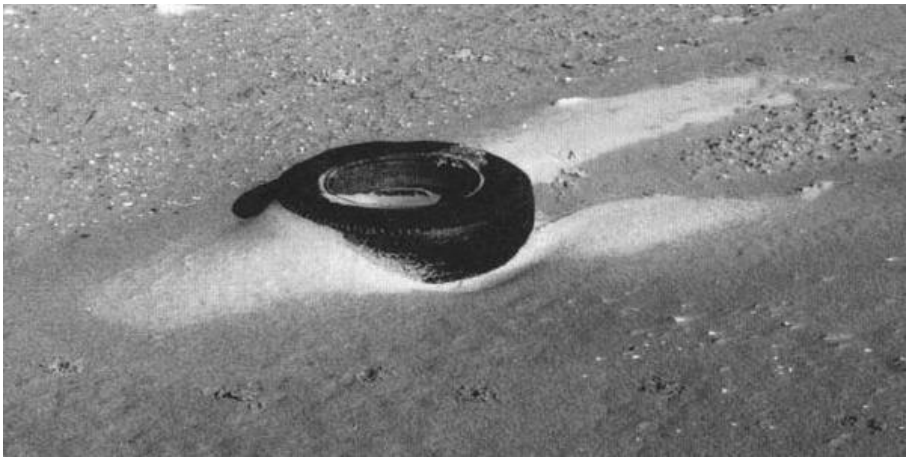

Figure 7.14 Development of paired lee accumulations and windward sand ramp adjacent to an obstacle (White and Tsoar, 1998).

7.6.2. Echo dunes

Echo dunes commonly form in front of cliffs (Fig. 7.15) but can only be maintained in the long term if sand is moved laterally along the cliff line by vortices located between the cliff and the echo dune. The sand may ultimately escape through drainage channels or other breaks in the cliff.

Figure 7.15 Echo dunes developed in front of a cuesta. The extremities of the dune develop into climbing dunes where drainage channels cut the cliff

7.6.3. Cliff-Top Dunes

A zone of reduced wind velocity is frequently observed just downwind of the crest of escarpments (Marsh and Marsh 1987). Consequently, sand often accumulates at such sites forming cliff-top dunes (Fig. 7.16). Since sand can be blown up slopes as steep as 60°, the formation of cliff-top dunes does not necessarily require cliff recession or erosion of a sand ramp.

7.16 Climbing and cliff-top dunes respectively, (a) on Earth (White and Tsoar, 1998) and in Coprates Chasma on Mars (Chojnacki et al, 2010).

Figure 7.17 A large barchan dune that sows an asymmetry due to elongation of the left horn by winds blowing from the right side of the dune.

7.6.4. Simple Barchans and Transverse Barchanoids

Barchans are isolated crescentic dunes whose horns point downwind. The windward slope is typically convex with an average maximum slope of 12° while the leeward slope is characterized by a slip face at 33–34°. Some barchan dunes have a separate crest and brink, whereas in other cases the two coincide. Small barchans tend to be flatter than larger forms and have a smaller angle between the windward flank and the desert floor (Hastenrath, 1987). Barchans are one of the best known dune types and their genesis has been much discussed (Wipperman and Gross, 1986).

Barchans can migrate long distances downwind without experiencing major changes in size or shape. In some instances they act almost as a closed system, in which sand is prevented from escaping from the dune by reverse flows associated with vortices on the leeward side of the dune. However, in most cases migrating barchans act as an open system in dynamic equilibrium, in which the input of sand from upwind is equal to the downwind losses from the horn tips. A change in wind conditions or sand supply will cause the barchan to change its size and probably its shape. The rate of barchan advance is directly related to the rate of sand transport over the brink and inversely related to the brink height. Where sand supply increases, individual barchan dunes may link up to form a sinuous-crested ridge oriented perpendicular to the strongest wind or resultant sand drift direction. Many transverse ridges display alternating *barchanoid* (downwind facing) and *linguoid* (upwind-facing) elements (White and Tsoar, 1998).

Transverse and barchan dunes in a reversing wind regime change their profile dramatically as the slip face alternates from one side of the dune to the other. Dunes which change their slip face orientation in this way are known as *reversing* dunes (McKee, 1982).

Figure 7.18 Photograph of complex transverse megadunes. Thar Desert of northwest India (Kar, 1990)

7.6.5. Linear Dunes

Linear dunes are characterized by their considerable length, relative straightness, parallelism, regular spacing, and low ratio of dune to inter-dune areas. As with other dune types, simple, complex, and compound varieties can be recognized. Simple linear dunes consist of a single narrow dune ridge with a straight or sinuous crest line which may be rounded or sharp in cross-section. Two major types are recognized (Tsoar, 1989), unvegetated and vegetated. Because of the lack of vegetation, the former has a sharp crest which gives it its name seif (sword). The second type is vegetated and has a more rounded crest. Seif dunes occur in many African sand seas, where they have often been referred to as silk dunes. They are also found extensively in Sinai and other parts of the Middle East. Vegetated linear dunes occur widely in Central Australia, the Kalahari, the Thar Desert of northwest India and Pakistan (Lancaster, 1986).

Figure 7.19 view of sinuous seif dunes.

References

Allen J.R.L. (1982) Sedimentary structures. Amsterdam: Elsevier.

Allen J.R.L. (1994) Fundamental properties of fluids and their relation to sediment transport processes. In: Pye K (ed) Sediment Transport and Depositional Processes, Blackwell Scientific Publications, Oxford, pp 25–60

Bourke M.C., Viles H.A. (2007) A Photographic Atlas of Rock Breakdown Features in Geomorphic Environments. Publisher: Planetary Science Institute

Chojnacki M., Jeffrey E. Moersch, Burr D.M. (2010) Climbing and falling dunes in Valles Marineris, Mars. Geophysical Research Letters, 37: L08201, doi: 10.1029/2009GL042263.

Hastenrath S.L. (1987) The barchan dunes of southern Peru revisited. Z. Geomorph. 31: 167–178.

Hunter R.E., Richmond B.M., Alpha T.R. (1985) Storm-controlled oblique dunes of the Oregon coast: reply. Bull. Geol. Soc. Am. 96: 410.

Illenberger W.K., Rust I.C. (1988) A sand budget for the Alexandria coastal dune field, South Africa. Sedimentology, 35: 513–521.

Kennedy S.K., Meloy T.P., Gurney T.E. (1985) Sieve data size and shape information. J. Sedim. Petrol., 55: 356–360

Kar A. (1990) Megabarchanoids of the Thar Desert: their environment, morphology and relationship with longitudinal dunes. Geography J. 156: 51–61.

Krinsley D., Dorn R., Tovey N.K. (1995) Nanometer-Scale Layering

in Rock Varnish: Implications for Genesis and Paleoenvironmental Interpretation, The Journal of Geology, 103(1): 106–113

Lancaster N. (1986) Grain size characteristics of linear dunes in the southwestern Kalahari. J. Sediment. Petrol. 56: 395–499.

Lancaster, N., 2005, Aeolian erosion, transport and deposition, in Selley, R.C., Robin, L., Cocks, M., and Plimer, I.R., eds., Encyclopedia of Geology: Oxford, Elsevier, p. 612–627.

Malcolm L.P., Raupach M.R. (1991) Measurements in an air settling tube of the terminal velocity distribution of soil material. J. Geophy. Res. 96(15): 275-286

Marsh W.M., Marsh B.D. (1987) Wind erosion and sand dune formation on high Lake Superior bluffs. Geog. Ann**.** 69A: 379–391.

Pye K. (1994) Properties of sediment particles, Chapter 1 In Pye, K. (ed.), Sediment Transport and Depositional Processes. Oxford: Blackwell Scientific, pp. 1–24.

Shao Y.P., Lu H. (2000) A simple expression for wind erosion threshold friction velocity. J. Geophys. Res. 105**:** 22437–43

Tsoar H. (1989) Linear dunes forms and formation. Prog. Phys. Geogr. 13: 507–528.

White B., Tsoar H. (1998): Geomorphology 22:159

Wipperman F.K., Gross G. (1986). The wind-induced shaping and migration of an isolated dune: a numerical experiment. Boundary-layer Meteorol. 36: 319–334.

Chapter 8
Aeolian processes on Mars

Introduction

Mars is a dusty, cold, desert world with a very thin atmosphere. The robotic explorers have found lots of evidence that Mars was much wetter and warmer, with a thicker atmosphere, billions of years ago. The days and seasons are likewise comparable to those of Earth. Liquid water cannot exist on the surface of Mars due to low atmospheric pressure. Data show Martian soil to be slightly alkaline and containing elements such as magnesium, sodium, potassium and chlorine. These nutrients are found in soils on Earth, and they are necessary for growth of plants. Mars is scarred by a number of impact craters. The largest confirmed of these is the Hellass impact basin which is visible from Earth. Due to the smaller mass of Mars, the probability of an object colliding with the planet is about half that of Earth. Mars has two relatively small moons, Phobos and Deimos. Wind erosion and deposition are powerful agents of surface change on Mars. The topography on Mars shows a large scale asymmetry between the northern lowlands and the southern highlands. Mars exhibits many of the same dune forms as seen on the Earth, including barchan, transverse, yardangs, as well as star and climbing dunes. Many dunes are located in the floors of impact craters where sediment could accumulate. Mars is a very dusty planet. Dust storms on Mars are full of water. In 2018, the largest recorded dust storm circled the entire Martian globe, so thick that it hid the surface from the sun and killed the Opportunity rover. Most of the time the lofting and rearranging of dust is done by the dust devils that spin across the

planetary surface. Dust on Mars is the most important driver of weather. The static electricity from rains rubbing against one another in these dry, sandy whirlwinds could be a problem. "It's possible that all of the dust grains clattering together in these storms could produce a lot of electricity and disable electronics. The electric fields associated with dust devils on Mars are so much drier and dustier than in devils on Earth. Mechanical weathering is the primary mode for the generation of sand-sized particles on Mars, mainly because of the dearth of water under present Martian conditions. Impact craters also provide an intense but much localized means to break up near-surface rocks into smaller constituent pieces. The sand dunes are widespread around Mars, but not in a systematic manner.

A ring of sand called the North Polar Erg (NPE) surrounds the north polar cap on Mars. The dune field on the floor of Proctor crater was the first to be identified on Mars which covers an area approximately 2275 km^2 in area. A variety of dune types have been recognized on Mars over the years, including barchan, barchanoid ridge, transverse, star, linear, dome, and complex dunes. Cater-related permanent wind streaks are observed around some craters on Mars.

8.1. Longevity of Wind Erosion on Mars

Wind erosion and deposition are powerful agents of surface change on Mars. Erosion is sensitive to the atmospheric density, so feedback between orbit variations and atmospheric density can enhance the sensitivity of erosion rates to orbital parameters. Some scientists have used statistics derived from a 1 Gyr (giaga-years = 10^9 years) integration of the spin axis of Mars, coupled with runs of the NASA Ames 3-D general circulation model (GCM) at a variety of orbital conditions and pressures, to explore this feedback. We find that wind erosion in the GCM is associated with two factors: baroclinic zone – a region in which a temperature gradient exists on a constant pressure surface – winds, and strong cross-equator solstice flows. Both of these factors are influenced by topography, producing an asymmetry in the erosion pattern between the north and the south. The erosion model,

averaged over 1 Gyr, produces potential erosion rates of 1.7×10^{-5} myr^{-1} in the north and 1.0×10^{-5} myr^{-1} in the south, which increase by an order of magnitude in an early 28 mbar atmosphere. The stability of these potential erosion patterns over geological time indicates that the lowland regions of Mars are continuously eroded, and that wind is capable of revealing ancient sedimentary deposits, or eroding substantial deposits that may have otherwise been preserved (Armstrong and Leovy, 2005).

Wind erosion and other aeolian formation processes dominate the geology of Mars today. Images from the Mars Global Surveyor (MGS) (Malin and Edgett, 2001) are replete with evidence for wind modification, from current dust storms and recent dust devils, to ubiquitous evidence for dunes and wind streaks.

Wind erosion is an important yet poorly constrained phenomenon on Mars. Evidence of wind erosion exists from Pathfinder images of ventifacts (Bridges, 1999) and orbital images show evidence for long term wind erosion in large, elongated formations known as yardangs (Edgett and Malin, 2000), as well as short term mobilization events such as dust storms and dust devils (Cantor et al, 2001). However, the cumulative effects of this erosion are poorly understood.

The topography on Mars is dominated by the global dichotomy, a large scale asymmetry between the northern lowlands and the southern highlands. The roughly six kilometers elevation difference between the north and the south strongly influences the global circulation of the planet (Richardson and Wilson, 2002) and affects the distribution of surface winds (Fenton and Richardson, 2001). The large elevation differences also cause persistent, dramatic differences in atmospheric pressure between the southern highlands and northern lowlands.

Sagan and Bagnold (1975) were the first to suggest a possible connection between erosion rates on Mars and the variable atmospheric density at the surface. They noted the importance of topography, suggesting that low areas with relatively high atmospheric density, such as Hellas Basin and the northern lowlands,

may be a source of dust injection into the Martian atmosphere. However, the density of the Martian atmosphere also changes over a range of time scales. Viking lander measurements show as much as a 25% change in the atmospheric pressure over the seasonal time scale (Hess et al, 1980). Efforts to model the changes in atmospheric pressure over longer time scales show substantial variation (Fanale and Salvail, 1994), and atmospheric loss models suggest a denser atmosphere in the past (Brain and Jakosky, 1998). Orbital variations impact surface pressure, wind patterns, and the distribution of wind erosion. Studies by Fenton and Richardson (2001) suggest that the overall wind patterns are quite stable with respect to changes in orbital conditions.

However, topographic factors have been shown to have a strong influence on the general circulation (e.g., Gierasch, 2002). Haberle et al. (2003), using a GCM coupled to a model for dust flux induced by saltation, showed that the pattern of potential surface erosion is also stable with respect to orbital variations. They also showed that the spatial distribution of erosion potential calculated by the GCM closely matches the observed distribution of surface thermal inertia, as expected if erosion tends to expose rocky surfaces or bedrock. However, no studies to date have examined the magnitude of the winds as the surface pressure changes. Since changes in surface pressure can result from long term orbital changes (Fanale and Salvail, 1994), as well as potential atmospheric loss (Brain and Jakosky, 1998), in order to examine the long term effects of wind erosion, we need to devise a method for quantifying these changes.

8.2. Aeolian Processes and Features on Mars

Aeolian processes have significantly modified the surfaces of all the terrestrial planets that have appreciable atmospheres, including the Earth, Mars, Venus, and Saturn's moon Titan. For over a century we have had indirect evidence of the importance of aeolian processes on Mars. Historical observations showed that dark features on the Martian surface waxed and waned with the seasons.

Originally this was interpreted to be the result of vegetation undergoing seasonal cycles similar to vegetation in temperate zones on the Earth. With the advent of spacecraft data, however, it became apparent that dusts from global storms, which occur fairly frequently during Southern Hemisphere summer (Kahn et al., 1992), were simply hiding dark albedo markings on the surface. Although there is abundant evidence in the form of valley networks, outflow channels and modified impact craters indicating that the early history of Mars supported rainfall and surface runoff (Craddock and Howard, 2002), aeolian processes have been a persistent geologic agent for the last 3–4 billion years (Carr, 2006), and the evidence for aeolian processes is ubiquitous at all scales from orbital data (e.g. Edgett and Christensen, 1994) to lander images (e.g. Greeley et al, 2004).

Mars exhibits many of the same dune forms as seen on the Earth, including barchan, transverse, yardangs, as well as star and climbing dunes (Bourke, 2010; Chojnacki et al., 2010; Fenton et al., 2005; Zimbelman and Griffin, 2010). Also, perhaps some of the most interesting images returned by the Mars Exploration Rovers show a series of large dust devils advancing across the surface (Greeley et al, 2006). Although not as common, seif and linear dunes have also been recognized (Lee and Thomas, 1995).

Many dunes are located in the floors of impact craters where sediment could accumulate. Perhaps one of the most significant developments to be made recently is the ability to determine sediment provenance and pathways on Mars, which is possible because of the variety of high-resolution images that are available. The High Resolution Stereo Camera (HRSC) with a spatial resolution of 10 m/pixel (Neukum and Jaumann, 2004) and the Mars Context Camera (CTX) with a resolution of *6 m/pixel (Malin et al, 2007) can provide the spatial coverage and resolution necessary to identify and characterize major dune fields along with their potential sources. In addition, the High Resolution Imaging Science Experiment (HiRISE) camera with a spatial scale of 25–32 cm/pixel (McEwen et al., 2007) and the Mars Observer Camera with a resolution of 1.4 m/pixel (Malin

et al., 1991) provide the detail necessary to observe small characteristics of individual dunes. Using these data, Silvestro et al. (2010) were able to were able to analyze the nature of complex dune field patterns located in Aonia Terra (52_S, 292.5_E) in the Thaumasia Quadrangle (MC-25) and determine that there were at least two episodes of dune construction, indicating that the local wind regimes changed over time. They also provided some of the first evidence of distant sediment transport on Mars (tens of kilometers) and identified the source areas as layered materials exposed in pits and crater walls.

High-resolution imagery has also provided some of the first evidence for recent dune movement on Mars. Silvestro and Fenton (2011) have begun a systematic search to identify areas of active sand transport outside of the polar regions (+65_ latitude) beginning with an analysis of dune fields in the Arabia Terra region of Mars. Using HiRISE images they found four sites where active sand transport appears to be occurring. The evidence is subtle, and most of the areas showing changes are less than a few meters in size. However, such observations are important for understanding physical processes on the surface. Results from such efforts will also lead to a better understanding of the current Martian climate and wind regimes.

8.3. Dust Storm

A dust storm or sandstorm is a meteorological phenomenon common in arid and semi-arid regions and arises when a gust front passes or when the wind force exceeds the threshold value where loose sand and dust are removed from the dry surface. Particles are transported by saltation and suspension, causing soil erosion from one place and deposition in another. The Sahara and dry lands around the Arabian Peninsula are the main source of airborne dust, with some contributions from Iran, Pakistan and India into the Arabian Sea, and China's storms deposit dust in the Pacific. It has been argued that recently, poor management of the Earth's drylands, such as neglecting the fallow system, are increasing dust storms from desert margins and

changing both the local and global climate, and also impacting local economies.

The term *sandstorm* is used most often in the context of desert sandstorms, especially in the Sahara, when, in addition to fine particles obscuring visibility, a considerable amount of larger sand particles are blown closer to the surface. The term *dust storm* is more likely to be used when finer particles are blown long distances, especially when the dust storm affects urban areas (Squires, 2007).

8.4. Dust Storms on Mars

In the 1870's astronomers first noted the presence of yellow clouds on the surface of Mars and suggested they were caused by windblown dust. Today, dust storms on Mars are well known and those that display visible structures are called "textured dust storms." Textured dust storms actively lift dust into the atmosphere, and can result from a range of meteorological effects including strong winds. Besides obscuring views of the Martian surface, dust in these storms affects atmospheric heating, and accumulation of dust on the surface can alter the surface albedo (reflectivity). These dust storms, despite being studied for more than a century, remain rather mysterious. It is not understood, for example, how textured storms are distributed over the surface of the planet, when their frequency peaks, or how much dust is actually swept up.

The astronomers found that textured dust storms are seasonally clustered: they occur mostly at the equinoxes (the "spring" and "fall" seasons of Mars) and not the solstices (the "summer" and "winter" seasons). They also occur most frequently in the north-polar region above mid-latitudes. They are able to quantify the relative importance of textured dust storms to dust in the atmosphere, and find that they can account for about half, the rest coming from local "dust devils" or other small-scale disturbances. Not least, they report that the dust in textured dust storms is mixed globally on a timescale of weeks. The new research, which analyzed eight years of spacecraft observations, uses the most complete set of data to date to obtain the most recent

understanding of Martian dust storms (Guzewich et al, 2015).

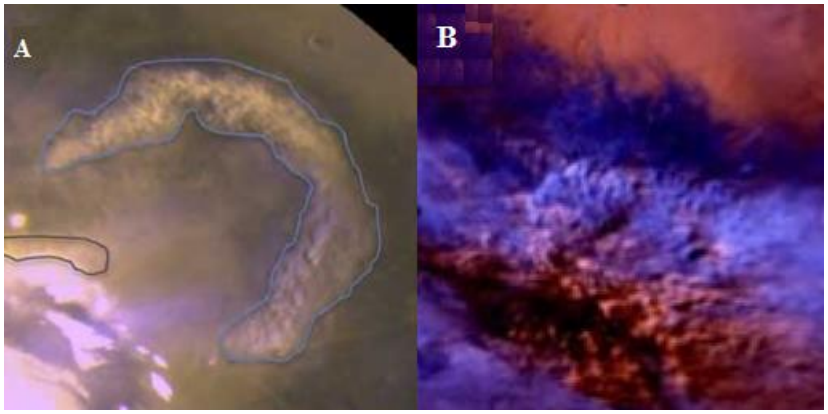

Figure 8.1 An image of a Martian textured dust storm taken with the Mars Global Surveyor (MGS) mission (A). The colored contours indicate the confidence level of the identifications. A new analysis of textured dust storms examines data over eight years of MGS observations and finds that such storms account for about half of all the dust in the Martian atmosphere (Guzewich et al. 2015). An image from the Mars Gobal Surveyor showing a "pebbled"-type dust storm (B). Astronomers have identified three kinds of textured dust storms on Mars, and in a study covering six years found that these textured storms have preferred seasons and locations (Kulowski Laura et al, 2017).

Dust storms on Mars aren't all about dust — they're also full of water. A satellite orbiting Mars has taken the most detailed measurements yet of how these rare events trap water at lower altitudes, which may help reveal what happened to the water that used to be abundant on the Red Planet.

In 2018, the largest recorded dust storm circled the entire Martian globe, so thick that it hid the surface from the sun and killed the Opportunity rover. The ExoMars Trace Gas Orbiter watched this cataclysmic storm from orbit. Just before sunset and just after sunrise on Mars, it examined the atmosphere to determine how the dust storm absorbed sunlight. Ann Carine Vandaele at the Royal Belgian Institute for Space Aeronomy and her colleagues used this data to determine

how water was behaving in the storm. They found that just before the storm, there were water ice clouds in the atmosphere, but no water vapour more than 40 kilometres above the surface. This changed a few days later when water vapour appeared at altitudes of 40 and 80 kilometers, seemingly replacing the water ice clouds.

This probably occurs because the dust absorbs heat, warming up the atmosphere and making it circulate more strongly, which prevents the formation of ice clouds, says Vandaele. The team believes that by observing the dust storms as they form, we may be able to figure out what causes them. Vandaele says "We hope to see something happening right at the beginning of the dust storms that could explain why they happen".

The dust storms puff up the atmosphere, making it easier for gases including water vapour to escape into space, so this could help explain how Mars became so inhospitable. "We are certain that in the past Mars was wetter and warmer, but we have to understand where the water went. Understanding where it goes during atmospheric events now is just the first step (Vandaele et al, 2019).

8.4.1. Dust Bowl

Mars is a very dusty planet. Having spent most of the past few billions of years in an extremely dry and frigid state its rocks just keep on eroding to tiny particles. And with sizes as small as individual talcum powder grains (about 3 microns) and a lower surface gravity than Earth, even the thin Martian atmosphere can loft these particles high into the sky (Guzewich, 2017).

Most of the time the lofting and rearranging of dust is done by the dust devils that spin across the planetary surface. At any given moment on Mars there are an estimated 10,000 or so active dust devils. Imaging data can reveal the tracks left by some of these on the Martian landscape, and barometric data from landers also provides clues to their occurrence rates. During the course of a single Martian day there may be several million of these swirling dervishes – each popping up for a few minutes at a time.

Not only do they maintain a dust load in the atmosphere (where the particles help warm the air and influences global climate), they also rearrange the dust. It's a bit like having a vast army of rather incompetent cleaners, siphoning up dust from one place and simply depositing it somewhere else. Unlike Earth, with a wet biosphere that washes dust from the atmosphere and helps bind rock particles into soil and sediments, dust on Mars is more or less eternal.
Although not fully understood, it also seems likely that the movement of dust grains generates electrical potentials – high enough perhaps for lightning-like discharges, and certainly enough to make the dust extra sticky for any robotic or human exploration.

But dust devils are typically highly localized phenomena. Mars also experiences dust storms on much grander scales. During the southern spring and summer on Mars, coinciding with the closest approach to the Sun in the elliptical Martian orbit, storms are common. At this distance there is 45 percent more solar radiation hitting Mars than at it's farthest from the Sun.

There's a double-barreled driver for these seasonal storms: The atmosphere warms up and winds get stronger, driven by greater contrasts in surface temperature and frozen carbon dioxide on the southern polar cap sublimates, raising the global atmospheric pressure. A thicker atmosphere means a longer hang time for dust particles, and storms can loft material up to over 60 kilometers altitude.

To add insult to planetary injury, it seems possible that dust storms can contribute to the drying out of Mars. Grains can carry water molecules to high enough altitudes that sunlight breaks molecular bonds, hydrogen escapes to space and those water molecules can never reform. Although they're large these seasonal storms generally remain confined to a particular geographical area (e.g., the great Hellas Basin in the south). But about every 3 Martian years (about 5.5 Earth years) they can explode into global events – in other words a roughly one-in-three-probability in a given year. Even though the wind speeds are never shocking by Earth standards, perhaps hitting 60 miles an hour (96 km an hour), the entire planet can become

enshrouded by dust in just days (Viúdez-Moreiras et al, 2019).

Figure 8.2 Massive storm on Mars **(**Guzewich et al, 2017)

8.4.2. Dust Devil

The Red Planet is plagued by devils. It now seems that Mars's surface is teeming with 10 times as many dust devils as we thought. These rotating columns of dust form around low-pressure air pockets and are common on Mars, where they send dust into the atmosphere, controlling the planet's climate. To get a better understanding of the Martian climate, as well as potential risks for future Mars missions, we need to know how many dust devils there are, but the barometers on landers there can't detect all of them.

They are only going to detect the biggest dust devils that have the strongest dips in pressure, and when they do detect them they're going to give you a skewed image of the structure of those dust devils. That's because there's no way to determine if they're sensing pressure changes at the edges or in the middle of a whirlwind.

Sensors can give us a snapshot of a small piece of the environment, but Jackson and his colleagues applied statistical methods to the barometer data to get a better idea of the full story (Brian et al, 2018).

Dust devils on Mars usually whirl across the surface for a few minutes before dissipating. And the team found that on any given day about one 13-metre-wide dust devil pops up per square kilometer of

surface, on average. That's about 10 times as many dust devils as originally thought, and they are also considerably smaller than earlier estimates that put them at 100 meters wide.

Mars's surface area is almost 145 million square kilometers – meaning that millions of dust devils blow across its surface every day. Jackson says if you were standing on the surface, you might be able to see dozens of kilometers-tall dust devils skittering across the ground at any one time.

Dust devils on Mars are whirlwinds that form the same way as dust devils on Earth. But on Mars, their paths can be traced by the dark tracks they leave behind. Some tracks run in roughly straight lines, while others curve, and a few even make curlicues. The track's shape is set by the movement of the dust devil.

The reason the tracks are dark is that a dust devil, as it passes over the ground, sweeps up and blows away the light-toned dust that forms a thin coating on the ground over nearly all of Mars. This exposes the bare ground underneath, which is often dark lava or basalt rock. But while dust devil tracks long outlive the whirlwinds that formed them, they still disappear rapidly on a geological time scale. As days and months pass, dust continues to settle out of the atmosphere onto the surface. After a Mars year or less, most dust devil tracks have disappeared or will do so shortly.

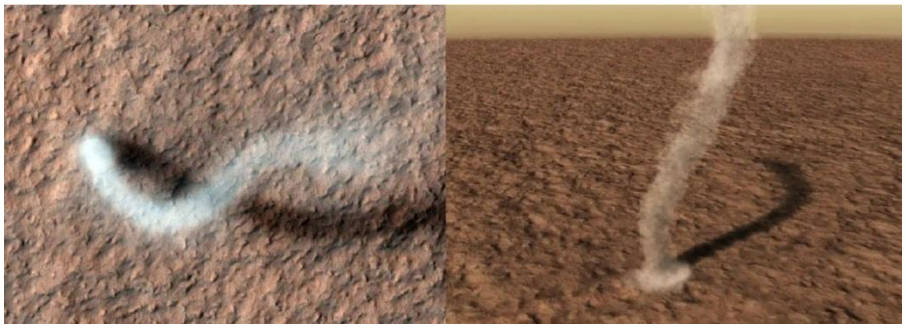

Figure 8.3 Dust devils skittering across the Mars at any one time (Kuepper and Wurm, 2016; Dennis et al, 2017).

"The place is really popping with atmospheric instabilities, especially in the afternoon," when heat from the sun churns the atmosphere, says (NASA's Goddard Space Flight Center in Maryland, William Farrell).

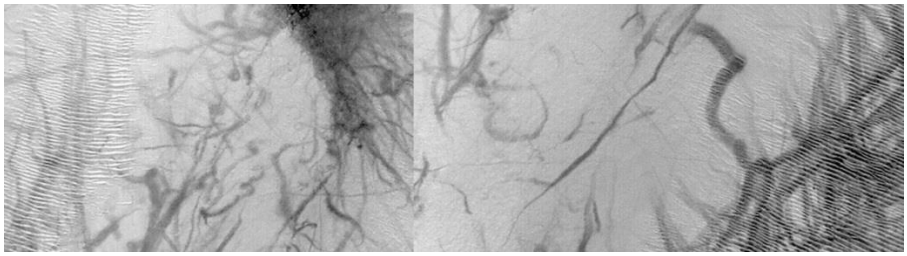

Figure 8.4 Wild looking dark streaks – dust devil tracks – going in all directions fill this images showing part of Argyre impact basin. The passage of dust devil picks up and disturbs the thin coating of dust, exposing the dark surface underneath, Dust devil fade in about a Mars year as more dust falls from the air covers the tracks (NASA/JPT-Caltech /Malin Space Agency Systems; Balme et al, 2003).

8.5. Electric Whirlwind

Dust devils are one of the most important ways that surface dust gets lofted into the atmosphere, where it traps warmth and is a crucial factor in controlling the planet's climate and weather. Dust on Mars kind of fills the role of water on Earth: it's the most important driver of weather. Understanding dust devils could also be important. While the planet's thin atmosphere keeps the high winds from being particularly dangerous since it's not dense with gas particles like Earth's, the dust grains themselves would be hard to keep out of spacesuits, future Mars shelters and just about everything else (Michael et al, 2016).

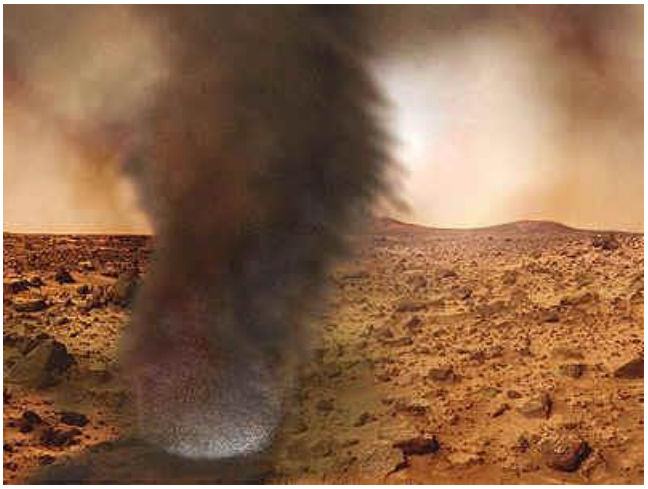

Figure 8.5 Giant columns of whirling dust on Mars add new surprises in planetary exploration. Experts now agree that analogous "dust devils" on Earth contain powerful electric fields (Ferral et al, 2003).

Plus, the static electricity from grains rubbing against one another in these dry, sandy whirlwinds could be a problem. "It's possible that all of the dust grains clattering together in these storms could produce a lot of electricity and disable electronics. The electric fields associated with dust devils on Earth probably aren't strong enough to be dangerous, but Mars is so much drier and dustier (Jackson et al, 2017).

Dust devils form via fluid micro-instability associated with the inversion of a surface-warmed air mass and cooler overlying layers (Renno et al, 1998). Pressure gradients develop in these systems, which force dust grains upward, and in the process act to form coherent convective miniature cyclones. Such dust formations are generated at the air-surface interfaces both on Earth and on Mars. In dust devils, grains in contact with each other and the surface are known to generate and transfer electric charge via frictional or triboelectric processes (Marshall, 1994). There is a tendency to charge-polarize grains based on mass and compositional differences (Desch and Cuzzi, 2000). This mass-based charging preference combined with the mass stratification within the convective devil

leads to a macroscopic, vertically-stratified charge distribution in the devil and consequently the development of a large inter-devil electrostatic potential. Large devil electric fields have been measured at kilovolt per meter strengths in the vicinity and within terrestrial dust devils (Delory et al, 2002) and the charge separation and potential development process has been simulated in Melnik and Parrot (1998).

8.6. Glacier

A glacier is a river of ice. It starts with a field of snow, usually high on a mountain. New snow falls on top, while older snow below is compressed. It becomes denser and recrystallizes as ice. Year-after-year, if winter snowfall is greater than summer melting, the stage is set for the snow field to become a glacier.

When the ice becomes thick enough, it deforms under its own weight and begins to flow downhill as a glacier. Speeds vary depending on conditions, but are typically slow: a meter (yard) or two per day, week, or month. As it flows, the glacier's front plows up rocks, soil, and vegetation (on Earth). At the same time, the bottom of the glacier grinds across the landscape like coarse sandpaper, scouring it with rocks picked up in its path and carried by the ice. Glaciers on Earth vary in thickness along their course, but are usually several hundred meters (yards) thick at least. At the height of the last ice age, the ice sheets (mega-glaciers) in North America were a kilometer (3,300 feet) thick or more.

The flow in a glacier is always downhill and outward. Even when scientists speak of a glacier "retreating," the ice is still continuing to flow forward. What retreats is only the glacier's front or edge, which is melting away faster than the forward-moving ice can resupply. As long as the snow supply is greater than the removal of ice through melting or sublimation, a glacier will advance. But if these forces reach a balance, even temporarily, the front of the glacier will remain in place, but the ice within the glacier will continue to flow. It carries the debris (rocks, sand, gravel, clay) forward and dumps it in a ridge called a moraine at the point where the ice melts.

A few places on Earth (in Antarctica) have temperatures cold enough

that the bottom layers of glaciers are frozen to the ground and do not move. The glacier can still flow, but only in the layers above the lowest ones. Scientists call such glaciers "cold-based," and they expect that the term describes a great many Martian glaciers (Head et al, 2006).

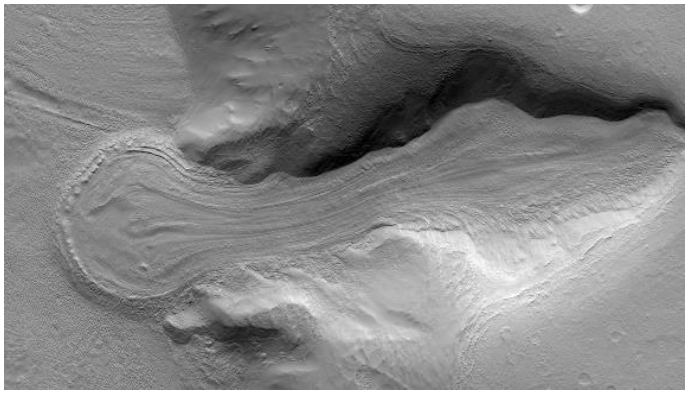

Figure 8.6 A valley glacier on Mars shows many features found on terrestrial glaciers. An accumulation zone lies at left; the ice surface shows flue lines and snout of the glacier shows an end moraine of debris pushed up in front up the glacier. (Head et al, 2006).

Like glaciers on Earth, glaciers on Mars are not pure water ice (Arfstrom, 2005). Many are thought to contain substantial proportions of debris, and a substantial number are probably better described as rock glaciers (Head and Marchant, 2003). For many years, largely because of the modeled instability of water ice in the mid-latitudes where the putative glacial features were concentrated, it was argued that almost all glaciers were rock glaciers on Mars. However, recent direct observations made by the SHARAD radar instrument on the Mars Reconnaissance Orbiter satellite have confirmed that at least some features are relatively pure ice, and thus, true glaciers. Some authors have also made claims that glaciers of solid carbon dioxide have formed on Mars under certain rare conditions (Kreslavsky and Head, 2011).

8.6.1. Moraines

A glacier moving across a landscape is like a giant bulldozer: it knocks down nearly everything in its path. Even big outcrops of

bedrock don't escape being scarred — bedrock is scratched, scraped, rounded, and has pieces of outcrop torn away. Where does all the debris go? When a glacier reaches its limit "where melting overtakes the flow of ice" the piled-up debris is left in what geologists call a moraine. (The name originated in French.) Glaciers can leave several kinds of moraine, but a terminal moraine is one of the most significant. Terminal moraines mark the farthest advance of a glacier or ice sheet. Long Island, New York, is built from two linked ones: the Harbor Hill and Ronkonkoma moraines. Every moraine represents a line on the ground that marks the outer edge of a glacier or ice sheet. Or it marks where a glacier paused as its front edge retreated. On Mars, scientists have identified probable moraines that were left by glaciers that formed on the northwest sides of the four giant Tharsis volcanoes. But these moraines lie on top of delicate landscape features that a moving sheet of ice would totally destroy. What happened? The moraines, scientists think, were left by cold-based glaciers (Arfstrom and Hartmann, 2005). These mountain-born ice sheets covered the ground, but the base of the glacier was frozen firmly to the surface and did not move, thus preserving the underlying landscape. The ice sheet flowed internally and dropped debris carried from upstream at points where the ice front paused or stopped.

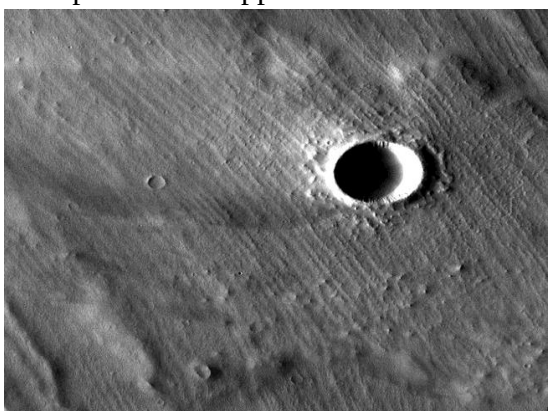

Figure 8.7 Grooved train (interrupted by impact crater) overlies lava flows near the giant shield volcano Asia Mons. The parallel ridges may be moraines, deposits of sands and rocks left by a cold-base-glacier on the side of the volcano (NASA/JPT-Caltech / Arizona State University; Arfstrom and Hartmann, 2005).

8.7. Sediments on Mars

Mechanical weathering is the primary mode for the generation of sand-sized particles on Mars, mainly because of the dearth of water under present Martian conditions. The large temperature swings experienced daily and seasonally will act (albeit slowly) to break apart rocks exposed at the surface, perhaps enhanced by intermittent films of water molecules when conditions allow localized condensation of the trace amount of water vapor present in the atmosphere.

Impact craters also provide an intense but much localized means to break up near-surface rocks into smaller constituent pieces. Still, when billions of years are available to carry out the mechanical weathering, it is not surprising that collections of sand-sized material can be found across much of Mars. When winds of sufficient intensity occur, the sand-sized material eventually tends to concentrate into protodunes or dune fields, usually within topographic depressions that act to trap the particles. The Viking, Pathfinder, and Phoenix landers, along with both MERs, all returned evidence of fine-grained material wherever these explorers looked, although only the last three spacecraft carried cameras that could resolve sand from the silt to clay-sized dust particles that settle ubiquitously out of the Martian atmosphere. The two rovers have documented particles ranging from dust and sand to granules and cobbles everywhere along the tens of kilometers of the surface over which they have ranged.

Sophisticated remote sensing instruments on both landed and orbiting spacecraft have revealed much about the fine particles present on the Martian surface. Measurements of the thermal infrared energy radiated from the surface provide important clues to the physical size of the constituent surface materials. As discussed before, thermal inertia refers to how well (or how poorly) the surface maintains its temperature through the course of a Martian day. Materials with high thermal inertia (large blocks and rock outcrops) tend to stay relatively cool through the day and warm through the night, in contrast to low thermal inertia materials (such as a thick dust mantle). When multiple

thermal wavelengths are measured, the distribution of high or low thermal inertia materials within a single pixel can be quantified, even when the individual particles are not resolved.

The thermal inertia of windblown deposits within impact craters on Mars indicates that these deposits respond to temperature changes as if they were comprised of a uniform layer of coarse sand (400–600 lm in diameter), which is larger than the fine sand that makes up most of the dunes on Earth (100–200 lm in diameter). Spectroscopic measurements of the dark deposits in craters also revealed that they consist primarily of a basaltic composition, some showing evidence of minerals called pyroxenes, which are common in basalt rocks. The Opportunity rover was able to investigate a dark sand deposit (named 'El Dorado') in the Columbia Hills, confirming the basaltic composition of the medium-to-coarse sand found there (discussed in more detail below). Both rovers have also obtained evidence of localized deposits of sand-sized aggregates that, when pressed upon by the rover arm, break up into dust; such aggregates may be similar to 'parna' on Earth, where sand-sized aggregates of clay particles form dunes around dried lakebeds. Aggregates on Mars likely could not survive the saltation required for transport over long distances, but they do appear to contribute to localized collections of sand-sized materials.

The observed distribution of sand dunes is widespread around Mars, but not in a uniform or systematic manner. By far the largest accumulation of sand dunes occurs in the sand sea that surrounds the North Pole within the 70–80 –N latitude band. Portions of the north polar erg were recently shown to include the spectral signature of the mineral gypsum, a material common around the margin of some saline lakes, leading to speculation that the dune field could incorporate materials derived from ancient lakebed deposits.

Outside of the north polar erg, more than 900 sand dune patches larger than 1 km^2 have been mapped across the rest of Mars, with the resulting collection of dune forms displaying a considerable diversity across the planet (Hayward et al, 2007). No obvious sources are

recognized for the identified dune deposits, although the north polar sand may be derived from a specific dark basal unit within the polar layered deposits. Dunes within craters appear to be trapped within the topographic depression rather than derived from a localized source exposed within the crater rims. Mars also lacks obvious sinks for mobile sand; the lack of current oceans makes it difficult to remove sand from the system except through burial inside impact craters that became buried by some later event.

8.8. Saltation on Mars

Saltation, the motion of sand grains in a sequence of ballistic trajectories close to the ground, is a major factor for surface erosion, dune formation, and triggering of dust storms on Mars. Although this mode of sand transport has been matter of research for decades through both simulations and wind tunnel experiments under Earth and Mars conditions, it has not been possible to provide accurate measurements of particle trajectories in fully developed turbulent flow. Here we calculate the motion of saltating grains by directly solving the turbulent wind field and its interaction with the particles. The calculations show that the minimal wind velocity required to sustain saltation on Mars may be surprisingly lower than the aerodynamic minimal threshold measurable in wind tunnels. Indeed, Mars grains saltate in 100 times higher and longer trajectories and reach 5-10 times higher velocities than Earth grains do. On the basis of our results, we arrive at general expressions that can be applied to calculate the length and height of saltation trajectories and the flux of grains in saltation under various physical conditions, when the wind velocity is close to the minimal threshold for saltation (Almeida et al, 2008).

8.9. Dunes

Dunes are familiar features on Earth and they also occur on Mars, Venus, and Saturn's moon, Titan. What all these bodies have in common is an atmosphere, plus substantial amounts of loose sand-size

particles. Of all the extraterrestrial dunes scientists know about, those on Mars are the most closely studied.

A dune is a heap of sand piled up and shaped by the wind. (Underwater dunes exist on Earth, but we can ignore these in regard to today's Mars.) The word "dune" implies a substantial size — at least several meters high. But small ripples of sand only a few centimeters (inches) high are made in the same way from the same materials. The difference lies mainly in the supply of particles and how much time the wind has had to work on them.

Sand grains range in size from 0.0625 mm to 2 mm. Sand forms when the wind picks up small particles of rock and flings them against other rocks and outcrops, chipping away small, sharp-edged bits. The wind grinds these pieces against each other, making them smaller and rounder through abrasion.

Stand barelegged on a beach on a day with strong winds. The sting of flying sand shows you the power of windblown particles, which can break down even the toughest rocks given enough time. The process never quits as long as the wind is blowing. Sand's mineral composition depends on its parent rocks. On Earth, where granitic rocks are common, most sand is quartz, or silicon dioxide (SiO_2). On Mars scientists still have much to learn about Martian sands and their compositions.

The most common rock on Mars is volcanic basalt, a dark rock, so sand particles made from it will appear dark. (Some beaches on Earth are made of dark volcanic sand.) Yet many Mars dunes are not dark in tone. Scientists interpret this to mean that light-tone dust has fallen from the atmosphere to cover the dunes. A dust coating suggests that the dune sand is not moving or active. In contrast, a line of dunes lying between where Mars rover Curiosity landed and Mt. Sharp appears dark in tone. A series of high-resolution images have shown scientists that sand ripples on the dunes are moving southwest as local winds blow from the northeast.

On Earth, dunes form in numerous characteristic shapes, many also occurring on Mars. The main Martian dune types are mega-ripples,

parabolic or barchan (bar-kan), transverse, and star. As wind blows sand, the grains slide, hop (saltate), and bounce across the surface. If sand grains are plentiful, they begin to collect in small mounds and drifts, creating dunes. A dune typically has a gentle slope (5° to 15°) leading up to a ridge or crest, then a steeper (30° to 35°) slope downward. The gentle rise is called the stoss or windward face, while over the crest lies the slip face or lee face.

With a steady wind blowing from one direction, a dune migrates downwind. Sand grains bounce up the stoss slope, cross the crest, and avalanche down on the slip face. As more grains arrive on the slip face they bury the earlier-arriving ones. Slowly, the dune crest moves downwind, and eventually the first grains emerge on the windward face once more. They get picked up and blown over the crest and onto the slip face again, and the process repeats endlessly.

This simplified picture has many variations. Dune shapes vary according to sand supply, the ground they move across, and wind directions. For example, winds that blow in two opposite directions (from day to day, or throughout the year) create sharp-crested dunes with roughly equal slopes on either side of the crest. Star dunes, which show several crest lines that meet, form wherever winds blow from several directions about equally.

Moreover, dunes do not remain fixed in type. Barchan dunes, for instance, can merge into barchanoid ridges, or the "horn" on one side of a barchan may grow steadily longer until it becomes a transverse dune. And so on. As you study dunes, remember that every dune is the result of constructive forces and destructive ones. One force breaks rocks down into grains, and another force pushes the grains together to build dunes. This cycle of building up, tearing down, and building again is a fundamental process in all geology and earth science. Whenever you look at a landscape, either an image or in real life, try to figure out what's being built and what's being destroyed in what you see.

8.10. Dune Locations

The Thermal Emission Imaging System (THEMIS) on the Mars Odyssey spacecraft has provided a uniform image base with global coverage and adequate resolution to evaluate dune morphology. Thus the global inventory of dunes could be systematically mapped (Fig. 8.9), starting with the equatorial and mid-latitudes (65 S to 65 N; Hayward et al, 2007), followed by both the north (Hayward et al. 2010) and south polar regions (Hayward et al. 2012). This mapping effort identified dune fields down to a size of *1 km^2; nearly 900 locations correspond to dune fields within impact craters of various sizes, and the North Polar Erg(NPE) is the only place where sand is abundant on a regional scale.

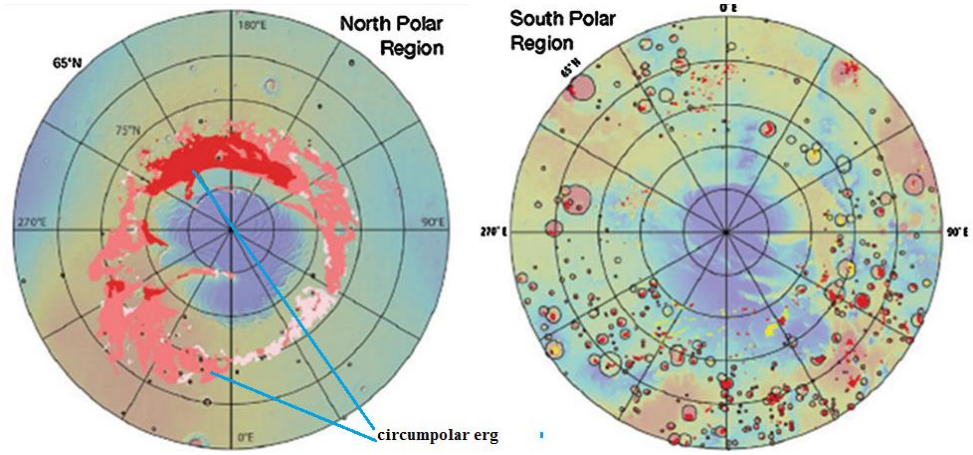

Figure 8.9 A map of dune fields on Mars assembled by the Mars Dune Consortium. Apart from the circumpolar erg in the north, most of the major dune fields are in craters (credit Hayward et al, 2010).

8.10.1. North Polar Erg

A ring of sand called the North Polar Erg (NPE) surrounds the north polar cap on Mars, the one area on the planet that approaches the scale of sand seas (ergs) on Earth. The International Astronomical Union (IAU) has established guidelines for the nomenclature of features identified on all mapped planetary surfaces.

The Compact Reconnaissance Imaging Spectrometer for Mars

(CRISM) instrument revealed that gypsum is a significant component of the Olympia Undae polar sands (Horgan et al. 2009).

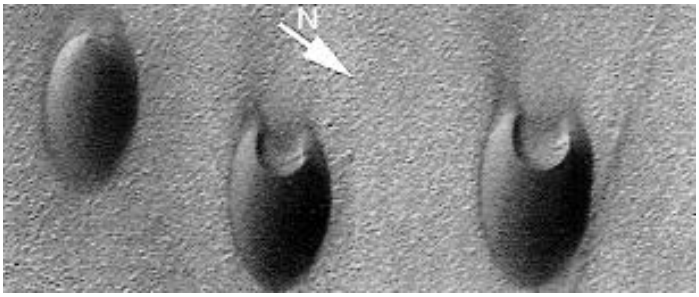

Figure 8.10 Dunes near the North Pole showing a "rectilinear" pattern (after Ryan Anderson, 2009).

Imaging from the High Resolution Imaging Science Experiment (HiRISE) camera allows the dune sands to be traced back to eroded exposures of a thick bed within the basal component of the polar layered deposits, which would indicate that the origin of polar sand likely preceded the emplacement of the thick sequence of polar layered deposits (Fishbaugh and Head, 2005). The NPE sand deposits can now be placed in context with other bedrock materials exposed throughout the north polar region (Tanaka and Fortezzo, 2012), but this provides no additional insight into where the sand may have originated prior to its involvement in the deposition of the polar layered deposits.

8.10.2. Proctor Crater

Proctor crater is 150 km in diameter, located in the southern cratered highlands to the west of the giant Hellas impact basin. The dune field on the floor of this crater was the first to be identified on Mars from Mariner 9 images; the field covers an area approximately 35 by 65 km in area, and the dune field has been targeted often by subsequent orbiters. The resolution of the Mariner 9 image is not sufficient to allow potential long term movement of the dunes to be detected; comparison of a higher-resolution image obtained in 1999 by the Mars Orbiter Camera (MOC) on the Mars Global Surveyor spacecraft to the

Mariner 9 image showed that any movement must have been less than the size of a Mariner pixel (62 m/pixel) during the 14 Mars years (28 Earth years) that elapsed between the two images. On-going study of the Proctor dune field, notably with the HiRISE camera has yielded many insights into the emplacement

8.10.3. Kaiser Crater

Kaiser crater is 210 km in diameter and is located in the southern cratered highlands to the west of Proctor crater. The dune field present on the crater floor was imaged late in the mission of Viking Orbiter 2, showing dune crests that are likely transverse to the winds that transported the sand into the crater.

Much later, the Mars Orbiter Camera (MOC) on the Mars Global Surveyor spacecraft provided higher-resolution images of individual barchan sand dunes near the main dune field, probably the result of sand that has escaped from the margin of the main dune field. The Hi-RISE camera obtained a stereo image pair from which very detailed elevation information is obtained for an individual dune in the Kaiser crater. This dune showed avalanche features on its slip face in MOC image R06- 00380, so HiRISE stereo data were collected to investigate the relief associated with avalanche modification of dune slip faces on Mars, in an effort to assess what mechanisms may have produced the avalanching of the sand.

8.10.4. Lyot Crater

Lyot crater is 240 km in diameter, located in the northern lowland plains of Vastitas Borealis. Lyot has the largest crater dune field found within the northern lowland plains of Mars. The Lyot dune field has been monitored regularly by orbiting cameras to see whether there are distinguishable variations in how dunes in the northern hemisphere change with time, as compared to the more numerous dune fields in the southern hemisphere, but so far the dunes in Lyot do not display unique characteristics.

8.10.5. Herschel Basin

Herschel is a 300 km diameter impact basin in the equatorial portion of the cratered southern highlands. MOC images of the dune field in Herschel showed a 'grooved' texture that was interpreted to suggest that the sand was moderately indurated and subject to erosion aeolian scour. However, recently the Herschel dune field has shown 1 m of movement between two HiRISE images taken on March 3, 2007 and 1 December, 2010, and the grooved appearance is resolved to be a confluence of aeolian ripples on the dune surface, so that induration of the sand is no longer required. This is merely one example of several locations where HiRISE repeat imaging is now documenting the planet-wide movement of sand under current climatic conditions (Bridges et al, 2012b).

8.10.6. Rabe Crater

Rabe crater is 108 km in diameter, and is located in the southern cratered highlands in what used to be called the Hellespontes region, the same general area where both Proctor and Kaiser Craters are located. Monitoring of the Rabe dune field using MGS/MO data was unable to document any observable dune movement, leading to an estimate for the local sand migration rate here of only 1–2 cm per Mars year (Fenton 2006a). The combination of THEMIS infrared and visible data provided interesting insights into the physical properties of this dune field.

Color represents the nighttime temperatures, where blue is relatively cold and red is warm, corresponding to dusty and rocky exposures, respectively. The crests of the 150–200 m tall dunes are consistently warmer (by ~6 ^{o}C) than the adjacent troughs between the dunes, suggesting that wind has swept most of the dust from the crest areas. Also, the red (rocky) areas are exposed layered material that may have provided a local source for at least some of the sand-sized materials.

8.10.7. Richardson Crater

Richardson crater is 55 km in diameter, and is located in the polar

region of the southern cratered highlands. The dunes in this crater have received considerable attention from multiple spacecraft camera teams because they show distinctive 'spotted' patterns as the seasonal cap of carbon dioxide frost vaporizes from the sand surface during southern spring.

The defrosted 'spots' may expose sand that could then be blown or avalanched onto adjacent frost-covered areas, which in turn would enhance the removal of the frost from these areas.

8.10.8. Nili Patera

Instead of occurring within an impact crater, this dune field (CRISM image) is located within the broad caldera present at the summit of the shallow-sloped Nili Patera volcano. The barchan dunes of Nili Patera were the first place to provide documented evidence of ripple and dune movement on Mars of at least a meter, using repeat HiRISE images (Silvestro et al, 2010a). The rippled surfaces of the barchans and barchanoid ridges in the Nili Patera region have continued to be monitored with HiRISE as part of the continuing effort to document dune and ripple movement occurring today across the entire planet (Bridges et al, 2012a), as well as the first place on Mars to apply the sophisticated COSI-Corr software which was designed to Rippled (not deeply eroded, as had been thought from lower-resolution MOC images) dunes on the floor of Herschel crater. HiRISE PSP_002860_1650. NASA/JPL/ U of A. Inset, portion of browse image. Documented 1 m movement in the Herschel dune field, which occurred between two HiRISE images taken 1.5 Mars years apart. Remarkably, given the non-detection of movement on Mars over the Mariner 9 to Mars Odyssey period of some 35 years, these latest results indicate that sand movement rates on Mars today are comparable to documented rates obtained in some places on Earth.

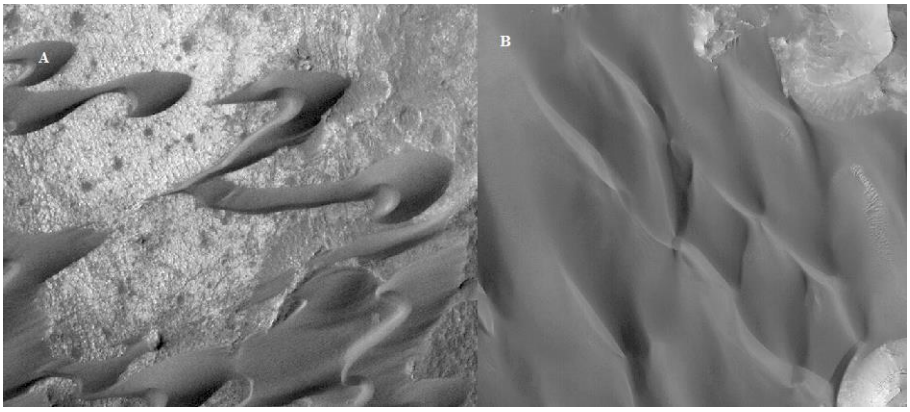

Figure 8.11 A field of sand dunes in the Nili Patera region toward the lower left, as indicated by duns's shape, which scientists call a Barchan (A). The dunes dark tons also that the sand is free of dust, therefore the dunes are actively moving. (B) The steepest slops on each dune faced toward the bottom / lower left of the image. This indicates that the dominants winds came from the north (top of the image). (NASA/JPT-Caltech /Malin Space Agency Systems).

8.10.9. Gale Crater

Gale crater is 154 km in diameter, and is located at the transition from the southern cratered highlands to the northern lowland plains, south of the Elysium Mons volcanic center. A massive mound of material covers the central peak of the crater, rising 5.5 km above the level of the crater floor; layered clay-rich materials near the base of the central uplift (Fig. 12.22) are the primary target for the Curiosity rover, The central mound in Gale crater is surrounded by an arc of dark sand dunes (orbital imaging of dune field reveals a rather complex wind flow pattern on the crater floor, likely strongly influenced both by the crater rim and the high central mound (Silvestro et al, 2013).

Figure 8.12 Curiosity Mastcam panorama of the floor of Gale crater, showing layered mounds in Mount Sharp (aka Aeolus Mons) with dark dunes in the foreground (after Lorenz and Zimbelman, 2014).

8.10.10. Victoria Crater

Victoria crater is substantially larger than Endurance crater, and thus the ripple field on its floor is correspondingly larger as well. Opportunity drove around roughly one-quarter of the rim of the crater, searching for the best path to gain access into it. During this drive, Opportunity crossed the surface of a broad dark wind streak that emanates from the northern side of the crater becoming the first rover to investigate a wind streak on Mars.

8.10.11. Endeavour Crater

Several separate dune patches are present on the floor of this broad crater, some of which are visible in distant views from Opportunity, but orbiter imaging provides the best viewing option thus far. The dunes in Endeavour crater have been documented to move at a rate that is substantially greater than what has been observed in HiRISE images from elsewhere on the planet (Chojnacki et al, 2011).

8.10.12. El Dorado, Gusev Crater

The only large patch of low albedo (dark) sand visited so far by a rover is

the site called ‘El Dorado’, on the northern side of Husband Hill, the largest of the Columbia Hills within Gusev crater. During its descent from the summit of Husband Hill, Spirit drove well into the margin of the El Dorado sand deposit (Fig. 8.13).

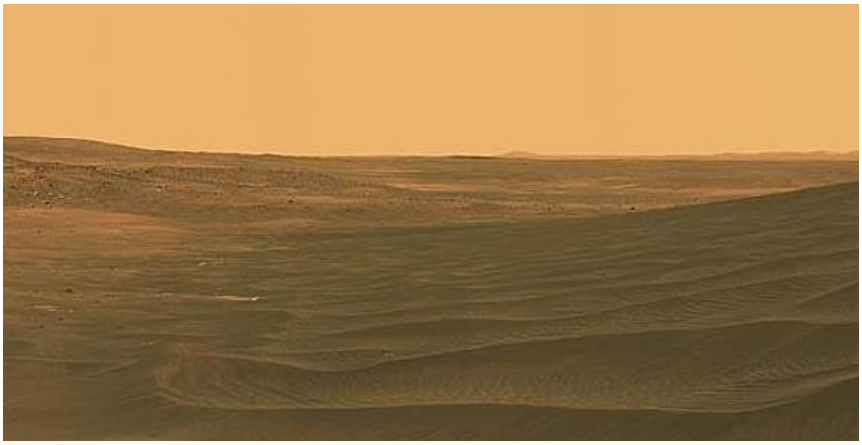

Figure 8.13 a portion of Pan Cam mosaic of El Dorado dunes, with Gusev crater rim visible in the background. Note the local slope. Image: NASA/JPL

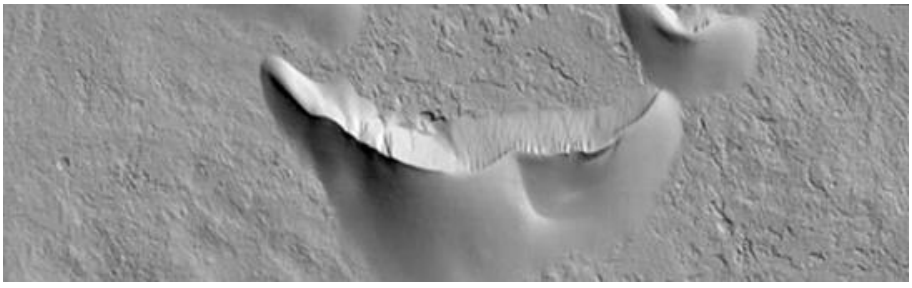

Figure 8.14 A barchan dune on the floor of Kaiser Crater. The elevation data were collected to investigate avalanche features on the slip face of the dune. The scale of this rather conventional-looking barchan is much larger than corresponding examples on Earth—the crest to the floor at the base of the slipface is a drop of some 300 m, over a magnitude larger than is typical for Earth barchans of the same shape. Image credit NASA/JPL/U of A/USGS, (after Ralph and Zimbelman, 2014).

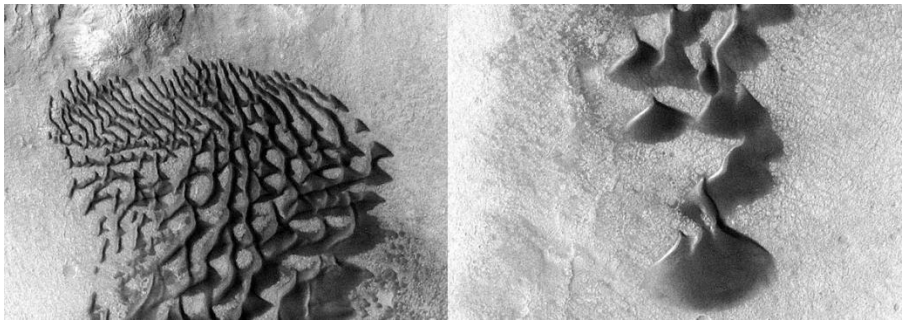

Figure 8.15 Interesting gradation between linear forms and 'teardrop' barchans across the floor of Bunge Crater in response to winds blowing from the direction at the top of the picture. The frame is about 14 kilometers wide. Mars Odyssey THEMIS. Image PIA13654, (after Ralph and Zimbelman, 2014)

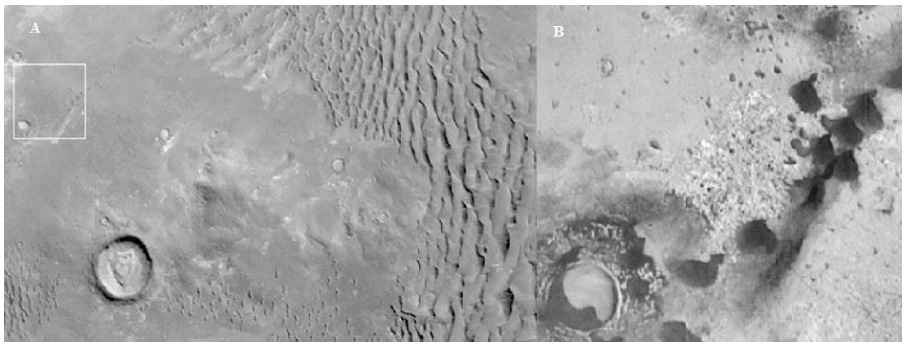

Figure 8.16 (A) Viking Orbiter 2 image (575B60) of the floor of Kaiser crater, acquired in 1978 with a resolution of about 50 m per pixel. North is up, illumination is from the top right. To the right are large transverse ridges, while towards the bottom a flock of small barchans can be seen migrating towards the left. A few small barchans can just be made out in the box in upper left; an area imaged 20 years later by the Mars Orbiter Camera (MOC) on Mars Global Surveyor, Image NASA/MSSS (B). (after Ralph and Zimbelman, 2014).

8.11. Types of Dunes

A variety of dune types have been recognized on Mars over the years, including barchan, barchanoid ridge, transverse, star, linear, dome, and complex dunes (the last displaying attributes of two or more dune

types). Notably, almost one-third of the dune fields identified in a global map of sand dunes on Mars do not seem to fit easily into one of the dune categories used to describe dunes on Earth (Hayward et al. 2007, 2010, 2012). The formation mechanism for Martian dunes is thought to be essentially the same as the recognized aeolian processes that generate similar dune forms on Earth.

However, Martian dunes tend to be up to an order of magnitude larger than their comparable terrestrial counterparts, similar to the large size displayed by many other Martian landforms. Here we will not necessarily discuss in detail each of the Martian dune types, but rather present examples of the more common types for comparison with dunes on the other planets.

Barchans are one of the most readily identifiable dune types on any planet, due to the distinctive crescentic shape of the entire dune mass. Barchans and barchanoid ridges are quite common near the margins of the NPE, particularly where the sand supply from the erg becomes more widely distributed as the sand spreads onto the surrounding plains. Barchans are also found at lower latitudes where the supply of sand is relatively limited, but still sufficient to produce large and impressive crescent-shaped sand deposits.

One of the most common dune types on Mars is the transverse ridge, comprised of one prominent crest line that is inferred to be transverse to the orientation of the wind that blew the sand to its present location. Martian transverse features are often quite symmetric with respect to the crest axis, making it difficult to decide from which of the two transverse directions the driving winds blew, but also suggestive that two nearly equal but opposite wind patterns may be present, perhaps driven by diurnal temperature and pressure variations, especially where winds are likely to be confined in valleys. For transverse features with wavelengths less than 100 m, the non-generic term ‘transverse aeolian ridge’ (TAR) has been applied, allowing for the smallest TARs to possibly be either small sand dunes or large ripples.

Invariably, where TARs and dunes co-exist, the dunes are usually

dark and the TARs bright, and the dunes are superposed on the TARs showing that they have been active more recently has yielded many insights into the emplacement and modification of dune fields within craters on Mars (Fenton 2006a).

Figure 8.17 Ripples covered by dark dunes on Mars, NASA / JPL-Caltech / University of Arizona.

8.11.1 Wind Streaks

Cater-related permanent wind streaks are observed around some craters on Mars. Such wind streaks are different from the “typical” wind streaks that commonly occur on Mars. Traditional wind streaks can be light or dark features, but they are non-permanent features that can change length and orientation over time. Additionally, traditional wind streaks are often considered to be depositional features based on their appearance and thermal properties. Conversely, crater-related permanent wind streaks do not change length or orientation over time. Hence, these streaks are proposed to be formed by impact-generated winds.

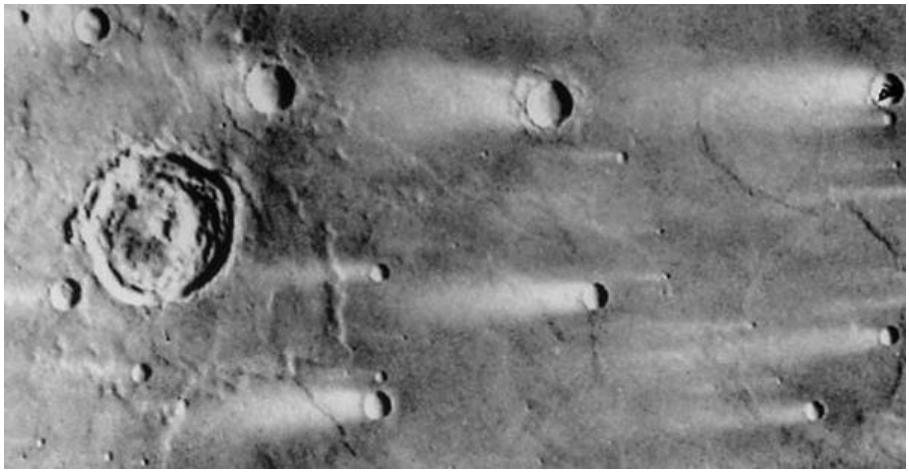

Figure 8.18 The bright streaks in this image indicate the direction of the prevailing winds (from east to west). These streaks are formed by the collection of windblown material in the lee of a crater. Most bright streaks maintain relatively constant direction and albedo over periods of many years, although subtle changes were noticed in some streak orientations in the five to seven years between the Mariner 9 and Viking encounters. The crater near the top of the image displays a prominent central pit that may be an indicator of subsurface volatiles.

Crater-related permanent wind streaks, known as "blast-wind" streaks, are nearly invisible unless imaged in the nighttime thermal infrared. At these wavelengths at night, the blast-wind streaks appear bright, and radiate away from a central crater. Existing topography, such as preexisting craters, leads to double wind streak tails, indicative of scouring by strong, sustained winds and vortices (Quintana and Schultz, 2014).

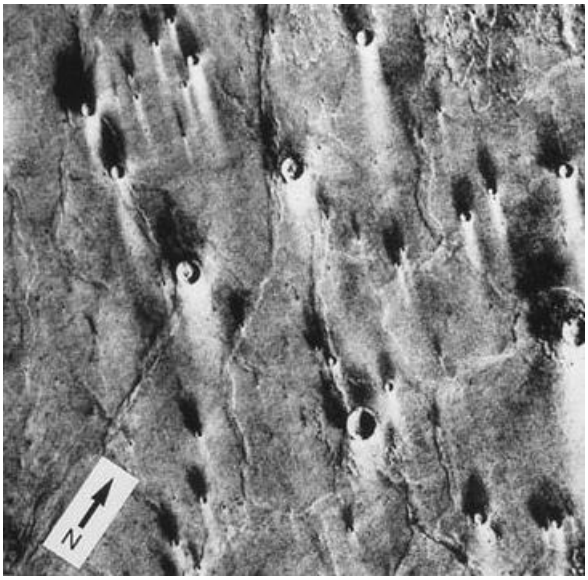

Figure 8.19 Bright and dark wind streaks are simultaneously present around craters on Mars. These presumably formed during different wind regimes and are the result of the differential vulnerability of dark basaltic sand and bright dust to wind erosion or deposition. Image is located at 28° S, 245° W in Hesperia Planum (Melosh, 2011).

References

Almeida Murilo P., Eric J. R. Parteli, Jose´ S. Andrade, Herrmann H.J. (2008) Giant saltation on Mars, in Proceedings of the National Academy of Sciences 105(17):6222-6. DOI: 10.1073/pnas.0800202105 · Source: PubMed

Arfstrom J., (2005) Terrestrial analogs and interrelationships. Icarus, 174: 321–335. doi:10.1016/j.icarus.2004.05.026.

Arfstrom J., Hartmann W. (2005) "Martian flow features, moraine-like ridges, and gullies; Terrestrial analogs and interrelationships". Icarus, 174 (2): 321–335.
doi:10.1016/j.icarus.2004.05.026

Armstrong J.C., Leovy Conway B. (2005) Long term wind erosion on Mars. Icarus 176:57–74.

Balme M.R., Whelley P.L., Ronal G. (2003) Mars: Dust devil track survey in Argyre Planitia and Hellas Basin. Journal of geophysical research, 108(8): E8, 5086, doi: 10.1029/2003JE002096, 2003

Bourke M.C. (2010) Barchan dune asymmetry: observations from Mars and Earth. Icarus, 205(1): 183–197.

Brian j., Ralph L., Karan D. (2018) A framework for relating the structures and recovery statistics in pressure time-series surveys for dust devils. Icarus 2018, 166-174. doi. 10.1016/j.icarus.2017.07.027

Brain D.A., Jakosky B.M. (1998). Atmospheric loss since the onset of the martian geologic record: combined role of impact erosion and sputtering. J. Geophys. Res., 103: 22689–22694.

Bridges, N.T., (1999) Ventifacts on Mars. In: The Fifth International Conference on Mars, July 19–24, 1999, Pasadena, California.

Abstract 6152.

Bridges N.T., Bourke M.C., Geissler P.E., et al, (2012a). Planet wide sand motion on Mars. Geology 40, 31-34, doi: 10.1130/ G32373.1

Cantor B.A., James P.B., Caplinger M., Wolff M.J. (2001) Martian dust storms: 1999 Mars Orbiter Camera observations. J. Geophys. Res., 106: 23653–23688.

Chojnacki M., Moersch J.E., Burr D.M. (2010) Climbing and falling dunes in Valles Marineris Mars. Geophysical Research Letters 37: L08201.

Chojnacki M., Burr D.M., Moersch J.E., Michaels T.I. (2011) Orbital observations of contemporary dune activity in Endeavour crater, Meridiani Planum, Mars. Journal of Geophysical Research 116: E00F19.

Craddock R.A., Howard A.D. (2002). The case for rainfall on a warm wet early Mars. Journal of Geophysical Research – Planets 107(E11): 5111.

Dennis R., Ralph D.L., Matthew B., Lynn D.N., Angelo P. R., Aymeric S., John Z. (2017) Special Issue on Dust Devils. Space Sciences Series of ISSI, 5: Page 1-4. doi: 10.1007/978-94-024-1134-8_1

Desch S. J., and Cuzzi J. N. (2000) The generation of lightning in the solar nebula. Icarus, 143: 87.

Edgett K.S., Malin M.C., (2000) New views of Mars eolian activity, materials, and surface properties: three vignettes from the Mars Global Surveyor Mars Orbiter Camera. J. Geophys. Res., 105: 1623–1650.

Fenton, L.K., Richardson, M.I., 2001. Martian surface winds: insensitivity to orbital changes and implications for aeolian processes. J. Geophys. Res. 106, 32885–32902.

Fenton L.K., Toigo A.D., Richardson M.I. (2005) Aeolian processes in Proctor Crater on Mars: Mesoscale modeling of dune-forming winds. Journal of Geophysical Research – Planets 110: E06005.

Ferral W.M., Dellory G.T., Cummer S.A., Marshall J.R. (2003). A simple electrodynamic model of a dust devil, Geophysical research letters, vol. 30, no. 20, 2050, doi: 10.1029/2003GL017606

Fishbaugh K, Head J.W. (2005) Origin and characteristics of the Mars north polar basal unit and implications for polar geologic history. Icarus 174, 444-474.

Gierasch P. (2002) Planetary science the north–south martian divide. Nature, 416: 269–270.

Greeley R., Whelley P.L., Arvidson R.E., Cabrol N.A., Foley D.J., Franklin B.J., et al. (2006) Active dust devils in Gusev crater Mars: Observations from the Mars Exploration Rover Spirit. Journal of Geophysical Research 111: E12S09.

Greeley R., Squyres S.W., Arvidson R.E., Bartlett P., Bell J.F., Blaney D, et al. (2004) Wind-related processes detected by the Spirit Rover at Gusev Crater Mars. Science 305(5685): 810–813.

Guzewich S.D, Anthony D.T., Laura K., HuiqunWang H. 2015. Mars Orbiter Camera climatology of textured dust storms. Icarus, 258:1-13.

Guzewich S.D., Newman C.E., Smith M. D., et al. 2017. "The Vertical Dust Profile Over Gale Crater, Mars." Journal of Geophysical Research: Planets, **122:** doi: 10.1002/2017je005420

Haberle R.M., Murphy J.R., Schaeffer J. (2003) Orbital change experiments with a Mars general circulation model. Icarus, 161: 66–89.

Hayward, R.K., Mullins, K.F., Fenton, L.K., et al. 2007. Mars Global Digital Dune Database and initial science results. Journal of Geophysical Research 112, E11007, doi:10.1029/2007JE002943.

Hayward, R.K. Titus, T.N., Michaels, T., Fenton, L., Colaprete, A. Christensen P.R. (2009) Aeolian dunes as ground truth for atmospheric modeling on Mars. Journal of Geophysical Research 114(E11), Cite ID E11012.

Hayward, R.K, Fenton, L.K., Tanaka, K.L., Titus, T.N., Colaprete, A. and Christensen, P.R. 2010. Mars Global Digital Dune Database: MC1. U.S. Geological Survey Open-File Report, 2010–1170.

Hayward R.K., Fenton, L.K., Titus T.N., Colaprete A., Christensen P.R. (2012) Mars global digital dune database: MC-30: U.S. Geological Survey Open-File Report 2012–1259.

Head J.W., Marchant David R. (2003). "Cold-based mountain glaciers on Mars: western Arsia Mons". Geology. 31 (7): 641–644. doi:10.1130/00917613(2003)031

Head J.W., et al. (2006). "Extensive valley glacier deposits in the northern mid-latitudes of Mars: Evidence for Late Amazonian obliquity-driven climate change". Earth and Planetary Science Letters, 241 (3): 663–671. doi:10.1016/j.epsl.2005.11.016

Horgan B.H., Bell J.F., Noe Dobrea E.Z., Cloutis E.A., Bailey D.T., Craig M.A., Roach L.H., Mustard, J.F. 2009. Distribution of

hydrated minerals in the north polar region of Mars. Journal of Geophysical Research, 114(E1), Cite ID E01005.

Jackson B., Lorenz R., Davis K. (2017) Earth and Planetary Astrophysics (astro-ph. EP). doi: 10.1016/j.icarus.2017.07.027

Kahn R.A., Martin T.Z., Zurek R.W., Lee S.W. (1992) The Martian dust cycle. In: Kieffer H.H., Jakosky B.M., Snyder C.W., Matthews M.S. (eds) Mars. Tucson, AZ: University of Arizona Press, 1017–1053.

Kreslavsky M.A., Head J.W. (2011) Carbon dioxide glaciers on Mars: Products of recent low obliquity epochs. Icarus, 216 (1): 111–115. doi:10.1016/j.icarus.2011.08

Kuepper M., Wurm G., (2016) Application of dust loading in Martian dust devils by self-shadowing. Icarus, 274 (org/10.1016/j.icarus.2016.02.049

Kulowski Laura et al (2017) The seasonal and spatial distribution of textured dust storms observed by Mars Global Surveyor Mars Orbiter Camera, Advances in Space Research. doi: 10.1016/j.asr.2016.10.028

Lee P. Thomas P.C. (1995) Longitudinal dunes on Mars: Relation to current wind regimes. Journal of Geophysical Research 100: 5381–5395.

Malin M.C., Danielson G.E., Ravine M.A., Soulanille T.A. (1991) Design and development of the Mars Observer Camera. International Journal of Imaging Systems and Technology 3: 76–91.

Malin M.C., Edgett K.S. (2001) Mars Global Surveyor Mars Orbiter

Camera: interplanetary cruise through primary mission. J. Geophys. Res., 106: 23429–23570.

Malin M.C., Bell J.F., Cantor B.A., Caplinger M.A., Calvin W.M., Clancy R.T., et al. (2007) Context camera investigation on board the Mars Reconnaissance Orbiter. Journal of Geophysical Research 112: E05S04.

McEwen A.S., Eliason E.M., Bergstrom J.W., Bridges N.T., Hansen C.J., Delamere W.A., et al. (2007) Mars Reconnaissance Orbiter's High Resolution Imaging Science Experiment (HiRISE). Journal of Geophysical Research 112: E05S02.

Melosh H.J. (2011) Planetary surface processes. Cambridge planetary science, ISBN 978-0-521-51418-7

Michael V.K., Ralph D.L., Nilton O.R. (2016) Dust Devil Steady-State Structure from a Fluid Dynamics Perspective Space Science Reviews, 203: Number 1-4, Page 209.

Marshall J.G., Particle Dispersion Experiment (PDE): Preliminary results from the USML-1glovebox, NASA CP 3272, 717, 1994.

Neukum G., Jaumann R. (2004) HRSC: The High Resolution Stereo Camera of Mars Express. In: Wilson A (ed.) Mars Express: The Scientific Payload. Noordwijk, Netherlands: ESA Publications Division ESA SP-1240: 17–35.

Quintana S.N., Schultz P.H (2014) 45th Lunar and Planetary Science Conference, The formation of crater-related blast wind streaks on Mars. Brown University, Department of Geological Sciences, 324 Brook Street, Providence, RI

Ralph D. Lorenz, James R. Zimbelman. How Windblown Sand

Shapes Planetary Dune Worlds Landscapes. ISBN 978-3-540-89724-8, DOI 10.1007/978-3-540-89725-5.
Springer Heidelberg New York Dordrecht London, 2014.

Richardson M.I., Wilson R.J. (2002) A topographically forced asymmetry in the Martian circulation and climate. Nature, 416: 298–301

Renno N.O., Burkett M.L., Larkin M.P. (1998) A simple thermodynamic theory of dust devils, Journal of Atmosphere Science, 55: 3244

Sagan C., Bagnold R.A., (1975) Fluid transport on Earth and aeolian transport on Mars. Icarus 26: 209–218.

Silvestro S., Di Achille G., Ori G.G. (2010b) Dune morphology, sand transport pathways and possible source areas in east Thaumasia Region (Mars), Geomorphology 121: 84–97.

Vandaele A.C., et al. (2019) Martian dust storm impact on atmospheric H2O and D/H observed by ExoMars Trace Gas Orbiter, Nature, 568: doi: 10.1038/s41586-019-1097-3

Viúdez-Moreiras D., Newman C.E., Torre M., et al. (2019) "Effects of the MY34/2018 Global Dust Storm as Measured by MSL REMS in Gale Crater." Journal of Geophysical Research: Planets, 124 (7): 1899-1912 doi:10.1029/2019je005985

Silvestro S., Fenton L.K. (2011) Present-day aeolian activity in Arabia terra: First results from a global mapping of active dune fields on Mars 1482. 42nd Lunar and Planetary Science Conference, Houston, TX: Lunar and Planetary Institute.

Silvestro S., Di Achille G., Ori G.G. (2010) Dune morphology sand

transport pathways and possible source areas in east Thaumasia Region Mars. Geomorphology 121: 84–97.

Squires V.R. (2007) Physics, Mechanics and Processes of Dust and Sandstorms (PDF). Adelaide University, Australia.

Sullivan, R. et al., 2008. Wind-driven particle mobility on Mars: Insights from Mars Exploration Rover observations at ‘‘El Dorado’’ and surroundings at Gusev crater. Journal of Geophysical Research 113, E06S07, doi: 10.1029/2008JE002541.

Tanaka, K.L., Fortezzo, C.M. (2012) Geologic map of the North Polar Region of Mars. U.S. Geol. Survey Sci. Invest. Map 3177, scale 1:2000, 000

Zimbelman J.R., Griffin L.J. (2010) HiRISEimages of yardangs and sinuous ridges in the lowermember of theMedusae Fossae Formation, Mars. Icarus, 205(1): 198–210.

Chapter 9
Aeolian Processes on Titan

Introduction

Vast fields of dunes have been discovered on Titan, the largest moon around Saturn (Lorenz et al, 2006), a world that is at once very different from Earth. Titan is a cold, icy world, with a surface gravity similar to the Moon around Earth. It is somewhat larger (5150 km diameter) than the planet Mercury and, uniquely among the moons of the solar system, has a thick atmosphere (1.5 bar surface pressure) predominantly of nitrogen with some methane. The action of sunlight on this methane produces heavier organic compounds, some of which accumulate as solids on the surface, and are sculpted by winds into dunes. Thousands of linear duneforms have been observed by the Cassini Radar instrument on the Cassini spacecraft, operating in Synthetic Aperture Radar (SAR) mode. These features are found mainly in equatorial regions, dominantly within ±30° of the equator, and they nearly encircle the globe. They may cover as much as 20% of the surface and have orientations indicative of time-averaged, W to E wind flow across the globe (Radebaugh et al, 2010).

Dunes Because sunlight is so faint at Saturn, it was originally thought that there would not be enough energy from solar insolation to drive surface winds, and thus Titan would not have any active aeolian processes (Lorenz et al, 2006). However, climatic models suggest that the tidal pull by Saturn generates pressure variations in Titan's atmosphere capable of driving near-surface winds (Tokano and Neubauer, 2002). Titan has a methane-rich atmosphere with a surface pressure of ~1.5 atm (146.7 kPa); coupled with a low gravity (0.14 g),

this results in a threshold wind speed of only ~10 cm/s necessary to move an average sand-sized particle (Lancaster, 2006).

Observations from the Cassini spacecraft's Radio Detection and Ranging (RADAR) instrument, which has a resolution similar to the Magellan spacecraft's radar images of Venus (Lorenz et al, 2001), show radar dark parallel features (Figure 3) that appear to be linear dunes (Lorenz et al, 2006). These features are ~100–150m high, have slopes of 6–10° (Lorenz et al, 2006), are tens of kilometers long, and resemble terrestrial linear dunes in all respects (Radebaugh et al, 2010). However, Titan is an icy satellite, and instead of consisting of quartz-rich sediments, the dunes on Titan are most likely composed of ice particles that were eroded from precipitation and runoff of liquid methane (Lorenz et al, 2006) or they consist of hydrocarbon particles that were generated by photochemistry in Titan's stratosphere and that simply accumulated over time (Wahlund et al, 2009).

Although the radar survey of Titan's surface is not complete, it appears that the linear dunes are ubiquitous in the equatorial region between ±30° latitude (Radebaugh et al, 2008), possibly due to Titan's global atmospheric circulation pattern (Lorenz and Radebaugh, 2009). Interestingly, the slope orientations of the dunes suggests that they are being driven by westerly winds (Lorenz et al, 2006), which is opposite to the wind directions predicted by global climatic models (Tokano and Neubauer, 2002). However, more recent models of global circulation that were integrated over an entire year on Titan suggests that there may be occasionally fast, turbulent westerlies initiated by the equinoctial passage of the intertropical convergence zone around the equator (Tokano, 2010).

The discovery of linear dunes on Titan has several important implications for understanding aeolian processes in planetary environments. Dunes have now been recognized on all terrestrial planets that have an appreciable atmosphere, and aeolian processes are now known to be literally universal in several meanings of the word. Generation and transport of sediment appears to be a basic geologic process on planetary surfaces. Aeolian processes also adjust to the

environment and occur in a range of atmospheric pressures and compositions as well as variations in surface gravities. It is interesting to note, however, that the only dune forms that appear to be ubiquitous are linear dunes (Craddock, 2011).

The Cassini mission continues to provide new insights into the unique sand dunes that cover nearly a fifth of the surface of Saturn's largest moon. Lorenz (2014) summarizes the key parameters involved with aeolian processes on Titan, including the sensitivity of saltation to these parameters, and also evaluates the dune-building timescales for Titan. Rodriguez et al. (2014) examined the Titan dunes correlating radar data with compositional information from the Visual and Infrared Mapping Spectrometer; the dune material is dominated by solid organics of atmospheric origin that represent the largest visible surface reservoir of hydrocarbons on Titan. Savage et al. (2014) report on analyzing 7000 measurements of the width and spacing of dunes obtained from five study sites on Titan; the average width is 1.3 km and the average crest spacing is 2.7 km, comparable to large dunes on Earth, and cumulative probability plots of the measurements indicate that the dunes on Titan are of a single population.

According to Greeley (2014) some researchers have used sophisticated modeling to investigate the dunes on Titan. Mastrogiuseppe et al (2014) used Cassini radar altimetry, restricted to locations where the altimeter foot prints were entirely on dunes, to investigate heights of the Fensal dune field on Titan, through application of a non-coherent electromagnetic echo model to the processing of the returned altimetry signal. Le et al (2014) modeled both the microwave backscatter and thermal emission from linear dune fields to compare to Cassini radar and radiometric data of Titan's dunes, in order to investigate regional variations among the dune fields on Titan. Paillou et al (2014) modeled multi-frequency synthetic aperture radar response of linear dunes of the Great Sand Sea in Egypt, along with topography obtained during space shuttle missions, to compare to the radar response obtained during the T8 flyby that included large sections of the dunes on Titan, concluding that a single

surface scattering term is insufficient to explain the radar signal strength backscattered by the dunes on Titan.

9.1. The Sand Seas of Titan

The low gravity and dense atmosphere on Titan make it a favorable environment for aeolian transportation of material (Lorenz et al, 1995) in the sense that the wind speeds needed to saltate surface particles are rather low. However, until recently (Lorenz and Mitton, 2002) it was thought that loose particles were difficult to generate and transport (erosive processes and wind, driven by the faint sunlight reaching Titan's surface, were expected to be weak) and would be susceptible to trapping by surface liquids.

Recently, numerical circulation models (Tokano and Neubauer 2002) incorporating the tide in Titan's atmosphere due to Saturn's gravity (Lorenz, 1992) (~400 times as strong as the moon's effect on Earth) show that near surface winds may be dominated by this effect rather than solar heating, and periodically varying winds comparable with the transport threshold may result. The winds vary both in strength and direction. Data from Cassini (Porco, 2005) and from the Huygens probe (Tomasko, 2005) that landed on Titan in January 2005 show a very geologically varied surface, modified by a mix of processes including strong fluvial erosion, impact, and cryovolcanism[1]. No evidence for large bodies of surface liquids has so far been found. Thus, the setting for aeolian transport now seems much more favorable.

Aeolian features appear on planetary surfaces at a wide range of scales, from cm-wide ripples to km-scale megadunes[2]; imaging resolutions of better than 1 km are therefore required to observe them (Lorenz et al, 2006). Early large-scale nearinfrared (near-IR) imaging

1 - Cryovolcanism is defined as the extrusion of liquids and vapors of materials that would be frozen solid at the planetary surface temperatures of the icy bodies of the outer solar system.

2 - A very large aeolian bedform.

at ~km resolution by the Cassini Imaging Science Subsystem (ISS) indicated large-scale albedo patterns such as dark streaks and asymmetric edge contrasts (sharp westward boundaries and diffuse eastward ones) that were suggestive of net-eastward fluid transport of materials on Titan's surface, possibly by wind, but individual features could not be resolved.

Radar imaging (Lorenz et al, 2006) on Cassini's T3 flyby, found many distinct radar-dark linear features (nicknamed "cat scratches" superposed on other geological units and having a spacing of 1 to 2 km and lengths of many tens of km, in a generally east-west orientation. These covered about 20% of that swath (covered ~1.8 million km^2, or almost 2% of Titan's surface), in patches with extents of up to 400 km.

The imaging on [1]T8 has found large expanses of these features, covering some 65% of that swath. Patches of these features vary from just a few km across to the width of the swath (~200 km), and one contiguous region is 1500 km long. Furthermore, in some places in T8 the feature size, favorable geometry, and resolution of the observations allow the detection of bright topographic glints (Fig. 9.1).

1 - One of the large expanse features on Titan.

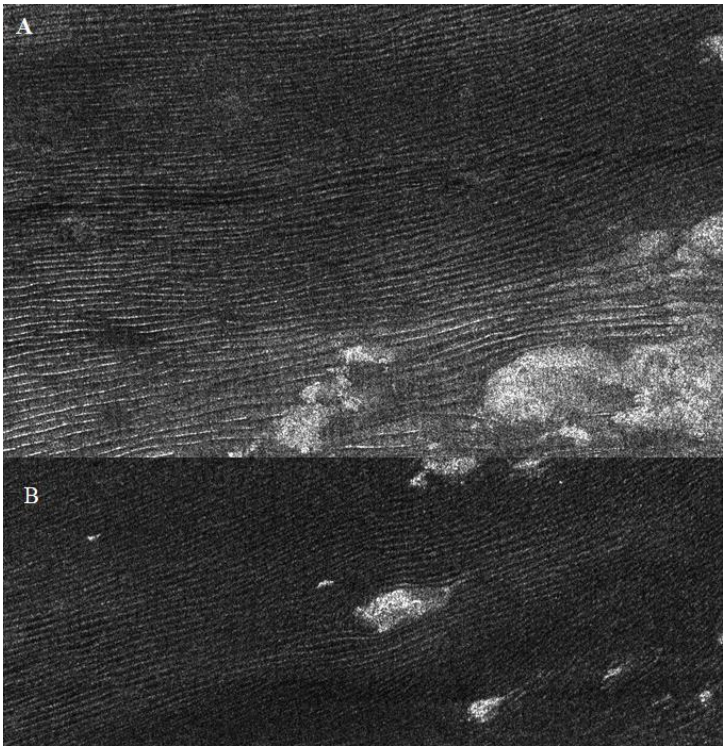

Figure 9.1 (A) an area 41125 km^2 (north up) of the Belet sand sea at ~12-S, 100-W. Topographic glints are evidence of slopes facing the observer (radar illumination is from above). The subparallel orientation of the dunes and the 1:2 dune to interdune gap ratio are typical of longitudinal dunes on Earth. (B) Bright areas are small hills; the flow diverges around them and reconverges. A tail toward the right is evident in the lower hill, suggesting an east-northeast transport direction (after Lorenz et al, 2006).

Data from Cassini and from the Huygens probe that landed on Titan in January 2005 show a very geologically varied surface, modified by a mix of processes including strong fluvial erosion, impact, and cryovolcanism. No evidence for large bodies of surface liquids has so far been found. Thus, the setting for aeolian transport now seems much more favorable.

Aeolian features appear on planetary surfaces at a wide range of scales, from cm-wide ripples to km-scale megadunes; imaging

resolutions of better than 1 km are therefore required to observe them. Early large-scale near-IR imaging at ~km resolution by the Cassini Imaging Science Subsystem (ISS) indicated large-scale albedo patterns such as dark streaks and asymmetric edge contrasts.

Morphologically, the features resemble longitudinal dunes such as those found in the Lut and other terrestrial deserts (Fig. 9.2).

Figure 9.2 Image of Lut sand sea (Iran) showing undulating topography

Their height, longitudinal symmetry, superposition on other features, and the way they merge (forming tuning fork) suggest that they are depositional. The interpretation as longitudinal dunes is supported by the way they divert and reconverge around topographic obstacles (Fig. 9.2). The asymmetric streamline pattern thus formed suggests that the net transport direction is generally eastward, with some regional variation (Fig. 9.3) and local deviations around elevated or bright topography.

Figure 9.3 A 515 km by 200 km segment of the T8 swath where the longitudinal dunes creeping from the left (west) encounter what appears to be a broad bright topographic rise. As the sand flows around this obstacle, it forms transverse dunes at the southwestern side before the longitudinal pattern resumes. Such a pattern confirms a depositional origin and is the only prominent example of dunes other than longitudinal ones observed so far (after Lorenz et al, 2006).

On Titan, the wind regime that forms longitudinal dunes may be a natural result of the interaction of the fluctuating tidal wind field with the steady zonal (west-east) winds that prevail higher in the atmosphere (Bird, 2005). A substantial instantaneous meridional (north-south) component is implied, and the fact that dunes are not oriented exactly west-east everywhere also suggests a net meridional component over the long term.

Whether or not the meridional component can be explained by other mechanisms, the presence of substantial meridional winds was not anticipated before the tidal model. It is evident that topography has a substantial effect on near-surface winds—the dune orientation can veer by some 45- over just 10 km.

9.2. Titan's Dune-Forming Winds

The Cassini mission made an unexpected discovery when it found evidence of linear dune fields on Titan's surface. The radar dark dunes have a mostly tropical distribution between +/−30° latitude that extends to all longitudes. Cassini has imaged thousands of dunes

throughout its mission, many of which are observed to divert around topography. The crestline orientations of the dunes and their interaction with topography allow scientists to estimate the dominant wind direction on the surface of Titan. There is some consensus in the community that the dune-forming winds produce an eastward net transport, and are therefore predominantly westerly (West to East) (Takano, 2010).

The Titan surface wind regimes that have been proposed, mostly based on studies of morphologically similar Earth dune fields, are as follows: westerly winds with a fluctuating tidal component, bimodal (coming from two directions) westerly, bimodal easterly, unimodal westerly, bimodal and slightly westerly, and both unimodal and bimodal westerly winds. Titan's dunes have been proposed to be longitudinal, which only form in a specific type of wind regime with bimodal winds having roughly equal magnitudes and divergence angles of greater than 90°. In which case, some of these theories are in conflict with maximum gross bedform-normal transport theory (MGBNT) for the alignment in a given wind regime. It is not certain that Titan's dunes are longitudinal, however, and there are other ways to form linear dunes (Larson, 2019).

There is an active debate about the dune-forming wind regimes. This debate has been guided by several studies of Earth dune fields considered analogous to the Titan dunes including those in Namibia, the Sahara, the Serengeti, and China. The linear dunes have been considered analogs to Namibian dunes due to morphological similarities (Radeaugh et al, 2008). The presence and morphology of these dunes can aid our understanding of the dune-forming winds on Titan. Complicating this active debate about the surface wind regime is the fact that global circulation models (GCMs) have historically not been able to reproduce westerly (prograde) surface winds in the tropics (Newman et al, 2011).

Several GCMs have offered detailed results of the surface wind patterns and how they relate to the dunes across different orbital periods. There are currently three leading hypotheses that overcome

the apparent discrepancy between GCM surface winds and dune orientations. First, one GCM found that despite predominantly easterly winds near equinox, there is a brief period of fast westerlies. The usual surface winds in this GCM are easterly and usually around 1 m/s, however near equinox there are strong westerly winds of a slightly higher magnitude, 1.5 m/s. Although westerly winds are rare, their increased velocity allows them to carry sand grains while the weaker easterly winds cannot, thus building the dunes (McDonald, 2016). This is based on the principle that the potential saltation flux is proportional to the cube of friction velocity, thus the sand flux is very sensitive to the wind strength. Other studies suggested that Titan's dunes form over orbital time scales and may not be in equilibrium with the current wind regime. Finally, there is a hypothesis that gust fronts from convective storms drive dune formation (Larson, 2019).

According to Larson (2019) topography may play a necessary role in shaping the surface winds on Titan that form dunes. Large areas of the tropics, especially those at higher elevations, and with dunes present, have westerly winds up to 1.1 m/s in this simulation. These winds are consistent in direction and velocity with the Huygens measurements. There is also a positive correlation between the wind speed in this simulation and dune presence. The correspondence in this simulation of westerly winds with the dune locations may suggest an as yet unknown physical process, such as downslope winds that may play an important role in dune formation.

Westerly winds may not be sufficient to form Titan's dunes. Rubin and Hesp (2009) showed that for longitudinal dunes, nearly equal bimodal winds are required with divergence angles greater than 90°. However, it is unclear if Titan's dunes are longitudinal or stabilized linear dunes. Figure 9.4 shows rose diagrams compiled over a Titan year for the whole tropics. The wind pattern for the base case model (upper left) is bimodal with both directions being easterly and about 68° apart. The simulation with topography (upper right) has a multitude of directions, but at any given location, the winds are predominantly bimodal with angles greater than 90°. It appears that

the forced dynamics (bottom two panels, Figure 9.4) remove much of the bimodality that is shown to create longitudinal dunes. The added torque in the bottom two simulations acts in different directions due to the pressure dependence of the torque term. Much of the tropics are at high elevations and experience a prograde torque. This bimodality is important for determining the type of dunes created. Thus, only the simulation with topography is consistent with longitudinal dune formation and westerly surface winds. However, as noted above, there are other methods of creating linear dunes, such as by stabilizing sediment.

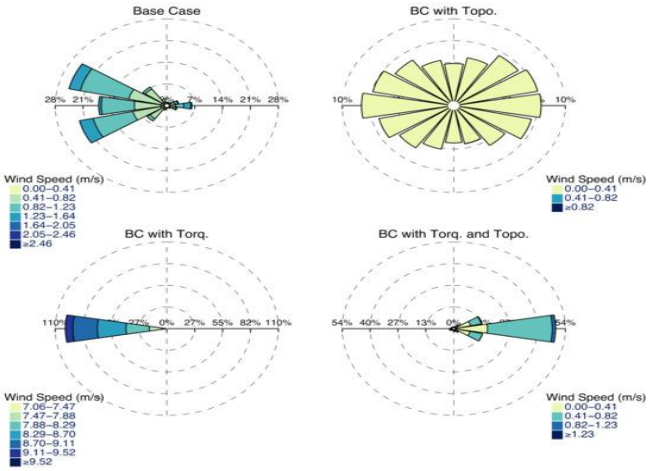

Figure 9.4 Downwind wind rose diagrams (wind directions from the center out) for the tropics (+/−30°) for one Titan year (after Larson, 2019).

Dune formation occurs due to a spatial or temporal decrease in the sand-carrying capacity of the wind in areas with strong enough wind that sand can be mobilized (Fryberger et al, 1979). Given Titan's fairly weak winds, a minimum condition needed for dune formation is sufficient wind speed to lift sand particles. Therefore, the threshold wind speed could be <1 m/s (Burr et al, 2015). According to Larson (2019) many other factors control Titan's dune including sediment availability and sufficiently low sediment cohesion. This could also potentially be due to the fact Larson's model resolution does not resolve the local winds. The wind speeds shown here are averaged

over several Titan days and are less than the maximum instantaneous wind speeds that would actually move the sediment. Furthermore, recent laboratory analysis suggests that sustained movement of grains on Mars, and presumably on Titan, can be maintained by impacts from saltating grains, which requires lower wind speeds than direct fluid drag (Sullivan and Kok, 2017).

9.3. Saltation Threshold in Titan

The optimum saltation diameter for particles on Titan is probably 200–600 μm, with threshold friction speeds of 0.03–0.06 m/s (free stream speeds of 0.8–1.5 m/s). These values, however, are all estimates, based on assuming a density consistent with organics and cohesion the same as terrestrial sands. The saltation mechanics of specified dry materials are rather well understood the challenge at Titan knows what the sand materials actually are and how the saltation threshold may be affected by cohesion which may be in turn influenced by methane or ethane moisture and thus variable with space and time on Titan. The efficacy of charge generation and retention on saltating materials on Titan may be high, and their effects on saltation mechanics may be profound.

9.3.1. Saltation Length and Ripple Formation

Aeolian ripples result from the preferential accumulation of material at ripple crests due to the shadowing of intercrest areas from incoming saltating particles. Thus while the saltation path length is an influence on ripple spacing (as suspected by Bagnold) it is only an upper limit to ripple dimensions.

The saltation trajectory results from the launch of a particle by aerodynamic forces lifting a particle off the bed, or the impact of a predecessor (i.e. impact ‘splash’) and the acceleration of the particle downwind. How fast it moves downwind depends on how high it gets, since the flow velocity immediately adjacent to the surface is very small due to the ‘no slip’ condition at the flow boundary (Law of the Wall). This in turn depends on the launch velocity, but also on how

quickly the particle is decelerated by fluid drag. On Mars, this drag is small, so particles can rise to heights of the order of a meter and be accelerated fast downwind, leading to fields of large ripples. On Titan, as noted by Lorenz et al, (1995), the saltation path length is very short – about 1 cm. This is because the terminal velocity of sand particles in the thick Titan atmosphere is very small, about 0.3 m/s for the optimum 300–500 μm particles.

On Titan, then, classic aeolian ripples are unlikely to form in the pseudoballistic way they do on Earth and Mars. As is also the case on Venus (e.g. Kok et al, 2012) and underwater surfaces on Earth, any bedforms must result from hydrodynamic effects. This may be important for radar remote sensing, in that regular ripples with a wavelength of several centimeters could cause resonant Bragg scattering and affect the radar reflectivity of dunes at the Cassini radar wavelength of 2 cm: the discussion here suggests such Bragg effects will not be significant.

9.4. Electrostatic effects on Titan sand

It is well-known that moving granular materials can generate electrical charges via triboelectrical effects (and such charging can present powder explosion hazards in certain industrial settings, e.g. Eckhoff, 2003). Blowing sand and dust can similarly develop electric fields and particle charges (e.g. Merrison, 2012) as can blowing snow, and the associated electrostatic forces can reduce the saltation threshold, and increase the sand transport rate for a given friction speed (Rasmussen et al., 2009) – indeed, when friction speeds are just above the threshold, the sand transport can be enhanced by a factor of several by likely electrostatic effects. On the other hand, a macroscopic electric field can instead increase the saltation threshold (von Holstein-Rathlou et al., 2012) and would thereby reduce transport.

Charging is strongest in dry (and thus electrically-insulating) conditions, and as reviewed by Merrison (2012), sand charging is broadly consistent with the measured charge to mass ratio observed in snow, of the order of 50 μC/kg. It is not surprising that electrically-

insulating materials like plastics (and by implication, organic solids in general) can develop charges too.

On Titan it can be expected that particles will retain their charge effectively. Furthermore, given the low gravity, the proportionate effect of electrostatic forces on wind threshold and on sand transport will be larger than for the Earth and Mars. Experimental investigation of triboelectric charging in Titan analog materials, and the possible effects on aggregation of particles, may be fruitful. Numerical or analytic simulation of saltation mechanics with electrostatic forces will also be of interest.

9.5. Dune Formation on Titan

Sand accumulation in dunes occurs as a result of transport instability. Airflow accelerates over a surface bump, and causes an increase in wind stress that depends on surface height and slope, reaching a maximum slightly upwind of the topographic peak (the crest). However, a finite distance (the 'saturation length' Ls) is required for the sand flux to 'catch up' with the increase in potential sand transport afforded by the accelerating wind. Providing the bump is large enough that the sand flux reaches a maximum upwind of the crest, then the crest can accumulate sand and the dune can grow (Kok et al, 2012). Thus dunes must be of a certain minimum ('elemental') size in order to form and grow.

Saturation length defines the wavelength scale at which a flat sand bed will destabilize (Claudin and Andreotti, 2006) to form 'elementary' dunes. The dunes observed by Cassini are presumably therefore 'giant' dunes, formed by the growth or aggregation of these smaller elementary bedforms (Lorenz et al, 2010).

Observable aerodynamic ripples are not expected on Titan. The length scale at which dunes can begin to grow is ~1.5 m, and so imaging resolution of the order of 0.2 m would be desirable on future missions to characterize the full spectrum of bedform sizes. Based on scaling of terrestrial transport relations, dunes likely reorient on timescale of ~50,000 years, comparable with the timescale of

astronomical climate forcing, and thus the dune pattern may lag the present-day wind field (Lorenz, 2014).

Dunes can grow and coalesce to form progressively larger dunes, but the growth rate asymptotically declines as the dune spacing approaches the thickness of the atmospheric boundary layer (Andreotti et al, 2009). The static stability at the top of this layer provides a 'capping' function, much as does the free surface of the water for subaqueous dunes, and limits the dune growth.

Lorenz et al, (2010) noted that the Huygens descent profile indicates a boundary layer height of ~3 km, close to the observed spacing of Titan's dunes – almost universally 2–3 km (Savage et al., 2014). The fact that the dunes appear to be of this scale means they are morphologically mature: once growing dunes reached this height and spacing, they would stop growing. Thus dividing the sand volume by a sand transport rate to derive a construction time gives only a lower limit on the age of the dunes.

9.6. Dune Growth and Reorientation Timescale

There is every reason to expect that Titan's climate has changed through time. Solar luminosity has changed over Solar System history (~4.5 Gyr) with resultant effects on climate, the methane inventory in the atmosphere may have changed both up and down (e.g. Lunine et al, 1998) on ~100 Myr timescales (and methane is a major greenhouse gas, as well as the principal source of 'moisture' at Titan's surface), and there is a climate forcing – much like the Croll–Milankovich cycles that drive Earth's glacial cycles – with a ~50,000 year period (Aharonson et al, 2009).

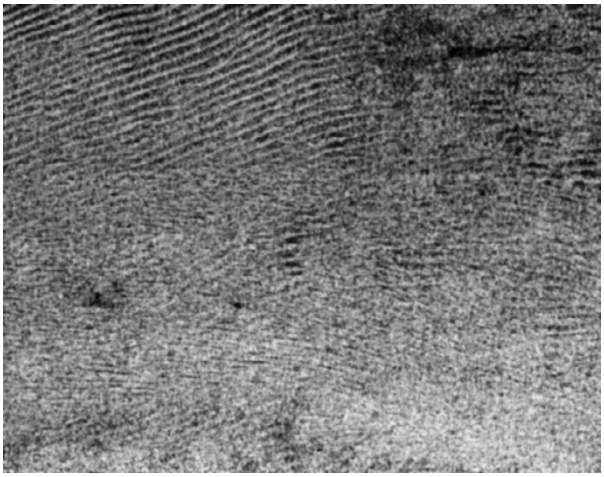

Figure 8.5 One of the few examples of interposed or superposed dune systems on Titan. This segment of the T8 near-equatorial swath is at ~10° S, 240° W. Image is 160 ~ 125 km and has been black–white inverted for clarity (after Lorenz, 2014).

This latter forcing likely redistributes surface liquids (explaining the preponderance of lakes and seas in the north polar regions in the present epoch) but probably also influences wind patterns and humidity distribution, and by extension, the orientation, size and distribution of dunes.

While Titan's dunes overall are remarkable for their striking uniformity in spacing, orientation and morphology (almost exclusively linear), closer examination does reveal some features which may indicate a reorientation of dune forms. Hayes et al. (2012) have noted some star and barchan-like features. One set of linear dunes (Fig. 9.5) has also been observed with an intervening, or possibly superposed, linear pattern.

References

Andreotti B., Fourriere A., Ould-Kaddour F., Murray B., Claudin P. (2009) Size of Giant Aeolian Dunes limited by the average depth of the atmospheric boundary layer. Nature 457: 1120–1123.

Bird M.K.M, Nature, 438: 800 (2005).

Burr D.M., Bridges N.T., Marshall J.R. et al, (2015) Higher-than-predicted saltation threshold wind speeds on Titan. Nature: 517: 60–63.

Craddock R.A. (2011) Aeolian processes on the terrestrial planets: Recent observations and future focus. Progress in Physical Geography, 36(1): 110–124

Eckhoff R. (2003) Dust Explosions in the process industries. Gulf Professional Publishing, 719p.

Fryberger S.G., Ahlbrandt T.S., Andrews S.(1979) Origin, sedimentary features, and significance of low-angle aeolian “sand sheet” deposits, Great Sand Dunes National Monument and vicinity, Colorado. J. Sediment. Res. 49: 733–746.

Greeley R. (2014) Introduction to the planetary dunes special issue, and the aeolian career of Ronald Greeley, Icarus, 230: 1-4. doi.org/10.1016/j.icarus.2014.01.003

Hayes A.G., Ewing R.C., Lucas A., et al, (2012) Determining timescales of the dune forming winds on titan, third international planetary dunes workshop, Flagstaff, AZ, June 2012. Lunar Planet Sci., Abstract 7057.

Kok J., Parteli E.J.R., Michaels T.I., Karam D.B. (2012) The physics

of wind-blown sand and dust. Rep. Prog. Phys. 75: 106901. doi.org/10.1088/00344885/75/10/106901

Larson E.J.L. (2019) Topographic Effects on Titan's Dune-Forming Winds. Atmosphere, 10(10), 600; doi.org/10.3390/atmos10100600

Lancaster N. (2006) Linear dunes on Titan. Science, 312: 702-703.

Le Gall A., Janssen M.A., Kirk R.L., Lorenz R.D., (2014) Modeling microwave backscatter and thermal emission from linear dune fields: Application to Titan. Icarus, 230: 198–207.

Lorenz R.D., Lunine J.I., Grier J.A., Fisher M.A. (1995) J. Geophys. Res. (Planets) 88: 26377.

Lorenz R.D., Mitton J., Lifting Titan's Veil (Cambridge Univ. Press, Cambridge, 2002).

Lorenz R.D., in Proceedings Symposium on Titan, Toulouse, France, 9-12 September 1991, B. Kaldeich, Ed. (European Space Agency SP-338, Noordwijk, Netherlands, 1992), pp. 119–123.

Lorenz R.D., Elachi C., West R.D., Johnson W.T.K., Janssen M.A., Moghaddam M., et al. (2001) Cassini Radio Detection and Ranging (RADAR): Earth and Venus observations. Journal of Geophysical Research 106: 30271–30279.

Lorenz R.D., Wall S., Radebaugh J., Boubin G., Reffet E., Janssen M., et al. (2006) The sand seas of Titan: Cassini RADAR Observations of longitudinal dunes. Science, 312: 724–727.

Lorenz R.D., Radebaugh J. (2009) Global pattern of Titan's dunes: Radar survey from the Cassini prime mission. Geophysical Research Letters 36: L03202.

Lorenz R.D., Claudin P., Radebaugh J., Tokano T., Andreotti B. (2010) A 3 km boundary layer on Titan indicated by dune spacing and Huygens Data. Icarus 205, 719–721.

Lorenz, R.D., 2014. Physics of saltation and sand transport on Titan: A brief review. Icarus, 230, 162–167.

Mastrogiuseppe M., Poggiali V., Seu R., Martufi R., Notarnicola C., (2014) Titan dune heights retrieval by using Cassini radar altimeter. Icarus, 230, 191–197.

Mc Donald G.D., Hayes A.G., Ewing R.C., et al (2016) Variations in Titan's dune orientations as a result of orbital forcing. Icarus, 270: 197–210.

Merrison J.P., et al, (2012) Factors affecting the electrification of wind-driven dust studied with laboratory simulations. Planet Space Sci. 60: 328–335.

Merrison J.P. (2012) Sand transport, erosion and granular electrification. Aeolian Res. 4: 1–6.

Newman C.E., Lee C., Lian, Y., Richardson M.I., Toigo A.D. (2011) Stratospheric superrotation in the Titan WRF model. Icarus, 213: 636–654.

Radebaugh J., Lorenz R.D., Lunine J.I., Wall S.D., Boubin G., Reffet E., et al. (2008) Dunes on Titan observed by Cassini Radar. Icarus, 194: 690–703.

Radebaugh J., Lorenz R., Farr T., Paillou P., Savage C., Spencer C. (2010) Linear dunes on Titan and earth: Initial remote sensing comparisons. Geomorphology, 121: 122–132.

Rubin D.M., Hesp P.A. (2009) Multiple origins of linear dunes on Earth and Titan. Nat. Geosci., 2: 653–658.

Paillou Ph., Bernard D., Radebaugh J., Lorenz R., Le Gall A., Farr, T. (2014) Modeling the SAR backscatter of linear dunes on Earth and Titan. Icarus, 230, 208–214.

Porco C.C., Nature, 434: 159 (2005).

Rodriguez S., et al, (2014) Global mapping and characterization of Titan's dune fields with Cassini: Correlation between RADAR and VIMS observations. Icarus, 230: 168–179.

Savage C.J., Radebaugh J., Christiansen E.H., Lorenz R.D. (2014) Implications of dune pattern analysis for Titan's surface history. Icarus 230, 180–190.

Tokano T., Neubauer F.M. (2002) Tidal winds on Titan caused by Saturn. Icarus 1582: 499–515.

Tokano T., (2010) Relevance of fast westerlies at equinox for the eastward elongation of Titan's dunes. Aeolian Research, 2: 113–127.

Tomasko M.G. et al, (2005) Nature, 438: 765.

von Holstein-Rathlou C., Merrison J.P., Braedstrup C.F., et al, (2012) The effects of electric fields on wind-driven particulate detachment. Icarus 220: 1–5.

Wahlund J-E, Galand M., Muller-Wodarg I., Cui J., et al, (2009) On the amount of heavy molecular ions in Titan's ionosphere. Planetary and Space Science, 57: 1857–1865